Syntheses of Heterocycles and Aroylhydrazones using Organic Nitriles: Molecular Structures and Self-assembly of their Transition Metal Complexes

Submitted by

Arkalekha Mandal

Roll 126122019

Under the Supervision of

Prof. Bhisma K. Patel

Department of Chemistry,

Indian Institute of Technology Guwahati

Dedicated to My

Ma and Baba

Contents

Chapter 1

Introduction and Literature Review

The first chapter is divided in two parts, the first part gives a concise description on how different non-covalent interactions determine the self-assembly of metal complexes. The second part discusses brief literature review on electrophilic behaviour of nitrile functional group which is exploited for the syntheses of different ligands throughout the thesis. It also gives a general overview on metal complexes of aroylhydrazones and their applications.

1. 1. The Role of Weak Interactions in Self-recognition and Self-assembly of Metal Complexes

The non-covalent weak interactions play a decisive role in the molecular recognition process and thus determine the crystal packing of organic and metallorganic solids.[1] Modern crystal engineering strategies involve judicious use of different weak non-covalent interactions to build up supramolecular assemblies. The non-covalent interactions discussed herein include classical hydrogen bond, weak non-classical hydrogen bond *e.g.* C−H···O, C−H···N, C−H···X C−H···π, halogen bond, π···π, cation···π, lp···π and agostic interactions.

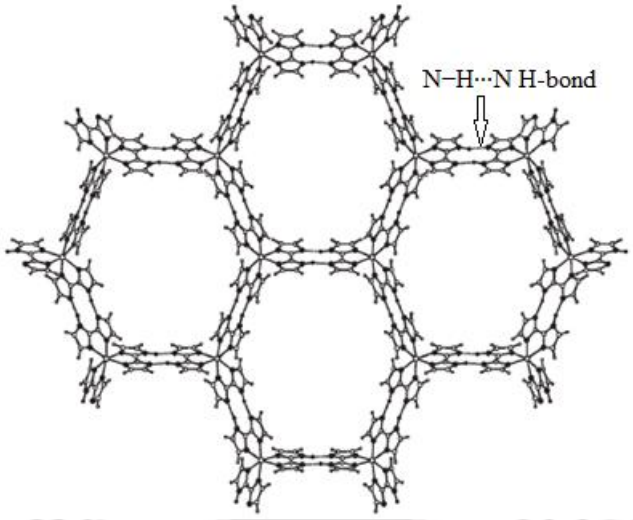

Figure 1. A two dimensional honeycomb network via double N−H···N hydrogen bond in $[Ni(HBIm)_3]^-$, BIm = biimidazolate.[3a]

Classical hydrogen bonding interaction is the major cohesive force in crystal packing. Owing to its strong directional nature associated with the lesser energy of formation or dissociation, hydrogen bonds build up robust intermolecular networks leading to large supramolecular assemblies.[2,3] Hydrogen bond donors/ acceptors in the periphery of ligand molecules together with other donor/ acceptor systems like co-ligands, lattice solvent molecules and counter-anions display various hydrogen bonding pattern induced by classical

O−H···O, N−H···O, N−H···N, N−H···X (X = F, Cl) hydrogen bonds.[4] Coordination complexes furnished with hydrogen bonding substituents on their periphery are used as templates for constructing and designing robust inorganic frameworks.[5] In past two decades hydrogen bonding interactions in coordination complexes and organometallic complexes have been explored by Desiraju, Braga and Grepioni *et al*.[6] The ability of metal bound hydride to act as moderate to strong hydrogen bond donors have been reported by Desiraju[7] and Shubina[8] *et al*.

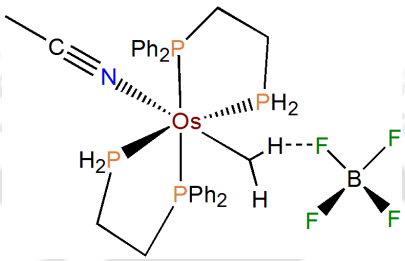

Figure 2. Metal bound hydride acting as hydrogen bond donor.[8]

The significance of non-classical hydrogen bonds *e.g.* C−H···O, C−H···N, C−H···X (X = F, Cl, Br) and C−H···π interactions in crystal packing of organometallic compounds have been comprehensively studied by Desiraju,[9] Brammer[10] and Palmore.[11] The nature of these weak interactions has remained a matter of debate and they are considered to be in the margin of weak hydrogen bond and Van der Waals interaction.[12] However, these interactions are considered to be weak hydrogen bonds when they follow considerable linearity.[13] Desiraju *et al* and Braga *et al* have demonstrated that weak C−H···O hydrogen bonds very often act as the most significant interaction in the crystal packing of metal carbonyls.[9] The role of weak C−H···X (X = F, Cl and Br) in determining the self-assembly of metal complexes of halopyridines have been systematically explored by Brammer *et al*. The interaction energy corresponding to such weak, non-classical hydrogen bonds range in between 2-10 kcal/mole.[14]

The halogen bond or the interaction of the electropositive region (σ-hole) contouring the halogen atom of C−X (X = Cl, Br and I) bond with an electronegative center has attracted much attention from scientific community.[15] Halogen bonds are known to have strong directional property (C−X···Nu ≥150°) along with the strength of weak to moderate hydrogen bonding interactions.[15] The prominent role of halogen bonds in crystal engineering of organic solid[16] and in biology[17] have been reckoned earlier. The incorporation of halogen bond in crystal engineering of metal complexes has been first introduced by Brammer *et*

al.[18] Consequently, it has been proved to be a useful tool to dictate supramolecular assembly of metal complexes of halo substituted ligands.[18c] Halogen substituted organic molecules have been reportedly introduced to the crystals of metal complexes and newly generated halogen bonds take part in self-assembly of metal complexes.[19] The halogen bond is reported to tether weak paramagnetic Co(II) centres in an one dimensional Co(II) coordination polymer and thus forming a strong ferromagnetic chain.[20a] Awadi *et al* have reported the concomitant involvement of interhalogen bond and C–H···X interactions along with metal ion bridging to form three dimensional Cu(II) coordination polymers.[20b]

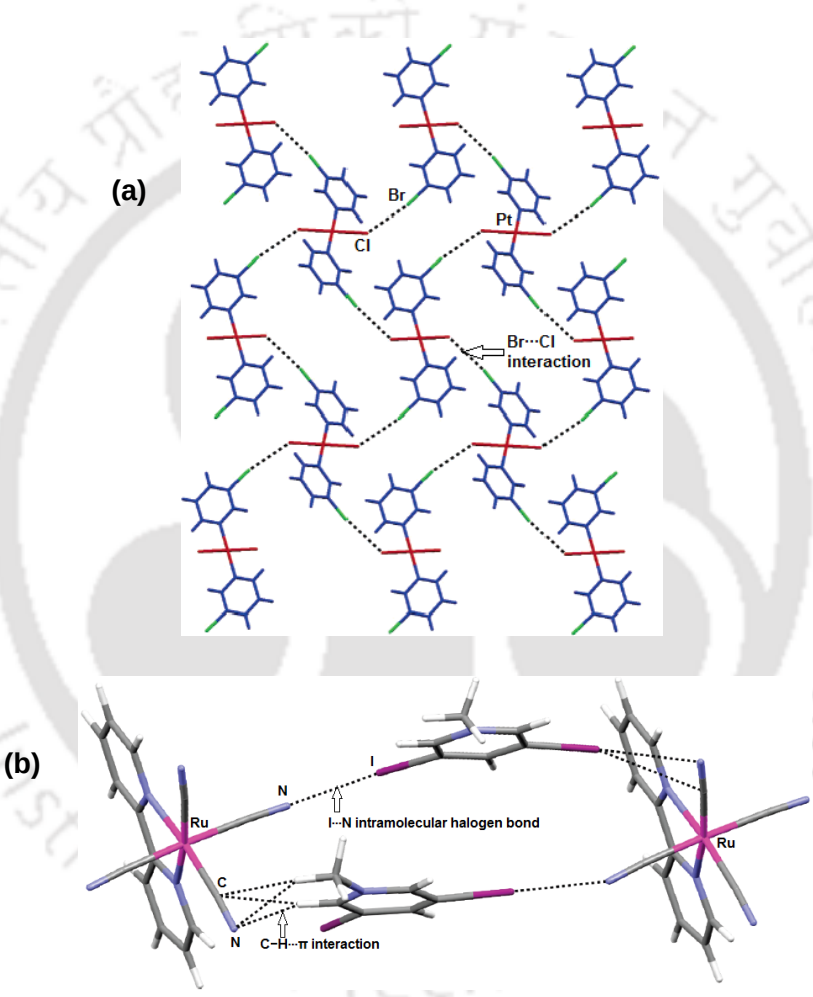

Figure 3. (a) Interhalogen Br···Cl interaction forming 2-D network in $PtCl_2(NC_5H_4Br\text{-}3)_2$;[18a] (b) Weak C–H···π hydrogen bond and intermolecular I···N interaction in $[Ru(bipy)(CN)_4]$.[18c]

The role of π···π interaction in crystal engineering of organic and organometallic solids has been recognised.[21] The π···π interactions are broadly classified into three categories; parallel π···π stacking interaction and anti-parallel or slipped π···π interaction and rare orthogonal π···π interaction.[22] Among these interactions parallel π···π stacking interaction are considered to be the most important as they can impart strong stabilisation

energy[23] as well as govern fluorescence properties.[24] The role of strong parallel π···π stacking interaction to increase the fluorescence intensity of organic molecules[24] and transition metal complexes[25] have been described earlier. The reason can be attributed to the fact that strong π···π stacking interaction helps in mixing of molecular orbitals and thereby reduces the HOMO-LUMO separation.[25] The role of π···π stacking interaction in spontaneous chiral resolution of tris-chelated Cu(II) and Fe(II) complexes of chiral ligands were reported earlier.[26] Diastereoselectivity of Cu(II) complex of a chiral Schiff base ligand via C−H···N hydrogen bond and π···π stacking interaction has also been cited.[27]

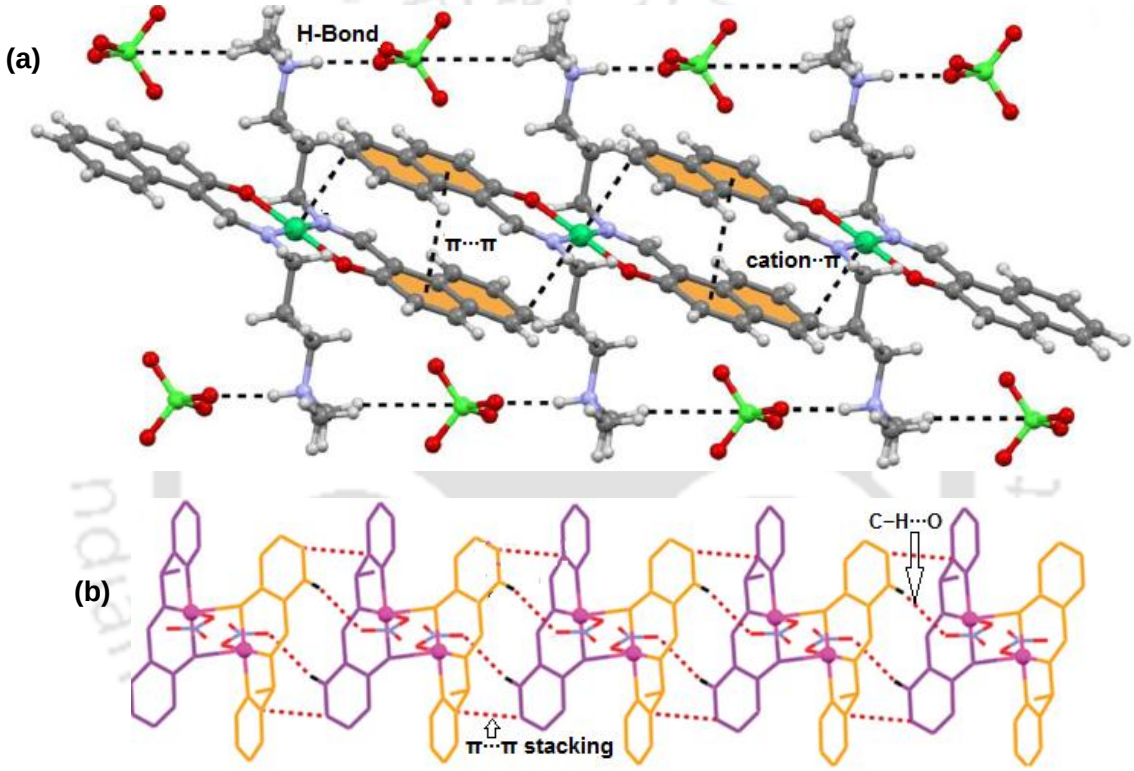

Figure 4. (a) Classical N−H···O hydrogen bond, π···π and cation···π interaction in Ni(II) complex of napthol derivative;[21] (b) π···π Stacking and non-classical C−H···O interaction dictating diasteroselectivity in Ni(II) complex of a chiral Schiff base.[27]

The interaction between an electron rich aromatic cloud and cation or the cation···π interaction very often plays an important role in determining the crystal packing of metal complexes.[28] The occurrence of cation···π interaction is frequently accompanied by π···π interactions in crystal structures of metal complexes of substituted aromatic or heterocyclic ligands.[29] Another interesting feature often associated with the crystal packing of metal complexes of aromatic ligand is the presence of anion···π interaction which is basically the interaction between the electropositive centre or a π-hole on an aromatic ring and an anion.[30]

This interaction is particularly important when the aromatic ring is substituted with electron withdrawing substituents. Banik *et al* reported anion···π interaction playing a prominent role in the crystal packing of Cd(II) complexes of N,N-dimethylvioluric acid which is a derivative of uracil.[31] The role of Br···π and weak C−H···Br hydrogen bond to act as the major forces in crystal packing of bromo substituted ferrocene derivatives has been reported by Chopra *et al*.[32]

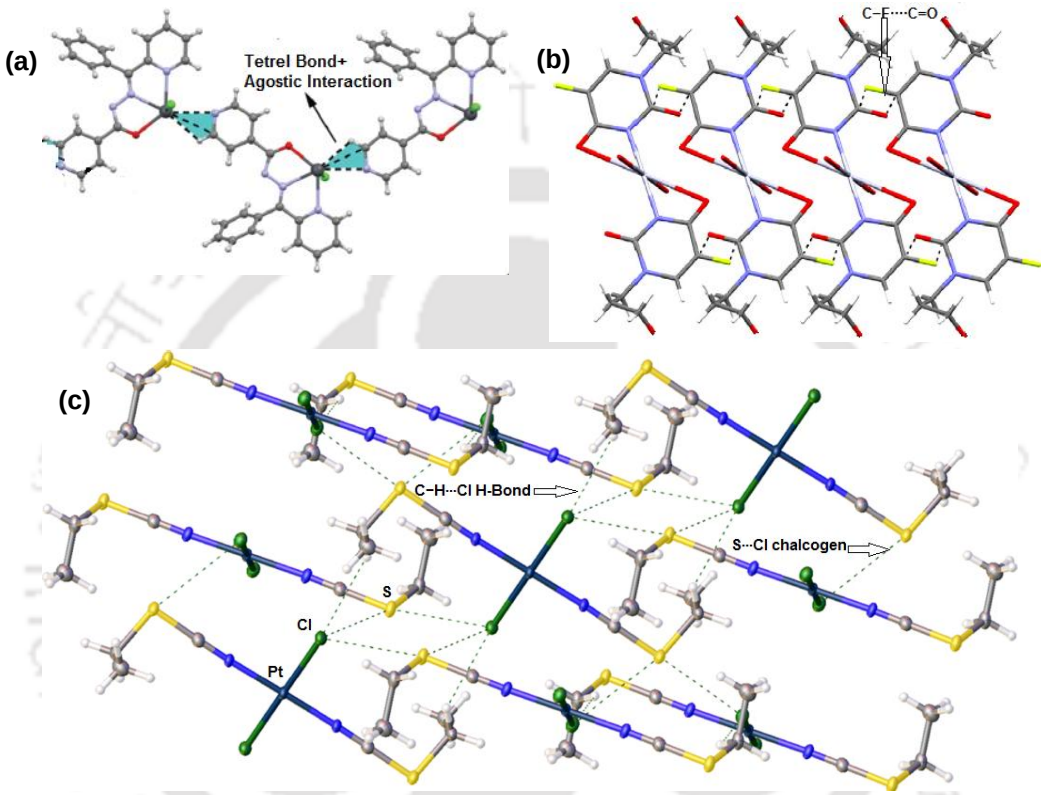

Figure 5. (a) Tetrel bond and agnostic interaction in Hg(II) complex of hydrazide ligand;[33] (b) C−F····C=O interaction in Ni(II) complex of fluoro substituted uracil;[35] (c) Chalcogen and C−H···Cl interaction in Pt complex of alkylthiocyanate.[34]

The wide application of halogen bonds in crystal engineering of organic and organometallic compounds encouraged the scientific community to explore similar σ-hole interactions e.g. tetrel bond (σ-hole on Si, Ge, Sn and Pb), pnictogen bond (σ-hole on P, Te) and chalcogen bond (σ-hole on S, Se). Recently, the application of these interaction in crystal engineering of metal complexes have been reported by Godhrat *et al*[33] and Kukushkin *et al*.[34] The interaction between electron cloud of a C−H bond with an electrophile is called agnostic interaction and such interaction is known to impart stabilization to crystal packing.[33,35] The role of agnostic interactions in crystal packing is reported for metal hydride

complexes.[35] Strong dipolar C−F····C=O interaction is known to play a significant role in the crystal packing of Hg(II) complex of fluoro substituted uracil has been reported by Frontera *et al*.[36] On the other hand, weak dispersive C−H···H−C interaction acts as a major force in the crystal Ni(II) complex of aminomethyl substituted naphthalene derivative.[19b]

Quantification and rationalisation of different weak interactions in crystal packing has emerged as the new realm of crystal engineering. Different methods used for the analyses of weak interactions include Hirsfeld surface analyses,[37] atoms in molecule (AIM),[38] natural bond orbital (NBO)[39] and PIXEL analyses.[40] Density functional theory (DFT) is also widely applied for quantification for intermolecular interaction energies.[41] Guru *Row et al*[42] and Aakeröy *et al*[43] have introduced rational modification of crystal structures of organic solids through quantitative analyses of non-covalent interactions. These concepts have been utilised in recent times for crystal engineering of organometallic compounds.[44]

The emergence of crystal engineering of inorganic solids as a promising field of chemistry has prompted us to pursue our interest in this field. We choose two ligand systems, 1,2,4-triazole and aroylhydrazone (−C(=O)−NH−N=C−). Quantitative crystal structure analyses of differently substituted triazoles or structurally similar thiadiazoles especially with halogen substitution have been reported earlier.[45] The intriguing features associated with crystal structures of these substituted triazoles are concomitant contribution of strong N−H···N, N−H···O hydrogen bonds and weak C−H···N, C−H···O, C−H···X hydrogen bonds as well as π···π and lp···π interactions. On the other hand, crystal engineering of substituted anilides particularly anilides with halo or aminophenyl substitution has received much attention from scientific community as they showcase the coexistence of strong and weak hydrogen bonds.[46] It has also been reported that careful disposition of the substitution on the phenyl group leads to the generation of new features in crystal packing.[46] Crystal engineering of hydrazides with aromatic substitution has been comprehensively studied by Li *et al*.[47] Amino or halophenyl substitutions on hydrazide moiety are known to generate N−H···N or N−H···X hydrogen bonded supramolecular architectures *viz.* ladder, helices and foldemer.[47]

Keeping these facts in mind, we have employed amino, hydroxy or halo substituted 1,2,4-triazole and aroylhydrazone ligands for the study. Metal complexes [M = Co(III), Ni(II), Cu(II), Zn(II) and Cd(II)] of these ligands were prepared and their crystal structures have been analysed. We used DFT, NBO and AIM analyses to understand different intra and

intermolecular interactions in the crystal structures of these ligands and their metal complexes. As metal complexes of 1,2,4-triazole particularly with d^{10} metal ions are known to be fluorescent, detailed investigation of fluorescence property of Zn(II)/ Cd(II) complexes of 3,5-disubstituted 1,2,4-triazole ligands along with their crystal structure analyses have been investigated. In addition, the reaction between organic nitriles and differently substituted hydrazides are used throughout this thesis to synthesise new ligands. We have also described the synthesis of different N-heterocycles using the reaction between organic nitrile and hydrazide functional groups in this thesis.

References

[1] (a) G. A. Jeffrey, W. Saenger, *Hydrogen Bonding in Biological Structures*; Springer-Verlag: Berlin, **1991**; (b) G. A. Jeffery, *An Introduction to Hydrogen Bonding*, Oxford University Press, Oxford, **1997**; (c) G. R. Desiraju, T. Steiner, *The Weak Hydrogen Bond in Structural Chemistry and Biology*, Oxford University Press, Oxford, **1999**; (d) P. Murray-Rust, J. P. Glusker, *J. Am. Chem. Soc*. **1984**, *106*, 1018; (e) G. A. Jeffrey, H. Maluszynska, J. Mitra, *Int. J. Biol. Macromol*. **1985**, *7*, 336. (f) T. Steiner, W. Saenger, *Acta Crystallogr. Sect. B* 1992, **B48**, 819.

[2] (a) P. Murray-Rust, J. P. Glusker, *J. Am. Chem. Soc.* **1984**, *106*, 1018; (b) T. Steiner, W. Saenger, *Acta Crystallogr. Sect. B* **1992**, *B48*, 819; (c) G. A. Maluszynska, J. Mitra, *Int. J. Biol. Macromol.* **1985**, *7*, 336.

[3] (a) A. H. Hoveyda, P. J. Lombardi, R. V. O′Brien, A. Z. Zhugralin, *J. Am. Chem. Soc.* **2009**, *131*, 8378; (b) T. L. Arbolea, F. L. Arbolea, M. J. Tapia, I. L. Arbolea, *J. Phys. Chem.* **1993**, *97*, 4704.

[4] D. Braga, S. L. Giaffreda, F. Grepioni, L. Maini, M. Polito, *Coord. Chem. Rev.* **2006**, *250*, 1267.

[5] (a) G. R. Desiraju, *Angew. Chem.* **1995**, *107*, 2541; (b) G. R. Desiraju, *Chem. Commun.* **1997**, *16*, 1475; (c) D. Braga, F. Grepioni, P. Sabatino, G. R. Desiraju, *Organometallics* **1994**, *13*, 3532.

[6] D. Braga, F. Grepioni, G. R. Desiraju, *J. Organnomet. Chem.* **1997**, *548*, 33.

[7] R. Banerjee, G. R. Desiraju, R. Mondal, J. A. K. Howard, *Chem. Eur. J.* **2004**, *10*, 3373; b) V. R. Thalladi, H. -C. Weiss, D. Bläser, R. Boese, A. Nangia, G. R. Desiraju, *J. Am. Chem. Soc.* **1998**, *120*, 8702.

[8] M. Epstein and E. S. Shubina, *Coord. Chem. Rev.* 2002, **231**, 165.

[9] (a) D. Braga, F. Grepioni, K. Biradha, V. R. Pedireddi, G. R. Desiraju, J. Am. Chem. Soc. **1995**, *117*, 3156; (b) D. Braga, *Acc. Chem. Res.* **2000**, *33*, 601; (c) D. Braga, F. Grepioni, G. R. Desiraju, *Chem. Rev.* **1998**, *98*, 1375; (d) F. Grepioni, G. Cojazzi, S. M. Draper, N. Scully, D. Braga, *Organometallics* **1998**, *17*, 296; (e) D. Braga, F. Grepioni, E. Tedesco, *Organometallics* **1998**, *17*, 2669.

[10] (a) F. Zordan, L. Brammer, P. Sherwood, *J. Am. Chem. Soc.* **2005**, *127*, 5979; (b) L. Brammer, G. M. Espallargas, S. Libri, *CrystEngComm* **2008**, *10*, 1712; (c) G. M. Espallargas,

L. Brammer, D. R. Allan, C. R. Pulham, N. Robertson, J. E. Warren, *J. Am. Chem. Soc.* **2008**, *130*, 9058.

[11] (a) M. T. McBride, T. -J. M. Luo and G. T. Palmore, *Cryst. Growth Des.* **2001**, *1*, 39; (b) T. -J. M. Luo and G. T. Palmore, *Cryst. Growth Des.* **2002**, *2*, 337.

[12] (a) P. K. Thallupally, A. Nangia, *CrystEngComm* **2001**, *3*, 114; (b) C. B. Aakeröy, T. A. Evans, K. R. Seddon, I. Pálinkó, *New J. Chem.* **1999**, *23*, 145.

[13] R. Taylor, *Cryst. Growth Des.* **2016**, *16*, 4165.

[14] (a) R. C. Johnston, P. H. -Y. Cheong, *Org. Biolmol. Chem.* **2013**, *11*, 5017; (b) V. R. Hathwar, S. M. Roopan, R. Subashini, F. N. Khan, T. N. Guru Row, *J. Chem. Sci.* **2010**, *122*, 677.

[15] (a) O. Hassel, *Nobel Lectures, Chemistry* 1963; Elsevier: Amsterdam, **1972**; (b) O. Hassel, *Science* **1970**, *170*, 497; (c) A. C. Legon, *Phys. Chem. Chem. Phys.* **2010**, *12*, 7736; (d) S. J. Grabowski, *J. Phys. Chem. A* **2011**, *115*, 12340.

[16] (a) D. Chopra, T. N. Guru Row, *Cryst. Growth Des.* **2005**, *5*, 1679; (c) J. Ridout, M. R. Probert, *Cryst. Growth Des.* **2013**, *13*, 1943; (c) R. B. Walsh, C. W. Padgett, P. Metrangolo, G. Resnati, T. W. Hanks, W. T. Pennington, *Cryst. Growth Des.* **2001**, *1*, 165; (d) K. Eichstaedt, A. Wasilewska, B. Wicher, M. Gdaniec, T. Połoński, Cryst. Growth Des. **2016**, *16*, 1282,

[17] (a) P. Auffinger, F. A. Hays, E. Westhof, P. S. Ho, *Proc. Natl. Acad. Sci.* **2004**, *101*, 16789; (b) R. Wilcken, M. O. Zimmermann, A. Lange, A. C. Joerger, F. M. Boeckler, *J. Med. Chem.* **2013**, *56*, 1363; (c) Y. Lu, Y. Wang, W. Zhu, *Phys. Chem. Chem. Phys.* **2010**, *12*, 4543.

[18] (a) L. Brammer, E. A. Bruton, P. Sherwood, *New J. Chem.* **1999**, *23*, 965; (b) G. M. Espallargas, F. Zordan, L. Arroyo Marín, H. Adams, K. Shankland, J. Streek, L. Brammer, *Chem. Eur. J.* **2009**, *15*, 7554; (c) S. Derossi, L. Brammer, C. A. Hunter, M. D. Ward, *Inorg. Chem.* **2009**, *48*, 1667; (d) P. Smart, Á. B. -Villafuerte, L. Brammer, *CrystEngComm.* **2013**, *15*, 3151.

[19] (a) M. C. Pfrunder, A. S. Micallef, L. Rintoul, D. P. Arnold, J. McMurtrie, *Cryst. Growth Des.* **2016**, *16*, 681; (b) B. N. Ghosh, M. Lahtinen, E. Kalenius, P. Mal, K. Rissanen, *Cryst. Growth Des.* **2016**, *16*, 2527.

[20] (a) J. M. C. -Juan, E. Coronado, G. M. Espallargas, H. Adams, L. Brammer, *CrystEngComm.* **2010**, *12*, 2339; (b) F. F. Awwadi, R. D. Willett, B. Twamley, M. M. Turnbull, C. P. Landee, *Cryst. Growth Des.* **2015**, *15*, 3746.

[21] (a) R. -P. Ye, X. Zhang, Y. -Y. Qin, Y. -G. Yao, DOI: 10.1039/c7ce00004a; (b) M. C. Carrión, G. Durá, F. A. Jalón, B. R. Manzano, A. M. Rodríguez, *Cryst. Growth Des.* **2012**, *12*, 1952; (c) R. Banik, S. Roy, Ľ. Dlháň, J. Titiš, R. Boča, A. M. Kirillov, A. D. Martin, A. Bauza, A. Frontera, A. R. -Diéguez, J. M. Salas, S. Das, *Dalton Trans.* **2016**, *45*, 16166; (d) M. Mirzaei, H. E. -Hosseini, Z. Bolouri, Z. Rahmati, A. Esmaeilzadeh, A. Hassanpoor, A. Bauza, P. Ballester, M. B.-Oliver, J. T. Mague, B. Notash, A. Frontera, *Cryst. Growth Des.* **2015**, *15*, 1351.

[22] (a) M. Nishio, Y. Umezawa, H. Suezawa, S. Tsuboyama, *The CH/π Hydrogen Bond: Implication in Crystal Engineering* in *The importance of Pi-interactions in crystal engineering: Frontiers in crystal engineering*, Wiley, **2012**; (b) M. L. Waters, *Curr. Opin. Chem. Biol.* **2002**, *6*, 736.

[23] C. R. Martinez, B. L. Iverson, *Chem. Sci.* **2012**, *3*, 2191; (b) I. Pecsi, I. Leveles, V. Harmat, B. G. Vertessy, J. Toth, *Nucleic Acids Res.* **2010**, *38*, 7179.

[24] A. Mukhopadhyay, V. K. Maka, J. N. Moorthy, *Phys. Chem. Chem. Phys.* **2017**, *19*, 4758.

[25] A. S. Roy, P. Saha, P. Mitra, S. S. Maity, S. Ghosh, P. Ghosh, *Dalton Trans.* **2011**, *40*, 7375.

[26] (a) E. C. Constable, G. Zhang, C. E. Housecroft, M. Neuburger, J. A. Zampese, *Chem. Commun.* **2010**, *46*, 3077; (b) E. C. Constable, G. Zhang, C. E. Housecroft, M. Neuburger, S. Schaffner, *Dalton Trans.* **2009**, 8165.

[27] H. S. Jena, *New J Chem.* **2014**, *38*, 2486.

[28] D. A. Dougherty, Science **1996**, *271*, 163.

[29] (a) M. Cametti, M. Nissinen, A. D. Cort, L. Mandolini, K. Rissanen, *J. Am. Chem. Soc.* **2005**, *127*, 3831; (b) A. Bhattacharyya, A. Bauzá, A. Frontera, S. Chattopadhyay, *Polyhedron* **2016**, *119*, 451.

[30] A. Frontera, P. Gamez, M. Mascal, T. J. Mooibroek, J. Reedijk, *Angew. Chem. Int. Ed.* **2011**, *50*, 9564.

[31] R. Banik, S. Roy, A. M. Kirillov, A. Bauza, A. Frontera, A. R. -Diéguez, J. M. Salas, W. Maniukiewicz, S. K. Das, S. Das, *CrystEngComm.* **2016**, *18*, 5647.

[32] R. Shukla, P. Panini, C. J. McAdam, B. H. Robinson, J. Simpson, T. Tegg, D. Chopra, *J. Mol. Struct*. **2017**, *2*, 494.

[33] G. Mahmoudi, A. Bauzá, A. R. -Diéguez, P. Garczarek, W. Kaminsky, A. Frontera, *CrystEngComm.* **2016**, *18*,102.

[34] E. S. Yandanova, D. M. Ivanov, M. L. Kuznetsov, A. G. Starikov, G. L. Starova, V.Y. Kukushkin, *Cryst. Growth Des.* **2016**, *16*, 2979.

[35] (a) J. P. Stambuli, C. D. Incarvito, M. Bühl, J. F. Hartwi, *J. Am. Chem. Soc.* **2004**, *126*, 1184; (b) W. Baratta, S. Stoccoro, A. Doppiu, E. Herdtweck, A. Zucca, P. Rigo, *Angew. Chem. Int. Ed.* **2003**, *42*, 105.

[36] A. Bauzá, A. Terrón, M. B. -Oliver, A. G. -Raso, A. Frontera, *Inorg. Chim. Acta* **2016**, *452*, 244.

[37] J. J. McKinnon, A. S. Mitchell, M. A. Spackman, *Chem. Eur. J.* **1998**, *4*, 2136.

[38] R. F. W. Bader, Y. Tal, S. G. Anderson, T. T. N. -Dang, *Isr. J. Chem.* **1980**, *19*, 8.

[39] A. E. Reed, L. A. Curtiss, F. Weinhold, *Chem. Rev.* **1988**, *88*, 899.

[40] A. Gavezzotti, *Z. Kristallog.* **2004**, *220*, 499.

[41] (a) Y. Zhan, D. G. Truhlar, *Acc. Chem. Res.* **2008**, *41*, 157; (b) A. Bauzá, I. Alkorta, A. Frontera, J. Elguero, *J. Chem. Theory Comput.* **2013**, *9*, 5201.

[42] (a) A. R. Choudhury, T. N. Guru Row, Cryst. Growth Des. 2004, 4, 47; (b) S. K. Nayak, M. K. Reddy, T. N. Guru Row, D. Chopra, *Cryst. Growth Des.* **2011**, *11*, 157; (c) P. Munshi, K. N. Venugopala, B. S. Jayashree, T. N. Guru Row, *Cryst. Growth Des.* **2004**, *4*, 1105; (d) D. Chopra, K. Nagarajan, T. N. Guru Row, *Cryst. Growth Des.* **2005**, *5*, 1035; (e) T. N. Guru Row, *Coord. Chem. Rev.* **1999**, *183*, 81.

[43] (a) C. B. Aakeröy, *Acta Cryst.* **1997**, *B53*, 569; (b) C. B. Aakeroy, N. R. Champness, C. Janiak, *CrystEngComm.* **2010**, *12*, 22; (c) C. B. Aakeröy, A. M. Beatty, B. A. Helfrich, *Angew. Chem. Int. Ed.* **2001**, *40*, 3240; (c) C. B. Aakeröy, A. M. Beatty, D. S. Leinen, *Angew. Chem. Int. Ed.* **1999**, *38*, 1815; (d) C. B. Aakeröy, J. Desper, B. Leonard, J. F. Urbina, *Cryst. Growth Des.* **2005**, *5*, 865.

[44] (a) A. J. Blake, N. R. Champness, P. Hubberstey, W. -S. Li, M. A. Withersby, M. Schröder, *Coord. Chem. Rev.* **1999**, *183*, 177; (b) L. Brammer, J. C. M. Rivas, R. Atencio, S. Fang, F. C. Pigge, *J. Chem. Soc., Dalton Trans.* **2000**, 3855; (c) L. Brammer, *Chem. Soc. Rev.* **2004**, *33*, 476; (d) L. Brammer, *Dalton Trans.* **2003**, 3145; (e) D. Braga, *J. Chem. Soc., Dalton Trans.* **2000**, 3705; (e) C. B. Aakeröy, A. M. Beatty, D. S. Leinen, K. R. Lorimer, *J. Chem. Soc., Dalton Trans.* **2000**, 3869.

[45] (a) R. Shukla, T. P. Mohan, B. Vishalakshi, D. Chopra, *CrystEngComm.* **2014**, *16*, 1702; (b) Y. -C. Li, C. Qi, S. -H. Li, H. -J. Zhang, C. -H. Sun, Y. -Z. Yu, S. -P. Pang, *J. Am. Chem. Soc.* **2010**, *132*, 12172; (c) P. Panini, T. P. Mohan, U. Gangwar, R. Sankolli, D. Chopra, *CrystEngComm.* **2013**, *15*, 4549.

[46] (a) V. R. Pedireddi, S. D. Reddy, B. S. Goud, D. C. Craig, A. D. Rae, G. R. Desiraju, *J. Chem. Soc. Perkin Trans. 2*, **1994**, 2353; (b) I. Saraogi, V. G. Vijay, S. Das, K. Sekar, T. N. Guru Row, *Crystallogr. Eng.* **2003**, *6*, 69; (c) G. Kaur, P. Panini, D. Chopra, A. R. Choudhury, *Cryst. Growth Des.* **2012**, *12*, 5096; (d) P. Du, X. K. Jiang, Z. -T. Li, *Tetrahedron Lett.* **2009**, *50*, 316; (e) J. -L. Hou, X. -B. Shao, G. J. Chen, Y. X. Zhou, X. K. Jiang, Z. -T. Li, *J. Am. Chem. Soc.* **2004**, *126*, 12386.

[47] (a) N. Galić, B. Perić, B. K. -Prodić, Z. Cimerman, *J. Mol. Struct.* **2001**, *559*, 187; (b) X. Zhao, X. -Z. Wang, X. -K. Jiang, Y. -Q. Chen, Z. -T. Li, G. -J. Chen, *J. Am. Chem. Soc.* **2003**, *125*, 15128; (c) D. -W. Zhang, X. Zhao, J. -L. Hou, Z. -T. Li, *Chem. Rev.* **2012**, *112*, 5271; (d) W. -J. Chu, J. Chen, C. -F. Chen, Y. Yang, Z. Shuai, *J. Org. Chem.* **2012**, *77*, 7815.

Literature Review Part A

1. 2. Literature review part A describes a concise literature survey on reactivity of nitrile functional (C≡N) group. The nitrile functional group due to its polar nature ($^{+}_{C}{=}{=}{=}\bar{N}$) acts both as a nucleophile[1] and electrophile.[2] Various addition reactions across nitrile functional group have also been reported earlier.[3] The nitrile functional group has been extensively employed to synthesise heterocycles including triazoles, oxazoles, pyridimine, pyrazine, pyridine and isoquinoline.[4] It is pertinent to mention in this regard that N-heterocyclic nitriles especially 2-cyanopyridine is worthy to mentioned due to its wide application to prepare heterocycles.

The nucleophilic nature of nitrile functional group is reportedly less pronounced inc comparison to the electrophilic behaviour. However, the nitrile functional group acts as a nuclophile in presence of strong Lewis acids *e.g.* $SbCl_5$,[5] CF_3SO_3H[6] and mercuric nitrate.[7]

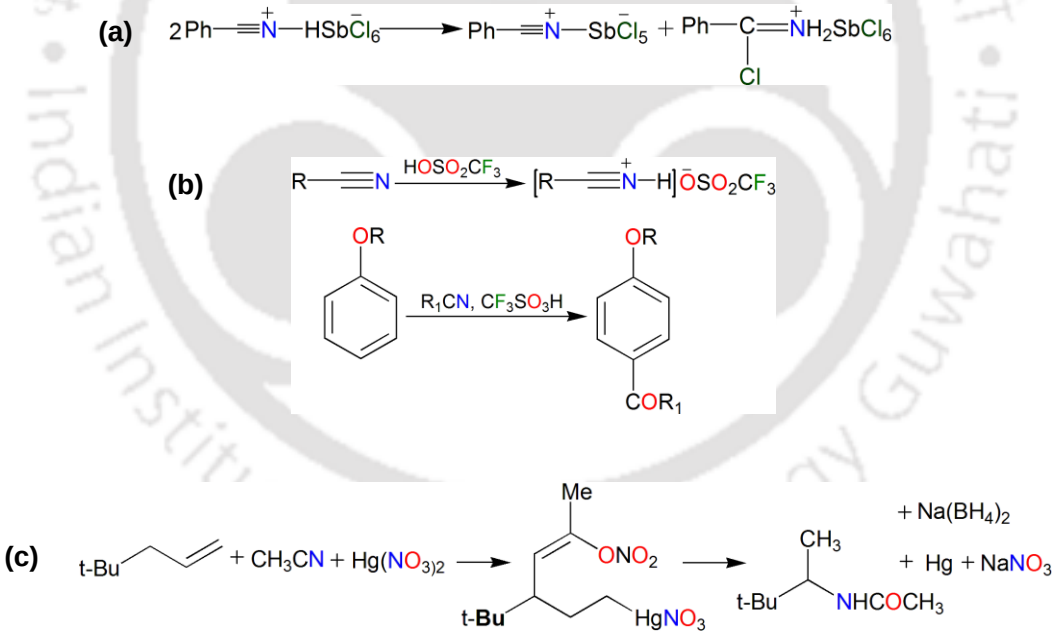

Scheme 1. (a) Reaction of nitrile group with $SbCl_5$;[5] (b) Reaction of nitrile group with $HOSO_2CF_3$;[6] (c) Reaction of nitrile group with mercuric chloride.[7]

The addition reactions across nitrile functional group have been explored long back and classical Pinner reaction[8] should be mentioned in this regard. In recent years, transition metal ion catalyzed addition reactions of nitrile functional group have gained attention. The metal ions such as Ni(II)/Cu(II)[9] and Pd(II)[10] have been used as catalysts. Cyclo-addition

reaction between nitrile group and silanes to result in penta substituted pyridines has been reported by Konakahara *et al*.[11]

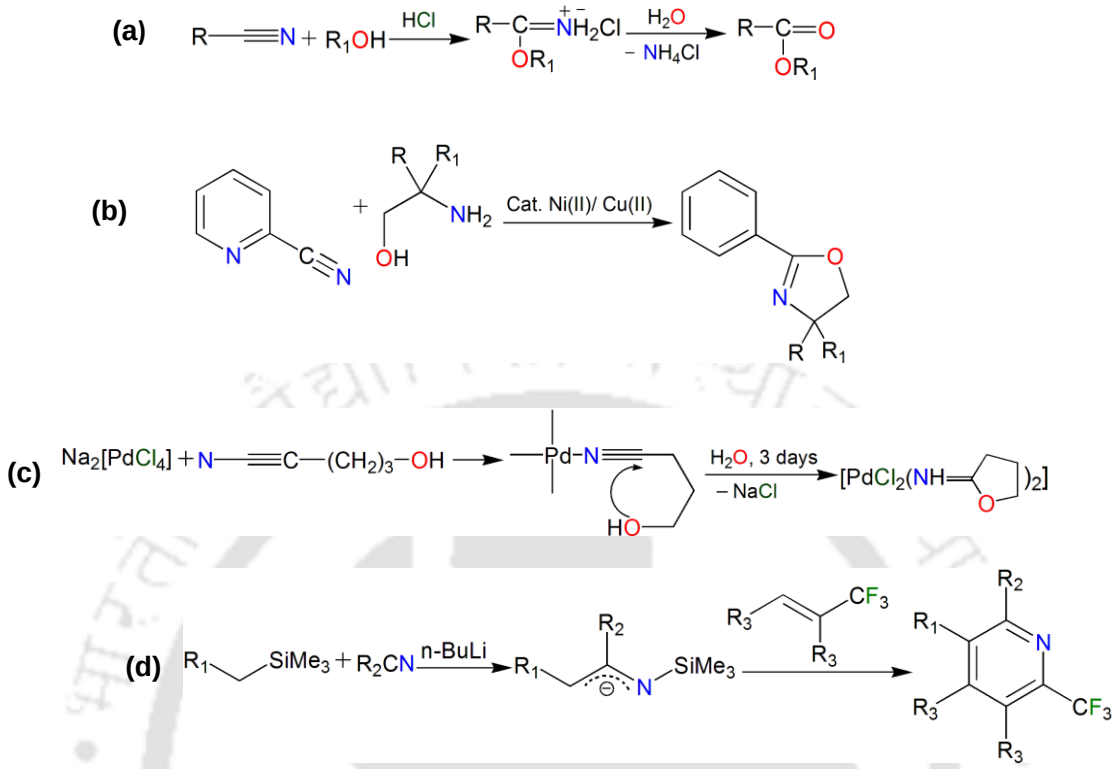

Scheme 2. (a) Classical Pinner reaction;[8] (b) Ni(II)/Cu(II) catalyzed addition reaction;[9] (c) Pd(II) catalyzed addition reaction;[10] (d) Cyclo-addition reaction between nitrile group and trimethyl silanes.[11]

The electrophilic nature of nitrile group is more profound than its nucleophilic nature and this has been extensively exploited to synthesise various heterocycles. The reaction between nitrile group and ethylenediamine under different conditions produces imidazoline[12] and imidazoles.[13] Similarly the reaction between 2-cyanopyridine and aromatic aldehydes in the presence of primary amine or ammonium acetate results in the formation of poly substituted 2-(2′-pyridyl)imidazoles.[14]

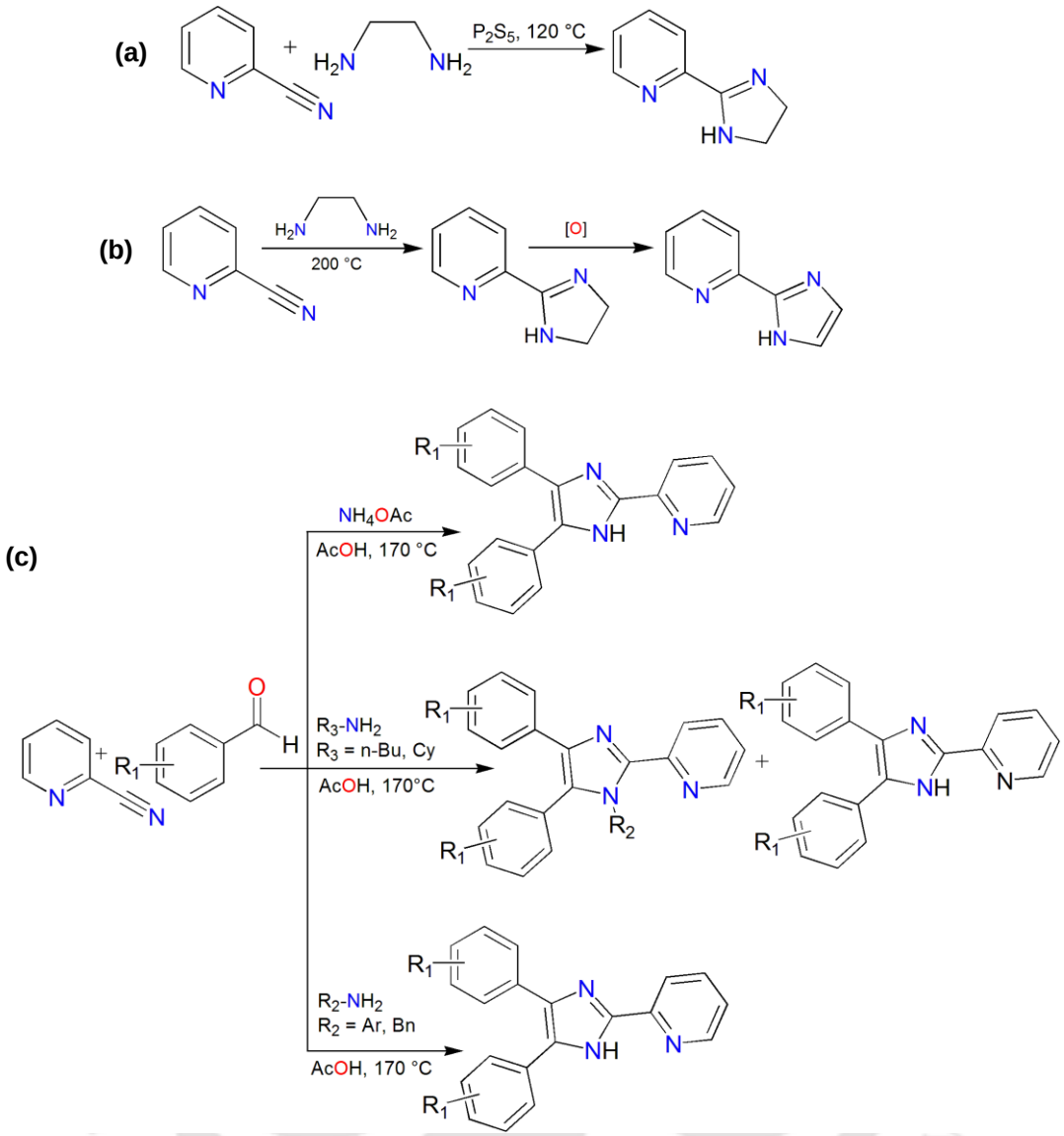

Scheme 3. (a) Synthesis of imidazoline;[12] (b) Synthesis of imidazole;[13] (c) Synthesis of tri substituted imidazole.[14]

The closely analogous hydrazide functional group is known to be reactive towards nitriles and the reactions between them have employed to prepare various heterocycles.[4] Geldard *et al* first prepared 1,2,4-triazole by the reaction between 2-cyanopyridine and hydrazine followed by deamination by nitrous acid.[4,15]

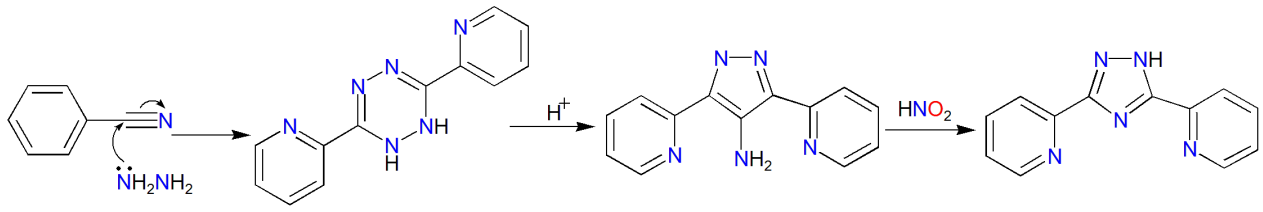

Scheme 4. Synthesis of 1,2,4-triazole the reaction of 2-cyanopyridine and hydrazine.[15]

An array of symmetrically 3,5-disubstituted 4-amino-1,2,4-triazoles including 3,5-di(2′-pyridyl)-4-amino-1,2,4-triazole have been reportedly synthesized by the reaction of aromatic nitriles with hydrazine hydrochloride in the presence of excess amount of hydrazine hydrate in ethylene glycol medium under microwave irradiation.[16] It has been reported that the reaction of hydrazine with 2-cyanopyrine followed by acidification by formic acid produces 3-(2′-pyridyl)-1,2,4-triazole.[17]

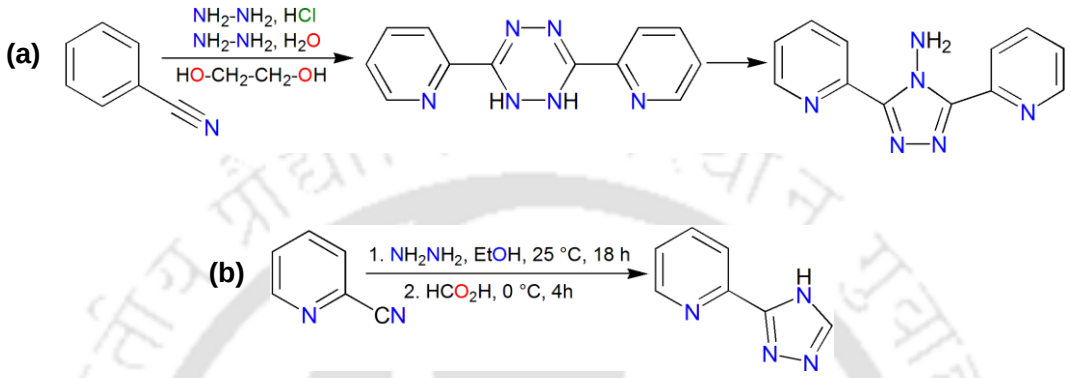

Scheme 5. Synthesis of 1,2,4-triazole under different conditions, (a);[16] (b).[17]

The 1,2,4-oxadiazole scaffold is found in many biologically active molecules and 5-(3′-cyanophenyl)-3-(2″-pyridyl)-1,2,4-oxadiazole is remarkable among them for its wide application as metabiotropic glutamate subtype 5 (mGlu 5) receptor antagonist. This compound has been reportedly synthesised by reacting 2-cyanopyridine with hydroxylamine which produces amidoxime. This amidoxime reacts with substituted acyl chloride to result in *o*-acyl amidoxime which undergoes intramolecular cyclisation to produce 1,2,4-oxadiazole.[18]

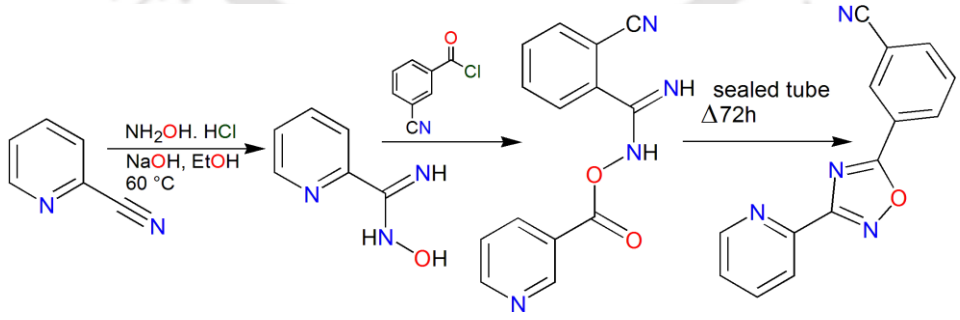

Scheme 6. Synthesis of 1,2,4-oxadiazole.[18]

Shintou *et al* reported that the reaction of 2-cyanopyridine with hydrazine hydrate yields 3-(2′-pyridyl)-amidohydrazone which further reacts with glyoxal to produce 3-(2′-

pyridyl)-1,2,4-triazine.[19] The reaction of 2-cyanopyridine and *o*-aminobenzhydrazide in presence of potassium carbonate results in the formation of 3,5-dipyridyl-1,2,4-triazole.[20]

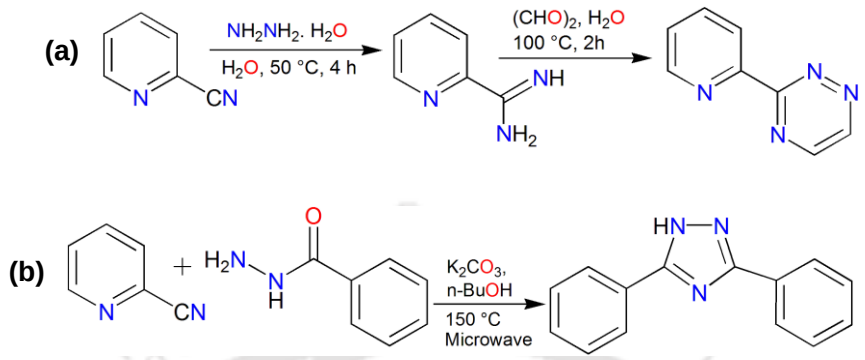

Scheme 7. (a) Synthesis of 1,2,4-triazine;[19] (b) Synthesis of 3,5-dipyridyl-1,2,4-triazole.[20]

The reaction of 2-cyanopyridine and hydrazine in presence of 2-phenyl glyoxal produces pyridyl substituted 1,2,4-triazine which upon reaction with 4-ethynyltoluene in *o*-dichlorobenzene medium forms substituted 2,2′-bipyridyls.[21]

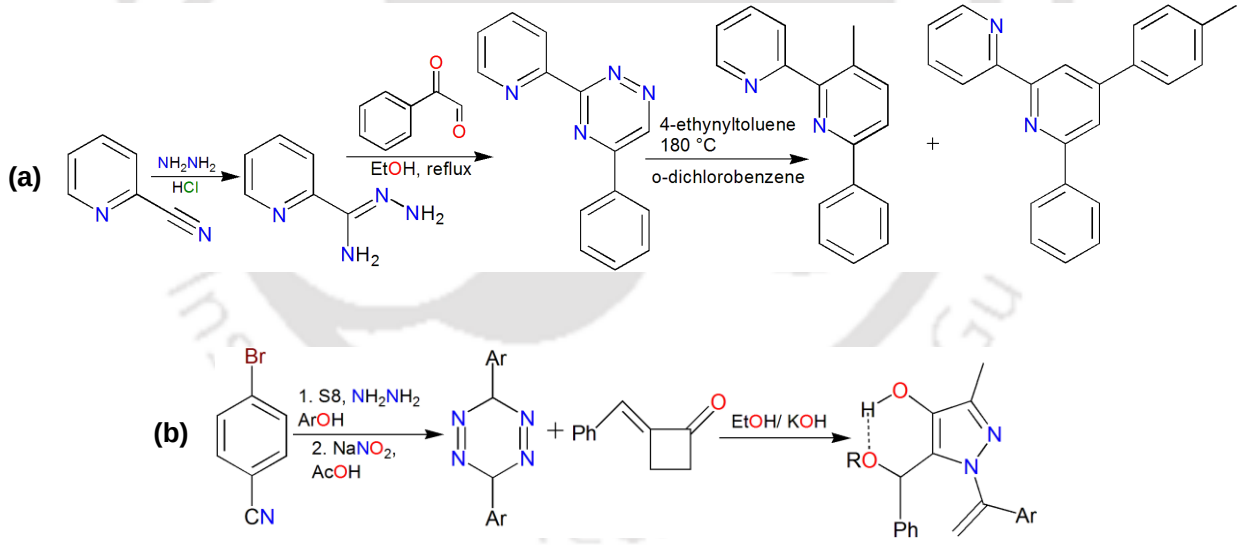

Scheme 8. (a) Synthesis of poly substituted 2,2′-bipyridine;[21] (b) Synthesis of substituted pyrazole. [22]

The reaction of *p*-bromo benzonitrile in presence of sulfur dissolved in aromatic alcohols and sodium nitrite resulted in the formation of 3,6-disubstitued dihydrotetrazine. This dihydrotetrazine further reacts with a functonalised cyclobutanone (thietanone) to produce fully substituted pyrazole.[22]

Reference

[1] (a) R. L. Elliott, R. M. Oliver, J. A. Laflamme, M. L. Gillaspy, M. Hammond, R. F. Hank, T. S. Maurer, D. L. Baker, P. A. DaSilva, R. W. Stevenson, C. M. Mack, J. V. Cassella, *Bioorg. Med. Chem. Lett*. **2003**, *13*, 3593; (b) A. S. Kiselyov, *Tetrahedron Lett*. **2005**, *46*. 1663.

[2] I. D. Gridnev, N. A. Gridneva, *Russ. Chem. Rev.* **1995**, *64*, 1091.

[3] (a) V. Y. Kukushkin, A. J. L. Pombeiro, *Chem. Rev*. **2002**, *102*, 1771; (b) Z. P. Demko, K. B. Sharpless, *J. Org. Chem*. **2001**, *66*, 7945.

[4] (a) J. -P. Zhang, Y. -Y. Lin, X. -C. Huang, X. -M. Chen, *J. Am. Chem. Soc.* **2005**, *127*, 5495; (b) R. L. Elliott, R. M. Oliver, J. A. Laflamme, M. L. Gillaspy, M. Hammond, R. F. Hank, T. S. Mauer, D. L. Baker, P. A. DaSilva-jardine, R. W. Stevenson, C. M. Mack, J. V. Cassella, *Bioorg. Med. Chem. Lett.* **2003**, *13*, 3593; (c) A. S. Kiselyov, Tetrahedron Lett. **2005**, *46*, 1663; (d) M. A. H. De Zwart, H. V. Goot, H. Timmerman, *J. Med. Chem.* **1998**, *32*, 487.

[5] (a) E. Allenstein, A. Schmidt, *Spectrochim. Acta* **1964**, *20*, 1451; (b) F. Klages, W. Grill, *Liebigs Ann. Chem*. **1955**, *594*, 21.

[6] B. L. Booth, G. F. Noori, *J. Chem. Soc., Perkin Trans.* **1980**, *1*, 2894.

[7] H. C. Brown, J. T. Kurek, *J. Am. Chem. Soc*. **1969**, *91*, 5647.

[8] (a) P. J. Dunn, In *Comprehensive Organic Functional Group Transformations*; A. R. Katrizky, O. Meth-Cohn, C. W. Rees, Eds. Elsevier: Oxford, **1995**, Vol. *5*, pp 741; (b) S. K. Sharma, M. Tandon, J. W. Lown, *J. Org. Chem*. **2001**, *66*, 1030.

[9] (a) D. Miklos, P. Segl'a, T. Glowiak, *Inorg. Chem. Commun*. **2001**, *4*, 66. (b) P. Segl'a, M. Koman, T. Glowiak, *J. Coord. Chem*. **2000**, *50*, 105; (c) P. Segl'a, M. Jamnicky, M. Koman, T. Glowiak, *Polyhedron* **1998**, *17*, 2765.

[10] N. V. Kaminskaia, I. A. Guzei, N. M. Kostic, *J. Chem. Soc., Dalton Trans*. **1998**, 3879.

[11] H. Suzuki, N. Sakai, R. Iwahara, T. Fujiwaka, M. Satoh, A. Kakechi, T. Konakahara, *J. Org. Chem.* **2007**, *72*, 5878.

[12] M. Anastassiadou, S. Danoun, L. Crane, G. B. Mouysset, M. Payard, D. -H. Rettori, P. Renard, *Bioorg. Med. Chem*. **2001**, *9*, 985.

[13] M. E. Voss, C. M. Beer, S. A. Mitchell, P. A. Blomgren, P. E. Zhickin, *Tetrahedon*, **2007**, *64*, 645.

[14] X. J. Wu, R. Jiang, X. P. Xu, X. M. Su, S. J. Ji, *J. Comb. Chem*. **2010**, *12*, 829.

[15] J. F. Geldard, F. Lions, *J. Org. Chem*. **1965**, *30*, 318.

[16] F. Bentiss, M. Lagrené, D. Barbry, *Tetrahedron Lett*. **2000**, *41*, 1539.

[17] J. Roppe, n. D. Smith, D. Huang, L. Tehrani, B. Wang, J. Anderson, J. Brodkin, J. Chung, X. Jiang, C. King, B. Munoz, M. A. Varney, P. Prasit, N. D. P. Cosford, *J. Med. Chem*. **2004**, *47*, 4645.

[18] D. Grant, R. Dahl, N. D. P. Cosford, *J. Org. Chem.* **2008**, *73*, 7219.

[19] T. Shintou, F. Ikeuchi, H. Kuwabara, K. Umihara, I. Itoh, *Chem. Lett.* **2005**, *34*, 836.

[20] K.S. Yeung, M. E. Farkas, J. F. Kadow, N. A. Meanwel, *Tetrahedron Lett.* **2005**, *46*, 3429.

[21] S. Diring, P. Retailleau, R. Ziesse, *Tetrahedron Lett.* **2007**, *48*, 8069.

[22] Y. F. Suen, H. Hope, M. H. Nantz, M. J. Haddadin, M. J. Kurth, *J. Org. Chem.* **2005**, *70*, 8468.

Literature Review Part B

1. 3. This section describes the chemistry of metal complexes of aroylhydrazones. Aroylhydrazone (Ar−C(=O)NH−N=C−) moiety represents a versatile coordination chemistry as a NO donor ligand.[1] Different heterocyclic *e.g.* pyridyl, pyrazinyl, imidazolyl, thiophenyl and substituted aromatic such that phenolic substitutions to the aroylhydrazone moiety also provide extra coordination sites. This group of ligands is widely known for the prolific biological activity of their metal complexes, catalytic activity and variable coordination modes.

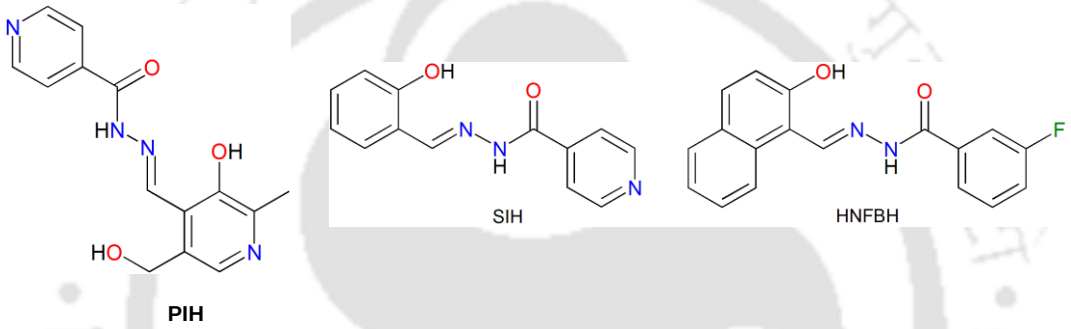

Scheme 1. Iron(III) chelator drug pyridoxal isonicotinyl hydrazone (PIH), salicylaldehyde isonicotinyl hydrazone (SIH) and 2-hydroxy-1-napthaldehyde *m*-fluorobenzoyl hydrazone (HNFBH). [2-3]

The most significant biological application of aroylhydrazone ligands is their use as Fe(III) chelators. Dietary iron restriction in tumor cells is a method to prevent the growth of tumor cell as Fe(III) helps in proliferation of cell. Pyridoxal isonicotinyl hydrazone (PIH) is one of the clinically proven drugs for iron chelation due to its low toxicity in *in vitro* cells (Scheme 1).[2] In addition, few aroylhydrazone based Fe(III) chelators *e. g.* salicylaldehyde isonicotinyl hydrazone (SIH) and 2-hydroxy-1-napthaldehyde *m*-fluorobenzoyl hydrazone (HNFBH) are reported to possess satisfactory anti-malarial activity.[3] Many other structurally similar aroylhydrazone ligands are also under the clinical trial including 311, 311m and N44pH (Scheme 2).[4,5]

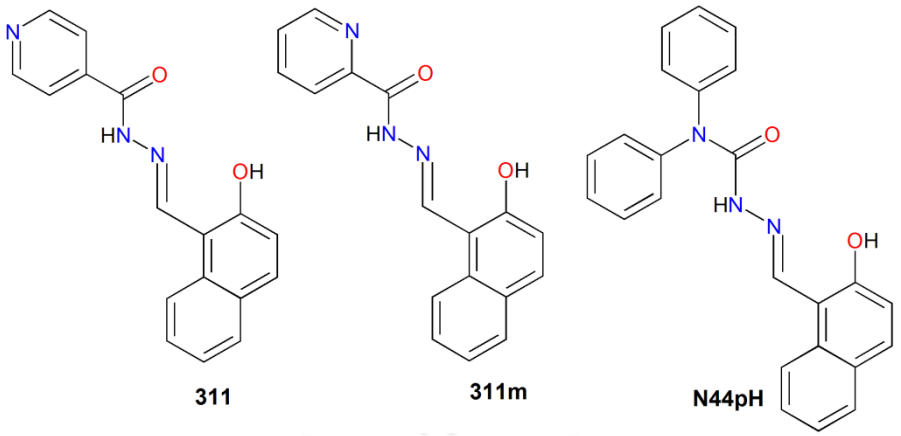

Scheme 2. (a) Few aroylhydrazone ligands under clinical trial as potential Fe(III) chelators;[3,4] (b) Sn(II) complex of aroylhydrazone ligand showing anti microbacterial activity.[5]

Pelizzi *et al* reported a Sn(IV) complex of di-2-pyridylketone-2-aminobenzoylhydrazone (Hdpa) showing high anti-bacterial property.[6] The MoO_2 complex of benzoylhydrazone of salicylaldehyde exhibits enhanced activity against Gram negative bacteria.[7] A vanadium (V) complex of aroylhydrazone based ligand N′-(2-hydroxy-4-methoxybenzylidene)-4-hydroxybenzhydrazide was reported by Zhao *et al*.[8] This complex is known to reduce blood glucose level for diabetic mice and currently under clinical trial (Scheme 3).

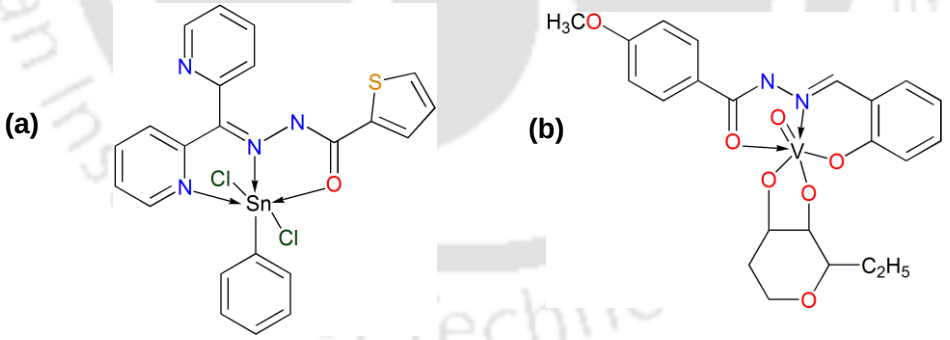

Scheme 3. (a) Sn(IV) complex of aroylhydrazone showing anti-bacterial property;[6] (b) VO complex of aroylhydrazone which can reduce blood glucose level.[8]

The substituted aroylhydrazone ligands often offer unusual higher coordination number to coordinated metal ions depending on the nature of substituents hydrazone moiety and suitable co-ligands. Chattopadhyay *et al* reported rare seven coordinated Mn(II) complex with a hydrazone based ligand.[9] The metal complex behaves as a one dimensional anti ferromagnetic chain through bridging amino group which results in the *hepta* coordination of

the Mn(II) center. In this regard, the μ-1,1-azido bridged dinuclear Mn(II) complex of (*E*)-N′-(phenyl)(pyridine-2-yl)methylene)furan-2-carbohydrazide ligand should be mentioned for the high anti ferromagnetic coupling between Mn(II) centers (Scheme 4).[10]

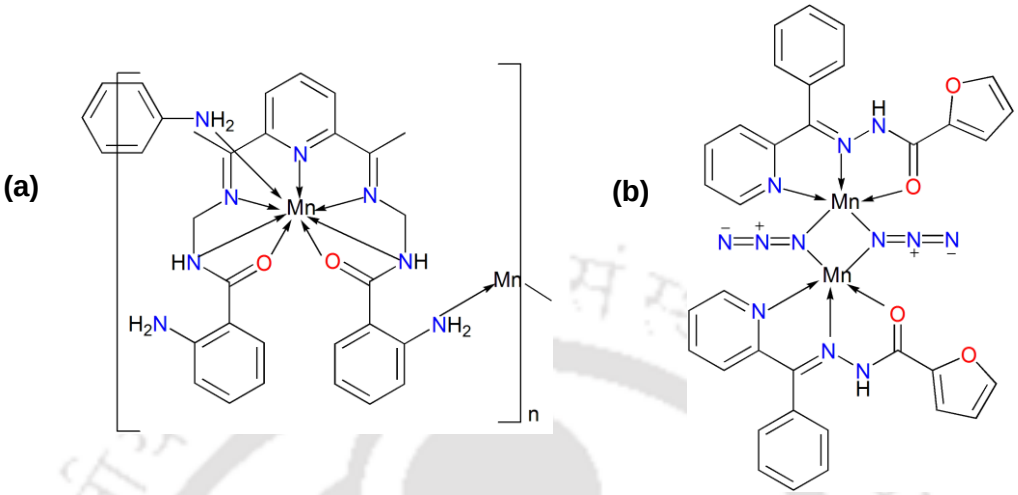

Scheme 4. Polynuclear Mn(II) complexes of aroyhydrazone ligands showing anti ferromagnetic coupling of Mn(II) centers, (a);[9] (b).[10]

Lanthanide metal complexes of aroylhydrazone ligands were reported earlier by Yang *et al* (Ln = Eu) and Yongxiang *et al* (Ln = La, Yb).[11] In recent time, lanthanide complexes of aroylhydrazone ligands have received much attraction for their magnetic properties and potential use as single molecule magnets (SMMs). Chandrashekhar *et al* reported a series of $Mn^{II}_2Ln^{III}_4$ (Ln = Gd, Tb, Dy, Ho) complex among which the Tb complex shows strong ferromagnetic coupling.[12] Single molecule magnet behaviour of a trinuclear lanthanide (Dy) complex of an aroylhydrazone ligand has been reported by Thompson et al.[13]

Aroylhydrazone ligands with aromatic substitution often exhibit interesting photo-physical property upon metal ion coordination. Cariati *et al* reported dinuclear Cu(II) and Pd(II) complexes of tridentate N-salicylidene-N′-aroylhydrazone ligands exhibit strong emission near infrared region (NIR).[14] Aroylhydrazone based ligands (*E*)-*N*′-(2,3-dihydroxybenzylidene)-4-hydroxybenzhydrazide and (*E*)-N′-(3,5-di-tert-butylsalicylidene)-2-benzoylhydrazine have been reportedly used for the selective Zn(II) sensing (Scheme 5). This ligand shows high selectivity for Zn^{2+} ions in presence of similar M^{2+} ions (M = Cd, Ca, Mg).[15]

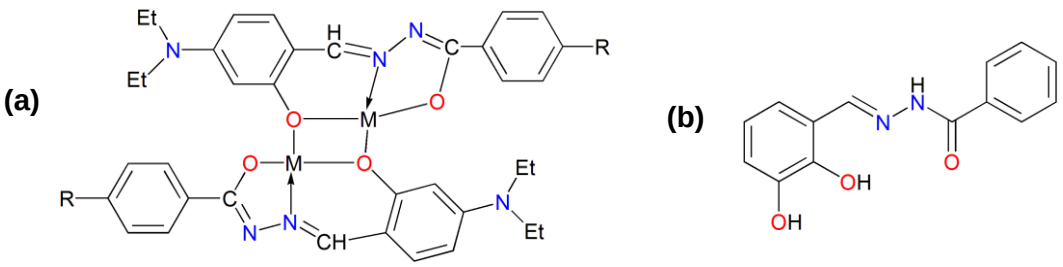

Scheme 5. (a) Metal complexes (M = Cu, Pd) of aroyhydrazone ligands showing emission at NIR region (R = NO_2, −CH=CH−NO_2);[12] (b) Aroylhydrazone ligand used for Zn^{2+} sensing.[13]

Transition metal complexes of aroylhydrazonamide ligands often exhibit remarkable catalytic activity. The Fe(III) complex (**1**) of (*E*)-N′-(2-hydroxy-3-methoxybenzylidene)benzohydrazide ligand promotes epoxidation of olefins using tertiary butyl peroxide as the oxidant and imidazole as co-catalyst.[16] This catalytic reaction is reported to exhibit wide substituent divergence which includes aliphatic, alicyclic as well as allylic double bonds (Scheme 6). Dinda *et al* reported a MoO_2 complex (**2**) of salicylhydrazone of 2-hydroxy-1-naphthaldehyde, which aids high product selectivity in the oxidation of benzoin using hydrogen peroxide.[17] The introduction of MoO_2 complex results in nearly 75% product selectivity of oxidation product benzil. This complex also helps to achieve high product selectivity in the oxidative bromination reaction of salicaldehyde and the mono brominated product is obtained in more than 65% selectivity (Scheme 7).

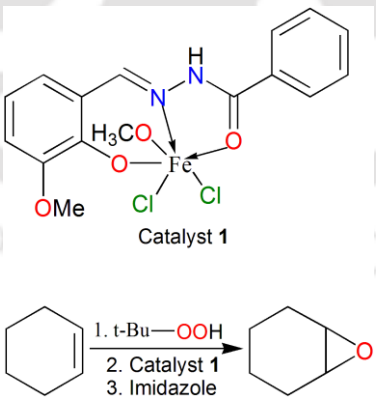

Scheme 6. Fe(III) complex of aroylhydrazone showing catalytic activity towards epoxidation of alkenes.[14]

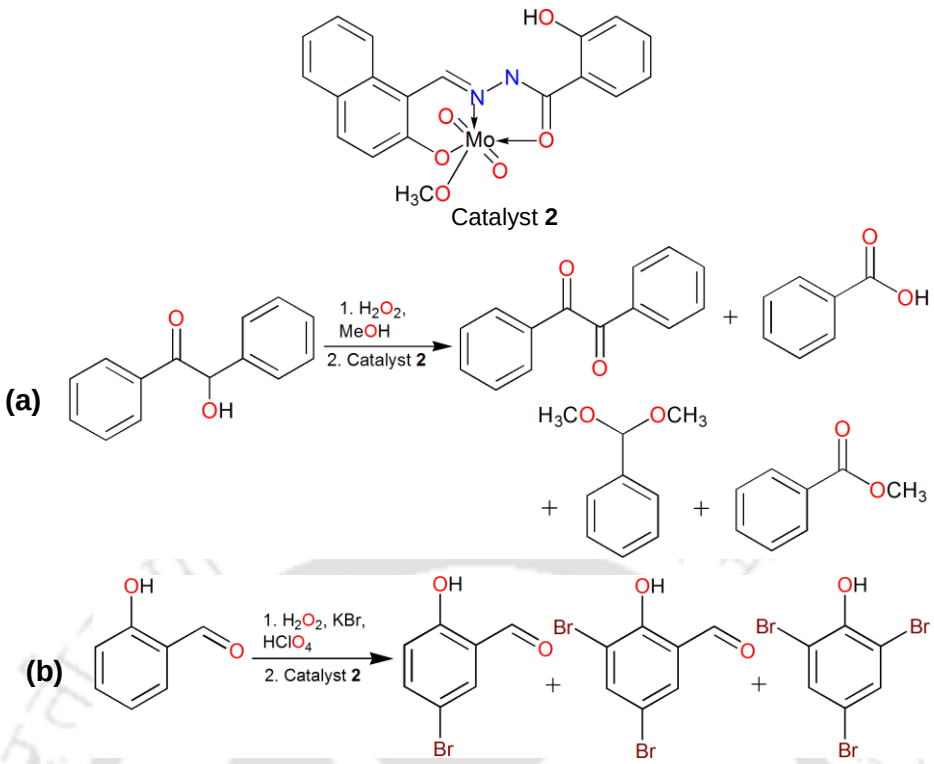

Scheme 7. MoO_2 complex of aroylhydrazone ligand showing catalytic activity in oxidation.[15]

One of the intriguing features of aroylhydrazone system is that it can undergo keto-enol tautomerism. The aroylhydrazonamide ligand system has often exhibit metal ion induced tautomerism which is otherwise rarely observed. Monfared *et al* reported a Cu(II) promoted keto-enol tautomerism in 2-acetylpyridine-3-hydroxy-2-naphthoylhydrazone ligand system.[18] The free ligand exists as a mixture of keto and enol tautomers as revealed by ^{1}H NMR spectroscopy. The Cu(II) coordination stabilizes the deprotonated keto form over enol form via intramolecular hydrogen bonding.

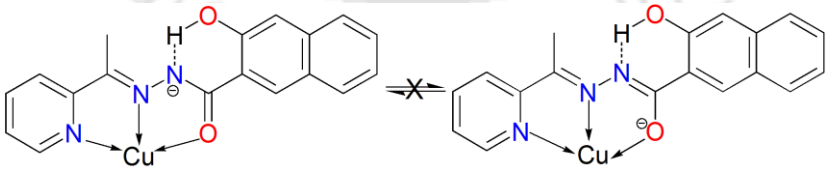

Scheme 8. Cu(II) coordination dictated keto-enol tautomerism in 2-acetylpyridine-3-hydroxy-2-naphthoylhydrazone ligand system.[16]

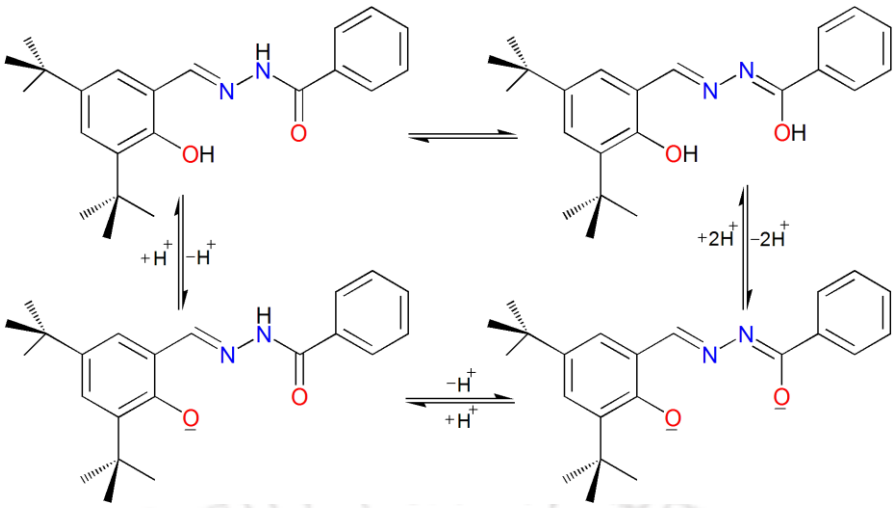

Scheme 9. Keto-enol tautomerism in iron(III) chelator H_2-(3,5-^{t}Bu$_2$).[19]

An interesting case of keto-enol tautomerism in aroylhydrazonamide system is reported by Matoga *et al* in potential Fe(III) chelator drug 3,5-di-tert-butylsalicylidene benzolhydrazine [H_2-(3,5-^{t}Bu$_2$)]. In this case both Fe(III) coordination and pH of the reaction medium dictate keto-enol tautomerism.[19] Likewise, metal ion coordination dictated conformation change around −C=N− is another intriguing feature of aroylhydrazone ligand. Angelusiu *et al* reported a aroylhydrazone ligand system wherein both keto-enol tautomerism and conformation change around −C=N− bond can take place.[20] The ^{1}H NMR spectrum of the ligand indicates the simultaneous presence of amido and imino form in the solution. However, only the amido form (conformation form I) gets stabilized during coordination with Ni^{2+}/Cu^{2+}.

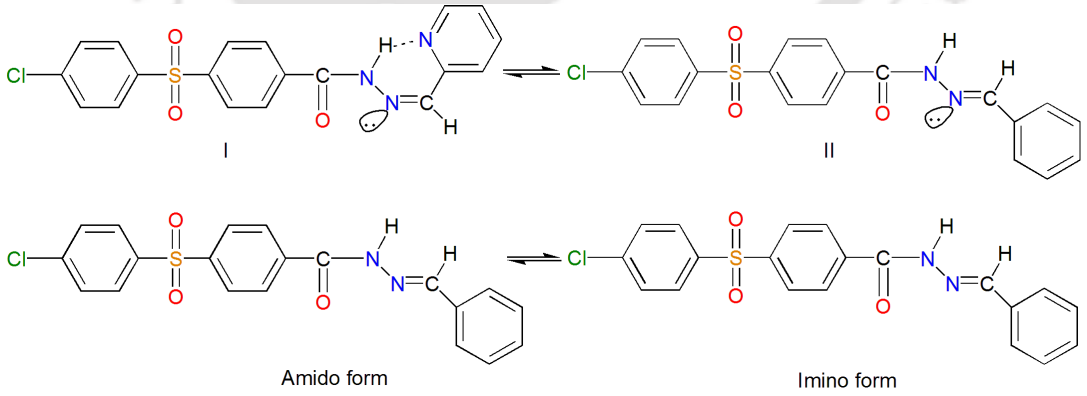

Scheme 10. Keto-enol tautomerism and conformation change around −C=N− bond in N-(2-pyridinecarboxyaldehyde)-N′-[4-(4-chloro-phenylsulfonyl) benzoyl] hydrazone system.[20]

Metal complexes of aroylhydrazone ligands often exhibit interesting supramolecular features. Yang *et al* reported interesting hydrogen bonding pattern in the Cu(II) complex of N3-salicyloylpyridine-2-carboxamidrazone, including the presence of an intraligand hydrogen bond.[21] Mahmoudi *et al* a series of Pb(II) complexes of the ligand N′-(phenyl(pyridin-2-yl)methylene)isonicotinohydrazide is worthy to be mentioned in this regard (Scheme 11).[22] Theses complexes first showcase the simultaneous presence agostic interaction and a tetrel bond involving the heaviest tetrel atom (Pb).

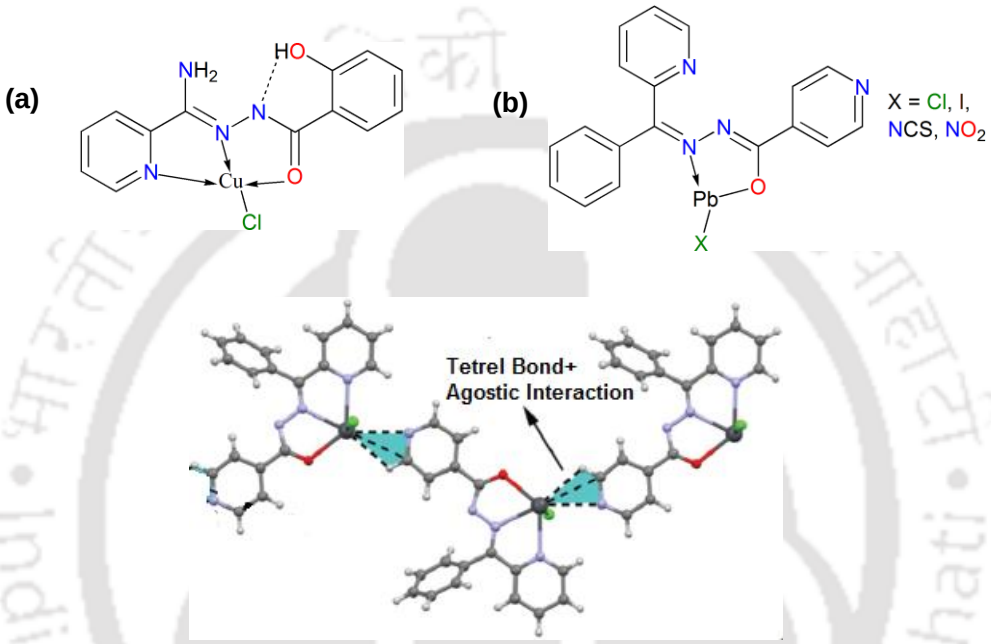

Scheme 11. (a) Cu(II) complex of aroylhydrazone showing interesting hydrogen bonding pattern;[21] (b) Pb(II) complex of N′-(phenyl(pyridin-2-yl)methylene)isonicotinohydrazide exhibiting tetrel bond and agnostic interactions;[22] (c) Agostic interaction and tetrel bond in the Pb(II) complex of *N*′-(phenyl(pyridin-2-yl)methylene)isonicotinohydrazide.[22]

References

[1] (a) M. Carcelli, G. Corazzari, S. Ianelli, G. Pelizzi, C. Solinas, *Inorg. Chim. Acta* **2003**, *353*, 310; (b) A. Bacchi, M. Carcelli, G. Pelizzi, C. Solinas, L. Sorace, *Inorg. Chim. Acta* **2006**, *359*, 2275; (c) C. Carini, G. Pelizzi, P. Tarasconi, C. Pelizzi, K. C. Molloy, P. C. Waterfield, *J. Chem. Soc., Dalton Trans.* **1989**, 289.

[2] D. R. Richardson, *Crit. Rev. Oncol. Hematol.* **2002**, *42*, 267.

[3] D. R. Richardson, K. Milnes, *Blood* **1997**, *89*, 3025.

[4] A. Walcourt, M. Loyevsky, D. B. Lovejoy, V. R. Gordeuk, D. R. Richardson, *Int. J. Biochem. Cell Biol.* **2004**, *36*, 401.

[5] D. B. Lovejoy, D. R. Richardson, *Blood* **2002**, *100*, 666.

[6] M. Carcelli, C. Pelizzi, G. Pelizzi, P. Mazza, F. Zani, *J. Organometal. Chem.* **1995**, *488*, 55.

[7] S. Pasayat, S. P. Dash, P. K. Majhi, Y. P. Patil, M. Nethaji, H. R. Dash, S. Das, R. Dinda, *Polyhedron* **2012**, *38*, 198.

[8] X. Zhao, X. Chen, J. Li, J. Chen, G. Sheng, F. Niu, D. Qu, Y. Huo, H. Zhu, Z. You, *Polyhedron* **2015**, *97*, 268.

[9] S. Naskar, D. Misshra, S. K. Chattopadhyay, M. Corbella, A. J. Blake, *Dalton Trans.* **2005**, 2428.

[10] H. H. -Monfared, R. Bikas, J. Sanchiz, T. Lis, M. Siczek, J. Tucek, R. Zboril, P. Meyer, *Polyhedron* **2013**, *61*, 45.

[11] (a) Z. -Y. Yang, R. -D. Yang, F. -S. Li, K. -B. Yu, *Polyhedron* **2000**, *19*, 2599; (b) M. Yongxiang, M. Zhongquian, Z. Gang, *Polyhedron*, **1989**, *8*, 2105.

[12] A. Chakraborty, P. Bag, J. Goura, A. K. Bar, J. -P. Sutter, V. Chandrasekhar, *Cryst. Growth Des.* **2015**, *15*, 848.

[13] M. U. Anwar, S. S. Tandon, L. N. Dawe, F. Habib, M. Murugesu, L. K. Thompson, *Inorg. Chem.* **2012**, *51*, 1028.

[14] (a) F. Cariati, U. Caruso, R. Centore, W. Marcolli, A. D. Maria, B. Panunzi, A. Raviello, A. Tuzi, *Inorg. Chem.* **2002**, *41*, 6597; (b) X. Peng, X. Tang, W. Qin, W. Dou, Y. Guo, J. Zheng, W. Liu, D. Wang, *Dalton Trans.* **2011**, *40*, 5271.

[15] B. Tang, H. Ma, G. Li, Y. Wang, G. Anwar, R. Shi, H. Li, *CrystEngComm* **2013**, *15*, 8069.

[16] H. H. Monafared, S. Sadighian, M. -A. Kamyabi, P. Meyer, *J. Mol. Cat. A* **2009**, *304*, 139.

[17] S. Pasayat, S. P. Dash, S. Roy, R. Dinda, S. Dhaka, M. R. Maurya, W. Kaminsky, Y. P. Patil, M. Nethaji, *Polyhedron* **2014**, *67*, 1.

[18] H. H. Monfared, H. Falakian, R. Bikas, P. Meyer, *Inorg. Chim. Acta* **2013**, *394*, 526.

[19] D. Matoga, J. Szlarzewicz, K. Stadnicka, M. S. Shongwe, *Inorg. Chem.* **2007**, *46*, 9042.

[20] M. V. Angelusiu, S. F. Barbuceanu, C. Dragchici, G. L. Almajan, *Eur. J. Med. Chem.* **2010**, *45*, 2055.

[21] S. -P. Xu, F. -L. Yang, G. -Z. Zhu, H. -L. Shi, X. -L. Li, *Polyhedron* **2014**, *68*, 1.

[22] G. Mahmoudi, A. Bauzá, A. Frontera, *Dalton Trans.* **2016**, *45*, 4965.

Chapter 2

Metal Ion Directed Tautomeric Polymorphism in a Hydrazonamide/ Hydrozonate System

Molecular structures of transition metal complexes of *ortho* and *para*-aminophenyl substituted hydrazonamide ligands *viz.* 2-amino-benzoic acid (amino-pyridin-2-yl-methylene)-hydrazide and 4-amino-benzoic acid (amino-pyridin-2-yl-methylene)-hydrazide) have been described herein. The ligands can exist in two tautomeric forms *viz.* hydrazonamide and hydrazonic acid via keto-enol tautomerism and the hydrazonamide form is only observed in free form of the ligands. The hydrazonamide form of the former ligand has a six membered intramolecular hydrogen bond between *o*-amino group and amide oxygen (O_A) as evident from the crystal structure. This ligand binds to Co^{3+} and Cu^{2+} centers in the conjugate base of hydrazonic acid (hydrozonate form), while it binds as a neutral molecule to Ni^{2+}, Zn^{2+} and Cd^{2+} in its hydrazonamide form. The *ortho* amino group remains intramolecularly hydrogen bonded to the imino nitrogen (N_I) of hydrazide moiety forming a six membered ring in the anionic hydrazonate form. Hydrazonamide versus hydrazonate tautomerism and consequent conformational change observed in metal complexes of 2-amino-benzoic acid (amino-pyridin-2-yl-methylene)-hydrazide is well supported by both DFT and NBO studies.

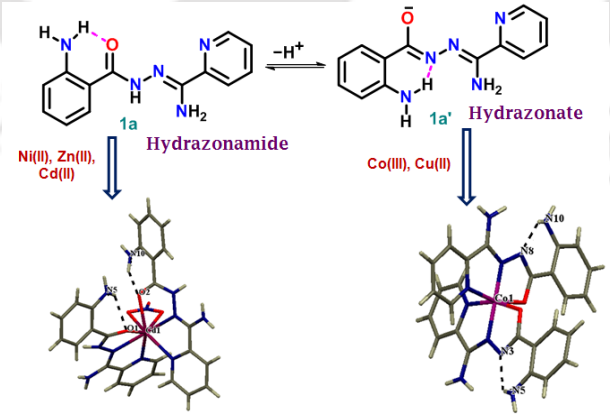

This work has been published in *ChemistrySelect* **2017**, *2*, 494-503.

2.1. Introduction

Tautomers of a compound show discernible difference in their physico-chemical properties such as dipole moment, hydrophobicity, acidity / basicity.[1] It is expected that the tautomers of same compound also exhibit distinct molecular conformation as their recognition in a supramolecular assembly should be dissimilar. The study of tautomers has ever been intriguing to organic chemists[2] and recently it attracted much attention in the realm of computational chemistry.[3] In comparison, reports on tautomerism in solid state are scarce and a recent Cambridge Structure Database (CSD) search demonstrated the existence of only 108 pairs of such tautomers.[4] Tautomerism in solid state has mainly been reported for azole and azine class of compounds including various active pharmaceutical ingredient (API) molecules such as omeprazole, rantidine, sulfasalazine, irbesartan.[5] The other studies of solid state tautomerism have been carried out on barbituric acid and its derivatives,[6] hydroxy-nicotinic acid,[7] tricyclobenzadazole[8] and pyrimidones.[9] In all cases the most discussed keto-enol tautomerism has been witnessed except for drug sulfamethizole wherein sulfonamide-sulphonimide tautomerism (Scheme 1) is present.[10]

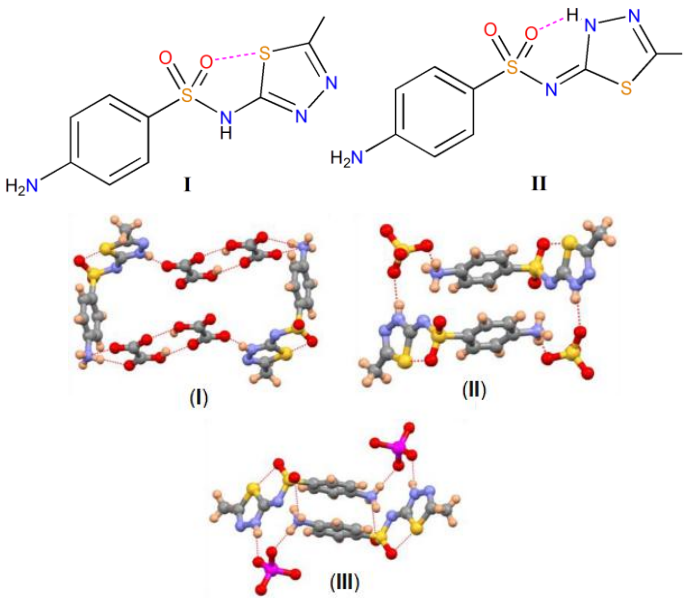

Scheme 1. Tautomeric form **I** of drug Sulpamethiazole is stabilized by oxalate (**I**), nitrate (**II**) and sulphate (**III**) salt formation.[10]

Most organic compounds (> 99.5 %) in solid state are isolated in their most stable tautomeric form and witnessing the other high energy tautomer is considered as a tremendously tough goal.[4] The rare cases wherein two tautomers could be obtained in pure

forms in the solid state, the energy difference between two tautomers lie in the range of weak to moderate hydrogen bonding interaction energy.[11] In order to stabilize the high energetic and unstable tautomers in solid state, reported crystal engineering strategies involve incorporation of a new component in crystal structure and thereby stabilizing the high energy tautomer through newly generated intra and intermolecular interactions. In this regard, salt formation (Scheme 1),[10] hydrate formation[7] and cocrystal formation (Scheme 2)[12] strategies have been explored so far. It is pertinent to mention that in last two methods one tautomer gets either protonated or deprotonated or remain in zwitterionic form. We presumed that as many of the organic compounds especially N and O containing molecules are potential metal ion chelators, utilising metal ion coordination can be another method to study different tautomeric forms in solid state.

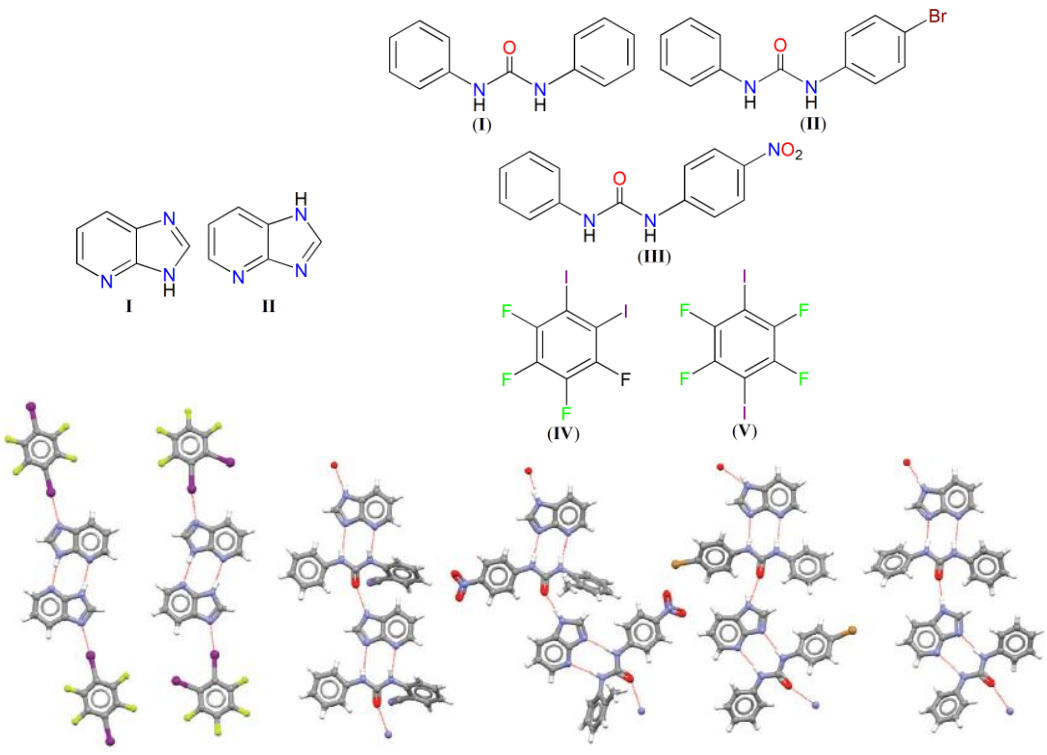

Scheme 2. Different tautomeric forms of 1-deazapurine stabilized by cocrystal formation.[12]

In order to demonstrate our envisaged strategy, hydrazonamide group of organic compounds has been chosen as numerous metal complexes of hydrazoanmide ligands were earlier reported. Many of the metal complexes show remarkable anti-tumor and analgesic properties[13] and few hydrazonamide molecules exhibit thermochromic property.[14] Keto-enol tautomerism (−C(=O)−NH−N=C− versus –C(OH)=N−N=C−) can easily be achieved in

hydrazonamide system. To witness the effectiveness of our proposed strategy, we considered of adding a new segment to hydrazonamide moiety to result in extra stabilisation of one of the tautomeric form. Intramolecular hydrogen bonding interaction by introduction of an *ortho* amino group are extensively reported in benzamide and hydrazide groups of molecules,[15] which are structurally similar to hydrazonamides. Keeping this in mind, we synthesised *orho* and *para* aminophenyl substituted hydrazonamide ligands *viz.* 2-amino-benzoic acid (amino-pyridin-2-yl-methylene)-hydrazide (**1a**) and 4-amino-benzoic acid (amino-pyridin-2-yl-methylene)-hydrazide) (**1b**). The hydrazonamide tautomeric form of the first ligand or **1a** is stabilised by a six membered intramolecular hydrogen bond which is the strongest of all hydrogen bonding interactions.[16] Scheme 3 depicts plausible tautomeric and rotameric forms of the former ligand **1a**.

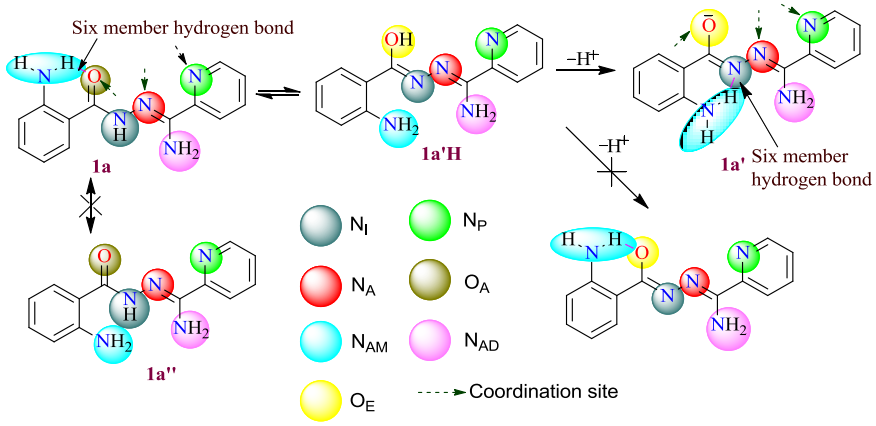

Scheme 3. Possible rotameric and tautomeric forms of ligand **1a**.

In order to achieve different tautomeric forms of ligand **1a**, we explored HSAB principle to choose the metal ions. Ligand **1a** was first reacted to Zn(II) and Cd(II) ions which are known as relatively softer Lewis acid. In Zn(II) and Cd(II) complexes the ligand **1a** behaves as a neutral, tridentate pincer type ligand which coordinates through the amide oxygen (O_A), azomethine (N_A) and pyridyl nitrogen (N_P). It was assumed that ligand **1a** might deprotonate and convert to an enolate *i.e.* hydrazoante form to coordinate with the harder Co(III) ion via enolate oxygen (O_E), which was indeed observed. The two tautomeric forms hydrazonamide (keto form) and anion of hydrazonic acid or hydrazonate (enolate form) are observed to exist in two different conformation *i.e.* rotameric / polymorphic forms. Different molecular conformation for tautomers of the same molecule or 'tautomeric polymorphism' is indeed a rare phenomenon and so far observed in only sixteen molecular systems.[4,7,8,10] The present

system illustrates a newer strategy to witness a high energy tautomeric forms and in addition it exhibits an example of rare 'tautomeric polymorphism'.

2. 2. Results and discussions

The aminophenyl substituted hydrazonamide ligands **1a** and **1b** can exist in two tautomeric forms *viz.* hydrazonamide and hydrazonic acid. Ligand **1a**, in addition, is able to exist in another rotameric form **1a″** which is due to *anti* orientation of hydrazonamide oxygen (O_A) with respect to *o*-amino group (Scheme 3). However, analogous rotameric form is not possible in ligand **1b** due to *para* disposition of the amino group. Nevertheless, PXRD of ligand **1a** shows significant phase purity as shown in Figure 1, indicating the presence of only hydrazonamide (**1a**) tautomeric form and not the other tautomeric / rotameric forms.

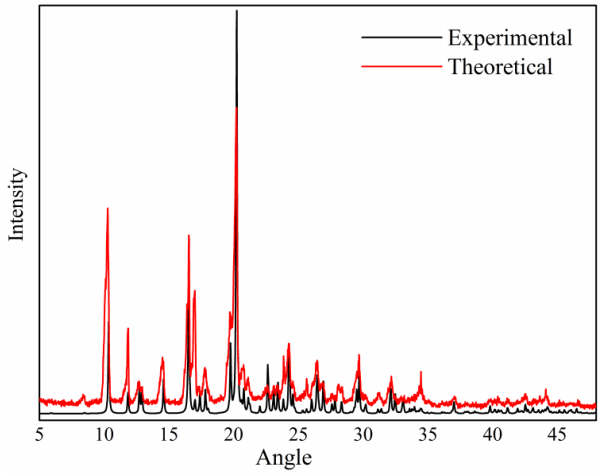

Figure 1. PXRD pattern of complex **1a**

2. 2. 1. Molecular structure description

A summary of crystallographic and refinement parameters of complexes **1-10** and hydrazonamide form of ligand **1a** have are listed in Table 1-4. In order to maintain uniformity on type of the donor atom / groups following conventions were used throughout this chapter: O_E = hydrazonate-O; O_A = hydrazonamide-O; O_N = nitrate-O; O_W = water-O; N_P = pyridine-N; N_A = azomethine-N; N_I = imino-NH/ imino-N; N_{AM} = aromatic-NH_2; N_{AD} = amidine-NH_2 and N_T = thiocyanate-N (Scheme 3).

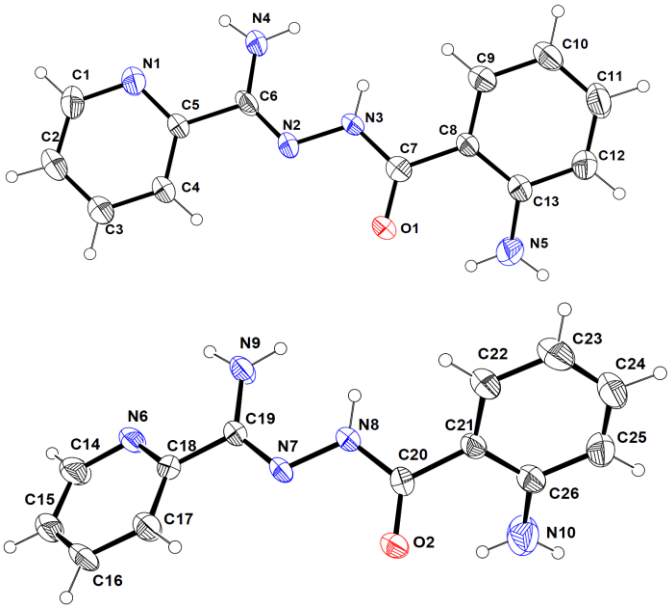

Figure 2. *ORTEP* diagrams of **1a** (both molecules), displacement ellipsoids are drawn on 30% probability level.

The *ORTEP* diagrams of two molecules present in the unit cell of ligand **1a** are shown in Figure 2. The two molecules primarily differ in (i) $O_A\cdots N_{AM}$ non-bonded contact (N5···O1, 2.926(3) Å, H5B···O1, 2.41(2) Å, N5−H5B···O1, 118.84(2)° and N10···O2, 2.716(4) Å, H10B···O2, 2.11(2) Å, N10−H10B···O2, 127.45(2)°); (ii) torsions involving O_A and N_{AM}, O1–C7–C8–C13, 46.2(3)°; O2–C20–C21–C26, 24.5(4)° and torsion angles involving N_P and N_{AD}, N4–C6–C5–N1, 17.2(3)°; N9–C19–C18–N6, -10.7(4)°. It is pertinent to mention that N_P and N_{AD} are oriented *cis* to each other in free form of this ligand as revealed by N_P–C–C–N_{AD}. In contrary, N_P and N_{AD} are observed to be *trans* to each other in coordinated form of the ligand, which is due to ring flipping of the pyridyl ring to favour coordination. Both N_I and N_{AD} groups donate hydrogen bond to O_A of the other molecule leading to the formation of $R_2^1(7)$ supramolecular motif (O1···N3, O1···N4, O2···N8, O2···N9). These intermolecular interactions generate two independent but similar hydrogen bonded chains as in Figure 3.

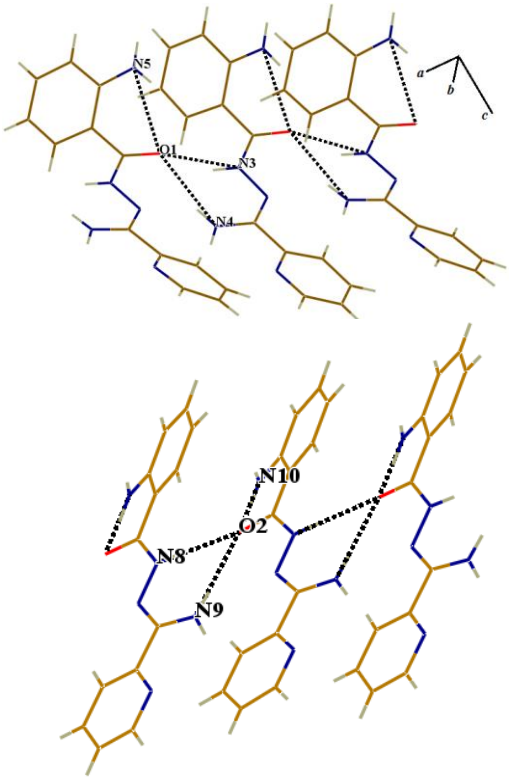

Figure 3. Hydrogen bonding in first molecule of ligand **1a**

2. 2. 1. 1. Crystal structure description of metal complexes of 1a

The *bis*-chelated metal complex [Ni(**1a**)$_2$]Cl$_2$·2H$_2$O (**1**) (Figure 4) adopt a distorted octahedral geometry by spanning the metal ion in $(N_A)_2(N_P)_2(O_A)_2$ coordination environment with *trans-cis-cis* disposition of donor sites. In complex **1**, the chelate bite angles lie in the range of 76.45(8)–78.13(9) and the *trans* angle O_A–Ni–N_P in complex **1** deviates from linearity by 25.4(1)° (Table 5).

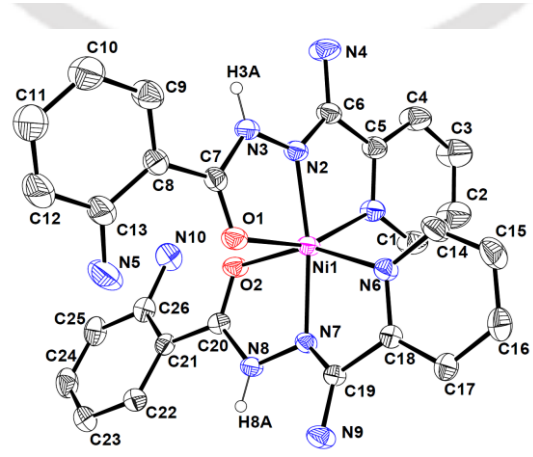

Figure 4. *ORTEP* diagram for compound [Ni(**1a**)$_2$]Cl$_2$·2H$_2$O (**1**), displacement ellipsoids are drawn on 30% probability level.

The lone-pair on N_I is inaccessible for any secondary interactions with two other hydrogen bond donor groups (*viz*. N_{AM} and N_{AD}), as a result, N_{AM} prefers to orient *syn* to O_A as the intraligand hydrogen bond acceptor. The parameters of intramolecular N−H···O hydrogen bond (N···O, 2.690(1) and 2.727(1) Å, O···H, 2.06 and 2.12 Å, N−H···O, 129.41(4) and 127.41(4)°) are in the range of classical intramolecular hydrogen bond.

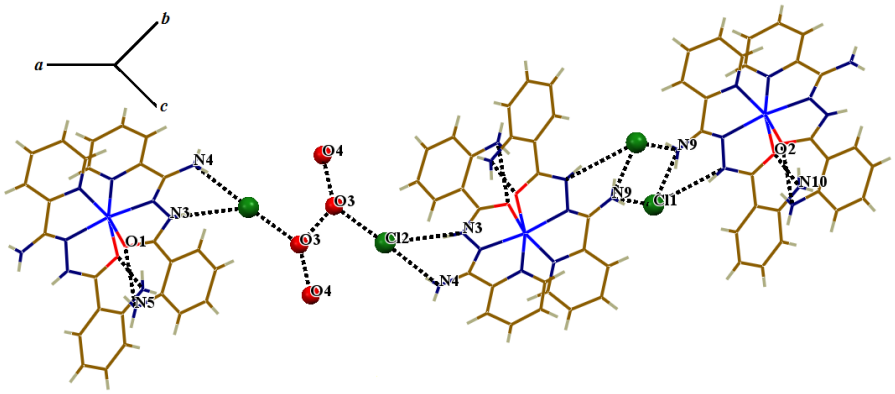

Figure 5. Hydrogen bonding in complex **1**, viewed along crystallographic *a* axis.

Complex **1** has two sets of N_I and N_{AD} (*viz.* N3N4 and N8N9), among which, the N3N4 set donate to chloride ion Cl2 (Figure 5) which in turn is hydrogen bonded to a Z-shaped water tetramer (O4O3O3O4) having O3···O3, 3.254(1) Å and O4···O4, 2.789(1) Å intermolecular contacts. In the N8N9 set, N_I donates to Cl1 while N_{AD} acts as a double donor to Cl1 and this brings two adjacent Cl1 ions within the non-bonded distance of 5.527(1) Å forming a $R_4^2(8)$ $R_2^1(7)$ supramolecular motif as shown in Figure 5.

Table 1. Crystallographic and refinement parameters of ligand **1a**, complex **1** and **2**

	1a	**1**	**2**
chem formula	$C_{13}H_{13}N_5O$	$C_{26}H_{30}N_{10}O_4NiCl_2$	$C_{19}H_{27}N_7O_3ZnCl_2$
formula wt	255.28	676.00	537.76
CCDC number	1451163	1451171	1451166
temp (K)	296	296	296
crystsyst	monoclinic	triclinic	triclinic
space group	*Pc*	*P*-1	*P*-1
a (Å)	11.1211(6)	8.6293(14)	8.6478(8)
b (Å)	14.9238(7)	9.2472(13)	11.9723(10)
c (Å)	8.3805(4)	19.390(3)	12.1429(9)
α (°)	90.00	92.864(8)	78.355(6)
β(°)	110.536(3)	91.983(7)	84.395(6)
γ(°)	90.00	95.917(8)	89.278(6)
V (Å^3)	1302.51(11)	1535.8(4)	1225.41(18)
Z	4	2	2
μ (mm^{-1})	0.088	0.858	1.254
ρ_{calcd}(g cm^{-3})	1.302	1.462	1.457
no. of unique rflns	4034	7429	4086
no. of rflns ($I \geq 2\sigma(I)$)	3140	4995	2638
R_1[a], wR_2[b] ($I \geq 2\sigma(I)$)	0.0412, 0.0986	0.0495, 0.1239	0.0551, 0.1415
R_1[a], wR_2[b] (all data)	0.0559, 0.1083	0.0825, 0.1398	0.0934, 0.1771
goodness of fit (F^2)	1.013	1.012	0.967
largest peak/hole (e Å^{-3})	0.125/-0.160	0.545/-0.345	0.537/-0.779

Table 2. Crystallographic and refinement parameters of complexes **3**-**5**

	3	**4**	**5**
chem formula	$C_{17}H_{19}N_5O_5Zn$	$C_{26}H_{26}N_{12}O_8Cd$	$C_{32}H_{40}N_{20}O_{10}Cd_2$
formula wt	438.76	747.00	1089.66
CCDC number	1451167	1451172	1451168
temp (K)	296	296	296
crystsyst	triclinic	triclinic	triclinic
space group	*P*-1	*P*-1	*P*-1
a (Å)	8.8215(16)	9.0525(4)	8.7849(4)

b (Å)	10.4024(19)	13.4096(8)	9.4710(4)
c (Å)	11.301(2)	14.2290(6)	14.1356(6)
α (°)	70.174(10)	63.219(5)	84.021(3)
β(°)	76.203(10)	82.617(4)	82.401(3)
γ(°)	82.541(10)	77.984(5)	66.865(2)
V (Å^3)	946.1(3)	1507.03(13)	1070.27(8)
Z	2	2	1
μ (mm^{-1})	1.338	0.795	1.072
ρ_{calcd}(g cm^{-3})	1.540	1.646	1.691
no. of unique rflns	3930	5707	3626
no. of rflns ($I \geq 2\sigma(I)$)	3286	4655	3201
R_1[a], wR_2[b] ($I \geq 2\sigma(I)$)	0.0361, 0.1092	0.0415, 0.0985	0.0247, 0.0573
R_1[a], wR_2[b] (all data)	0.0441, 0.1143	0.0551, 0.1123	0.0306, 0.0599
goodness of fit (F^2)	1.030	0.992	1.026
largest peak/hole (e Å^{-3})	0.349/-0.474	1.216/-0.443	0.246/-0.326

Table 3. Crystallographic and refinement parameters of complex **6-8**

	6	**7**	**8**
chem formula	$C_{26}H_{34}N_{11}O_{10}Co$	$C_{26}H_{33}N_{12}O_{13}Cu_2$	$C_{40}H_{52}N_{16}O_6Cu_2S_2$
formula wt	719.51	848.74	1044.20
CCDC number	1451170	1451173	1451165
temp (K)	296	296	296
crystsyst	triclinic	triclinic	triclinic
space group	*P*-1	*P*-1	*P*-1
a (Å)	11.5900(5)	10.3597(3)	7.7078(6)
b (Å)	11.6117(5)	12.7331(3)	12.7998(11)
c (Å)	13.1572(5)	14.7811(4)	13.0923(11)
α (°)	92.008(4)	114.8950(10)	88.608(7)
β(°)	110.133(4)	100.6440(10)	74.027(7)
γ(°)	108.548(4)	99.3820(10)	80.750(7)
V (Å^3)	1555.22(11)	1673.59(8)	1225.38(17)
Z	2	2	1
μ (mm^{-1})	0.627	1.355	1.014
ρ_{calcd}(g cm^{-3})	1.536	1.684	1.415

no. of unique rflns	5771	5172	4658
no. of rflns ($I \geq 2\sigma(I)$)	4716	4355	3751
R_1[a], wR_2[b] ($I \geq 2\sigma(I)$)	0.0507, 0.1340	0.0322, 0.0888	0.0598, 0.1743
R_1[a], wR_2[b] (all data)	0.0637, 0.1444	0.0404, 0.0941	0.0742, 0.1927
goodness of fit (F^2)	1.025	1.018	1.031
largest peak/hole (e Å^{-3})	0.819/-0.551	0.452/-0.268	0.792/-0.530

Table 4. Crystallographic and refinement parameters of complex **9** and **10**

	9	**10**
chem formula	$C_{13}H_{13}N_5OZnCl_2$	$C_{20}H_{22}N_{10}O_{10}Cd$
formula wt	391.57	674.89
CCDC number	1451169	1451161
temp (K)	296	296
crystsyst	monoclinic	orthorhombic
space group	$P2_1/c$	$P2_1$
a (Å)	7.6631(3)	8.4302(3)
b (Å)	17.7463(7)	17.2914(7)
c (Å)	11.7318(4)	17.9214(7)
α (°)	90.00	90.00
β(°)	109.062(2)	90.00
γ(°)	90.00	90.00
V (Å^3)	1507.94(10)	2612.40(17)
Z	4	4
μ (mm^{-1})	1.991	0.910
ρ_{calcd}(g cm^{-3})	1.725	1.716
no. of unique rflns	3455	6535
no. of rflns ($I \geq 2\sigma(I)$)	3419	5132
R_1[a], wR_2[b] ($I \geq 2\sigma(I)$)	0.0759, 0.1653	0.0335, 0.0874
R_1[a], wR_2[b] (all data)	0.0763, 0.1654	0.0475, 0.0938
goodness of fit (F^2)	1.002	1.001
largest peak/hole (e Å^{-3})	0.730/-0.767	0.564/-0.515

Table 5. Bond parameters of complex $[Co(\mathbf{1a'})_2]NO_3{\cdot}5H_2O$ (**6**) and $[Ni(\mathbf{1a})_2]Cl_2{\cdot}2H_2O$ (**1**)

1				**6**			
Ni1–O1	2.116(2)	O1–Ni1–N1	154.60(9)	Co1–O1	1.926(2)	N6–Co1–N7	82.1(1)
Ni1–O2	2.122(2)	N6–Ni1–O2	154.57(9)	Co1–O2	1.937(3)	O1–Co1–O2	92.8(1)
Ni1–N1	2.081(3)	N2–Ni1–N7	169.6(1)	Co1–N1	1.934(2)	N1–Co1–O1	163.5(1)
Ni1–N2	1.984(2)	N7–Ni1–N1	112.18(9)	Co1–N2	1.854(4)	N6–Co1–O2	163.2(1)
Ni1–N6	2.090(3)	O1–Ni1–N6	94.02(9)	Co1–N6	1.944(3)	N2–Co1–N7	179.5(1)
Ni1–N7	2.007(2)	O1–Ni1–N7	93.21(8)	Co1–N7	1.852(3)	N6–Co1–N1	92.6(1)
O1–Ni1–N2	76.71(9)	O2–Ni1–N1	98.13(9)	O1–Co1–N2	81.5(1)	O1–Co1–N6	89.8(1)
N1–Ni1–N2	77.9(1)	O2–Ni1–N2	100.37(9)	N1–Co1–N2	82.0(1)	O1–Co1–N7	98.9(1)
O2–Ni1–N7	76.45(8)	O1–Ni1–O2	88.01(7)	O2–Co1–N7	81.0(1)	O2–Co1–N1	89.7(1)
N6–Ni1–N7	78.13(9)	N2–Ni1–N6	104.8(1)	N6–Co1–N7	82.1(1)	O2–Co1–N2	99.3(1)
N1–Ni1–N6	90.8(1)			N1–Co1–N6	92.6(1)		

Table 6. Bond parameters of complex $[Zn(\mathbf{1a})Cl_2]{\cdot}2DMF$ (**2**), $[Zn(\mathbf{1a})(OAc)_2]$ (**3**) and $[Zn(\mathbf{1b})Cl_2]$ (**9**)

2		**3**		**9**	
Zn1–O1	2.239(4)	Zn1–O1	2.214(2)	Zn1–O1	2.269(5)
Zn1–N1	2.192(4)	Zn1–N1	2.167(2)	Zn1–N1	2.210(5)
Zn1–N2	2.080(5)	Zn1–N2	2.044(2)	Zn1–N2	2.028(5)
Zn1–Cl1	2.257(2)	Zn1–O2	1.960(2)	Zn1–Cl1	2.248(2)
Zn1–Cl2	2.247(2)	Zn1–O4	1.966(2)	Zn1–Cl2	2.273(2)
N1–Zn1–N2	74.1(1)	N1–Zn1–N2	75.41(8)	N1–Zn1–N2	74.0(2)
N2–Zn1–O1	72.3(1)	N2–Zn1–O1	73.52(7)	N2–Zn1–O1	73.2(2)
N1–Zn1–O1	143.5(2)	N1–Zn1–O1	148.90(7)	N1–Zn1–O1	147.3(2)
O1–Zn1–Cl1	95.7(1)	N1–Zn1–O2	103.15(8)	O1–Zn1–Cl1	95.5(1)
O1–Zn1–Cl2	100.0(1)	N2–Zn1–O4	129.82(8)	O1–Zn1–Cl2	96.9(1)
N1–Zn1–Cl1	97.6(1)	N1–Zn1–O4	104.28(8)	N1–Zn1–Cl1	105.1(2)
N1–Zn1–Cl2	105.0(1)	N2–Zn1–O2	137.58(8)	N1–Zn1–Cl2	97.0(2)
N2–Zn1–Cl1	134.2(1)	O2–Zn1–O4	92.12(8)	N2–Zn1–Cl1	130.0(2)
N2–Zn1–Cl2	111.3(1)	O1–Zn1–O2	98.77(7)	N2–Zn1–Cl2	114.6(2)
Cl1–Zn1–Cl2	114.37(6)	O1–Zn1–O4	96.60(7)	Cl1–Zn1–Cl2	115.07(7)

Table 7. Bond parameters of complex [Cd(**1a**)$_2$(NO$_3$)]NO$_3$ (**4**)

Cd1–O1	2.505(3)	O2–Cd1–N2	108.1(1)	N2–Cd1–N7	150.8(1)
Cd1–N1	2.417(3)	O3–Cd1–N7	79.9(1)	O1–Cd1–O4	121.3(1)
Cd1–N2	2.302(2)	O4–Cd1–N7	117.7(1)	O2–Cd1–O4	70.6(1)
Cd1–O2	2.414(4)	O4–Cd1–N2	85.2(1)	O3–Cd1–O4	46.2(1)
Cd1–N6	2.419(4)	O1–Cd1–O3	147.8(1)	O2–Cd1–O3	75.9(1)
Cd1–N7	2.302(2)	O2–Cd1–N7	67.5(1)	N1–Cd1–O4	68.9(1)
Cd1–O3	2.559(3)	N6–Cd1–N7	67.8(1)	N1–Cd1–O3	77.0(1)
Cd1–O4	2.803(6)	O1–Cd1–N6	92.8(1)	N1–Cd1–N7	135.2(1)
N1–Cd1–N2	67.7(1)	N6–Cd1–O3	108.0(1)	O3–Cd1–N2	128.2(1)
N2–Cd1–O1	66.0(1)	O1–Cd1–O4	121.3(1)	O1–Cd1–O2	71.9(1)
O1–Cd1–N1	130.9(1)	N2–Cd1–N6	104.5(1)		
O2–Cd1–N6	133.6(1)	N1–Cd1–N6	83.6(1)		

Table 8. Bond parameters of complex [Cd(**1a**)(NO$_3$)(N$_3$)]·DMF (**5**)

Cd1–O1	2.348 (2)	O2–Cd1–N1	102.03(7)	N1–Cd1–N6	88.9(1)
Cd1–N1	2.383 (3)	O1–Cd1−N6$^{/}$	136.34(8)	N1–Cd1–N6$^{/}$	98.13(8)
Cd1–N2	2.301 (2)	O2–Cd1–N6	89.96(8)	O1–Cd1–N6	88.70(8)
Cd1–O2	2.350 (2)	O3–Cd1–N6	75.14(9)	N6–Cd1–N6$^{/}$	76.10(9)
Cd1– N6$^{/}$	2.316 (2)	O2–Cd1–O1	87.51(7)	N2–Cd1–N6	155.74(8)
Cd1–O3	2.801 (3)	O2–Cd1–N2	87.65(7)	N2–Cd1–N6	113.40(8)
O3–Cd1–O1	71.13(7)	O2–Cd1–O3	47.87(8)		
N1–Cd1–N2	68.12(7)	O3–Cd1–N1	144.60(7)	O2–Cd1–N6$^{/}$	155.21(9)
N2–Cd1–O1	67.69(7)	O3–Cd1–N2	119.37(7)	O3–Cd1–N6$^{/}$	107.98(9)
O1–Cd1–N1	134.23 (7)				

Table 9. Bond parameters of complex $[Cu_2(\mathbf{1a'})_2(H_2O)_2](NO_3)_2{\cdot}3H_2O$ (**7**) and $[Cu_2(\mathbf{1a'})_2(NCS)_2]{\cdot}2DMF$ (**8**)

		7			**8**
Cu1–O1	1.990(2)	Cu2–O3	1.976(2)	Cu1–O1	1.983(3)
Cu1–N1	2.047(3)	Cu2–O4	1.939(4)	Cu1–N1	2.056(4)
Cu1–N2	1.889(2)	Cu2–N6	2.032(3)	Cu1–N2	1.898(2)
Cu1–N5	2.421(3)	Cu2– N7	1.898(2)	Cu1–N5	2.501(4)
Cu1–O2	1.946(2)	Cu2– N10	2.433(3)	Cu1–N6	1.928(4)
O1–Cu1–N2	79.37(9)	O3–Cu2–O4	96.2(1)	N2–Cu1–N1	79.5(1)
N2–Cu1–N1	79.7(1)	N6–Cu2–N7	80.1(1)	O1–Cu1–N5	97.1(1)
O1–Cu1–N5	108.67(9)	N6–Cu2–O3	156.97(9)	N1–Cu1–N5	91.3(1)
N1–Cu1–N5	88.0(1)	N7–Cu2–O3	79.76(9)	N2–Cu1–N5	94.7(1)
N2–Cu1–N5	99.2(1)	O4–Cu2–N6	101.2(1)	O1–Cu1–N1	157.8(1)
O1–Cu1–N1	155.01(9)	O4–Cu2–N7	167.9(1)	N5–Cu1–N6	94.6(2)
O2–Cu1–N2	170.6(1)	N6–Cu2–N10	89.1(1)	O1–Cu1–N6	101.2(1)
O1–Cu1–O2	98.50(9)	N7–Cu2–N10	99.2(1)	N2–Cu1–N6	170.5(2)
N1–Cu1–O2	99.9(1)	O3–Cu2–N10	105.14(9)	N1–Cu1–N6	94.6(2)
N5–Cu1–O2	90.2(1)	O4–Cu2–N10	92.8(1)	O1–Cu1–N2	98.6(2)

Table 10. Bond parameters of complex $[Cd(\mathbf{1b})(\mathbf{1b'})(H_2O)](NO_3)_2{\cdot}H_2O$ (**10**)

Cd1–O1	2.411(2)	O2–Cd1–N6	70.21(9)	O3–Cd1–N6	88.1(1)
Cd1–N1	2.417(3)	O1–Cd1–O3	81.40(8)	N1–Cd1–N6	145.3(1)
Cd1–N2	2.334(3)	O1–Cd1–N8	84.43(9)	N1–Cd1–N8	86.9(1)
Cd1–N6	2.395(3)	O1–Cd1–N6	79.58(9)	O2–Cd1–N2	138.69(9)
Cd1–N8	2.473(3)	N2–Cd1–N8	94.1(1)	O2–Cd1–N6	70.21(9)
Cd1–O2	2.310(2)	O2–Cd1–O3	83.79(9)	O2–Cd1–N8	108.04(9)
Cd1–O3	2.398(3)	N6–Cd1–N8	88.7(1)	N2–Cd1–O3	81.15(9)
N1–Cd1–N2	68.0(1)	O3–Cd1–N8	165.82(9)	N2–Cd1–N8	94.1(1)
N2–Cd1–O1	67.65(9)	O3–Cd1–N1	103.5(1)	O2–Cd1–N1	78.60(9)
O1–Cd1–N1	133.96(9)	O1–Cd1–O2	146.66(8)		

Table 11. Hydrogen bonding parameters in complex $[Ni(\mathbf{1a})_2]Cl_2{\cdot}2H_2O$ (**1**), $[Cd(\mathbf{1a})_2(NO_3)]NO_3$ (**4**)

Compound	D–H···A	D···A (Å)	H···A (Å)	∠D–H···A (°)	Symmetry
	N3–H3A···Cl2	3.250(1)	2.43	158.99(3)	x, y, z
	N4–H4A···Cl2	3.188(1)	2.37	159.18(4)	x, y, z
	N4–H4B···Cl2	3.356(1)	2.53	160.68(4)	-x+2, -y+1, -z
1	N5–H5B···O1	2.690(1)	2.06	129.41(4)	x, y, z
	N8–H8A···Cl1	3.300(1)	2.48	160.22(3)	-x+1, -y+1, -z
	N9–H9A···Cl1	3.229(1)	2.45	150.37(3)	-x+1, y, z
	N9–H9B···Cl1	3.279(1)	2.46	158.25(4)	x, y+1, z
	N10–H10A···O2	2.727(1)	2.12	127.41(4)	x, y, z
	N4–H4A···O4	2.716(4)	2.07	126.74(4)	-x+2, -y, -z+1
	N4–H4B··O2	3.014(3)	2.22	153.26(4)	-x+2, -y+1, -z
	N5–H5B···N3	2.716(4)	2.07	126.74(4)	x, y, z
	N4–H4A···O4	2.947(7)	2.23	148.18(4)	-x+2, -y, -z+1
	O6–H6A···O10	2.895(6)	2.57	106.61(3)	-x+1, -y+1, -z+1
	N3–H3A···O7	2.824(5)	1.91	172.55(5)	-x+1, -y+1, -z+1
4	N4–H4B···O8	2.952(6)	2.10	166.15(3)	-x+1, -y+1, -z+1
	N5–H5A···O1	2.903(6)	2.35	122.63(5)	x, y, z
	N8–H8A···O3	2.942(4)	2.13	174.10(4)	-x, -y, -z+2
	N9–H9A···O1	2.910(5)	2.08	153.20(4)	x, y, z
	N10–H10A···O2	2.780(7)	2.08	130.82(4)	x, y, z

Table 12. Hydrogen bonding parameters in complex $[Co(\mathbf{1a'})_2]NO_3{\cdot}5H_2O$ (**6**), and $[Cu_2(\mathbf{1a'})_2(H_2O)_2](NO_3)_2{\cdot}3H_2O$ (**7**)

Compound	D–H···A	D···A (Å)	H···A (Å)	∠D–H···A (°)	Symmetry
	N4–H4A···O4	2.716(4)	2.07	126.74(4)	-x+2, -y, -z+1
	N4–H4B··O2	3.014(3)	2.22	153.26(4)	-x+2, -y+1, -z
	N5–H5B···N3	2.716(4)	2.07	126.74(4)	x, y, z
	N4–H4A···O4	2.947(7)	2.23	148.18(4)	-x+2, -y, -z+1
	O6–H6A···O10	2.895(6)	2.57	106.61(3)	-x+1,-y+1, -z+1

6	O7–H7A···N10	3.067(7)	2.41	175.20(6)	2-x, 1-y, -z
	N9–H9A···O4	2.920(5)	2.18	164.81(4)	-x+1,-y+1, -z+1
	N9–H9B···O1	2.961(5)	2.07	152.87(4)	x-1, y, z-1
	N10–H10A···O8	3.168(6)	2.33	175.30(4)	-x+1,-y+1, -z+1
	N10–H10B···N8	2.697(5)	2.05	129.85(3)	x, y, z
	O2–H2A···O12	2.624(4)	1.79	178.56(4)	x, y, z
	O2–H2B···O5	2.823(4)	2.08	163.35(4)	x, y, z
	O11–H11A···O13	2.771(4)	1.84	159.43(5)	x, y, z
	O12–H12B···O11	2.745(4)	1.95	173.45(7)	x, y, z
	N9–H9A···O10	3.037(4)	2.31	157.22(4)	-x, -y+1, -z+1
	N5–H5A···N3	2.700(4)	2.15	129.22(3)	x, y, z
7	N10–H10B···N8	2.716(4)	2.12	131.19(3)	x, y, z
	N4–H4B···O6	2.965(4)	2.25	153.65(4)	-x+2,-y+1, -z+1
	N10–H10B···O10	2.995(4)	2.49	122.64(3)	-x, -y+1, -z+1
	N10–H10A···O5	3.327(3)	2.53	165.87(3)	-x, -y+2, -z+1
	N5–H5B···O8	3.159(4)	2.41	156.23(3)	-x+1, -y, -z+1
	N4–H4A···O13	2.986(5)	2.33	142.0 6(3)	x+1, y, z
	O4–H4C···O9	2.688(4)	1.96	176.98(4)	x, y, z-1
	O13–H13A···O3	2.809(4)	2.32	143.92(5)	x, y, z
	O4–H4D···O7	2.704(6)	2.00	171.71(5)	-x+1,-y+1, -z+1
	N9–H9B···O11	3.018(5)	2.35	159.67(3)	x-1, y, z
	O11–H11B···O1	2.836(4)	2.18	158.92(5)	x, y, z

The mono-chelates of **1a** with Zn(II) ion *viz.* [Zn(**1a**)Cl_2]·2DMF (**2**), [Zn(**1a**)$(OAc)_2$] (**3**) crystallize in *P*-1 space group. The coordination geometry around the bivalent zinc in **2** can be best described as distorted trigonal bipyramidal, even though calculated τ value 0.49 is inconclusive (Figure 6a). The sum of the three angles subtended at metal center (359.9(1)°) in trigonal plane is very close to the ideal value. Two axial sites are occupied by O_A and N_P with O_A–Zn–N_P angle being 143.5(1)° which is smaller as expected from inflexibility present in ligand framework. Lengths of Zn–Cl1 (2.257(2)Å) and Zn–Cl2 (2.247(2)Å) bonds are within the expected range. Useful bond lengths and bond angles for complex **2**, **3** and **9** are listed in Table 6. In complex **2**, N_{AM} is oriented *anti* to N_I, now having attached with hydrogen and it

forms intraligand hydrogen bond with carbonyl oxygen O_A (N5···O1, 2.679(5)Å). Among two DMF molecules present in the lattice, one is hydrogen bonded with N_I (N3···O3, 2.944(3) Å) and N_{AD} (N4···O3, 2.823(1) Å) groups forming a $R_2^1(7)$ motif while the other DMF molecule is hydrogen bonded with N_{AD}, N4···O2, 2.841(6) Å) only (Figure 6b).

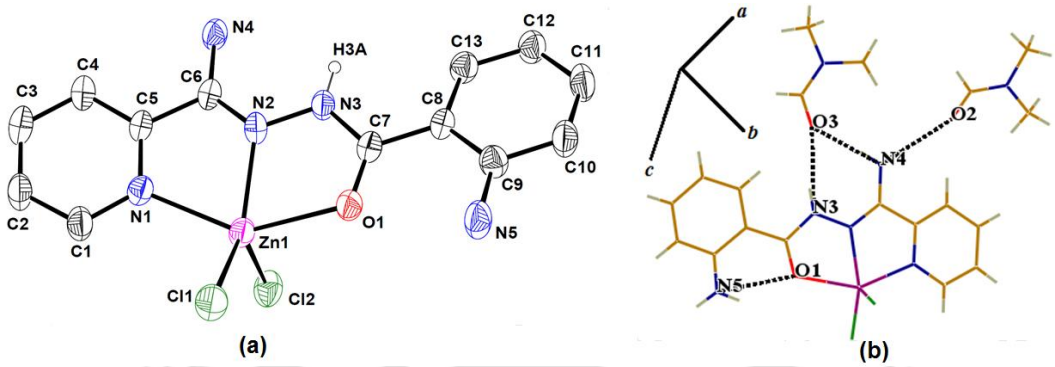

Figure 6. (a) *ORTEP* diagram of [Zn(**1a**)Cl_2]·2DMF (**2**), displacement ellipsoids are drawn on 30% probability level and hydrogen atoms except H3A are removed for clarity; (b) Hydrogen bonding in complex [Zn(**1a**)Cl_2]·2DMF (**2**).

In complex **3**, bivalent zinc is penta-coordinated having distorted trigonal bipyramid geometry (τ = 0.945). The trigonal plane is composed of N_A and oxygen atoms O2, O4 from two acetate ions and carbonyl oxygen O_A, N_P occupying two axial positions (Figure 7). Two Zn–O bond lengths for the acetate ion are (1.959(2) Å and 1.966(2) Å) shorter and indicate the stronger metal to ligand interaction in the trigonal plane. Deviation of bond angles N1–Zn–O2 (103.18(8)°); N1–Zn–O4 (104.28(8)°); O1–Zn–O2 (98.77(7)°) and O1–Zn–O4 (96.60(7)°) from ideal value of 90° suggesting that axial bonds are considerably bent. The equatorial plane is nonetheless no less deformed as revealed by bond angle values of O2–Zn–O4, N2–Zn–O2, N2–Zn–O4 which are 92.13(8)°, 137.58(8)° and 129.82(8)° respectively.

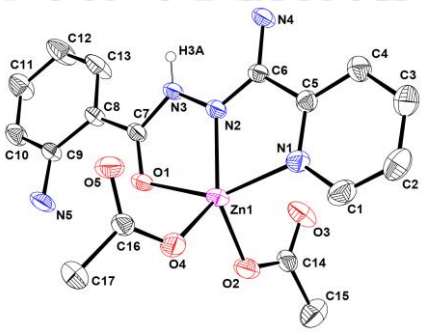

Figure 7. *ORTEP* diagram of [Zn(**1a**)$(OAc)_2$] (**3**), ellipsoids are drawn on 30% probability level and hydrogen atoms except H3A are removed for clarity.

Complex [Zn(**1a**)$(OAc)_2$] (**3**) exhibits intramolecular $N_{AM}\cdots O_A$ (N5···O1, 2.703(3) Å, H5B···O1, 2.07 Å and N5−H5B···O1, 129.63(2)°) hydrogen bond. Intermolecular hydrogen bonding interactions among N_I, N_{AD} and un-coordinated oxygen atoms of the metal bound acetate ion (N3···O5 and N4···O3) forming a $2R_2^1(7)$ motif and thus tether two molecules of complex **3** with respect to a three-fold symmetry axis passing through acetate oxygen atom O5. These acetate oxygen zippered polymeric units are interlinked through a short non-bonded contact of O1···N4, 3.155 Å (Figure 8).

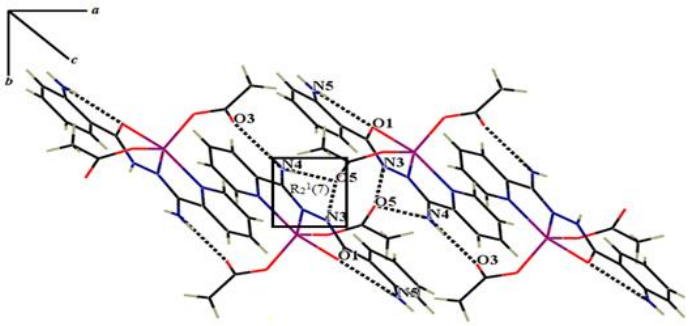

Figure 8. Centro-symmetric motif formed through hydrogen bonding in complex **3**.

The ligand is bound to Cd(II) in its neutral **1a** form in complex [Cd(**1a**)$_2$$(NO_3)$]$NO_3$ (**4**). The central metal ion has a $(O_A)_2(N_A)_2(N_P)_2(O_N)_2$ coordination environment in which the nitrate ion is bound as a chelating ligand (Figure 9a). Among two coordinated nitrate oxygen atoms, Cd–O3 distance (2.559(3) Å) is within the reported value while Cd–O4 distance (2.803(6) Å) is higher than the earlier reported values.[17] Useful bond distances and bond angles in complex **7** are listed in table 7. Intramolecular $O_A\cdots N_{AM}$ hydrogen bond (O1···N5, 2.903(6) Å and H5B···N5, 2.35 Å, N5−H5B···O1, 122.63(5)° and O2···N10, 2.780(7) Å, H10A···O2, 2.08 Å, N10−H10A···O2, 130.82(4)°) owing to *syn* orientation of N_{AM} and O_A. Among two sets of N_I and N_{AD} groups, one set (N3 and N4) is involved in the hydrogen bonding interaction (N3···O7 and N4···O8) exclusively with lattice nitrate (Figure 9b). The other set (N8 and N9) interacts with O3 and O5 atoms of the coordinated nitrate ion (N8···O3 and N9···O5) and thus forms a $2R_2^2(9)$ motif (Figure 9b). Such interactions generate a centrosymmetric hydrogen-bonded dimer and additional interaction between N_{AD} with O_A (N9···O1) links these dimers to a 1D hydrogen-bonded polymeric chain (Figure 9b).

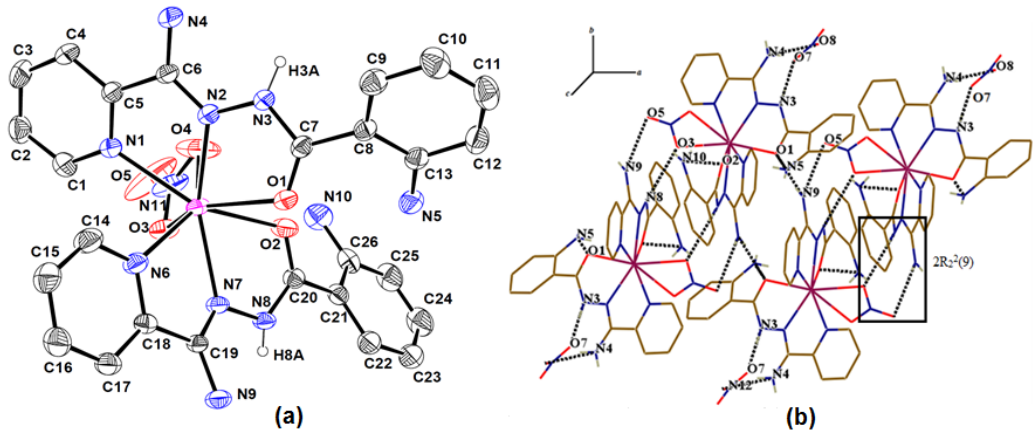

Figure 9. (a) *ORTEP* diagram of **4**, elliposoids at 30% probability level and aromatic hydrogens are removed; (b) Hydrogen bonded 1D-chain in complex **4** viewed along *a* axis.

The di-$\mu_{1,1}$-azido bridged dimeric unit present in complex [Cd(**1a**)(NO_3)(N_3)]·DMF (**5**) contains a Cd_2N_2 core having a crystallographic inversion centre (Figure 10). The coordination geometry of the eight coordinated metal centre can be best described as a monocapped octahedron with the basal plane composed of O1, N2, N1 and N6 atoms. The axial positions are taken up by N6′ and O2 atoms whereas O3 serves as the capping atom (Figure 10). All Cd–O bond distances (Table 8) are close to the reported values except Cd–O3 (nitrate, capped oxygen atom) bond length (2.802(3) Å).[17] The basal plane is distorted due to bite angle restrictions by ligand **1a**, with remarkably low bite angles (67.79(7)–68.12(7)°) and *trans* angles N2–Cd1–N6 (155.73(8)°) and N1–Cd1–O1(134.21(8)°) deviating largely from 180°. The axial atoms O2 and N6' are displaced from their ideal positions as revealed by the *trans* angle O2–Cd1–N6' (155.21(9)°). Relevant bond angles and bond lengths in complex **5** are given in table 8.

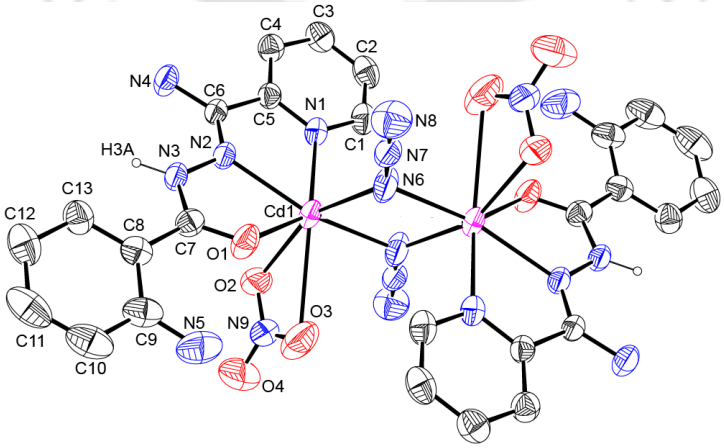

Figure 10. *ORTEP* diagram of [Cd(**1a**)(NO_3)(N_3)]·DMF (**5**), ellipsoids at 30% probability.

Intraligand hydrogen bond exists between N_{AM} and O_A [N5···O1, 2.675(4) Å, H5A···O1, 2.14 Å and N5−H5A···O1, 125.30(3)°]. The N_I and N_{AD} groups are involved in intermolecular hydrogen bonding with the oxygen atom (N3···O5, 2.858(4) Å; N4···O5, 2.842(2) Å) of DMF molecule forming a $R_2^1(7)$ motif (Figure 11).

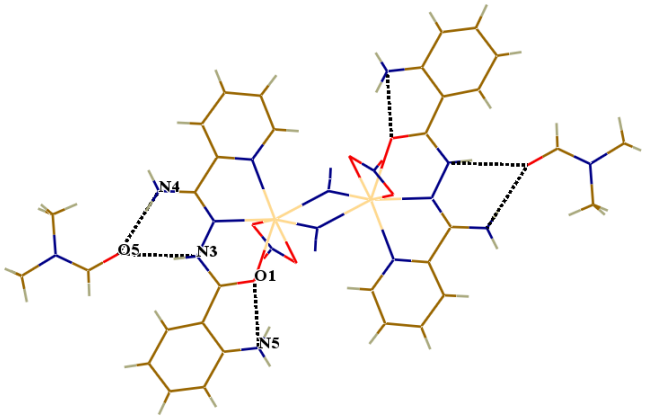

Figure 11. Hydrogen bonding in complex [Cd(**1a**)(NO_3)(N_3)]·DMF (**5**).

In crystal engineering a general query arises whether molecular conformation determines the crystal packing or the crystal packing dictates the molecular conformation.[18] However, it has been consistently observed that N_I and N_{AD} are both hydrogen bonded to the same acceptor in metal complexes bearing hydrazonamide (**1a**) form of the ligand. As a result, typically two types of supramolecular motifs are observed: (i) $R_2^1(7)$ motif with N_I, N_{AD} as hydrogen bond donors and one N, O or Cl atom from other molecule as the acceptor, which is more common, (ii) a larger motif $R_2^2(9)$ possessing more than one hydrogen bond acceptor. From investigation of the crystal packing of metal (Ni^{2+}, Zn^{2+} and Cd^{2+}) complexes of hydrazonamide form (**1a**) the former motif [$R_2^1(7)$] is observed in metal complexes **1**, **2**, **3** and **5** while the other larger motif [$R_2^2(9)$] is found only in complex [Cd(**1a**)$_2$(NO_3)]NO_3 (**4**).

2. 2. 1. 2. Crystal structure description of metal complexes of 1a′

The bis-chelated metal complex [Co(**1a′**)$_2$]NO_3·$5H_2O$ (**6**) (Figure 13) adopt a distorted octahedral geometry similar to [Ni(**1a**)$_2$]Cl_2·$2H_2O$ (**1**) with $(N_A)_2(N_P)_2(O_E)_2$ coordination environment. In complex **6**, the chelate bite angles lie in the range of 81.0(1)–82.1(1)° and the *trans* angle O_E–Co–N_P deviates largely from linearity by ~16.6(1)°. The bite angles are greater by 4.5(2)–5.1(1)° than observed in complex **1**. The trans angle $O_{E/A}$–M–N_P in the crystal structure of complex **6** shows deviation from linearity by ~ 13.8° while for complex **1**,

the deviation is much higher ~26.5°. These deviations in angle are manifestations of more flexibility in the hydrazonamide form than in the hydrazonate form.

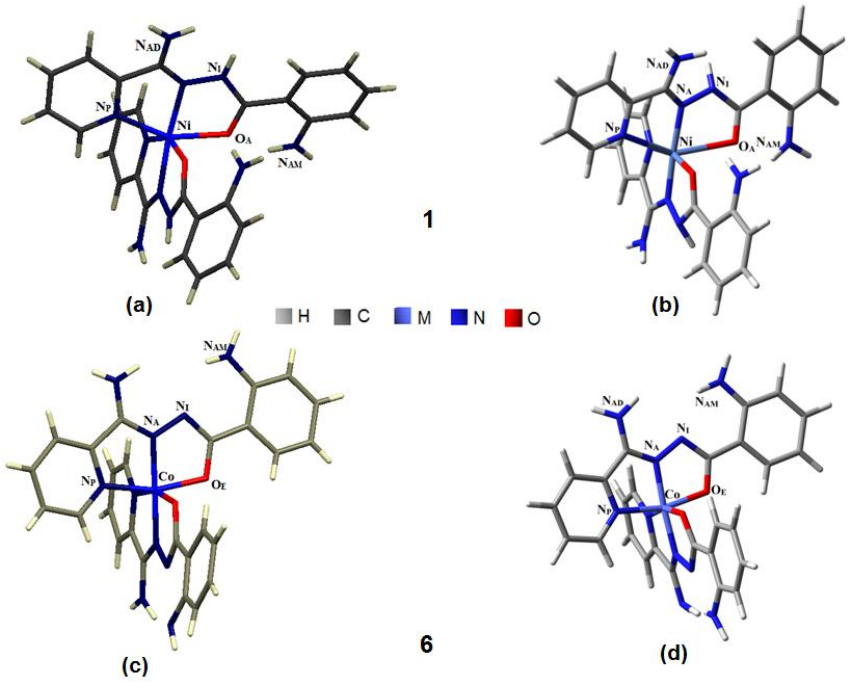

Figure 12. (a) Crystal structure of complex [Ni(**1a**)$_2$]Cl$_2$.2H$_2$O (**1**). (b) Optimised gas phase geometry of complex **1** obtained at B3LYP/ 6-31(d,p) level; (c) Crystal structure of complex [Co(**1a′**)$_2$]NO$_3$·5H$_2$O (**6**). (d) Optimised gas phase geometry of complex **6** obtained at B3LYP/ 6-31(d,p) level.

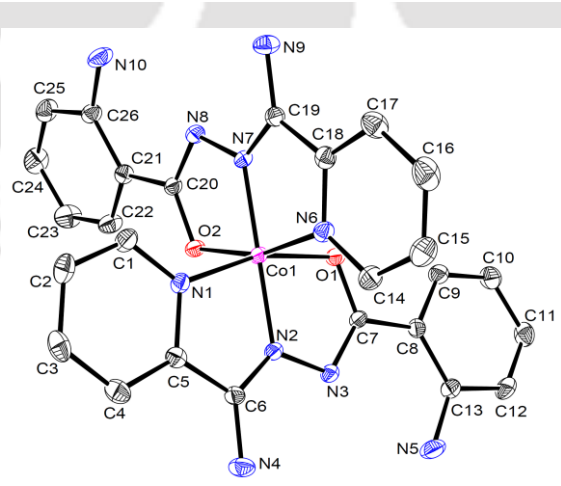

Figure 13. *ORTEP* diagram of **6**, displacement ellipsoids are drawn on 30% probability level and hydrogen atoms are removed for clarity.

In complex [Co(**1a′**)$_2$]NO$_3$·5H$_2$O (**6**), N_I has one lone-pair of electron which act as an intraligand hydrogen bond accepter with N_{AM} which is located marginally closer than N_{AD}

(Figure 14a). Intraligand N5−H5B···N3 (N3···N5, 2.716(4) Å, N3···H5B, 2.07 Å, N5−H5B···N3, 126.74(4)°) and N10−H10B···N8 (N8···N10, 2.697(5) Å, N8···H10B, 2.05 Å, N10−H10B···N8, 129.85(3)°) interactions are indeed observed. Both N_{AM} and N_{AD} groups are involved in inter-molecular hydrogen bonding interaction with O_E (N9···O1 and N4···O2) and nitrate oxygen (N9···O4 and N4···O4). Interaction of N_{AM} with water (N5···O9 and N10···O7) generates a chain along the *b* axis (Figure 14a). This chain is inter-linked to a 3D-hydrogen bonded network structure including a hexameric $(O6O7O10)_2$ ring of water molecules which is connected to O3 of nitrate by O8···O9 bridge (Figure 14b). The intermolecular O···O distances in the hexameric ring fall in the range of 2.709(6)−2.911(8) Å.

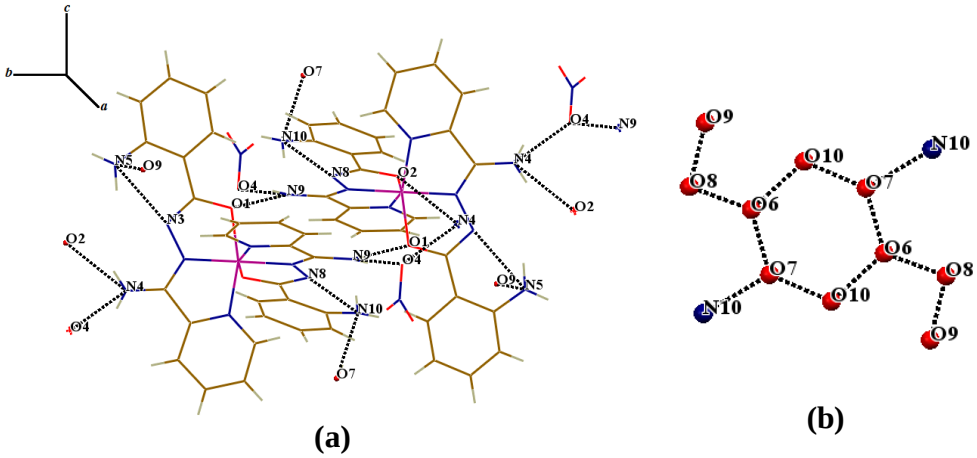

Figure 14. (a) Hydrogen bonding in complex **6** viewed along *bc* plane. (b) Hexameric water cluster in complex **6**.

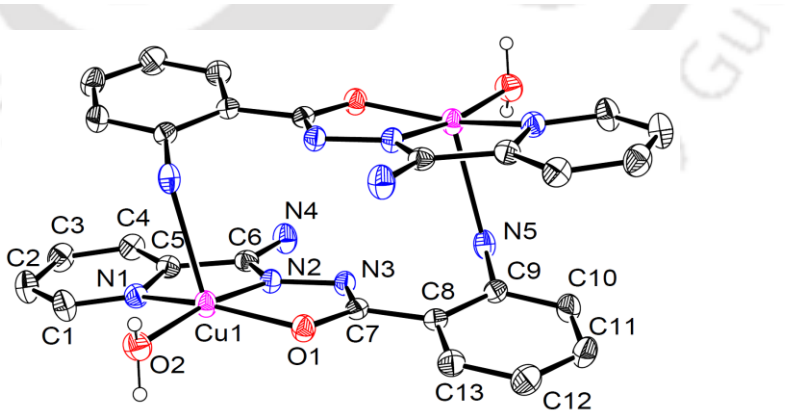

Figure 15. *ORTEP* diagram of **7**, displacement ellipsoids are drawn on 30% probability level and hydrogen atoms except those attached with O2 are removed for clarity.

The molecular structures of both $[Cu_2(\mathbf{1a'})_2(H_2O)_2](NO_3)_2{\cdot}3H_2O$ (**7**) and $[Cu_2(\mathbf{1a'})_2(NCS)_2]{\cdot}2DMF$ (**8**) show that the ligand is bound in its mono-anionic **1a′** form to

Cu(II) by using O_E, N_A and N_P. The fourth coordination site is occupied by a water molecule in **7** and nitrogen atom of the thiocyanate ion in **8**. Thus N_{AM} of one [Cu(**1a′**)(**L**)] (**L** = H_2O in **7** and NCS^- in **8**) unit coordinates to the copper centre of another at an axial site resulting in a dimeric $[Cu(\mathbf{1a'})(\mathbf{L})]_2$ unit, in which the metal centre having a distorted square-pyramidal geometry (Figure 15 and 17a). A centre of symmetry is present at the centre of Cu_2N_2 unit and two distinctive monomeric units are disposed in opposite fashion thus conserving centro symmetry. The relevant bond parameters for complex **7** and **8** are included in table 9.

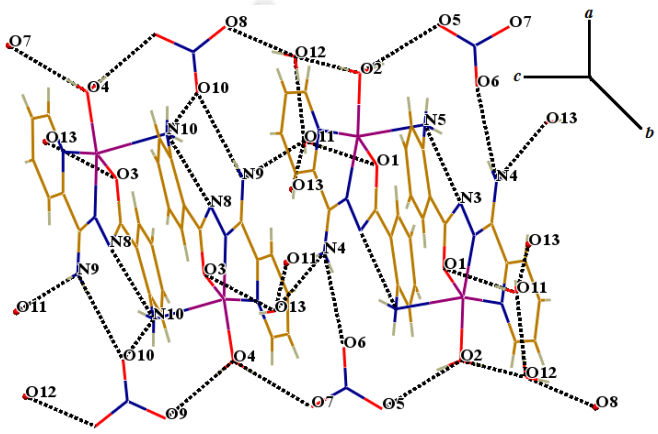

Figure 16. Hydrogen bonding in complex **7** viewed along *ac* plane.

An inspection on bond lengths reveals that $Cu–N_A < Cu–O_W < Cu–O_E < Cu–N_P$ in **7** and $Cu–N_A < Cu–N_T < Cu–O_E < Cu–N_P$ in **8**. Hence in both complexes the O_E behaves as weaker donor than water oxygen in **7** and thiocyanate nitrogen in **8**. The apical nitrogen is situated far away from the copper centre compared to other donor atom, the distances lie near the upper limit of $Cu^{II}–N$ bond length. Two Cu(II) ions are located at a distance of 5.699(7) Å (in **7**) and 6.005(1) Å (in **8**), which is unusually high for a true dinuclear copper complex. The dimeric units, nitrate ion and lattice water molecules are involved in hydrogen bonding interactions. Notably, N_{AM} acts as an intraligand hydrogen bond donor to deprotonated N_I (N5···N3 and N10···N8). Also N_{AM} (N10) is hydrogen-bonded with O10 of nitrate ions. The interactions among N_{AD} and nitrate ion exist as N4···O6 and N9···O10, moreover both N_{AD} are doubly hydrogen bonded with lattice water molecules (N4···O13 and N9···O11). The coordinated water donates to oxygen atoms (O7 and O9) from two nitrate ions and O_E also interacts with water oxygen (O13). These dimeric units are interlinked to form a 2D layered structure by hydrogen bonding interactions among nitrate oxygen (O5, O7, O8 and O9), coordinated (O2) and lattice (O11, O12 and O13) water molecules as shown in Figure 16.

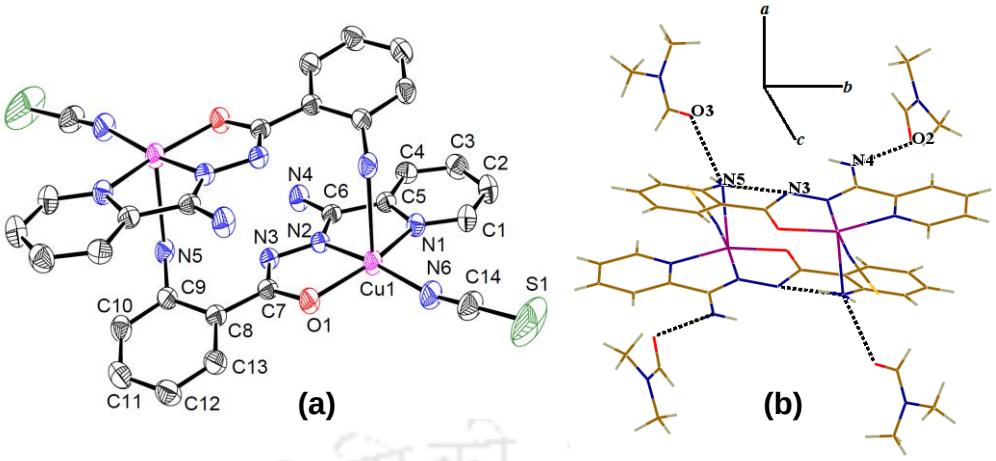

Figure 17. (a) *ORTEP* diagram of **8**, displacement ellipsoids are drawn on 30% probability level and hydrogen atoms are removed for clarity; (b) Hydrogen bonding in complex **8**.

In complex **8**, an intramolecular hydrogen bonding interaction between N_{AM} and N_I (Figure 17b) is present (N5···N3, 2.710(5) Å, H5B···N3, 2.10 Å and N5−H5B···N3, 127.99(2)°). Also both N_{AD} and N_{AM} groups are involved in intermolecular hydrogen bonding with the oxygen atom of DMF molecule; N5···O3, 2.930(8) Å and N4···O2, 2.879(6) Å (Figure 17b). In all metal complexes having hydrazonate (**1a′**) form *viz.* **6**, 7 and **8**, N_{AM} and N_{AD} are hydrogen bonded to different acceptors while the deprotonated N_I does not take part in intermolecular interactions.

No common supramolecular motif is observed in metal complexes of **1a′** form *i.e.* complexes **6**, **7** and **8** unlike found in most complexes of **1a** form. Thus, it can be inferred that molecular conformation can influence crystal packing in some cases but it is not always the case. However, analyses of crystal packing of **1-8** revealed that crystal packing does not determine molecular conformation in these complexes. The hydrazonamide form (**1a**) of the ligand is observed (Scheme 3) in metal complexes **1-5** and the hydrazonate form is present in complexes **6-8**. An inspection on C−$O_{A/E}$ and C−N_I bond lengths in complexes **1-8** reveals the following: (i) metal complexes having hydrazonate (**1a′**) form show a longer C–O_E bond length while those having hydrazonamide (**1a**) form exhibit a shorter C–O_A bond length, thereby suggesting the single bond character in C–O_E and double bond character in C–O_A.[19] (ii) A reverse trend is indeed observed in C–N_I bond lengths in complexes of **1a** and **1a′**. Metal complexes which possess the hydrazonamide form (**1a**) have C−O_A and C−N_I bond lengths respectively in the range of 1.240(4)−1.259(4) Å and 1.343(4)−1.366(3) Å. This supports double bond character in C−O_A and a single bond character in C−N_I. In contrast,

$C-O_E$ and $C-N_I$ bond lengths in metal complexes **6**, **7** and **8** lie in the range of 1.293(5)−1.323(3) Å and 1.316(3)−1.323(4) Å. Thus the $C-O_{E/A}$ and $C-N_I$ bond length values of **1a** and **1a′** in their metal complexes indicate '–C(=O)−NH− versus –C(O^-)=N' *i.e.* hydrazonamide (**1a**) versus hydrazonate (**1a′**) tautomerism. The $C-O_{E/A}$ and $C-N_I$ bond length variation in metal complexes **1-8** along with earlier discussed conformation variation in two tautomeric forms *viz.* **1a** and **1a′** suggest the metal ion coordination induced tautomeric polymorphism.

2. 2. 1. 3. Crystal structure description of metal complexes of 1b

Central Zn(II) ion of the complex [Zn(**1b**)Cl_2] (**9**) has distorted trigonal bipyramidal coordination geometry similar to that observed in **2** and **3**, though calculated τ value 0.54 is inconclusive (Figure 18a). The bond lengths and bond angles involving the metal centre are close to those found in complex **2**. Useful bond distances and bond angles in complex 9 are listed in Table 6. A zigzag chain is assembled through intermolecular hydrogen bonding interaction N4···N5 (3.06(1)Å) (Figure 18b).

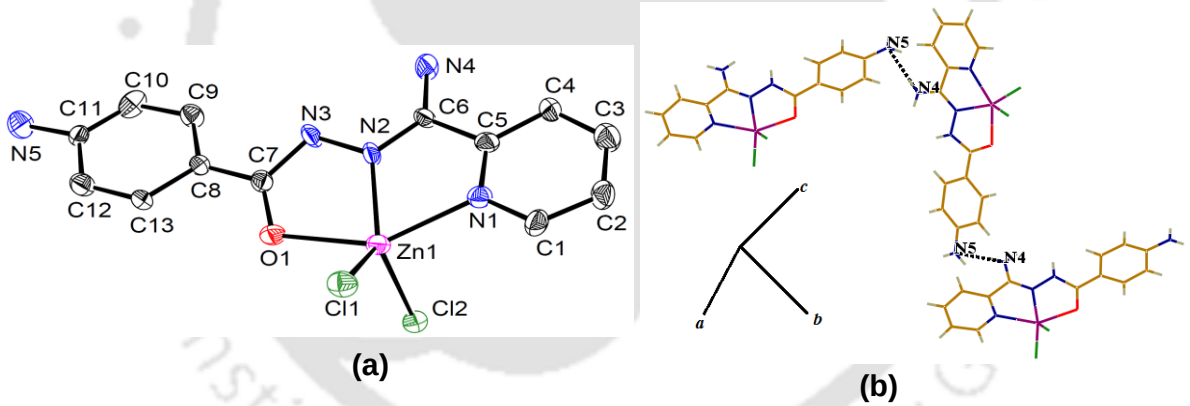

Figure 18. (a) *ORTEP* diagram of [Zn(**1b**)Cl_2] (**9**), displacement ellipsoids are drawn on 30% probability level and hydrogen atoms except H3 are removed for clarity. (b) Hydrogen bonding in complex [Zn(**1b**)Cl_2] (**9**).

A zigzag chain is assembled through intermolecular hydrogen bonding interaction between N_{AM} and N_{AD}; N4···N5, 3.06(1) Å (Figure 18b). In complex [Cd(**1b**)(**1b′**)(H_2O)](NO_3)$_2$·H_2O (**10**) {**1b′**=4-aminobenzhydrazide}, one of the ligand is coordinated to Cd(II) centre while the other is hydrolysed to a hydrazide unit (**1b′**) during the course of the reaction (Scheme 4).

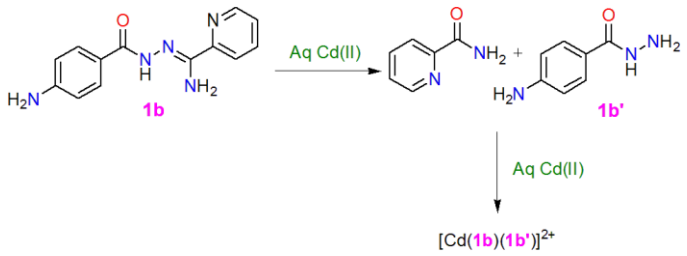

Scheme 4. Plausible pathway of formation of **10**.

Thus, the metal center is coordinated by ligand **1b** in its neutral tridentate hydrazonamide form, a bidentate chelating ligand **1b′**, a molecule of water and a nitrogen atom of the *p*-amino group from **1b′** that is coordinated to the neighbouring Cd(II) ion as shown in Figure 19. The *hepta* coordination in complex **10** imparts distorted pentagonal bipyramidal geometry around the metal ion. The basal plane consists of N_P, N_A, O_A (from **1b**), hydrazide-N, hydrazide-O (from **1b′**) and the axial positions are occupied by O_W (oxygen atom of water) and nitrogen (N8) from *p*-amino of **1b′** (Scheme 4) bound to neighbouring Cd(II) ion, thus bridging to the coordination polymer (Figure 19). In complex **10**, bite angles restrictions of ligand **1b** [67.65(9)–68.0(1)°] is more severe than open chain hydrazide ligand **1b′** [70.21(9)°]. All relevant bond parameters are listed in Table 10. The coordinated water molecule acts as a double hydrogen bond donor to both the lattice nitrate ions (O3···O4, 2.881(4) Å; O3···O7, 2.811(4) Å). The nitrogen atom from the hydrazide group is hydrogen bonded (N7···O10, 2.892(4) Å) to the lattice water molecule. The C−O_A and C−N_I bond lengths are respectively in the range of 1.236(4)−1.236(8) Å and 1.362(4)−1.374(8) Å in complex **9** and **10** in which ligand **1b** is found only in its hydrazonamide tautomeric form. The C−O_A and C−N_I bond length values in **9** and **10** are indeed similar to the respective values found in metal complexes of hydrazonamide form of the former ligand (**1a**).

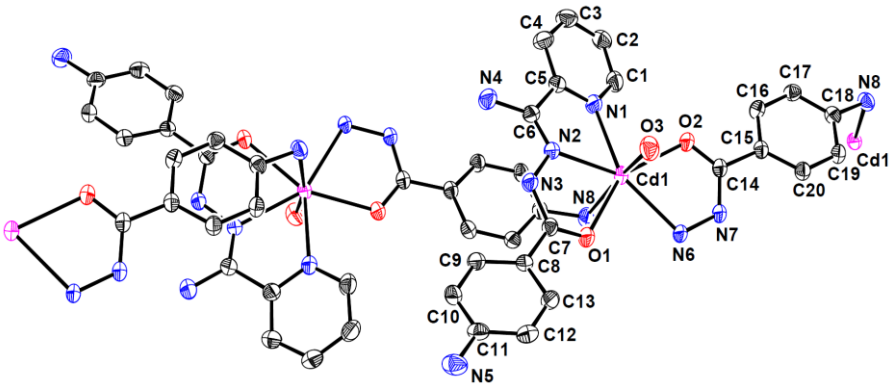

Figure 19. *ORTEP* diagram of **10**, displacement ellipsoids are on 30% probability level.

2. 2. 2. 1. Computational Studies

a) Evidence of conformational tautomerism in complexes of 1a from DFT study

Comparison of C−O_A and C−N_I bond lengths of optimised gas phase geometries of ligand **1a** and its metal complexes (**1**-**8**) with their crystal geometries revealed that the C−$O_{A/E}$ bond lengths in gas phase structure closely resemble the values obtained from their crystal structure. In contrary, the C−N_I bond lengths differ in crystal and gas phase geometries by ~ 0.02−0.05 Å in all metal complexes except **7** and **8** (Table 13). The C−O_A and C−N_I bond lengths in metal complexes of **1b**, which is found only in the hydrazonamide tautomeric form are consistent with the respective bond lengths (Table 13) found in metal complexes of hydrazonamide form of the ligand (**1a**).

Table 13. Bond length (Å) and N_I–C–C–C_{AM} and $O_{A/E}$–C–C–C_{AM} torsion angle (°) variation in ligand framework of **1a** and **1b** in crystal and gas phase DFT optimised structure

Compound	C–$O_{A/E}$	C–N_I	N_I–C–C–C_{AM}	$O_{A/E}$–C–C–C_{AM}
1a	1.243(3)	1.351(5)	-135.2(3)	46.2(3)
	1.231	*1.382*	*-153.51*	*23.75*
	1.235(7)	1.339(5)	-156.3(2)	24.5(4)
	1.230	*1.390*	*-159.69*	*21.19*
1	1.251(3)	1.360(4)	149.8(3)	-27.5(4)
	1.274	*1.400*	*-169.18*	*11.48*
	1.259(4)	1.351(3)	160.0(2)	22.4(4)
	1.241	*1.410*	*165.85*	*-14.65*
2	1.246(7)	1.345(6)	168.6(5)	-12.2(8)
	1.239	*1.404*	*165.87*	*-14.20*
3	1.245(3)	1.366(3)	-167.1(2)	13.6(4)
	1.240	*1.390*	*-166.75*	*15.09*
4	1.240(4)	1.343(4)	-135.9(4)	42.7(6)
	1.242	*1.403*	*-156.75*	*22.85*
	1.241(4)	1.351(7)	148.2(4)	-34.4(6)
	1.244	*1.400*	*157.22*	*-22.70*
5	1.247(3)	1.356(4)	161.9(3)	-17.0(4)
	1.237	*1.396*	*-150.51*	*27.84*
6	1.323(4)	1.320(5)	-7.5(5)	171.4(3)
	1.310	*1.344*	*-1.57*	*178.26*
	1.322(4)	1.322(4)	-9.1(5)	171.0(3)
	1.311	*1.344*	-9.08	*170.87*

7	1.303(3)	1.323(4)	-11.8(4)	170.0(3)
	1.298	*1.325*	*48.88*	*160.92*
	1.310(3)	1.317(4)	-12.5(4)	169.7(3)
	1.302	*1.321*	*42.95*	*-140.25*
8	1.293(5)	1.322(5)	15.7(6)	-167.6(4)
	1.283	*1.337*	*-33.17*	*149.65*
9	1.236(8)	1.374(8)		
	1.231	*1.402*		
10	1.236(4)	1.362(4)		
	1.252	*1.409*		

The values in italics denote corresponding parameters in optimised gas phase geometries.

The *syn* / *anti* orientation of N_{AM} with respect to N_I can be inferred from the values of N_I–C–C–C_{AM} and $O_{E/A}$–C–C–C_{AM} torsion angles (Table 13). Two different trends are witnessed in free ligand **1a** and its complexes **1-8**: (i) the free ligand and complexes of hydrazonamide form (**1a**) have N_I–C–C–C_{AM} torsion angle in the range 135.2(3)–168.6(5)° in crystal structures and 150.51−165.87° in the optimised gas phase structures implying that C–N_I and C–N_{AM} are oriented *anti* to accommodate intramolecular $N_{AM}\cdots O_A$ hydrogen bond. (ii) In complexes of hydrazonate (**1a′**) form, the *o*-amino group and N_I are oriented *syn* to each other resulting in the formation of an intramolecular $N_I\cdots N_{AM}$ hydrogen bond. The N_I–C–C–C_{AM} torsion angle lies in the range of 7.5(5)−15.7(6)° in crystal structures of complexes **6**, **7** and **8**, while the corresponding value in the optimised gas phase structure is in the range of 1.57−48.88°. The values of relevant bond lengths and bond distances in crystal and optimised gas phase geometry are not always in close conformity but the trends have always been maintained. The reason for this variation may be attributed to the absence of other hydrogen bond donors / acceptors *viz.* solvent molecules or counter anions in gas phase. Similar deviation in corresponding dihedral angle values in crystal and optimised gas phase structure has been reported earlier.[20]

b) Natural bond orbital (NBO) analysis of metal complexes (1-8)

NBO analyses of complex **1-8** and ligand **1a** show the following trends: (i) Electron charge density transfer from lone pair of amide oxygen (O_A) to an empty antibonding N_{AM}–H orbital takes place in free ligand and in the metal complexes of hydrazonamide (tautomeric form **1a**). (ii) Charge transfer occurs from the lone pair of imino nitrogen (N_I) to an empty antibonding N_{AM}–H orbital in metal complexes of tautomeric form **1a′**. (iii) A near perfect '*syn*' alignment of C–N_{AM} and C=O results in better charge transfer compared to slight higher values of O_A–C–C–C_{AM} in **1a**.

Table 14. NBO analyses of metal complexes of ligand **1a**

Molecule	Donor→ Acceptor	Second Order Perturbation Energy $E^{(2)}$ in kcal/mol
1a	lp O_A→ N_{AM}–H*	10.16
	lp O_A→ N_{AM}–H*	2.72
1	lp O_A→ N_{AM}–H*	2.41
	lp O_A→ N_{AM}–H*	1.86
2	lp O_A→ N_{AM}–H*	3.13
3	lp O_A→ N_{AM}–H*	3.07
4	lp O_A→ N_{AM}–H*	2.95
	lp O_A→ N_{AM}–H*	2.94
5	lp O_A→ N_{AM}–H*	3.19
6	lp N_I→ N_{AM}–H*	6.05
	lp N_I→ N_{AM}–H*	5.76
7	lp N_I→ N_{AM}–H*	2.24
8	lp N_I→ N_{AM}–H*	4.09

c) Potential energy surface analysis via scan of O–C–C–C_{AM} dihedral angle in 1a and 1a′

Potential energy surface analysis through relaxed scan of O_A−C−C−C_{AM} dihedral angle confirms the preferred *syn* orientation of O_A and N_{AM} (Figure 20) in hydraozonamide form (**1a**). The local minimum at 160° corresponds to the rotameric form **1a′′** (Scheme 3) which has considerable higher energy than rotameric form **1a**. Figure 20 reveals that the structure with *syn* orientation of N_I and N_{AM} is preferred in the hydrazonate form (**1a′**) and the global minimum exists at 170° value of O_E−C−C−C_{AM} dihedral angle. It also shows a local minimum which has *syn* orientation of O_E and N_{AM} with O_E−C−C−C_{AM} dihedral angle being 10°. The local minimum is higher in energy than the global minimum by a very small difference of 0.094 kcal/ mol.

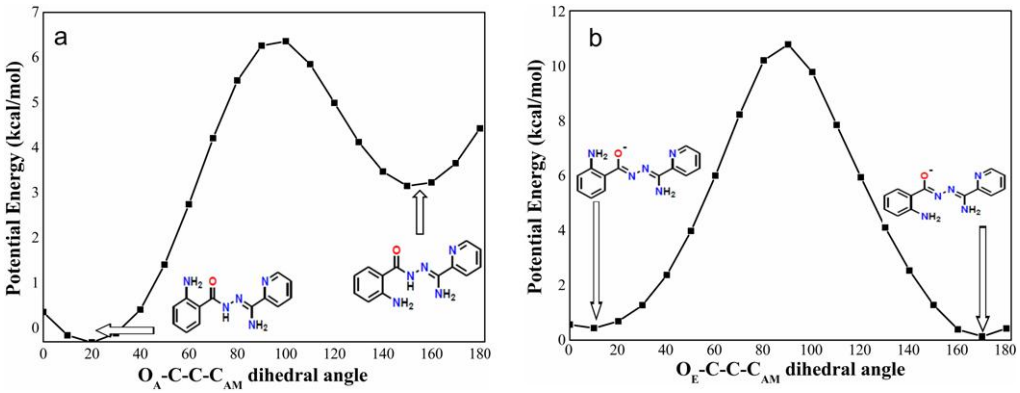

Figure 20. Potential energy is plotted against dihedral angle $O_{A/E}$−C−C−C_{AM} in **1a** and **1a′**

2. 2. 2. 2. Spectroscopic evidence of intramolecular hydrogen bond and tautomerism

The existence of an intramolecular N−H···O hydrogen bond in hydrazonamide form (**1a**) can be revealed from ^{1}H NMR. The signal for amidine NH_2 (N_{AD}) appears at around δ 6.85 ppm for both the ligands **1a** and **1b**. On the other hand, the signal for the amino group on the phenyl ring (N_{AM}) is significantly upfield shifted (Δδ ≈ 0.51 ppm) in **1a** (Figure 21) owing to its involvement in intramolecular but not in intermolecular hydrogen bonding. On the other hand, the amino group of **1b** is involved in intermolecular hydrogen bonding which is weakened in DMSO d_6 solution resulting in ligand molecules to remain in the single state. Similar upfield shift due to intramolecular interaction has been reported earlier.[15a]

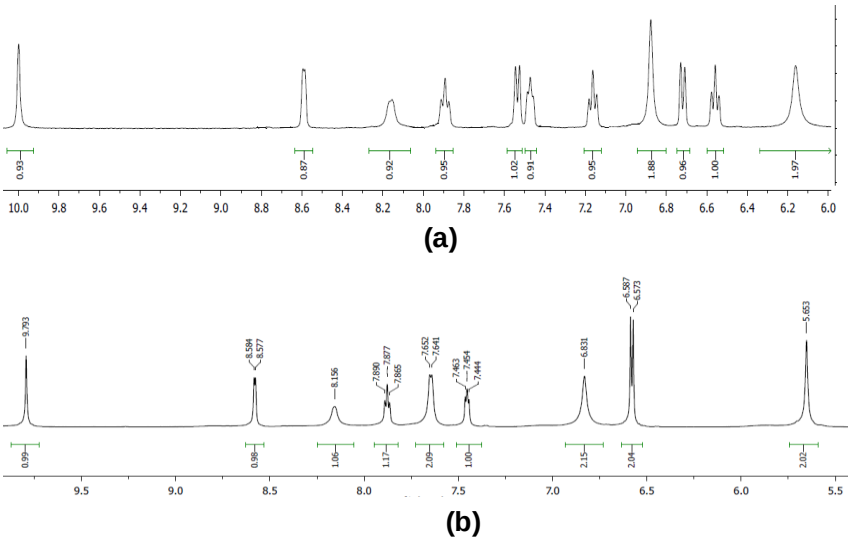

Figure 21. ^{1}H NMR spectra of ligands **1a** and **1b** in DMSO d_6.

Fluorescence behaviour of ligand **1a** and complexes **1-8** in methanolic solution at room temperature has been studied. The emission peaks exhibited by complexes **1-8** are not shifted significantly from ligand emission peak at 435 nm, which suggests the existence of intraligand charge transfer (Figure 22). It has been observed that all complexes of hydrazonamide (**1a**) form except complex **1** show increased emission compared to the free ligand. This increase in fluorescence intensity in metal complexes of hydrazonamide form (**1a**) might be due to enhanced rigidity of the ligand framework due to chelation, thereby reducing energy loss via radiationless decay through an intraligand photo-induced electron transfer (PET) process.[21]

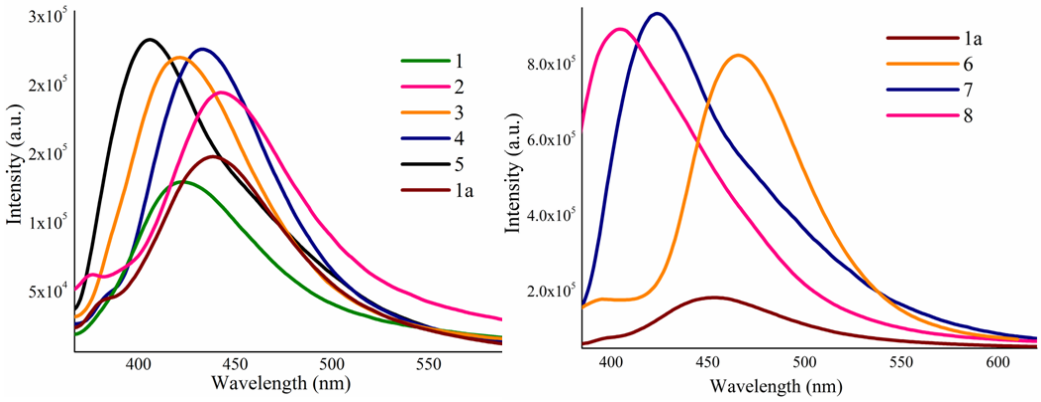

Figure 22. Fluorescence spectra of **1a** and complexes **1-8**, 10^{-5} M concentration for all compounds.

It is pertinent to note that complex **6**, **7** and **8** show significantly stronger emission than free ligand **1a**, which is due to the presence of more conjugated hydrazonte form **1a′**. In contrast, the intensity of emission in metal complexes possessing hydrazonamide (**1a**) form is not remarkably enhanced compared to the free lignd. Thus less conjugated hydrazonamide (**1a**) to a more conjugated hydrazonate (**1a′**) tautomerisation can be predicted by fluorescence spectroscopy as well.

2. 3. Conclusion

In summary, we have demonstrated a metal ion induced tautomerism and consequent change in conformation of the tautomers due to intramolecular hydrogen bonding interactions of a hydrazonamide ligand in the solid state. This system is an interesting illustration of rare 'tautomeric polymorpism'. This work describes a new build-up approach to witness an unstable tautomeric form of an organic molecule in the solid state. As many organic compounds have potential to act as coordinating ligand, this strategy could be of significant use to visualise an unstable tautomer in the solid state. Furthermore, considering diverse biological activity exhibited by hydrazonamide ligands and their metal complexes, a systematic study of molecular conformation and tautomerism of one of these compounds will be of significant importance.

2. 4. Experimental Section

2. 4. 1. Crystal growth, diffraction data collection and structure solution

Single crystals of complexes **1-10** and ligand **1a** were grown by slow evaporation from different common organic solvents (methanol, ethanol and DMF) or a mixture of solvents (methanol / DMF or methanol / acetonitrile / DMF) at room temperature. X-ray crystallographic data were collected using a Bruker SMART APEX-CCD diffractometer and Agilent Supernova diffractometer with Mo-Kα radiation (λ= 0.71073 Å). The intensity data were corrected by Lorentz and polarisation effects and empirical absorption corrections were made using either SADABS or multi-scan method. All structures were solved by direct methods using SHELX-97. Non hydrogen atoms were refined anisotropically by full matrix least-squares on F^2, using SHEXL-97 and further refined using PLATON.[22a] All hydrogen atoms were included in the calculated positions and refined isotropically using a riding model except for the water of crystallization. The O−H hydrogen of lattice water in most cases could neither be added at calculated positions nor be located at ideal positions from FMAP due to

large O−H distances. Useful parameters for hydrogen bond and other non-covalent interactions were calculated using PARST program[22b] implemented in PLATON.

2. 4. 2. Computational methods

The optimised gas phase geometries were obtained by Becke's three parameter functional[23] (B3LYP) at 6-31G(d,p) level using crystal co-ordinates as starting geometry. Stuttgart-Dresden (SDD) pseudo potential was used for Cd atoms in complexes **4**, **5** and **10**. Gaussian09[24] and GaussView05[25] program packages were used for calculation and visualisation. The relaxed scan of O–C–C–C_{AM} dihedral angle for hydrazonamide and hydrazonate forms of ligand **1a** was performed at B3LYP/ 6-31G(d,p) level in the angle range 0-180° at 10° intervals. NBO 3.1 version[26] intrinsically implemented on Gaussian09 version was used for NBO analyses at the same level of theory used for geometry optimisation.

2. 4. 3. Syntheses procedure and characterisation data

2-Amino-benzoic acid (amino-pyridin-2-yl-methylene)-hydrazide (1a). 2-aminobenzhydrazide (0.943 g, 6.0 mmol) and 2-cyanopyridine (0.677 g, 6.5 mmol) were suspended in PEG 400 (1.3 mL) in an oven dried 25 mL round bottom flask. The reaction mixture was then heated in a preheated oil bath at 80 °C for 6 h. To the resultant golden yellow liquid was then added water (20 mL) to precipitate out yellow solid. To this precipitate was then added ethylacetate (50 mL) and stirred for additional 10 min. The organic layer was separated in a separating funnel, washed with water (2 x 5 mL). The separated organic layer was dried over anhydrous $MgSO_4$ and evaporated under vacuum. The yellow solid so obtained was purified over a column of basic alumina by eluting with EtOAc:hexane (3:7). Yield of (**1a**): 1.26 g (82%). 400 MHz ^{1}H NMR (δ): 6.16 (s, 2H), 6.56 (t, *J* = 7.4 Hz, 1H), 6.72 (d, *J* = 8 Hz, 1H), 6.88 (s, 2H), 7.16 (t, *J* = 7.6 Hz, 1H), 7.47 (t, *J* = 5.6 Hz, 1H), 7.54 (d, *J* = 7.6 Hz, 1H), 7.89 (t, *J* = 7.6 Hz, 1H), 8.16 (s, 1H), 8.59 (d, *J* = 3.6 Hz, 1H), 10.00 (s, 1H). 150 MHz ^{13}C NMR (δ): 114.69, 115.17, 116.06, 128.67, 131.73, 142.80, 142.85, 144.86, 145.33, 146.36, 149.40, 165.37. ESI-MS: *m/z* calcd. for $C_{13}H_{13}N_5O$ $(M+H)^+$ 256.118, found $(M+H)^+$ 256.122.

4-Amino-benzoic acid (amino-pyridin-2-yl-methylene)-hydrazide (1b). Ligand **1b** was synthesized following the aforementioned procedure but using 4-aminobenzhydrazide (0.943 g, 6.0 mmol) and 2-cyanopyridine (0.677 g, 6.5 mmol). Pale yellow crude solid was

purified through a basic alumina column eluting with 4:6 mixture of EtOAc:hexane. Yield of (**1b**): 0.995 g (65%). 600 MHz ^{1}H NMR (δ): 5.65 (s, 2H), 6.58 (d, *J* = 8.4 Hz, 2H), 6.83 (s, 2H), 7.45 (t, *J* = 6.0 Hz, 1H), 7.64 (d, *J* = 6.0 Hz, 2H), 7.88 (t, *J* = 7.2 Hz, 1H), 8.15 (s, 1H), 8.57 (d, *J* = 4.2 Hz, 1H), 9.79 (s, 1H). 150 MHz ^{13}C NMR (δ): 112.50, 120.53, 120.85, 124.44, 129.17, 136.78, 146.30, 148.00, 150.89, 151.69, 163.37. ESI-MS: *m/z* calcd. for ($C_{13}H_{13}N_5O$+H) 256.118, found $(M^+$+H$)^+$ 256.123.

[Ni(1a)$_2$]Cl$_2$·2H$_2$O (1). To a solution of ligand **1a** (51 mg, 0.20 mmol) in methanol (10 mL), was added solid $NiCl_2·6H_2O$ (24 mg, 0.10 mmol) and stirred for two hours. The resultant pale green solution was transferred to a 25 mL conical at room temperature and left for crystallisation. Green, prismatic crystals suitable for X-ray diffraction study were obtained after one week by slow evaporation. Yield: 63 mg (93%). *Anal*. calcd. for $C_{26}H_{30}N_{10}O_4Cl_2Ni$: C, 46.18%; H, 4.47%; N, 20.71%. Found: C, 46.10%; H, 4.42%; N, 20.50%. IR (KBr, cm^{-1}): 1681 (s), 1617 (m), 1580 (m), 1531 (s), 1465 (m), 1416 (m), 1382 (s), 1330 (s), 1256 (s), 1162 (s), 1081 (w), 800 (s), 752 (s), 667 (m). UV-Vis [λ_{max}(nm), (ε, M^{-1}cm^{-1}), DMSO solution]: 265 (16540), 325 (12155), 373 (18885), 398 (10385), 602 (13), 964(32). ESI-MS: *m/z* found (calcd.): [**1a** + H]$^+$ 256.10 (255.11); [^{58}Ni(**1a**-H)]$^+$ 312.01(312.04); [^{58}Ni(**1a**)(**1a**-H)]$^+$ 567.11 (567.15).

[Zn(1a)Cl$_2$]·2DMF (2). Upon addition of solid anhydrous $ZnCl_2$ (34 mg, 0.25 mmol) to stirred DMF solution of ligand **1b** (64 mg, 0.25 mmol), the colour of the solution intensified to golden yellow. The golden yellow solution was kept in a 25 mL conical at room temperature. Yellow coloured prismatic crystals were deposited after two weeks. Only small crystals of complex **2** could be obtained even after repeated attempts and thus data completeness is relatively low (93%). Yield: 100 mg (79%). *Anal*. calcd. for $C_{19}H_{27}N_7O_3Cl_2Zn$: C, 42.44%; H, 5.06%; N, 18.23%, Found: C, 42.31%; H, 5.00%; N, 18.10%. IR (KBr, cm^{-1}): 3376 (w), 3202 (w), 2963 (m), 1680 (m), 1638 (s), 1612 (s), 1593 (m), 1560 (m), 1536 (m), 1478 (s), 1424 (m), 1389 (s), 1337 (m), 1287 (s), 1260 (s), 1240 (s), 1183 (w), 1151 (w), 1109 (s), 1047 (m), 1017 (s), 983 (w), 857 (m), 798 (s), 757 (s), 744 (s), 718 (s), 673 (s), 637 (m), 578 (m), 550 (m). UV-Vis [λ_{max}(nm), (ε, M^{-1}cm^{-1}), DMSO solution]: 254 (8770), 322 (8835), 356 (10460), 390 (5020). ESI-MS: *m/z* found (calcd.): [**1a**$^+$+H] 256.10 (256.11); [^{64}Zn(**1a**)^{35}Cl]$^+$ 353.99 (354.01).

[Zn(1a)(OAc)$_2$] (3). To a stirred methanolic solution of **1a** (40 mg, 0.17 mmol), solid $Zn(OAc)_2·2H_2O$ (37 mg, 0.17 mmol) was added. A pale yellow precipitate deposited was

separated by filtration, dissolved in 5 mL of DMF and left in a 10 mL beaker for slow evaporation at room temperture. Bright golden yellow crystals of diffraction quality were collected after one month. Yield: 48 mg (64%). *Anal*. calcd. for $C_{17}H_{19}N_5O_5Zn$: C, 46.54%; H, 4.36%; N, 15.96%. Found: C, 46.40 %; H, 4.31%; N, 15.79%. IR (KBr, cm^{-1}): 3533 (s), 3404 (s), 3313 (s), 1687 (s), 1644 (m), 1617 (s), 1583 (s), 1553 (s), 1518 (s), 1480 (s), 1447 (m), 1426 (s), 1344 (m), 1297 (s), 1252 (s), 1167 (m) 1156 (s), 1118 (s), 1032 (m), 1015 (s), 896 (m), 797 (s), 784 (w), 749 (s), 667 (m), 651 (m), 638 (m), 548 (w), 522 (w), 483 (w). UV-Vis [λ_{max}(nm), (ε, $M^{-1}cm^{-1}$), DMSO solution]: 255 (2405), 378 (2370), 400 (1760). ESI-MS: *m/z* found (calcd.): [**1a**+H]$^+$ 256.07 (256.11); [^{64}Zn(**1a-H**)]$^+$ 317.98 (318.03).

[Cd(1a)$_2$(NO$_3$)]NO$_3$ (4). Crystalline $Cd(NO_3)_2{\cdot}4H_2O$ (31 mg, 0.10 mmol) was added to methanolic solution of ligand **1a** (48 mg, 0.19 mmol) in methanol (15 mL), the resulting bright yellow solution was stirred for 1h. The solution was left undisturbed in a 25 mL conical for crystallisation and long needle shaped yellow coloured crystals of complex **4** deposited after 4 days. Yield: 63 mg (85%). *Anal*. calcd. for $C_{26}H_{26}N_{12}O_8Cd$: C, 41.81%; H, 3.51%; N, 22.50%. Found: C, 41.68%; H, 3.43%; N, 22.33%. IR (KBr, cm^{-1}): 3365 (m) 3300 (w), 3243 (m), 3068 (w), 2923 (w), 2854 (w), 1680 (s), 1648 (w), 1619 (s), 1580 (s), 1532 (s), 1470 (s), 1413 (m), 1383 (s), 1328 (s), 1290 (w), 1257 (s), 1205 (w), 1163 (s), 1119 (w), 1082 (w), 1042 (w), 1007 (w), 978 (w), 919 (w), 800 (s), 751 (s), 723 (w), 667 (w), 635 (w). UV-Vis [λ_{max}(nm), (ε, $M^{-1}cm^{-1}$), DMSO solution]: 256 (18250), 337 (3980). ESI-MS: *m/z* found (calcd.): [**1a**$^+$+H]$^+$ 256.18 (256.11); [^{114}Cd(**1a**-H)]$^+$ 368.11 (368.01); [^{114}Cd(**1a**)(NO$_3$)]$^+$ 431.11 (431.00); [^{114}Cd(**1a**-H)(**1a**)]$^+$ 623.30 (623.12).

[Cd(1a)(NO$_3$)(N$_3$)]·DMF (5). Ligand **1a** (64 mg, 0.25 mmol) and NaN_3 (16 mg, 0.25 mmol) were dissolved together in a mixture containing MeOH (9 mL), MeCN (9 mL) and DMF (3 mL). To this stirred solution, crystalline $Cd(NO_3)_2{\cdot}4H_2O$ (77 mg, 0.25 mmol) and resultant pale yellow solution was kept for one week in 25 mL conical at room temperature, which produced colourless cubic crystals of **5**. Yield: 95 mg (75%). *Anal*. calcd. for $C_{29}H_{33}N_{19}O_9Cd_2$: C, 34.27%; H, 3.27%; N, 26.18%. Found: C, 34.18%; H, 3.22%; N, 26.11%. IR (KBr, cm^{-1}): 2034 (s), 1647 (s), 1609 (s), 1581 (s), 1513 (s), 1475 (s), 1437 (m), 1385 (s), 1288 (m), 1230 (s), 1166 (s), 1100 (w), 1083 (w), 1045 (w), 1026 (w), 995 (w), 924 (w), 824 (s), 791 (s), 752 (s), 740 (w), 711 (w), 689 (m), 668 (m), 636 (m), 568 (w), 531 (w). UV-Vis [λ_{max}(nm), (ε, $M^{-1}cm^{-1}$), DMSO solution]: 252 (15550), 332 (6985). ESI-MS: *m/z* found (calcd.): [**1a**+H]$^+$ 256.09 (256.11); [^{114}Cd(**1a**-H)]$^+$ 367.97 (368.01).

[Co(1a′)$_2$]NO$_3$·5H$_2$O (6). To a solution of **1a** (102 mg, 0.40 mmol) in methanol (10 mL), was added Co(NO$_3$)$_2$·6H$_2$O (63 mg, 0.211 mmol), the resultant deep red coloured solution was stirred for 1 h and transferred to a 25 mL conical flask and left undisturbed at room temperature for crystallisation. The dark reddish brown needle shaped crystals deposited after one week was collected by filtration. Yield of (**6**): 135 mg (92%). *Anal*. calcd. for $C_{26}H_{34}N_{11}O_{10}Co$: C, 43.40%; H, 4.76%; N, 21.41%. Found: C, 43.32%; H 4.70%; N 21.25%. IR (KBr, cm^{-1}): 3382(b), 1660 (s), 1612 (s), 1570 (w), 1560 (w), 1512 (w), 1490(w), 1474 (w), 1436 (w), 1384 (s), 1343 (w), 1323 (w), 1249 (w), 1192 (w), 1163 (w), 1123 (w), 1082 (w), 1019 (w), 825 (w), 777 (w), 751 (w), 707 (w), 695 (w). UV-Vis [λ_{max}(nm), (ε, M^{-1} cm^{-1}), DMSO solution]: 261(32220), 305 (22535), 383 (17510), 433 (21350), 796 (18). ESI-MS: *m/z* found (calcd.): [Co(**1a′**)$_2$]$^+$ 567.10 (568.14).

[Cu$_2$(1a′)$_2$(H$_2$O)$_2$](NO$_3$)$_2$·3H$_2$O (7). To a methanol solution (10 mL) of **1a** (50 mg, 0.20 mmol), crystalline Cu(NO$_3$)$_2$·3H$_2$O (48 mg, 0.2 mmol) was added and resulting dark green solution was stirred for 2 h. The dark green solution was kept in 25 mL conical and dark green crystals suitable for X-ray diffraction studies were collected after five days from the undisturbed solution. Yield: 76 mg (90%). *Anal*. calcd. for $C_{26}H_{34}N_{12}O_{13}Cu_2$: C, 36.75%; H, 4.03%; N, 19.78%. Found: C, 36.59%; H, 3.97%; N, 19.64% IR (KBr, cm^{-1}): 3439 (b), 1654 (s), 1610 (m), 1593 (m), 1572 (w), 1560 (w), 1519 (s), 1504 (w), 1478 (s), 1384 (s), 1289 (w), 1235 (w), 1154 (w), 1101 (w), 1023 (m), 994 (m), 825 (s), 797 (s), 748 (m), 724 (w), 694 (w), 648 (w). UV-Vis [λ_{max}(nm), (ε, M^{-1}cm^{-1}), DMSO solution]: 267 (15905), 377 (12490), 425 (11,645), 690 (240). ESI-MS: *m/z* found (calcd.): [^{63}Cu(**1a**-H)]$^+$ 316.99 (317.03). EPR (DMF solution, 298K): g_{av} = 2.14, A = 93G.

[Cu$_2$(1a′)$_2$(NCS)$_2$]·2DMF (8). To a methanolic (15 mL) solution of **1a** (50 mg, 0.2 mmol), solid Cu(NO$_3$)$_2$·3H$_2$O (48 mg, 0.2 mmol) and NaSCN (16 mg, 0.2 mmol) were added. After stirring for 1h, dark green precipitate deposited were separated by filtration and dried in vacuo over CaCl$_2$. The precipitate was dissolved in 5 mL DMF and kept at room temperature. Block shaped crystals of X-ray diffraction quality were obtained by slow evaporation of DMF solution after one week. Yield: 165 mg (92%). *Anal*. calcd. for $C_{34}H_{38}N_{14}O_4S_2Cu_2$: C, 45.48%; H, 4.27%; N, 21.84%. Found: C, 45.50%; H, 4.22%; N, 21.80%. IR (KBr, cm^{-1}): 2085 (s), 1667 (s), 1597 (m), 1572 (w), 1514 (s), 1494 (w), 1472 (m), 1406 (s), 1384 (s), 1286 (w), 1256 (w), 1198 (w), 1161 (m), 1124 (m), 1092 (w), 1072 (w), 1010 (m), 825 (m), 809 (s), 787 (s), 751 (s), 704 (m), 688 (w), 664 (m), 647 (w), 522 (w). UV-Vis [λ_{max}(nm), (ε,

$M^{-1}cm^{-1}$), DMSO solution]: 252 (24370), 308 (16445), 362 (18260), 390 (16100), 409 (16080), 672 (105). ESI-MS: *m/z* found (calcd.): $[^{63}Cu(\mathbf{1a}\text{-}H)]^+$ 317.01 (317.04). EPR (DMF solution, 298K): g_{av} = 2.33, A = 190 G.

[Zn(1b)Cl$_2$] (9). Upon addition of solid $ZnCl_2$ (34 mg, 0.25 mmol) to a stirred DMF (5 mL) solution of ligand **1b** (64 mg, 0.25 mmol), the solution colour changed to golden yellow. This solution was transferred to a 10 mL conical, from which golden yellow coloured prismatic crystals deposited after two weeks. Yield: 88mg (90%). Anal calcd. for $C_{13}H_{13}N_5OCl_2Zn$: C, 39.87%; H, 3.35%; N, 17.88%. Found: C, 39.75%; H, 3.30%; N, 17.79%. IR (KBr, cm^{-1}): 3435 (m), 3333 (m), 3219 (m), 1683 (s), 1597 (m), 1503 (s), 1411 (s), 1301 (s), 1185 (m), 1140 (w), 1015 (m), 853 (s), 788 (w), 696 (w), 631 (w), 515 (w), 469 (w). UV-Vis [λ_{max}(nm), (ε, $M^{-1}cm^{-1}$), DMSO solution]: 279 (6520), 306 (7035), 325 (sh. 8090), 354 (10585). ESI-MS: *m/z* found (calcd.): [**1b**+H]$^+$ 254.97 (255.11); $[^{64}Zn(\mathbf{1b})^{35}Cl]^+$ 355.14 (354.01).

[Cd(1b)(1b′)(H$_2$O)](NO$_3$)$_2$·H$_2$O (10). Crystalline $Cd(NO_3)_2{\cdot}4H_2O$ (31 mg, 0.10 mmol) was added to a stirred methanolic (20 mL) solution of ligand **1b** (51 mg, 0.20 mmol) yielding a bright yellow solution. After stirring for 30 min, acetonitrile (7 mL) was added and left undisturbed. The solution was then stirred for another 1 h and transferred to a 25 mL conical at room temperature. Long needle shaped yellow coloured crystals deposited after six days were collected. Yield: 55 mg (81%). *Anal*. calcd. for $C_{20}H_{26}N_{10}O_{10}Cd$: C, 35.38 %; H, 3.86%; N, 20.63%. Found: C, 35.31 %; H, 3.83%; N, 20.50%. IR (KBr, cm^{-1}): 3455 (m), 3361 (s), 3204 (s), 1680 (s), 1629 (s), 1566 (m), 1507 (m), 1414 (s), 1297 (s), 1181 (s), 1115 (w), 1043 (w), 1077 (w), 1011 (w), 966 (w), 904 (w), 840 (s), 790 (s), 738 (m), 678 (w), 622 (m), 552 (m), 506 (w). UV-Vis [λ_{max}(nm), (ε, $M^{-1}cm^{-1}$), DMSO solution]: 274 (20380), 329 (43110). ESI-MS: *m/z* found (calcd.): [due to protonated 4-(3-(pyridin-2-yl)-1H-1,2,4-triazol-5-yl)aniline formed from **1b**] 238.06 (238.11); $[^{112}Cd(\mathbf{1b}\text{-}H)]^+$ 365.94 (366.01); $[^{114}Cd(\mathbf{1b})(NO_3)]^+$ 430.90 (431.00).

2. 4. 4. Selected spectra

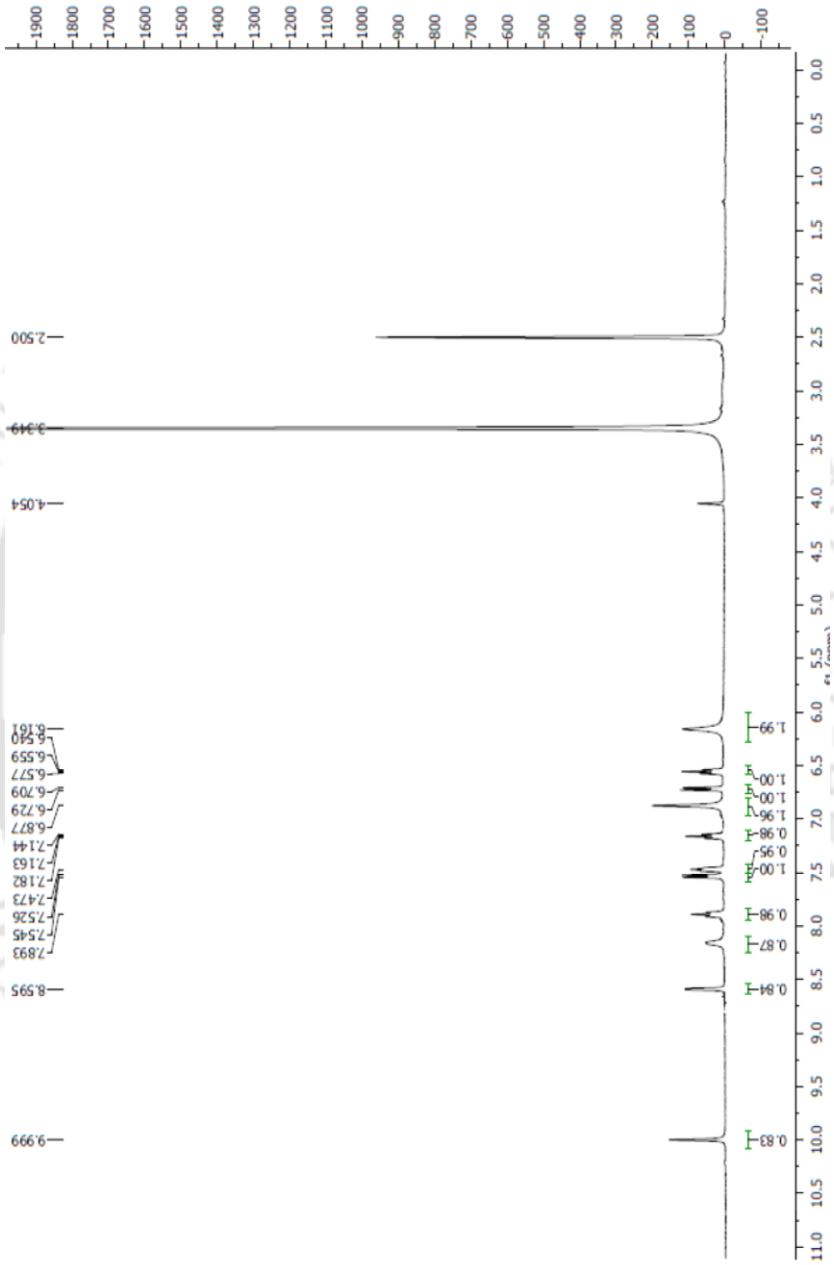

Spectrum 1. ^{1}H (400 MHz, DMSO d_6) NMR of **1a**

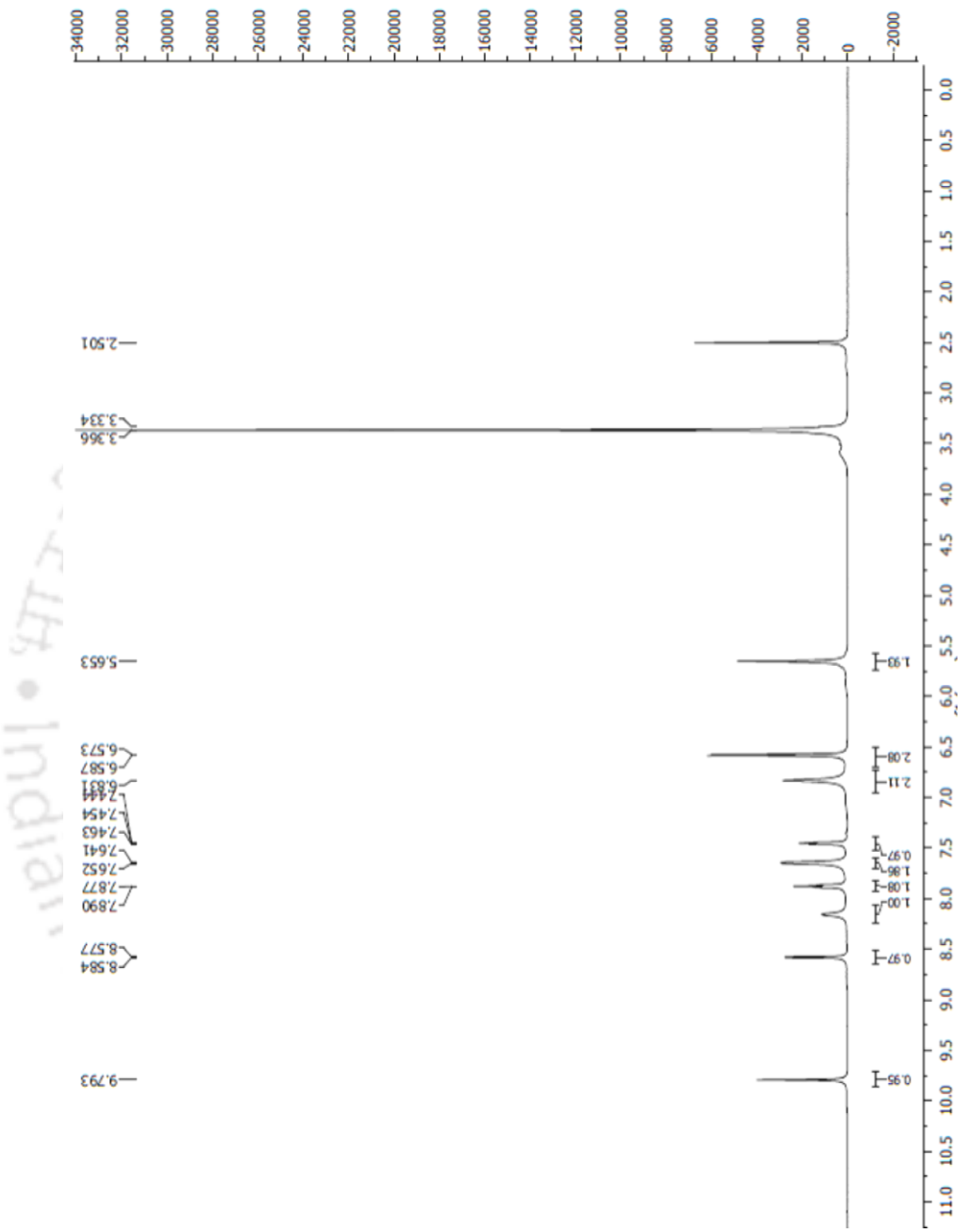

Spectrum 2. ^{1}H NMR (600 MHz, DMSO-d_6) of ligand **1b**

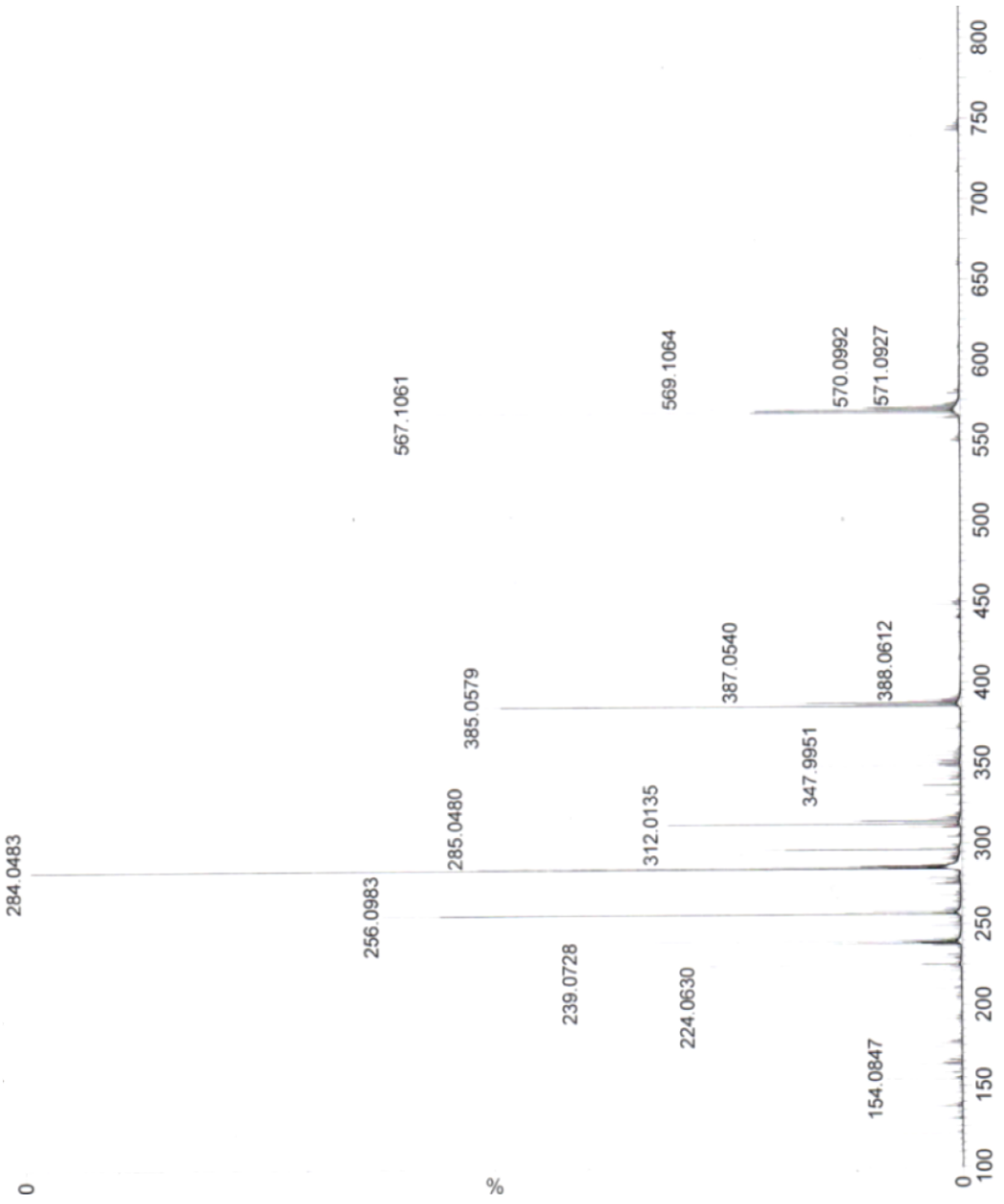

Spectrum 3. ESI-MS spectrum of complex [Ni(**1a**)$_2$]Cl$_2$·2H$_2$O (**1**)

Spectrum 4. ESI-MS spectrum of complex $[Cd(\mathbf{1a})_2(NO_3)]NO_3$ (**4**).

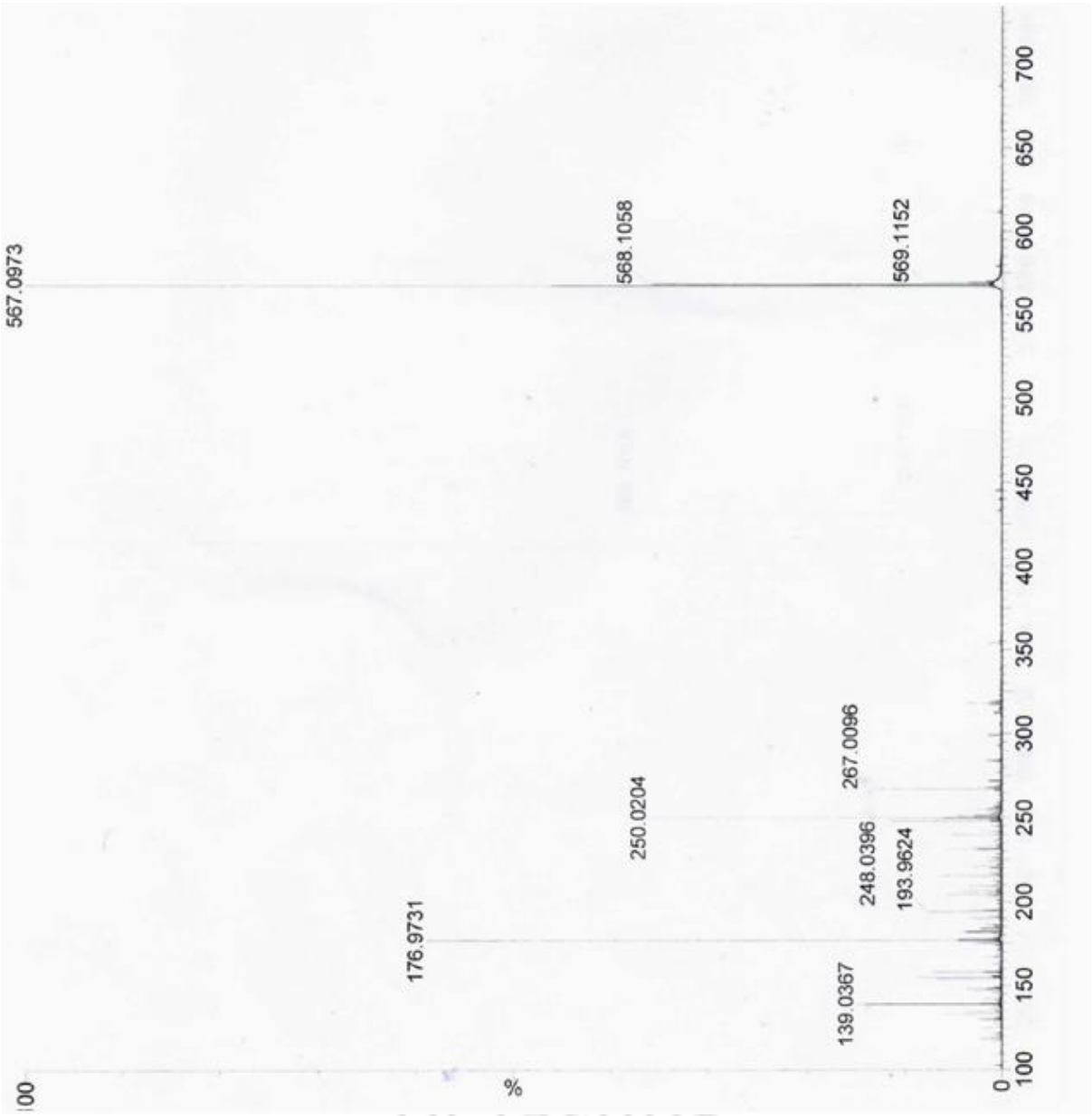

Spectrum 5. ESI-MS spectrum of complex $[Co(\mathbf{1a'})_2]NO_3{\cdot}5H_2O$ (**6**).

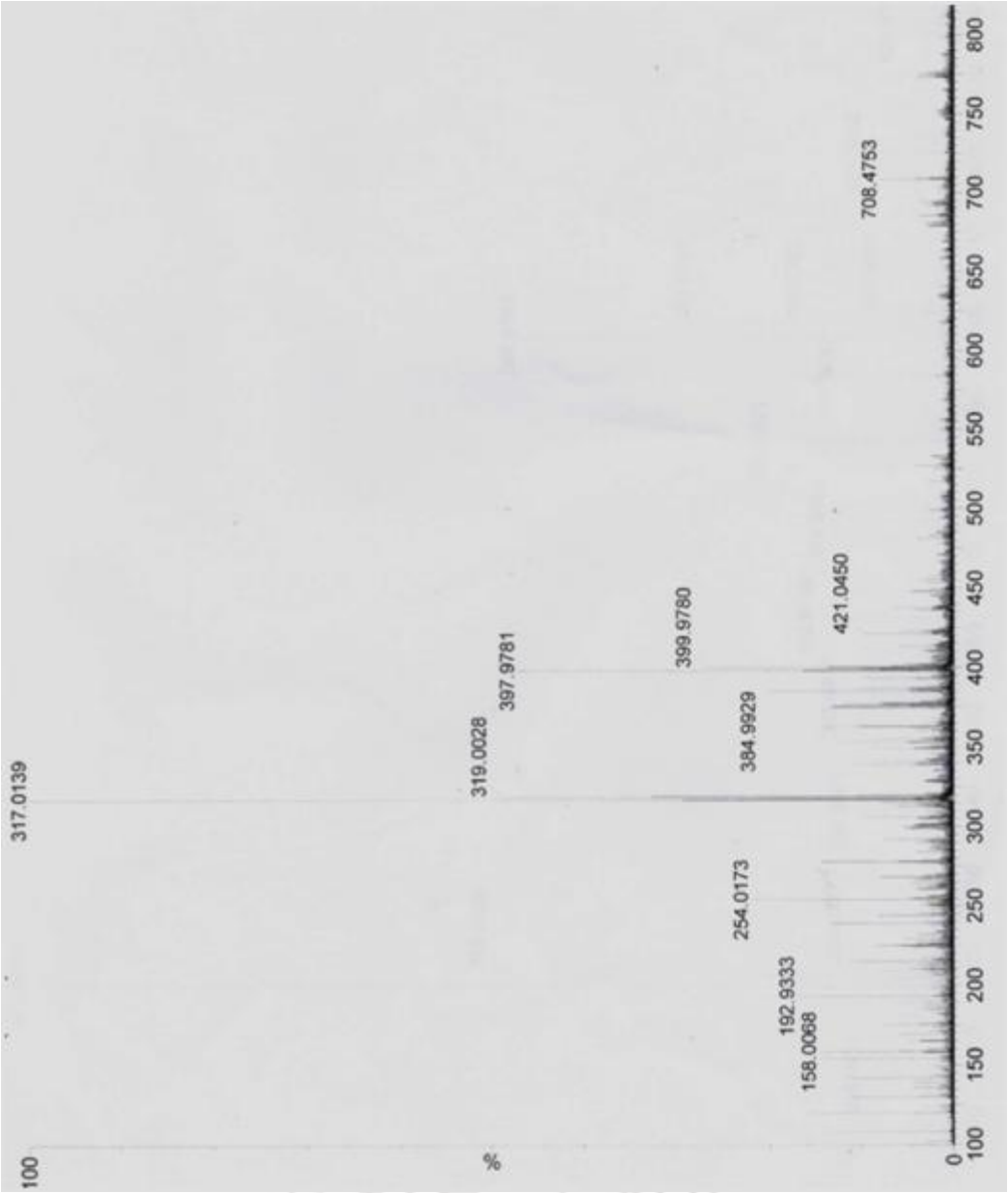

Spectrum 6. ESI-MS spectrum of complex $[Cu_2(\mathbf{1a'})_2(NCS)_2]\cdot 2DMF$ (**8**).

Reference

[1] Y. C. Martin, *J. Comput.-Aided Mol. Des*. **2009**, *23*, 693.

[2] (a) J. Elguero, A. R. Katritzky, O. V. Denisko, *in Advances in Heterocyclic Chemistry*, **2000**, vol. 76, pp. 1−84. (b) O. Martín, M. P. Torralba, M. Á. García, R. M. Claramunt, M. C. Torralba, M. R.Torres, I. Alkorta, J. Elguero, *ChemistrySelect* **2016**, *4*, 861.

[3] (a) W. A. Warr, *J. Comput.-Aided Mol. Des.* **2010**, 24, 497. (b) R. A. Sayle, *J. Comput. Aided Mol. Des*. **2010**, *24*, 485.

[4] A. J. Cruz-Cabeza, C. R. Groom, *CrystEngComm* **2011**, *13*, 93.

[5] (a) P. M. Bhatt, G. R. Desiraju, *Chem. Comm.* **2007**, 2057. (b) M. Mirmehrabi, S. Rohani, K. S. K. Murthy, B. Radatus, *J. Cryst. Growth* **2004**, *260*, 517. (c) A. J. Blake, X. Lin, M. Schroder, C. Wilson, R. X. Yuan, *Acta Crystallogr*. *Sect. C: Cryst. Struct. Commun*. **2004**, 60, o226–o228. (d) M. Bauer, R. K. Harris, R. C. Rao, D. C. Apperley, C. A. Rodger, J. *Chem. Soc. Perkin Trans.* **1998**, *2*, 475.

[6] (a) M. R. Chierotti, L. Ferrero, N. Garino, R. Gobetto, L. Pellegrino, D. Braga, F. Grepioni, L. Maini, *Chem. Eur. J.* **2010**, *16*, 4347. (b) M. U. Schimdt, J. Brüning, J. Glinnemann, M. W. Hützler, P. Mörschel, S. N. Ivashevskaya, J. Streek, D. Braga, L. Maini, M. R. Chierotti, R. Gobetto, *Angew. Chem. Int. Ed.* **2011**, *50*, 7924.

[7] S. Long, M. Zhang, P. Zhou, F. Yu, S. Parkin, T. Li, *Cryst. Growth Des.* **2016**, *16*, 2573.

[8] S. Tothadi, B. R. Bhogala, A. R. Gorantla, T. S. Thakur, R. K. R. Jetti, G. R. Desiraju, *Chem. Asian J*. **2012**, *7*, 330.

[9] L. M. Toledo, K. Musa, J. W. Lauher, F. W. Fowler, *Chem. Mater*. **1995**, *7*, 1639.

[10] (a) S. P. Thomas, S. P. K. P. Veccham, L. J. Farrugia, T. N. Guru Row, *Cryst. Growth Des*. **2015**, *15*, 2110; (b) S. P. Thomas, K. Shashiprabha, K. R. Vinutha, S. P. Nayak, K. Nagarajan, T. N. Guru Row, *Cryst. Growth Des.* **2014**, *14*, 3758.

[11] A. J. Cruz-Cabeza, A. Schreyer, W. R. Pitt, *J. Comput.-Aided Mol.Des*. **2010**, *24*, 575.

[12] K. Epa, C. B. Aakeröy, J. Desper, S. Rayat, K. L. Chandra, A. J. Cruz-Cabeza, *Chem. Commun.* **2013**, *49*, 7929.

[13] (a) M. Carcelli, P. Mazza, C. Pelizzi, G. Pelizzi, F. Zani, *J. Inorg. Biochem*. **1995**, *57*, 43; (b) P. B. Sreeja, M. R. P. Kurup, A. Kishore, C. Jasmin, *Polyhedron* **2004**, *23*, 575.

[14] D. J. Dijken, P. Kovaricek, S. P. Ihrig, S. Hecht, *J. Am. Chem. Soc.* **2015**, *137*, 14982.

[15] (a) P. Du, X. K. Jiang, Z. -T. Li, *Tetrahedron Lett.* **2009**, *50*, 316; (b) J. -L. Hou, X.-B. Shao, G. J. Chen, Y. X. Zhou, X. K. Jiang, Z. -T. Li, *J. Am. Chem. Soc.* **2004**, *126*, 12386; (d) C. Li, S. F. Ren, J. L. Hou, H. P. Yi, S. Z. Zhu, X. K. Jiang, Z. T. -Li, *Angew. Chem. Int. Ed.*

2005, *44*, 5725; (e) Y. Y. Zhu, J. Wu, C. Li, J. Zhu, J. L. Hou, C. Z. Li, X. K. Jiang and Z. -T. Li, *Cryst. Growth Des.* **2007**, *7*, 1490.

[16] (a) M. C. Etter, *J. Phys. Chem.* **1991**, *95*, 4601; (b) M. C. Etter, *Acc. Chem. Res.* **1990**, *23*, 120.

[17] (a) Md. B. Zaman, M. D. Smith, D. M. Ciurtin, H. C. Loye, *Inorg. Chem.* **2002**, *41*, 4895−4903; (b) Y. B. Dong, R. C. Layland, M. D. Smith, N. G. Pschirer, U. H. F. Bunz, H. C. Loye, *Inorg. Chem.* **1999**, *38*, 3056.

[18] W. H. Ojala, K. M. Lystad, T. L. Deal, J. E. Engebretson, J. M. Spude, B. Balidemaj, C. R. Ojala, *Cryst. Growth Des.* **2009**, *9*, 964.

[19] (a) A. Bacchi, M. Carcelli, M. Costa, A. Fochi, C. Monici, P. Pelagatti, C. Pelizzi, G. Pelizzi, L. M. S. Roca, *J. Organomet. Chem.* **2000**, *593*, 180; (b) T. Ghosh, S. Bhattacharya, A. Das, G. Mukherjee, M. G. B. Drew, *Inorg. Chim. Acta* **2005**, *358*, 989; (c) E. B. Seena, N. Mathew, M. Kuriakose, M. R. P. Kurup, *Polyhedron* **2008**, *27*, 1455; (d) B. Mondal, M. G. B. Drew, T. Ghosh, *Inorg. Chim. Acta* **2009**, *362*, 3303.

[20] P. Panini, T. P. Mohan, U. Gangwar, R. Sankolli, D. Chopra, *CrystEngComm* **2013**, *15*, 4549.

[21] S. L. Zheng, J. H. Yang, X. L. Yu, X. M. Chen, W. T. Wong, *Inorg. Chem.* **2004**, *43*, 830.

[22] (a) A. L. Spek, *Acta Cryst. D* **2009**, *65*, 148; (b) M. Nardelli, *J. Appl. Cryst.* **1995**, *28*, 659.

[23] (a) A. D. Becke, *J. Chem. Phys.* **1993**, *98*, 5648; (b) C. Lee, W. Yang, R. G. Parr, *Phys. Rev.* B **1988**, *37*, 785.

[24] Gaussian 09, M. J. Frisch, G. W. Trucks, J. R. Cheeseman, G. Scalmani, M. Caricato, H. P. Hratchian, X. Li, V. Barone, J. Bloino, G. Zheng, T. Vreven, J. A. Montgomery, Jr., G. A. Petersson, G. E. Scuseria, H. B. Schlegel, H. Nakatsuji, A. F. Izmaylov, R. L. Martin, J. L. Sonnenberg, J. E. Peralta, J. J. Heyd, E. Brothers, F. Ogliaro, M. Bearpark, M. A. Robb, B. Mennucci, K. N. Kudin, V. N. Staroverov, R. Kobayashi, J. Normand, A. Rendell, R. Gomperts, V. G. Zakrzewski, M. Hada, M. Ehara, K. Toyota, R. Fukuda, J. Hasegawa, M. Ishida, T. Nakajima, Y. Honda, O. Kitao and H. Nakai.

[25] GaussView, Version 5, Roy Dennington, Todd Keith, and John Millam, *Semichem Inc*., Shawnee Mission, KS, 2009.

[26] NBO Version 3.1, E. D. Glendening, A. E. Reed, J. E. Carpenter and F. Weinhold.

Chapter 3

Impact of Complementary Electronic Nature of C−X and M−X Halogens and Intramolecular X···O Interaction in Supramolecular Assemblies of Zn(II) Complexes of *O*-Halophenyl Substituted Hydrazides

The disparity in electronic nature of organic (C−X) and inorganic (M−X) halogen in supramolecular context has been demonstrated herein. Metal complexes [Zn(**hyd-X**)Cl_2].nDMF of three *o*-halophenyl substituted hydrazide based ligands **hyd-X** (hyd = hydrazide, X = F, Cl and Br) have been synthesised and characterised by single crystal XRD. C−X halogen atom in these complexes is involved either in intramolecular X···O interaction (when X = Cl/Br) or intramolecular N−H···X (when X = F) hydrogen bond. Supramolecular networks propagated via intermolecular C−X···N halogen bonds and N−H···X(M) hydrogen bonds are observed in crystal structures of the complexes. Intramolecular X···O interaction and intramolecular N−H···F hydrogen bond exert decisive roles in locking the molecular conformation in these compounds. DFT, AIM and NBO studies have been employed to acquire quantitative accounts of the halogen mediated non-covalent interactions.

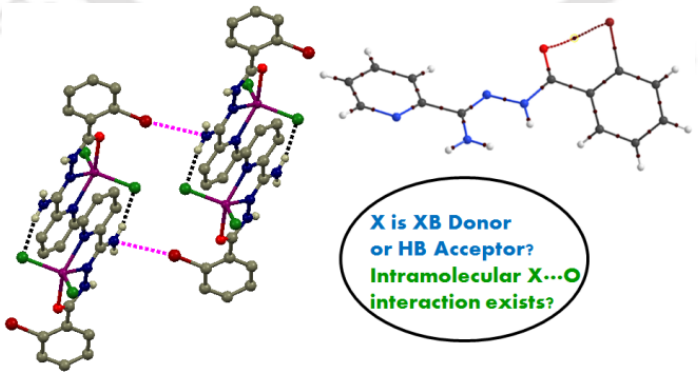

This work has been published in *CrystEngComm.* **2017**, *19*, 1607.

3. 1. Introduction

Halogen atoms are the most abundant peripheral atoms after hydrogen, which includes being the common substituent to a large number of biologically active organic compounds[1] as well as serving monodentate or bidentate bridging ligands to transition or main group metal complexes.[2] The charge cloud encompassing a halogen atom bonded to carbon is anisotropic in nature as C−X bond is comprised of the electrons on outermost surface of X. Consequent depletion of electronic charge on the surface of X atom results a positive electrostatic potential called σ-hole which contours the halogen atom. This σ-hole in turn is surrounded by a negative electrostatic potential forming a small negatively charged belt around the central part of the X atom.[3] The charge cloud surrounding the halogen atom of the C−X bond is anisotropic in nature and the positive electrostatic potential, known as the σ-hole contours the halogen atom. Owing to the simultaneous presence of both the halogen atom of C−X can act together as a Lewis acid and a Lewis base.[3] 'Halogen bond' or the electrostatic interaction between a nucleophile and the halogen atom of a C−X bond, are known for their high directionality and significant robustness.[4] Halogen bond and other weak interactions involving halogen atom have been exploited in designing metal organic framework,[5] liquid crystals,[6] pharmaceutical agents[7] and in material chemistry.[8] It has been reported that these interactions play decisive roles to determine molecular conformation,[9] polymorphism of solids[10] and *in situ* cryocrystallization of liquids.[11]

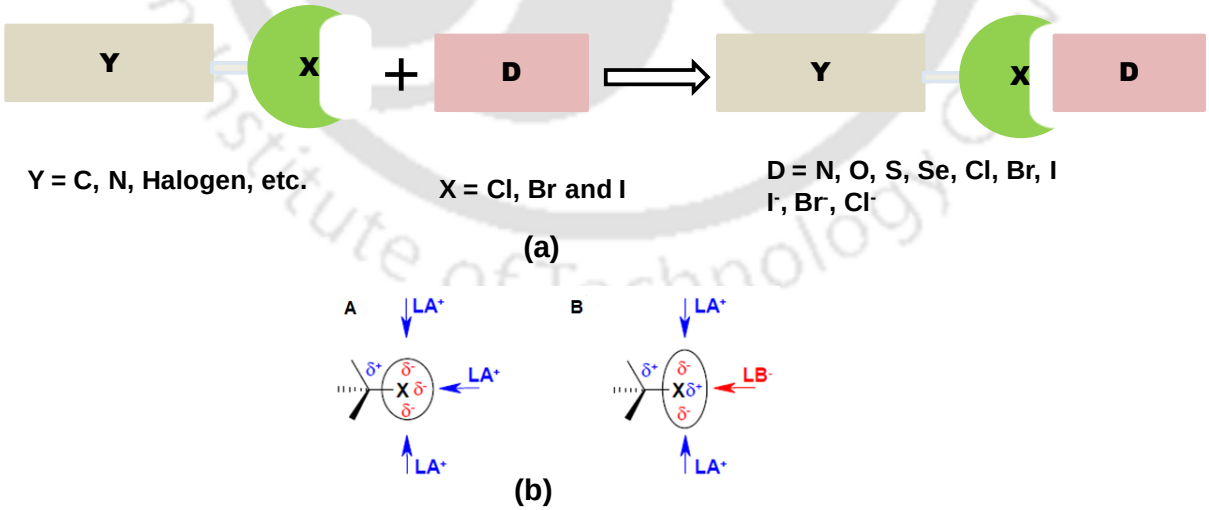

Scheme 1. (a) General scheme for the formation of halogen bond; (b) Anisotropy of electronic charge cloud around the halogen atom of C−X bond.

Intramolecular especially five or six membered N−H···X (X = F, Cl, Br) hydrogen bonds have been cited to exert prominent role on molecular conformation and supramolecular assemblies either in the presence or in the absence of any strong hydrogen bond.[12] Six membered intramolecular N−H···F interaction is the most remarkable amongst them as this has been utilized extensively in designing folding architectures of amides and hydrazides.[13] However, intramolecular halogen bond has not been studied as comprehensively as the intermolecular halogen bond or the intramolecular N−H···X hydrogen bond. This is due to the stringent requirement of linearity for the halogen bond which renders its presence within a molecular framework. So far only one example is reported in which the criterion of linear C−X···Nu arrangement was fulfilled within the molecular framework.[14] In the realm of hydrogen bonding interactions, a hydrogen bond constituting a six-membered ring is considered to be the most stable, amongst all the weak interactions, particularly when an aromatic ring current is delocalized over the hydrogen bonded ring.[15] This finding is of relevance to consider the possibility of an analogous five-membered halogen bonded ring stabilised by aromatic ring current. Computational studies carried out on 3-halopropenal[16] and perhalogenated ethanes[17] deem the possibility of such a robust, stabilizing five-membered intramolecular halogen bond interactions questionable. However, stabilizing five membered, intramolecular C−F···O interactions were reported for 2-fluoroflavonol[18a] and *o*-fluoro substituted benzoyl chlorides.[18b] Intramolecular C−F···O interactions in these molecules dictate the molecular conformation. In this regard, it should be mentioned that an analogous stabilizing intramolecular Br···S interaction has been reported earlier.[18c]

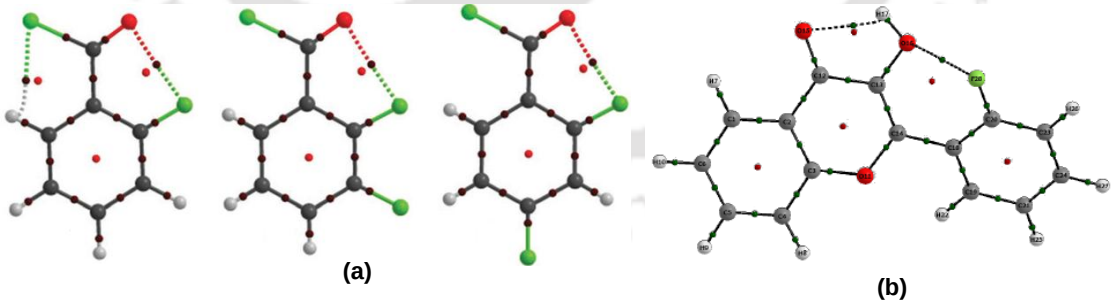

Scheme 2. Proof of intramolecular C−F···O−C interaction by AIM analyses, in (a) *Ortho* fluoro substituted bezoyl chlorides;[18b] (b) 2-fluoroflavonol.[18a]

Halogen substituted hydrazide or anilide systems have been considered to be one of the best choice to explore the regime of strong hydrogen bonds (N−H···O and O−H···O), intermolecular halogen bond, weak C−H···O, C−H···N, C−H···X (activated C−H) hydrogen

bonds especially C−H···F (organic fluorine) as well as intramolecular N−H···F interaction and the weakest interactions *i.e.* C−H···π, halogen···π and π···π.[19]

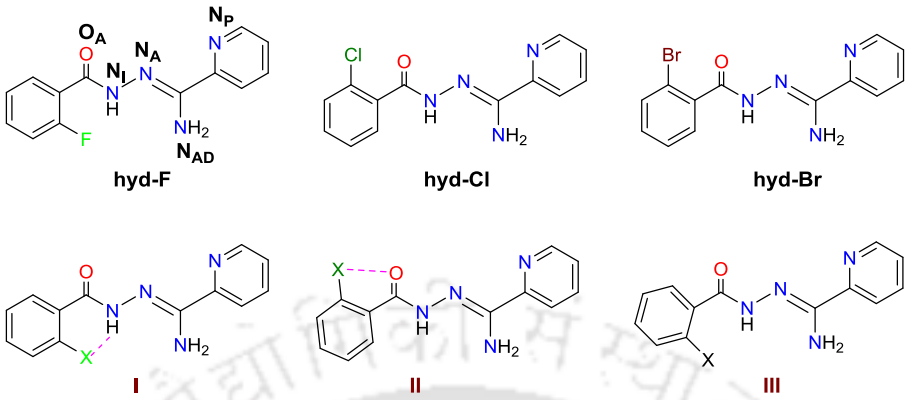

Scheme 3. Ligands used in the study and their conformational variants **I**, **II** and **III**.

Considering this fact, we have used three *o*-halophenyl substituted hydrazonamide ligands *viz.* 2-fluorobenzoic acid(amino-pyridin-2-yl-methylene)hydrazide (**hyd-F**), 2-chlorobenzoic acid(amino-pyridin-2-yl-methylene)hydrazide (**hyd-Cl**) and 2-bromobenzoic acid(amino-pyridin-2-yl-methylene)hydrazide (**hyd-Br**) in this study. Three conformational variants of these ligands have been observed either in the free form or in their zinc complexes (Scheme 3). In the conformational variant **I**, the dihedral angle N−C−C−C_X (13.4°) favours the existence of a six-membered intramolecular N−H···X hydrogen bond. A five-membered intramolecular O···X halogen bond can be viable in the conformational variant **II** as confirmed by O−C−C−C_X (≈ 44−45°). Another conformational variant **III** is also observed, in which the halogen atom stays apart from both the oxygen atom and the imine group and thus no intramolecular interaction of X is geometrically feasible. The conformational variant **I** was observed for only the ligand **hyd-F** in its zinc complex while the variant **II** is observed for ligand **hyd-Cl** and **hyd-Br** in the free form. This conformational disparity of *o*-fluoro substituted ligand has not been reckoned surprising as organic fluorine prefers hydrogen bond over halogen bond unlike other organic halogen.[20] Conformational variants **II** and **III** are present in their zinc complexes of ligand **hyd-Cl** and **hyd-Br**.

One of the most important aspects of supramolecular chemistry of the halogen is the marked difference between organic (C−X) and inorganic (M−X) halogen. This is caused by far greater polarity of M−X bond compared to C−X bond. While the charge clouds surrounding both the inorganic and organic halogen are anisotropic in nature, the degree of anisotropy in the first case is more pronounced.[21] Inorganic halogens are known to be

moderately strong hydrogen bond acceptor with their strength comparable to free chloride ion.[21a] The hydrogen bond acceptor property of inorganic halogen has been exploited earlier to construct N−H···X−M, N−H···X_2−M or O−H···X−M supramolecular synthons.[22] The systematic variation of Lewis acid nature of organic halogen and Lewis base nature of inorganic halogen has been successfully employed to design supramolecular architecture of metal complexes of halopyridines.[23] Keeping in line with this supramolecular synthetic strategy, we reacted the ligands **hyd-F**, **hyd-Cl** and **hyd-Br** with $ZnCl_2$ and have prepared metal complexes [Zn(**hyd-X**)Cl_2].nDMF (X = F, Cl, Br) (Scheme 4). The crystal packing of these complexes is dictated by the cooperation and competition between intermolecular C−X···N halogen bond and N−H···X−M hydrogen bond. We have changed the organic halogen from F to Br while the inorganic halogen is kept unaltered. This strategy helps to witness the impact of intermolecular C−X···N halogen bond in supramolecular assembly as well as rationally modify the crystal packing based on the hierarchy of weak interactions of the halogen.

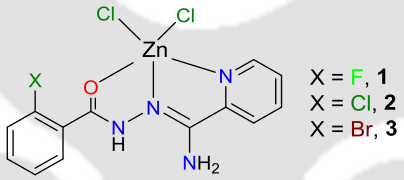

Scheme 4. Metal complexes [Zn(**Hyd-F**)Cl_2] (**1**), [Zn(**Hyd-Cl**)Cl_2] (**2**), [Zn(**Hyd-Br**)Cl_2] (**3**).

3. 2. Results and Discussion

3. 2. 1. Syntheses of ligands and complexes

The ligands **hyd-Cl** and **hyd-Br** were synthesized by heating equimolar mixture of *o*-halophenyl benzhydrazides with 2-cyanopyridine at 100 °C in PEG 400 medium (Scheme 5).

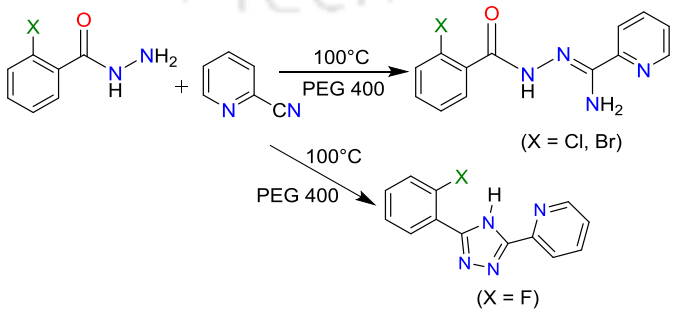

Scheme 5. Synthesis of ligands.

The same reaction conditions yielded *o*-halophenyl substituted 1,2,4-triazole which gets hydrolyzed and coordinated to Zn(II) centre upon reaction with $ZnCl_2$ (Scheme 6).The metal complexes [Zn(**hyd-X**)Cl_2].nDMF (X = Cl, Br) were prepared by reacting **hyd-Cl** and **hyd-Br** with anhydrous $ZnCl_2$ in DMF medium. These complexes have been well characterized by single crystal XRD, elemental analyses and ESI-MS spectra.

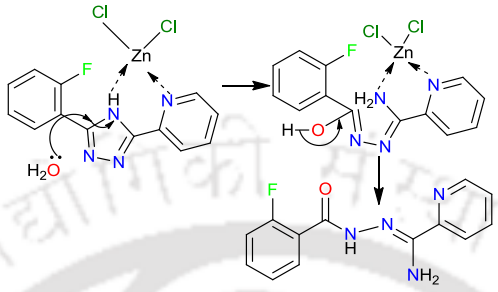

Scheme 6. Conversion of **trz-F** to **hyd-F**.

3. 2. 2. Description of Crystal structures

The structural and refinement parameters for complexes **1-3** and ligands **hyd-Cl**, **hyd-Br** have been included in Table 1. Figure 1 and 2 show the *ORTEPs* for all the compounds. These three ligands have multiple donor sites but they behave as a pincer type of tridentate ligand coordinating through O_A, N_A and N_P atoms. The ligands can exist in three conformational variants (**I**, **II** and **III**) as described earlier in Scheme 3. We have used the terms 'closed' to denote the variant **II** (conformation with intramolecular X···O contact) and 'open' to mention both the forms **I**, **III** (conformation without intramolecular X···O contact) throughout this text following the terminology used earlier for similar systems.[16] The salient features associated with supramolecular assembly of the complexes **1-3** and ligands **hyd-Cl**, **hyd-Br** include reproducibility of intramolecular X···O and intermolecular X···N halogen bond as well as N−H···X, C−H···X hydrogen bonds, and halogen···π interaction. The following conventions were used throughout the chapter for crystal structure description: O_A = hydrazide-O; N_P = pyridine-N; N_A = azomethine-N; N_I = imino-NH; N_{AM} = aromatic-NH_2; N_{AD} = amidine-NH_2.

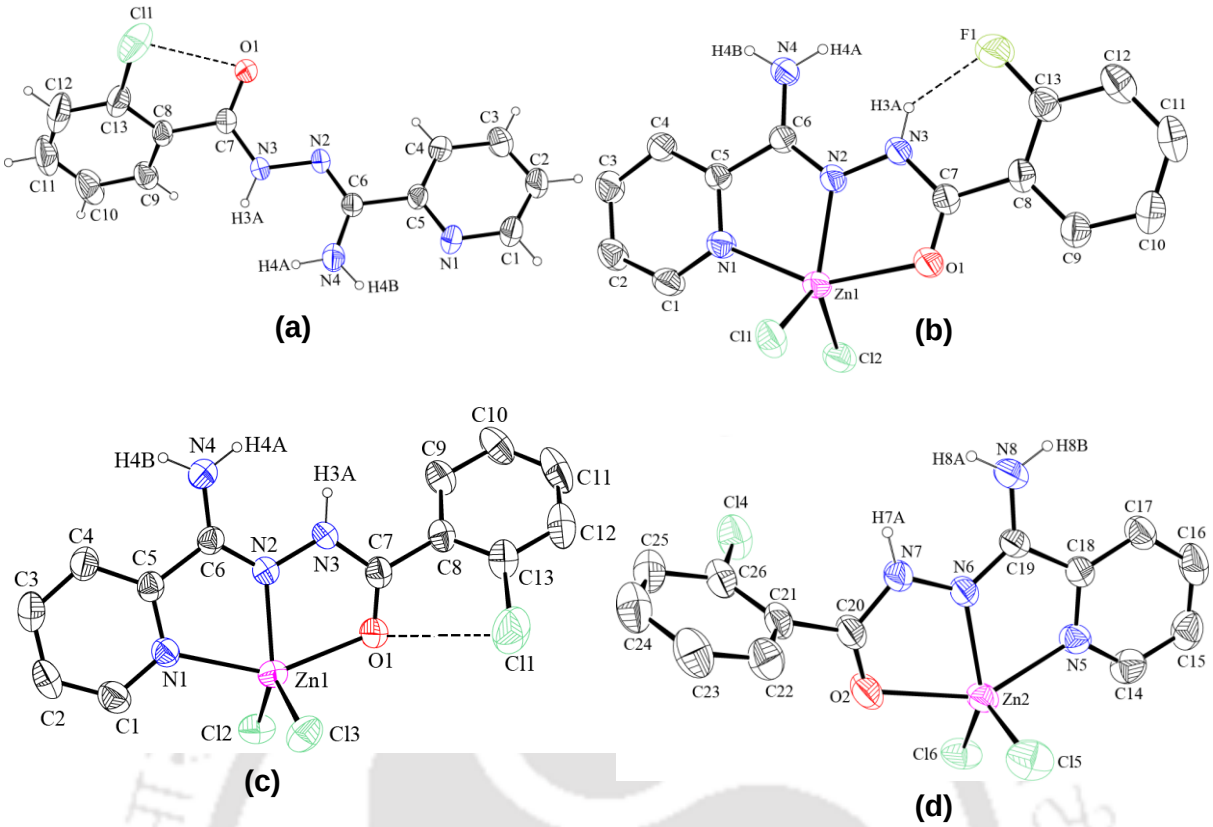

Figure 1. (a) *ORTEP* (40% probability) of ligand **hyd-Cl** showing conformation **II;** (b) *ORTEP* (40% probability) of complex **1** showing conformation **I**; (c) *ORTEP* (40% probability) of 'closed' complex molecule (conformation **II**) of complex **2**; (d) *ORTEP* (40% probability) of 'open' complex molecule (conformation I**II**) of complex **2**.

Table 1. Crystallographic and refinement parameters of ligand **hyd-Cl**, **hyd-Br** and complexes **1-3**

	hyd-Cl	**hyd-Br**	**1**
chem formula	$C_{13}H_{11}N_4OCl$	$C_{13}H_{11}N_4OBr$	$C_{13}H_{11}N_4OFZnCl_2$
formula wt	274.71	319.18	394.55
CCDC no	1519617	1519616	1519613
temp (K)	296	296	296
crystsyst	orthorhombic	orthorhombic	monoclinic
space group	*Pbca*	*Pbca*	$P2_1/n$
a (Å)	14.3577(10)	14.7684(10)	8.4436(3)
b (Å)	7.9468(6)	7.9893(4)	14.1669(5)
c (Å)	23.1682(14)	23.0430(11)	13.0108(4)
α (°)	90.00	90.00	90.00
β(°)	90.00	90.00	100.946(2)
γ(°)	90.00	90.00	90.00
V (Å^3)	2463.5(3)	2718.8(3)	1528.03(9)
Z	8	8	4
μ (mm^{-1})	0.286	3.021	1.972
ρ_{calcd}(g cm^{-3})	1.380	1.560	1.715
no. of unique rflns	2654	2785	3774
no. of rflns ($I \geq 2\sigma(I)$)	1516	1442	3044
R_1[a], wR_2[b] ($I \geq 2\sigma(I)$)	0.0618, 0.1350	0.0613, 0.1260	0.0276, 0.0717
R_1[a], wR_2[b] (all data)	0.1136, 0.1666	0.1191, 0.1490	0.0395, 0.0792
goodness of fit (F^2)	0.997	1.017	1.007
largest peak/hole (e Å^{-3})	0.237/-0.242	0.645/-0.623	0.299/-0.264
	2	**3**	
chem formula	$C_{16}H_{18}N_5O_2ZnCl_3$	$C_{16}H_{18}N5O_2Cl_2BrZn$	
formula wt	484.09	528.54	
CCDC no	1519614	1519615	
temp (K)	296	296	
crystsyst	monoclinic	monoclinic	
space group	$P2_1/c$	$P2_1/c$	
a (Å)	24.5875(9)	24.6067(13)	
b (Å)	9.1372(3)	9.1723(3)	
c (Å)	19.5598(7)	19.6072(14)	
α (°)	90.00	90.00	
β(°)	109.513(2)	110.211(7)	
γ(°)	90.00	90.00	
V (Å^3)	4141.9(3)	4166.4(4)	

Z	8	8
μ (mm^{-1})	1.594	3.374
ρ_{calcd}(g cm^{-3})	1.553	1.685
no. of unique rflns	10149	7727
no. of rflns ($I \geq 2\sigma(I)$)	5594	5231
R_1[a], wR_2[b] ($I \geq 2\sigma(I)$)	0.0423, 0.0991	0.0436, 0.0822
R_1[a], wR_2[b] (all data)	0.0948, 0.1127	0.0813, 0.0979
goodness of fit (F^2)	1.020	0.994
largest peak/hole (e Å^{-3})	0.422/-0.279	0.491/-0.567

Table 2. Relevant bond lengths (Å) and bond angles (°) in metal complex **1**

Zn1–O1	2.212(2)	N1–Zn1–N2	74.43(6)
Zn1–N1	2.159(2)	N2–Zn1–O1	72.97(6)
Zn1–N2	2.079(2)	N1–Zn1–O1	147.40(6)
Zn1–Cl1	2.250(6)	O1–Zn1–Cl1	97.86(4)
Zn1–Cl2	2.258(6)	O1–Zn1–Cl2	100.64(4)
		N1–Zn1–Cl1	99.29(5)
N1–Zn1–Cl2	97.27(5)	N2–Zn1–Cl2	122.69(5)
N2–Zn1–Cl1	123.08(5)	Cl1–Zn1–Cl2	114.23(2)

Table 3. Relevant bond lengths (Å) and bond angles (°) in metal complexes **2** and **3**

Complex **2**		Complex **3**	
Zn1−N1	2.222(3)	Zn1−N1	2.189(4)
Zn1−N2	2.070(3)	Zn1−N2	2.079(3)
Zn1−O1	2.250(3)	Zn1−O1	2.241(4)
Zn1−Cl2	2.231(9)	Zn1−Cl1	2.249(1)
Zn1−Cl3	2.262(9)	Zn1−Cl2	2.218(1)
Zn2−N5	2.198(3)	Zn2−N5	2.225(3)
Zn2−N6	2.078 (2)	Zn2−N6	2.086(4)
Zn2−O2	2.250(3)	Zn2−O2	2.256(4)
Zn2−Cl5	2.228(9)	Zn2−Cl3	2.260(1)
Zn2−Cl6	2.249(9)	Zn2−Cl4	2.221(1)
N1−Zn1−N2	73.71(9)	N1−Zn1−N2	73.5(1)
N1−Zn1−O1	147.25(9)	N1−Zn1−O1	145.5(1)
N2−Zn1−O1	73.60(9)	N2−Zn1−O1	73.1(1)
N1−Zn1−Cl2	98.78(7)	N1−Zn1−Cl1	99.9(1)
N1−Zn1−Cl3	99.40(7)	N1−Zn1−Cl2	100.1(1)
N2−Zn1−Cl2	125.33(7)	N2−Zn1−Cl1	132.4(1)
N2−Zn1−Cl3	116.31(7)	O1−Zn1−Cl1	96.1(1)
O1−Zn1−Cl2	98.42(6)	O1−Zn1−Cl2	98.6(1)

O1−Zn1−Cl3	96.62(6)	N2−Zn1−Cl1	132.4(1)
Cl2−Zn1−Cl3	118.33(4)	N2−Zn1−Cl2	108.9(1)
N5−Zn2−N6	73.8(1)	N5−Zn2−N6	73.7(1)
N5−Zn2−O2	146.1(1)	N5−Zn2−O2	146.8(1)
N6−Zn2−O2	73.29(9)	N6−Zn2−O2	73.3(1)
Cl5−Zn2−Cl6	118.84(4)	Cl3−Zn2−Cl4	118.03(5)
N5−Zn2−Cl5	100.08(8)	N5−Zn2−Cl3	100.09(9)
N6−Zn2−Cl5	108.83(7)	N6−Zn2−Cl3	115.2(1)
N5−Zn2−Cl6	99.27(7)	N5−Zn2−Cl4	98.47(9)
N6−Zn2−Cl6	132.26(7)	N6−Zn2−Cl4	126.7(1)
O2−Zn2−Cl5	98.03(7)	O2−Zn2−Cl3	96.66(9)
O2−Zn2−Cl6	96.68(7)	O2−Zn2−Cl4	98.58(9)

Table 4. Classical hydrogen bonding interactions in crystal structures of **hyd-Cl**, **hyd-Br** and complexes **1-3**

Compound	D−H···A	D···A (Å)	H···A (Å)	D−H···A(°)	Symmetry
hyd-Cl	N4−H4A···O1	2.886(3)	2.01	178	-x+1/2, y+1/2, z
	N3−H3···O1	2.932(3)	2.11	160	-x+1/2, y+1/2, z
	C9−H9···N2	3.414(4)	2.61	145	-x+1/2, y+1/2, z
hyd-Br	N4−H4A···O1	2.887(1)	2.03	180	-x+1/2, y+1/2, z
	N3−H3···O1	2.968(1)	2.14	161	-x+1/2, y+1/2, z
	C9−H9···N2	3.376(1)	2.86	143	-x+1/2, y+1/2, z
2	N4−H4A···O3	2.793(4)	1.94	170	x,-y+1/2,z+1/2
	N3−H3A···O3	2.737(4)	1.88	171	x,-y+1/2,z+1/2
	N7−H7A···O4	2.776(3)	1.92	171	x,y-1,z
	N8−H8A···O4	2.881(5)	2.04	167	x,y-1,z
3	N3−H3···O3	2.781(2)	1.93	169	x,y,z
	N4−H4A···O3	2.868(4)	2.02	167	x,y,z
	N7−H7A···O4	2.729(2)	1.87	173	x,-y+1/2+1,z+1/2
	N8−H8A···O4	2.794(3)	1.94	172	x,-y+1/2+1,z+1/2

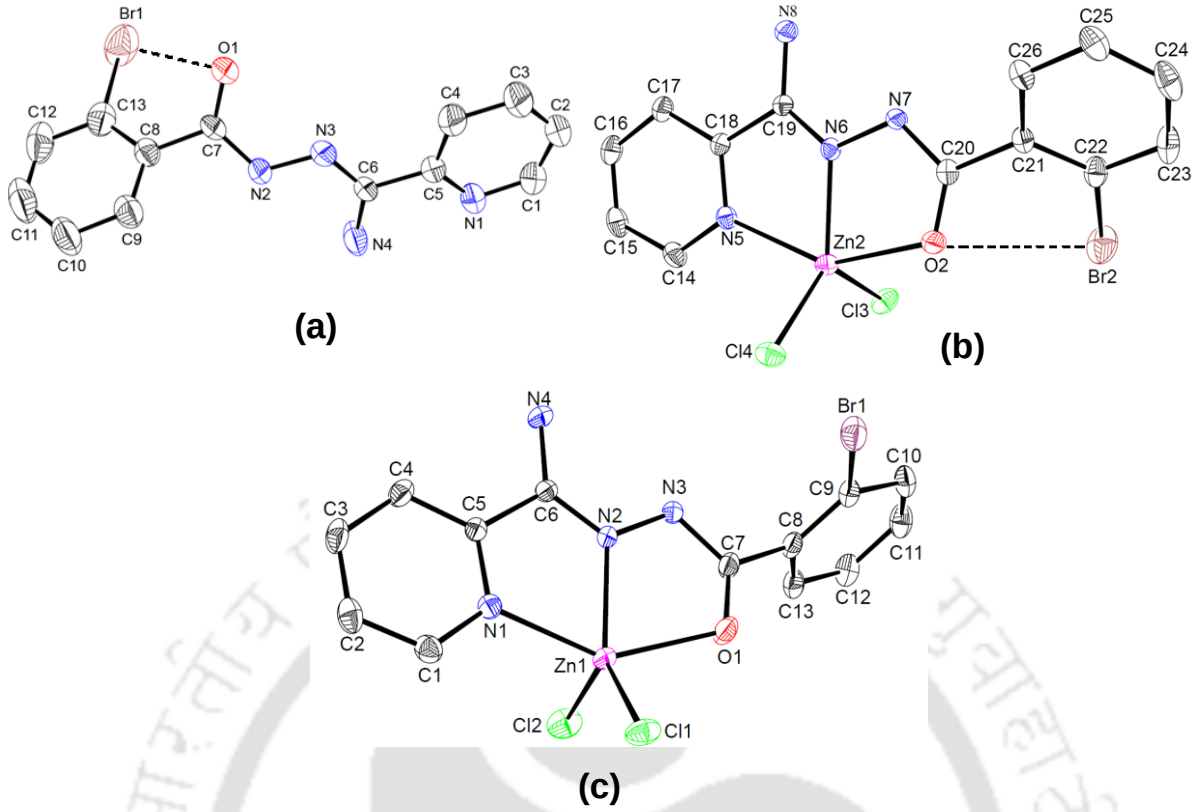

Figure 2. (a) *ORTEP* (40% probability) of ligand **hyd-Br** showing conformation **II**; (b) *ORTEP* (40% probability) of 'closed' complex **3**; (c) *ORTEP* (40% probability) of 'open' complex **3**.

Crystal structure description of ligand hyd-Cl and hyd-Br

Ligands **hyd-Cl** and **hyd-Br** are *isostructural* and crystallizes in the orthorhombic space group *Pbca*, the asymmetric unit contains one molecule having 'closed' conformation **I** (Figure 1a and 2a). The value of r_{OX} ($r_{OX} = d_{RX}/(r_O+r_X)$, d_{RX} is the distance between O and X atoms and r_O, r_X denote Van der Waals radius for the respective atoms) for intramolecular O···X interaction is around 0.92, which deems the possibility of a strong X···O interaction. The strength of the weak interactions is described using r_{DA} parameters throughout this chapter by following the convention used earlier to describe similar interactions.[24] However, the dihedral angle O−C−C−C_X (X = Cl, Br) [44.2(4)-45.4(7)°] values are higher for the strong intramolecular O···X interaction. The pyridyl (N_P) and amidine (N_{AD}) nitrogen atoms are *syn* in the free form of the ligand but they are oriented *anti* in the coordinated form (Figure 1a and 1c). The molecules of **hyd-X** form an infinite linear chain along the crystallographic *a* axis via N−H···O hydrogen bonds between strong donors *viz.* imine, amidine group and strong acceptor amide oxygen (Figure 3, Table 5). X···π interaction and C−H···N hydrogen bonds act

synergistically with N−H···O hydrogen bonds and contribute towards the further stabilisation of this supramolecular chain (Figure 3).

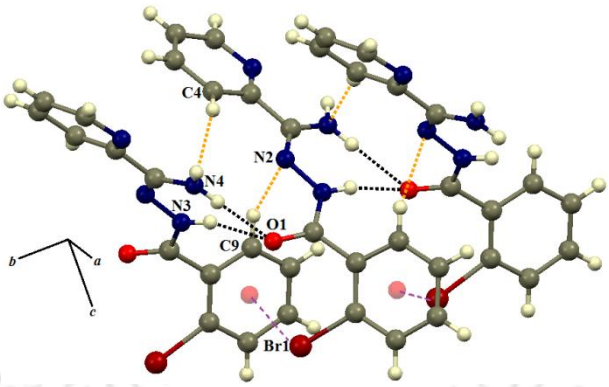

Figure 3. N−H···O, weak C−H···N hydrogen bonds and X···π interaction form an infinite chain of the ligand **hyd-Cl** along crystallographic *b* axis.

Crystal structure description of complex 1

Ligand **hyd-F** in complex [Zn(**hyd-F**)Cl_2] (**1**) adopts the conformational variant **I** and the presence of the intramolecular N−H···F interaction locks the molecular conformation (Figure 1b). Complex **1** crystallizes in the monoclinic space group $P2_1/n$, the asymmetric unit contains one molecule of the complex. The geometry around the penta-coordinated Zn^{2+} is the trigonal bipyramidal geometry (τ = 0.553) with the trigonal plane formed by azomethine nitrogen N_A, two chlorides while two axial positions are occupied by amide oxygen O_A and pyridyl nitrogen N_P (Figure 1b). The sum of three angles extending in the basal plane is 360(5)°, suggesting the basal plane is perfectly trigonal. However, the chelate bite angle O_A−Zn−N_P (147.40(6)°) demonstrates that the axial atoms are bent away from the chlorine atoms. The bond length trend Zn−O_A (2.212(2) Å) >Zn−N_P (2.159(2) Å) > Zn−N_A (2.079(2) Å) follows the trend of a pincer type ligand. The dihedral angle N−C−C−C_F (13.4(4)°) suggests the existence of a six-membered ring, near the planar intramolecular hydrogen bonded ring formed via N−H···F hydrogen bond (N3−F1, 2.687 (2) Å). Bifurcated N−H···Cl hydrogen bonds by metal bound halogen, namely, N4−H4A···Cl2 and N3−H3A···Cl2 interactions produce distinct dimeric motifs. These dimeric motifs are further joined by classical N4−HB···Cl1 and non-classical C−H···Cl hydrogen bonds to form a two dimensional sheet like structure (Figure 4a). The values of r_{NCl} (r_{NCl} = $d_{NCl}/(r_N+r_{Cl})$, r_N and r_{Cl} are the Van der Waals radii for the two atoms, d_{NCl} is the distance between N and Cl) being 0.97-0.99, indicate a moderate interaction but N−H···Cl interactions are directional (138-162°). This is

consistent with earlier reports by Brammer *et al*, which suggest that the 'inorganic halogen' possesses hydrogen bond acceptor ability in comparison to the free chloride.[23a] However, N3−H3A···Cl2 interaction (r_{NCl}, 1.06 and N−H···Cl, 139°) should be considered as a weak hydrogen bond. Non-classical hydrogen bonds *viz.* C−H···O and C−H···Cl(Zn) forms an infinite one dimensional supramolecular chain which is further supported by C−H···π interaction (Figure 4c). These one dimensional chains are connected by halogen···π interaction to form a two dimensional sheet like network. Dimeric motif formed by N−H···Cl hydrogen bond, C−F···Cl−Zn interhalogen interaction and face to face π···π stacking interaction is found in supramolecular assembly of complex **1** (Figure 4b). C−X···X'−M type synthons are common in metal halide complexes but C−F···Cl−M synthon in particular has not been reported yet.[21-23]The angle C−F···Cl (125.11°) does not strictly follow linearity while Zn−Cl···F (112.31°) angle is nearly obtuse, which is consistent with the earlier reports on C−X···X'−M synthon.[22,23a]

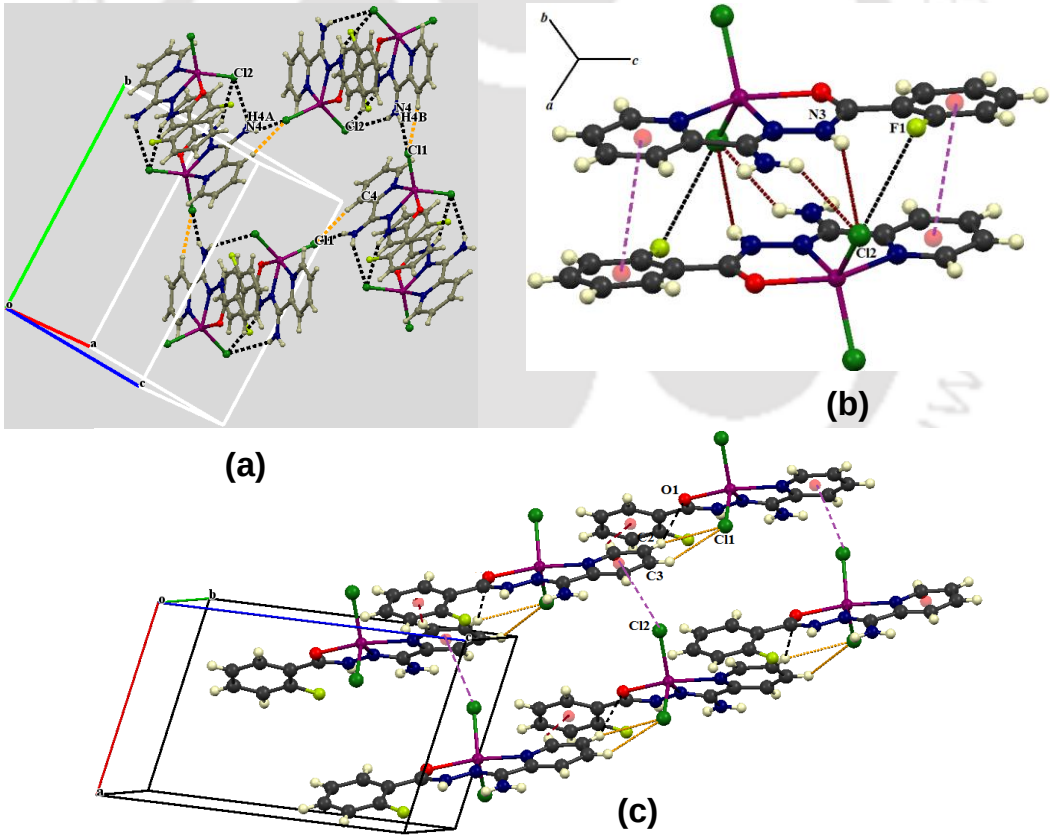

Figure 4. (a) A two dimensional ladder like structure formed by N−H···Cl interaction and weak C−H···Cl hydrogen bond in complex [Zn(**hyd-F**)Cl_2] (**1**); (b) Dimeric motif formed via N−H···Cl hydrogen bond, F···Cl and π···π interaction; (c) π···Cl interaction and C−H···Cl−Zn and C−H···O hydrogen bonds forming two dimensional architecture.

Table 5. Non-covalent interactions in crystal structures of **hyd-Cl**, **hyd-Br** and complex **1**

Compound	D−H···A	D···A (Å)	H···A (Å)	D−H···A(°)	Symmetry
	O1···Cl1	3.035(2)			x,y,z
hyd-Cl	Cg···Cl1	3.487(2)			-x+1/2,+y-1/2,+z
hyd-Br	O1···Br1	3.130(1)			x,y,z
	Cg···Br1	3.580(1)			-x+1/2,+y-1/2,+z
	N3−H3···F1	2.687(2)	2.09	126	x, y, z
	N4−H4B···Cl1	3.290(2)	2.45	162	-x+1/2, y-1/2,-z+1/2+1
1	N3−H3A···Cl2	3.509(2)	2.81	139	-x,-y+2,-z+1
	N4−H4A···Cl2	3.206(2)	2.55	137	-x,-y+2,-z+1
	C4−H4···Cl1	3.589(2)	2.67	170	-x+1/2,y-1/2,-z+1/2+1
	F1···Cl2	3.362(2)			-x,-y+2,-z+1
	Cg···Cl2	3.663			-x,-y+2,-z+1
	Cg···Cg	3.784			-x,-y+2,-z+1

Crystal structure description of complex 2 and 3

The asymmetric unit of the complexes [Zn(**hyd-Cl**)Cl_2].DMF (**2**) and [Zn(**hyd-Br**)Cl_2].DMF (**3**) is comprised of two complex molecules and two lattice DMF molecules. One complex molecule present in the asymmetric unit has 'closed' variant **II** of the conformation of the ligand while the other has an 'open' conformation variant **III** (Scheme 3, Figure 1c, 1d, 2b and 2c). The O−C−C−C_X dihedral angle values in 'closed' complex molecule are comparable to the free ligand [43.9(5)-45.2(6)°] while the values in 'open' molecule are much higher [107.8(6)-108.9(4)°]. The co-ordination geometry around the metal ion is trigonal bipyramidal and is extended by an azomethine nitrogen N_A and the two chlorine atoms and the axial positions are occupied by amide oxygen O_A and the pyridyl nitrogen N_P. The bite angle constraint on the ligand framework is evidenced by the values [146(1)°-147(1)°] for the *trans* angle O_A−Zn−N_P.

Amidine and imine groups on the 'closed' molecular conformation are hydrogen bonded to the oxygen atom of the solvent DMF forming a $R_2^1(7)$ hydrogen bonded motif (Figure 5a). The 'closed' complex molecule (having conformational variant **II** of the ligand) forms a distinct centro-symmetric dimeric motif via intermolecular N−H···Cl interaction between inorganic chlorine and the amidine nitrogen [N···Cl, 3.265(6)-3.286(3) Å]. The dimeric

motifs are interlinked to form an infinite two dimensional ladder like architecture along the crystallographic *b* axis by an intermolecular N···X halogen bond [N···X, 3.254(3) Å in **2** and 3.261(4) Å in **3**]. The values of C−X···N angle (150°) approach towards considerable linearity and X···N values lie in the reported range.[25] It is pertinent to note that 'organic fluorine' in complex **1** does not form intermolecular halogen bond unlike Cl or Br atoms of C−Cl / C−Br bond. As found in complex **1**, N−H···Cl(Zn) interactions are characterized by directionality (147°) and r_{NCl} values (0.98-0.99) suggest that the inorganic chlorine has moderate strength as the hydrogen bond acceptor (Table 6). Metal bound chloride forms hydrogen bond also with the aromatic ring [C···Cl, 3.425(3)-3.790(2) Å and C−H···Cl(Zn), 121-149°).

Table 6. Intermolecular interactions in crystal structures of complex **2** and **3**

Compound	D−H···A	D···A (Å)	H···A (Å)	D−H···A(°)	Symmetry
	O1···Cl1	3.305(3)			x,y,z
	N4···Cl1	3.254(3)			x,y-1,z
	N4−H4B···Cl3	3.286(2)	2.53	147	-x+1,-y+1,-z+1
2	N8−H8B···Cl6	3.353(3)	2.69	136	x, y-1,z
	C2−H2···Cl2	3.698(4)	2.87	149	-x+1, y-1/2, -z+1/2
	C29−H29···Cl2	3.750(4)	2.91	143	x, y-1, z
	C15−H15···Cl4	3.637(5)	2.95	131	-x,-y,-z+2
	C14−H14···Cl4	3.725(4)	2.84	160	x,-y+1/2,z+1/2
	C17−H17···Cl6	3.425(3)	2.85	121	-x,-y,-z+2
	C25−H25···Cl6	3.734(3)	2.83	163	x,-y+1/2,z-1/2
	O2····Br2	3.137(1)			x,y,z
	N8···Br2	3.261(1)			x,y-1,z
	N8−H8B···Cl3	3.265(2)	2.51	147	-x+1,-y+2,-z+1
	N4−H4B···Cl1	3.334(3)	2.68	134	x,y-1,z
	C4−H4···Cl1	3.411(2)	2.83	121	-x+1, y+1/2,-z+1/2
	C15−H15···Cl4	3.706(3)	2.89	148	-x,-y+2,-z+1
3	C23−H23···Cl2	3.790(3)	2.98	146	x,y-1,z
	C1−H1···Br1	3.764(2)	2.92	152	-x,y+1/2,-z+1/2
	C2−H2···Br2	3.789(2)	3.08	134	-x,-y+2,-z+1
	C29−H29···Br2	3.832(1)	3.08	141	x,y,z

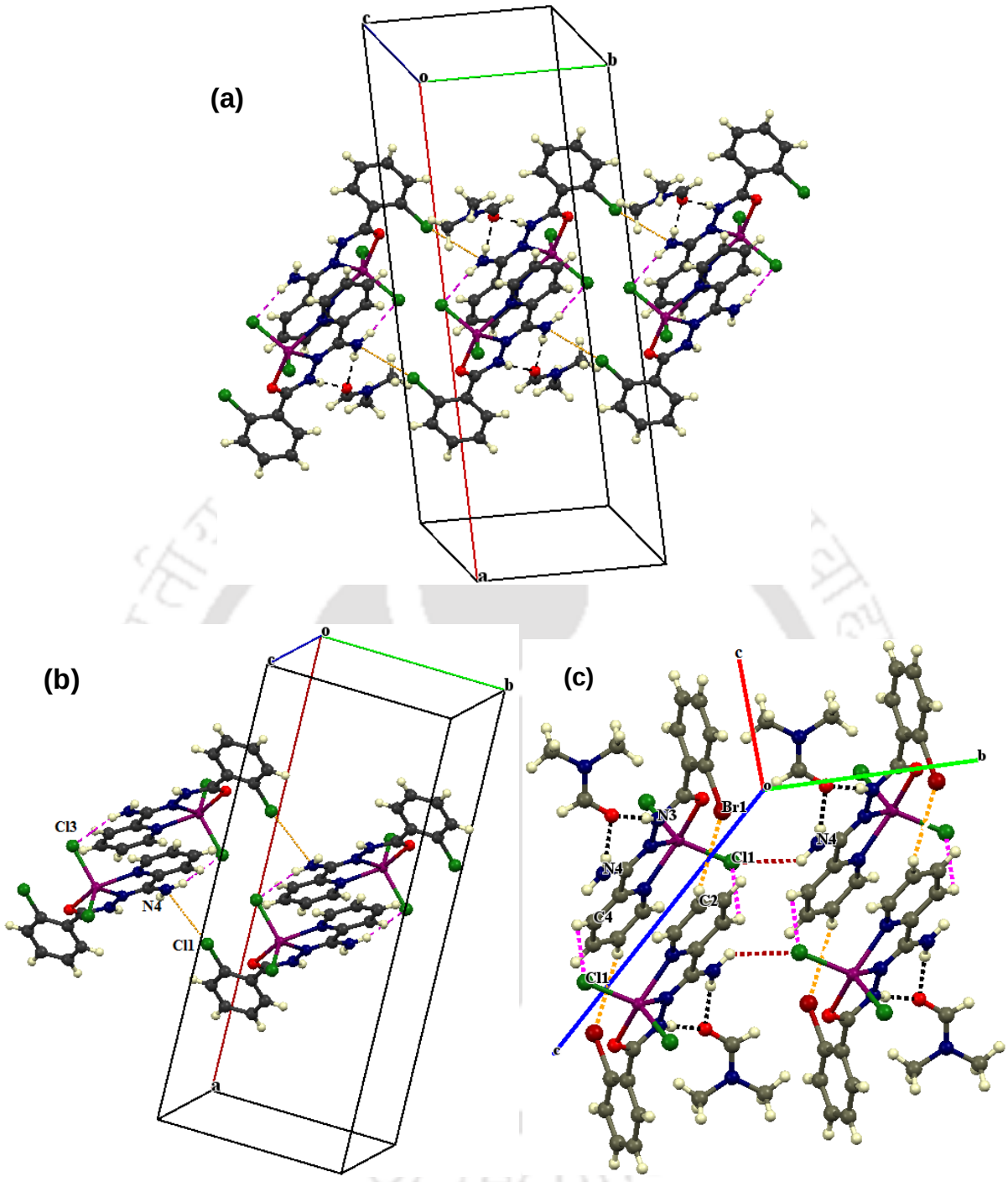

Figure 5. (a) Ladder like architecture formed by 'closed' complex and lattice DMF molecules in complex [Zn(**hyd-Cl**)Cl_2].DMF (**2**); (b) Complementary supramolecular behaviour of 'organic' and 'inorganic' halogen; (c) Classical N−H···O, N−H···Cl and non-classical C−H···X hydrogen bonds in 'open' molecule of complex [Zn(**hyd-Br**)Cl_2].DMF (**3**).

The dihedral angles O−C−C−C_X (~108(1)°) and N−C−C−C_X (~75(1)°) in 'open' molecule confirm that neither intramolecular X···O halogen bond nor intramolecular N−H···X hydrogen bond is present in this molecule. The 'open' molecule is hydrogen bonded with

oxygen atom of the DMF molecule through N_I and N_{AD} groups (Figure 5c). Weak C−H···Cl(Zn) hydrogen bonds in the supramolecular assembly of 'open' molecule exhibit directionality (146-159°) while C···Cl(Zn) distances [3.411(2)-3.734(3) Å] also suggests significant interaction (Table 6, Figure 5c). The C−H···X interaction involving the organic halogen shows considerable linearity [C−H···X, 152-160°] while C···X [3.725(4)-3.789(2) Å] distances are higher. This difference between C···X(Zn) and C···X(C) distances indicates that the inorganic halogen is a stronger hydrogen bond acceptor than the organic halogen.

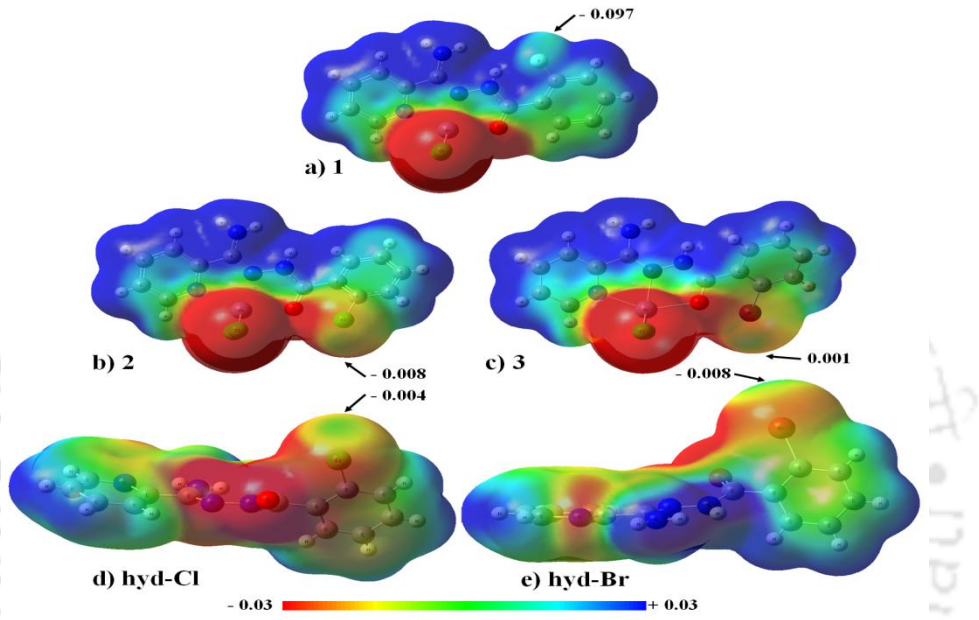

Figure 6. MEP diagrams of complex **1** (a), 'closed' molecule in complex **2** (b) and **3** (c) and ligand **hyd-Cl** (d), **hyd-Br** (e), calculated by DFT method at B3LYP/ 6-311G(d,p) level.

3. 2. 3. Computational Studies

3. 2. 3. 1. Electronic insights from calculations on the molecular electrostatic potential

Molecular electrostatic potential map was drawn for all the complex using DFT level calculations performed at B3LYP/6-311G(d,p) level (Figure 6). The electrostatic potential map clearly depicts the presence of highly negative electrostatic potential region on the chlorine atom attached to Zn in complex **1-3**. In contrast to this, σ-hole was observed on the organic halogen, Cl in **2** and **hyd-Cl**. Similarly, substantial σ-hole characteristics was also observed in the case of organic Br in **3** and **hyd-Br**. In case of **1**, it was interesting to observe the presence of a positive electrostatic region on the organic fluorine present in the complex which can be attributed to the electron withdrawing characteristics of Zn(II).

The reliability of the non-covalent interactions and motifs in supramolecular synthetic strategy depend on their geometric reproducibility and robustness. Halogen bond and other interactions of halogen in metal complexes have been known to play decisive roles in developing efficient supramolecular motifs for molecular recognition process.[4,6,7a,21-23] In the present study four classes of non-covalent interactions of halogen are observed, namely, intramolecular X···O interaction, intermolecular N···X halogen bond, N−H···X and C−H···X interactions and the weakest of all, halogen···π interaction.

3. 2. 3. 2. Intramolecular X···O interaction

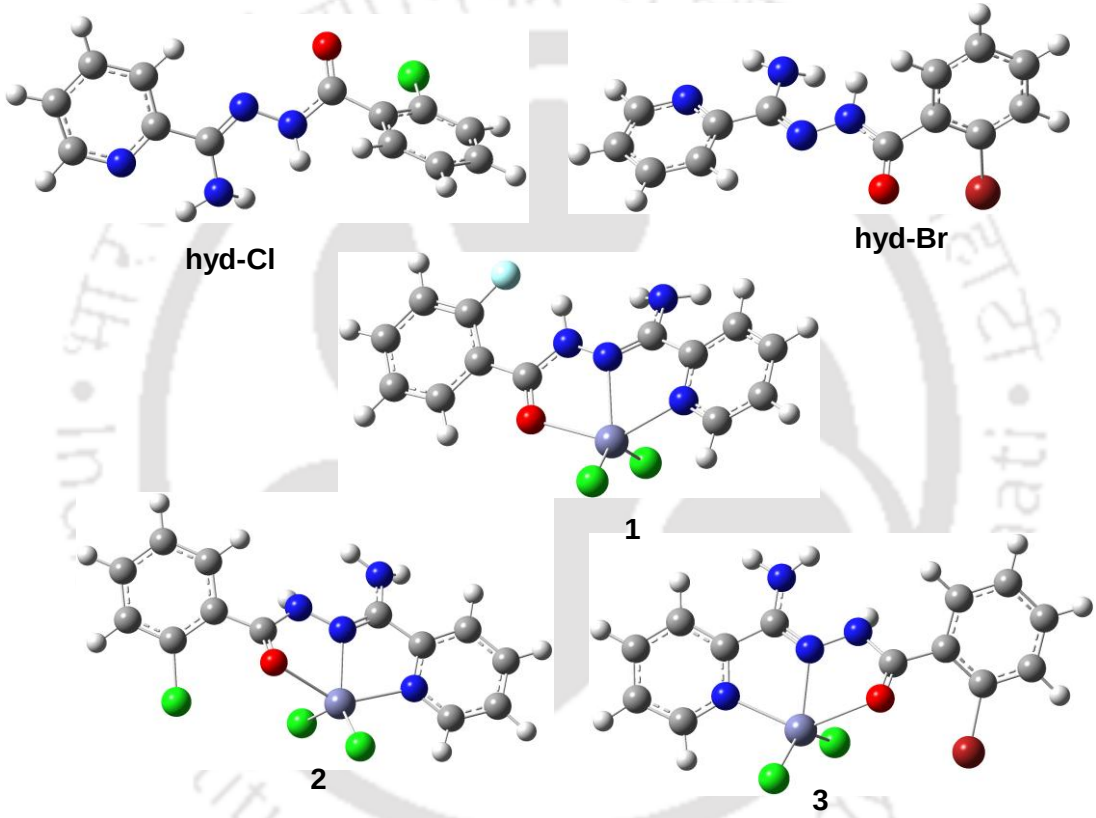

Figure 7. Optimised gas phase geometries of ligands **hyd-Cl**, **hyd-Br** and complex **1-3**.

Intramolecular X···O separation in ligand **hyd-Cl**, **hyd-Br** and 'closed' molecule of complex **2** and **3** fall below the sum of the Van der Waals radii of O and X atoms. However, the corresponding dihedral angle O−C−C−C_X in ligands and 'closed' molecule of complex **2** and **3** (~ 45°) indicates that X and O atoms are not in the same plane. Instead the O−C−C−C_X dihedral angle demonstrates that X and O atoms are inclined *synclinal*. Geometry optimisation performed at both M06-2X/6-31G(d,p) and dispersion corrected B3LYP/6-31G(d,p) leads to a decrease of the O−C−C−C_X dihedral angle by 4-5° in 'closed' molecule

(having conformation **II**) in complex **2** and **3**. In contrast, O−C−C−C_X dihedral angle opens up by ~14° in the optimised geometry of the ligands and thus O and X atoms are orientated *gauche* to each other.

The presence of intramolecular X···O bond in 'closed' molecule of **2** and **3** as well as their presence in **hyd-Cl** and **hyd-Br** was established from a topological analysis using QTAIM (Figure 8). A (3, -1) bond critical point between the halogen and oxygen atom was observed in all molecules (except for **1** where an intramolecular N-H···F interaction was observed) and thus the presence of an intramolecular Cl/Br···O interaction could be confirmed. The bond path length (BPL) in case of Cl···O contact was shorter than those observed for the corresponding Br···O contact and the trend resembles with experimentally observed X···O distances. The magnitude of ρ listed in Table 7 shows that the metal ion coordination does not have any effect on the intramolecular X···O interaction. The magnitude of the Laplacian of electron density ($\nabla^2\rho$) ranges from 1.031 e/Å^5 to 1.147 e/Å^5, having values slightly greater in case of Cl···O interaction as compared to the Br···O interaction. In addition to $\nabla^2\rho > 0$ for all X···O interactions, $H_b > 0$ and the ratio of $-G_b/V_b$ is greater than one, which points towards the fact that the intramolecular Cl/Br···O interactions under investigation are all weak closed-shell interactions. The ρ and Laplacian $\nabla^2\rho$ values are similar to the values reported earlier for moderate hydrogen bonding and typical halogen bonding interactions.[26] Similar values have also been cited for intramolecular C−F···O=C interaction.[18b]

Table 7. Topological and geometrical parameters of intramolecular X···O interaction

Compound	Intramolecular interaction	X···O distance in crystal (Å)	Bond path length (Å)	ρ (e/Å^3)	$\nabla^2\rho$ (e/Å^5)	H_{bcp}	$-G_b/V_b$	O−C−C−C_X in crystal (°)
Hyd-Cl	Cl···O	3.035(2)	3.045	0.082	1.133	0.002	1.194	44.4(2)
Hyd-Br	Br···O	3.130(1)	3.138	0.087	1.031	0.000	1.092	45.4(7)
2	Cl···O	3.035(3)	3.045	0.080	1.147	0.002	1.212	43.9(5)
3	Br···O	3.137(1)	3.145	0.080	1.031	0.001	1.173	45.2(6)
1	N−H···F		2.144	0.121	2.021	0.002	1.199	

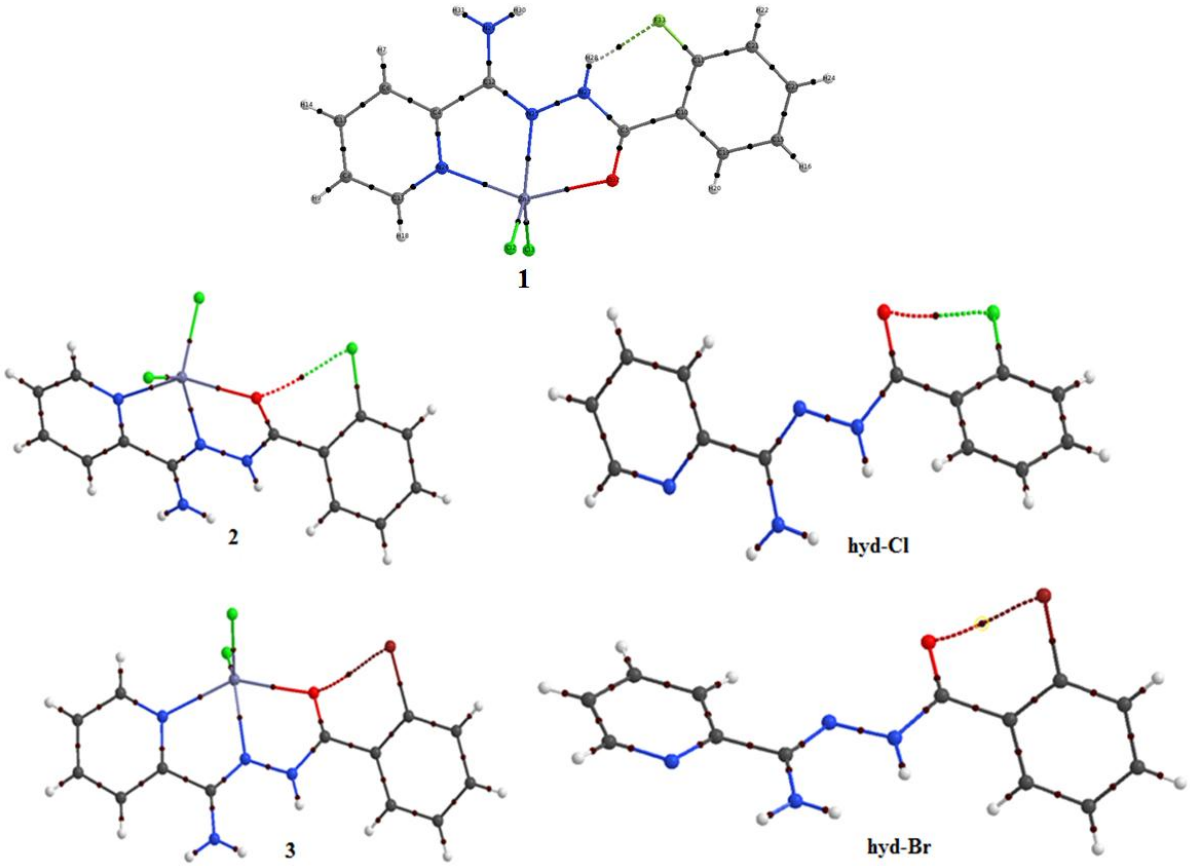

Figure 8. Molecular graph depicting intramolecular X···O (X = Cl, Br) interaction.

Earlier it has been reported for 3-halopropenals that the presence of a bond path and a bond critical point always does not ensure an attractive intramolecular X···O interaction.[16] The authors claim that the five-membered intramolecular X···O interaction should be a non-attractive especially when the molecule exhibiting 'open' conformation *i.e.* without X···O interaction is also experimentally observed. Single point calculations indicate that the 'closed' complex molecule has energy higher than 'open' complex molecule by around 2.0 kcal/ mol (Table 8). Therefore, intramolecular X···O interaction does not contribute to the overall stabilisation of the molecule. Similar results were cited for intramolecular F···F interaction in polyfluorinated biphenyls by Boyd *et al.*[27] The authors regarded that intramolecular F···F interaction imparts local stabilisation energy. A similar argument can be drawn for intramolecular X···O interaction in our investgation. It is pertinent to mention that complex **1** shows an intramolecular N−H···F hydrogen bond instead of X···O interaction. Second order perturbation energy E(2) for (lp)F→σ*(N−H) charge transfer amounts to 2.64 kcal/mol. Previously we reported six membered intramolecular N−H···N/O hydrogen bond determining molecular conformation in *o*-amino substituted hydrazide.[28] It demonstrates that

N−H···F hydrogen bond can exert same effect of N−H···N/O hydrogen bond in molecular recognition process.

Table 8. Energy of 'closed' and 'open' molecules in complex **2** and **3** determined at M06-2X/6-31G(d,p) and B3LYP-D3/6-31G(d,p) level

E ('closed' molecule of complex **2**, at M06-2X/6-31G(d,p) = -3955.38534 a.u.
E ('closed' molecule of complex **2**, at B3LYP-D3/6-31G(d,p) = -3955.88634 a.u.
E ('open' molecule of complex **2**, at M06-2X/6-31G(d,p) = -3955.38843 a.u.
E ('open' molecule of complex **2**, at B3LYP-D3/6-31G(d,p) = -3955.89017 a.u.
E ('closed' molecule of complex **3**, at M06-2X/6-31G(d,p) = -6067.00176 a.u.
E ('closed' molecule of complex **3**, at B3LYP-D3/6-31G(d,p) = -6067.00278 a.u.
E ('open' molecule of complex **3**, at M06-2X/6-31G(d,p) = -6067.00278 a.u.
E ('open' molecule of complex **3**, at B3LYP-D3/6-31G(d,p) = -6067.40137 a.u.

We have performed a relaxed potential surface energy scan with the change of dihedral angle O−C−C−C_X in ligand **hyd-Cl** to examine if the intramolecular X···O interaction indeed dictates molecular conformation. A local minimum exists at 40° value of dihedral angle O−C−C−C_X while the global minimum can be found at 140° (Figure 9).

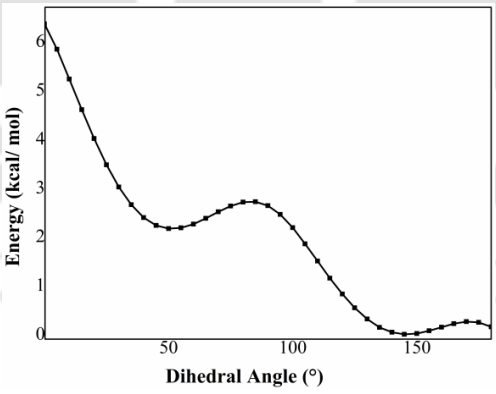

Figure 9. Relaxed scan of potential energy surface with change of O−C−C−C_X dihedral angle, 5° interval is taken.

The values of O−C−C−C_X (≈ 40°) dihedral angles in gas phase optimised geometry of 'closed' complex molecule of **2** and **3** correspond to the local minima of energy. However, O−C−C−C_X (≈ 105°) dihedral angle value in crystal geometry of 'open' complex molecule suggests that it should have little lower energy than the 'closed' molecule. The

conformational variant **III** (found in 'open' complex molecule of **2** and **3**) is *metastable* as it is neither a global nor a local minimum. Therefore, gas phase geometry optimisation of the molecular conformation for **III** leads to the global minimum in the potential energy surface.

3. 2. 3. 3. Intermolecular N···X halogen bond or N−H···X hydrogen bond?

'Organic' halogen (X = Cl, Br) atoms of 'closed' complex molecule in **2** and **3** are involved in intermolecular N···X halogen bond. The values of r_{NX} parameter in these complexes (0.99 in **2** and 0.96 in **3**) indicate a weak attractive interaction. In contrast, the metal bound chlorine atom in all three complexes is observed to form intermolecular N−H···Cl hydrogen bonds of a highly directional nature (N−H···Cl, ~148°). Table 9 contains BSSE corrected interaction energies associated with these intermolecular interactions. The complementary electronic nature of 'organic' versus 'inorganic' halogen can be interpreted *via* molecular electrostatic potential diagrams (Figure 6).

Table 9. Binding and charge transfer energies for N···X and N−H···X interactions

Molecule	Criteria	B3LYP-D3/6-31G(d,p)	M06-2X/6-31G(d,p)
1	ΔE(kcal/mol) N4−H4···Cl2	-24.75	-18.91
	E(2)kcal/mol (lp)Cl2→σ*(N−H)	2.68	2.55
	ΔE(kcal/mol) N4−H4···Cl1	-14.92	-12.53
	E(2)kcal/mol (lp)Cl1→σ*(N−H)	5.47	5.53
2	ΔE(kcal/mol) N···Cl	-7.31	-5.36
	E(2)kcal/mol (lp)N→σ*(C−Cl)	0.49	0.53
	ΔE(kcal/mol) N−H···Cl	-20.72	-20.02
	E(2)kcal/mol (lp)Cl→σ*(N−H)	4.01	3.93
3	ΔE(kcal/mol) N···Br	-7.34	-5.23
	E(2)kcal/mol (lp)N→σ*(C−Br)	0.84	0.89
	ΔE(kcal/mol) N−H···Cl	-21.13	-18.02
	E(2)kcal/mol (lp)Cl→σ*(N−H)	4.44	4.35

Natural bond orbital (NBO) analyses show value of (lp)N→σ*(C−X) charge transfer corresponding to intermolecular halogen bond is remarkably lower than (lp)Cl→σ*(N−H) charge transfer for intermolecular N−H···Cl hydrogen bond. This indicates that intermolecular

N···X interaction is much weaker than intermolecular N−H···X interaction. The second order perturbation energies show higher value for the C−Br (0.84 kcal/mol) than C−Cl (0.49 kcal/mol) orbital, which is almost unequivocal to the size of σ-hole on chlorine and bromine of C−X bond. It has been observed that perturbation energies E(2) does not always correspond to the binding energy for N···X or N−H···X interaction. This can be explained on the basis of the fact that the binding energies are calculated by taking into account the role of the basis sets in the whole molecule in the molecular pair while E(2) energies consider only the interaction between two interacting orbitals.

Table 10. NBO charge on halogen atoms calculated at B3LYP-D3/6-31G(d,p) level of theory

Molecule	Halogen atom	NBO charge
hyd-Cl	Cl	0.0264
% of *s* character in C hybrid orbital of C−X		22.59
hyd-Br	Br	0.0910
% of *s* character in C hybrid orbital of C−X		22.25
1	F	-0.3515
% of *s* character in C hybrid orbital of C−X		21.01
2-closed	Cl	0.0602
% of *s* character in C hybrid orbital of C−X		23.15
2-open	Cl	0.0049
% of *s* character in C hybrid orbital of C−X		22.26
3-closed	Br	0.1454
% of *s* character in C hybrid orbital of C−X		22.79
3-open	Br	0.0667
% of *s* character in C hybrid orbital of C−X		21.22

The *s* character of C hybrid orbital of C−X bond will increase if X acts as Lewis acid *i.e.* a halogen bond donor.[29] This is a direct consequence of Bent's rule[30] which states that atoms maximize the *s* character in hybrid orbitals toward electropositive substituents and the atoms maximize their *p* character toward more electronegative substituents. The *s* character of C hybrid orbital of C−X bond decreases if X acts as Lewis base *i.e.* hydrogen bond acceptor. It has been observed that the *s* character of C hybrid orbital of C−X bond in 'closed' complex molecule is slightly higher than that of the 'open' molecule in **2** and **3** (Table 10). This is consistent with the fact that the organic halogen serves as a hydrogen bond acceptor in 'open' molecule while it acts a halogen bond donor in the 'closed' molecule.

3. 2. 3. 4. C−H···X and halogen···π interaction

The weak interactions of halogen in these complexes include C−H···X(C), C−H···X(M) and halogen···π interactions. It has been observed in complexes **1-3** that both C−H···X(M) and C−H···X(C) interactions on certain occasions deviate from linearity while C···X(C) distances are always higher (Table 5, 6). The C−H···X(M) and C−H···X(C) interactions have not been unequivocally accepted as pure hydrogen bonding interactions.[31] Following the same arguments, C−H···X interactions in these compounds cannot be classified purely as either van der Waals interaction or weak hydrogen bond. Halogen···π interaction is considered the weakest of all interactions amongst the halogens, however it does contributes towards the crystal packing.[32] The angles θ = 44.06-44.31°, ω = 75.13° when X = Cl, 83.26° when X = Br (Figure 10) and Cg···X distance (3.487 Å for Cl and 3.580 Å for Br) corresponding to C−X···π interaction in ligands **hyd-Cl** and **hyd-Br** fall in the reported range.[32a] Halogen···π interaction by metal bound chloride in complex **1** is weak as Cl···π distance (3.663 Å) lies in the upper limit of such interaction.

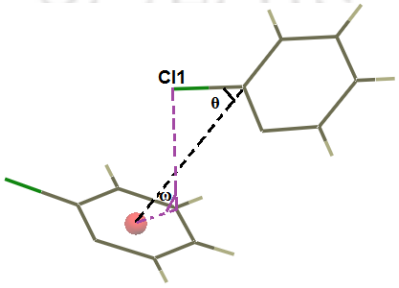

Figure 10. The parameters of C−X···π interaction.

3. 3. Conclusion

We have systematically explored weak interactions involving halogen in *o*-halophenyl substituted hydrazide ligands and their Zn(II) complexes. The existence of intramolecular X···O interaction in *o*-chloro/bromophenyl substituted ligands and their complexes has been proved by topological analysis. Further analyses reveal that this interaction energy imparts local stabilisation energy and corresponds to a local minimum in the potential energy surface. Complementary electronic nature of organic and inorganic halogen results in the formation of C−X···N and N−H···X−M supramolecular synthons in the zinc complexes **1-3**. The strength of intermolecular C−X···N halogen bond follows the order Br>Cl while 'organic fluorine' does not take part in such an interaction. Various moderate to weak hydrogen bonding interactions of halogen, namely, N−H···Cl−Zn, C−H···Cl−Zn and C−H···X−C interactions are observed in the crystal structures of these complexes. These weak hydrogen bonds act cooperatively as well as competitively with classical hydrogen bonds. Analyses of crystal structures of these complexes give an interim perspective of weak interactions of organic and inorganic halogen. In addition, this study demonstrates two important aspects of weak interactions of halogen; difference of 'organic fluorine' from other C−X halogen and the disparity between electronic nature of organic and inorganic halogen.

3. 4. Experimental Section

3. 4. 1. Computational methods

Gas phase geometry optimisation of the ligand **hyd-Cl** and zinc(II) complexes **1-3** have been performed using density functional theory at M06-2X/6-31G(d,p) level of theory. M06-2X functional is known to give reliable outcome taking in account the dispersion forces when weak non-covalent interactions in transition metal complexes are considered.[33] Geometry optimisation in gas phase by dispersion corrected DFT with standard 'zero damping' at B3LYP/6-31G(d,p) level of theory has also been carried out as it has been cited earlier that this method gives reliable interaction energy for long range weak dispersion interactions like halogen bond and π···π stacking force.[34] The optimised geometries using both the functional are in close agreement with each other. Single point energy calculations were performed using dispersion corrected DFT with standard 'zero damping' at B3LYP/6-31G+(d,p) level of theory. Energies associated with intermolecular halogen and hydrogen

bonds were calculated using the same level of theory and basis set superposition error (BSSE) was corrected by the method of Boys and Bernardi.[35] All calculations were carried out using Gaussian 09 programme package.[36] NBO analyses were performed at the same level of theory used for geometry optimisation using NBO 3 implemented in Gaussian 09. Crystal coordinates have been used as initial coordinates for all calculations. Molecular electrostatic potential were calculated using DFT performed at B3LYP/6-311G(d,p) level. Topological analysis was also performed to obtain properties such as electron density(ρ), Laplacian of the electron density ($\nabla^2\rho$), energy density (H_b) which is a sum of kinetic energy density (G_b) and potential energy density (V_b) at the bond critical point using B3LYP/6-311G(d,p) level on ligands under investigation using AIMALL[37] (13.11.04) which is based on the Quantum Theory of Atoms in Molecule.[38]

3. 4. 2. Materials and methods

2-Fluorobenzhydrazide, 2-chlorobenzhydrazide, 2-bromobenzhydrazide (Alfa Aeser), 2-cyanopyridine (Aldrich, USA), anhydrous $ZnCl_2$ (Merck India) and solvents were used as received without further purification. Single crystals of complexes **1-3** and ligands **hyd-Cl** and **hyd-Br** were grown by slow evaporation from common organic solvents (methanol and DMF) at room temperature. X-ray crystallographic data were collected using a Bruker SMART APEX-CCD diffractometer and Agilent Supernova diffractometer with Mo-Kα radiation (λ= 0.71073 Å). The intensity data were corrected by Lorentz and polarisation effects and empirical absorption corrections were made using multi-scan method. All structures were solved by direct methods using SHELX-97. Non hydrogen atoms were refined anisotropically by full matrix least-squares on F^2, using SHEXL-97 and further refined using PLATON.[39] All hydrogen atoms were included in the calculated positions and refined isotropically using a riding model. Useful parameters for hydrogen bond and other non-covalent interactions were calculated using PARST[40] program implemented in PLATON.

3. 4. 3. Syntheses procedure and characterisation data

2-[5-(2-Fluoro-phenyl)-1*H*-[1,2,4]triazol-3-yl]-pyridine (trz-F). 2-Fluorobenzhydrazide (0.925 g, 6 mmol) and 2-cyanopyridine (0.677 g, 6.5 mmol) were taken together in 1.5 gm of PEG 400 and heated for 12 h at 100°C. The resulting gummy yellow liquid was added to 50 mL water and stirred overnight which produced pale yellow residue. It

was filtered, washed thoroughly with water and hexane to remove impurities and dried over anhydrous $CaCl_2$. Dried product was subjected to column chromatography on basic alumina, in order to remove adhered PEG and pure **trz-F** was eluted with EtOAc : hexane (2:1) mixture. White solid; yield 1.155 g, 80%. IR (KBr, cm^{-1}): 3564, 3344, 3135, 1691, 1641, 1615, 1590, 1543, 1495, 1384, 1334, 1286, 1232, 1102, 1026, 985, 823, 790, 759. ^{1}H NMR (600 MHz, DMSO-d_6): δ 8.59 (d, *J* = 4.5 Hz, 1H), 8.12 (d, *J* = 7.9 Hz, 1H), 8.04 (dd, *J* = 10.6, 4.5 Hz, 1H), 7.87 (td, *J* = 7.8, 1.6 Hz, 1H), 7.47-7.41 (m, 1H), 7.40-7.36 (m, 1H), 7.26 (dd, *J* = 11.0, 4.1 Hz, 1H), 7.21 (dd, *J* = 10.5, 8.8 Hz, 1H).^{13}C NMR (150 MHz, DMSO-d_6): δ 161.11, 159.45, 149.53, 148.17, 137.58, 131.82, 131.77, 130.19, 124.67, 121.74, 116.23, 116.08. ESI MS calcd for $C_{13}H_{10}N_4F^+$ $(M+H)^+$ 241.089, found 241.088.

2-Chlorobenzoic acid(amino-pyridin-2-yl-methylene)hydrazide (hyd-Cl). Ligand **hyd-Cl** was synthesised by heating 2-chlorobenzhydrazide (0.925 g, 6 mmol) with 2-cyanopyridine (0.677 g, 6.5 mmol) in 1.2 g of PEG 400 under same reaction conditions as described for **trz-F**. White solid obtained after treating with water was purified by column chromatography using EtOAc : hexane (1:1) as eluent. White solid; yield 1.233 g, 75%. IR (KBr, cm^{-1}): 3416, 3201, 1667, 1639, 1603, 1591, 1580, 1545, 1505, 1467, 1443, 1422, 1399, 1366, 1309 (s), 1262, 1250, 1171, 1148, 1128, 1054, 1036, 1012, 910, 797, 776, 747, 738. ^{1}H NMR (600 MHz, DMSO-d_6): δ 8.72 (s, 1H), 8.13 (d, *J* = 7.7 Hz, 1H), 8.01 (s, 1H), 7.92 (s, 1H), 7.64-7.40 (m, 5H). ^{13}C NMR (100 MHz, DMSO-d_6) δ 160.92, 154.79, 150.30, 146.75, 138.55, 137.72, 132.31, 132.06, 131.13, 127.87, 125.86, 122.14. ESI MS calcd for $C_{13}H_{12}N_4{}^{35}Cl^+$ $(M+H)^+$ 275.070 found 275.063.

2-Bromobenzoic acid(amino-pyridin-2-yl-methylene)hydrazide (hyd-Br). Solid **hyd-Br** was obtained by heating a mixture of 2-bromobenzhydrazide (1.290 g, 6 mmol) and 2-cyanopyridine (0.677 g, 6.5 mmol) in PEG 400 and purified through column chromatography by eluting with 4:6 mixture of EtOAc : hexane. White solid; yield 1.145 g, 60%. IR (KBr, cm^{-1}): 3443 (s), 3318 (m), 3191 (m), 3043 (m), 3008 (m), 2925 (w), 2852 (w), 1670 (s), 1642 (s), 1588 (m), 1550 (s), 1473 (s), 1440 (m), 1397 (s), 1313 (s), 1269 (m), 1168 (s), 1089 (w), 1050 (s), 1030 (s), 996 (m), 971 (w), 952 (m), 904 (s), 866 (w), 795 (s), 777 (m), 742 (s). ^{1}H NMR (400 MHz, DMSO-d_6): δ 8.71 (d, *J* = 3.8 Hz, 1H), 8.12 (d, *J* = 7.6 Hz, 1H), 7.99 (t, *J* = 7.9 Hz, 1H), 7.89 (s, 1H), 7.62- 7.40 (m, 5H). 100 MHz ^{13}C NMR (δ DMSO-d_6): 160.73, 158.22, 149.62, 147.15, 137.74, 131.08, 131.00, 129.98, 124.81, 124.64, 121.43, 116.67, 116.46. ESI MS calcd for $C_{13}H_{11}N_4{}^{79}Br^+$ $(M+H)^+$ 319.019, found 318.990.

[Zn(hyd-F)Cl_2] (1). To a solution of ligand **trz-F** (48 mg, 0.20 mmol) in DMF (5mL), solid anhydrous $ZnCl_2$ (34 mg, 0.25 mmol) was added and stirred for five hours. Then the solution was left undisturbed and block shaped colourless crystals of **1** obtained after two weeks. Yield: 55 mg, 70%. *Anal*. Calcd. for $C_{13}H_{11}N_4OFCl_2Zn$: C, 39.57; H, 2.81; N, 14.20%. Found: C, 39.85; H, 2.85; N, 14.05%. IR (KBr, cm^{-1}): 3195 (b), 3115 (m), 1622 (s), 1588 (w), 1562 (s), 1497 (s), 1453 (s), 1387 (s), 1282 (s), 1263 (w), 1229 (s), 1181 (s), 1151 (s), 1127 (w), 1094 (s), 1046 (s), 1025 (s), 1006 (m), 985 (s), 945 (w), 865 (w), 824 (s), 792 (s), 771 (s), 746 (s), 716 (m), 695 (w), 664 (w), 644 (m), 496 (m). UV-Vis [λ_{max} (nm), (ε, $M^{-1}cm^{-1}$), DMSO solution]: 270 (21490), 314 (38515), 327 (29850). ESI MS *m/z* found (calcd.) [^{64}Zn(**hyd-F**)(^{35}Cl)]$^+$ 357.65 (356.99).

[Zn(hyd-Cl)Cl_2]·DMF (2). Upon addition of solid anhydrous $ZnCl_2$ (41 mg, 0.30 mmol) to stirred DMF solution of ligand **hyd-Cl** (69 mg, 0.25 mmol) the colour of the solution intensified to light yellow, which was left undisturbed. White prismatic crystals deposited after two weeks were collected, washed with cold methanol. Yield 89 mg, 74%. *Anal*. Calcd. for $C_{16}H_{18}N_5O_2Cl_3Zn$: C, 39.70; H, 3.75; N, 14.47%. Found: C, 39.81; H, 3.68; N, 14.55%. IR (KBr, cm^{-1}): 3627 (m), 3419 (b), 1703 (s), 1655 (w), 1613 (s), 1556 (s), 1476 (s), 1385 (s), 1320 (s), 1282 (s), 1182 (s), 1155 (s), 1130 (w), 1113 (w), 1091 (m), 1067 (s), 1049 (m), 1031 (m), 1002 (m), 984 (m), 876 (w), 845 (s), 802 (s), 775 (s), 757 (m), 737 (m), 712 (s), 655 (m), 637 (m), 570 (m), 452 (s). UV-Vis [λ_{max} (nm), (ε, $M^{-1}cm^{-1}$), DMSO solution] 269 (7800), 313 (15840), 377 (2520). ESI MS *m/z* found (calcd.) [**hyd-**^{35}**Cl**+H]$^+$, found 275.14 (275.07); [^{64}Zn(**hyd-**^{35}**Cl**)^{35}Cl]$^+$ 373.05 (372.96).

[Zn(hyd-Br)Cl_2]·DMF (3). Same procedure as adopted for synthesis of complex **2**, yielded pale yellow crystals of **3**. Yield 84 mg, 64%. *Anal*. Calc. for $C_{16}H_{18}N_5O_2Cl_2BrZn$: C, 36.36; H, 3.43; N, 13.25%. Found: C, 36.43; H, 3.32; N, 13.19%. IR (KBr, cm^{-1}): 3653 (s), 3473 (b), 3182 (b), 3049 (w), 1704 (s), 1656 (m), 1616 (m), 1533 (s), 1486 (m), 1473(m), 1445(m), 1426(s), 1318(s), 1275(s), 1198(m), 1173 (m), 1157 (w), 1141 (w), 1121 (m), 1094 (s), 1044 (m), 1030 (m), 1017 (s), 970 (w), 915 (m), 897 (w), 825 (w), 793 (s), 763 (w), 750 (m), 724 (m), 687 (s), 641 (m), 570 (m). UV-Vis [λ_{max}(nm), (ε, $M^{-1}cm^{-1}$), DMSO solution]: 265 (9750), 312 (26180), 329 (19870). ESI MS *m/z* found (calcd.) [^{64}Zn(^{79}**hyd-Br**)(^{35}Cl)$^+$] 416.99 (416.91).

3. 3. 4. Selected spectra

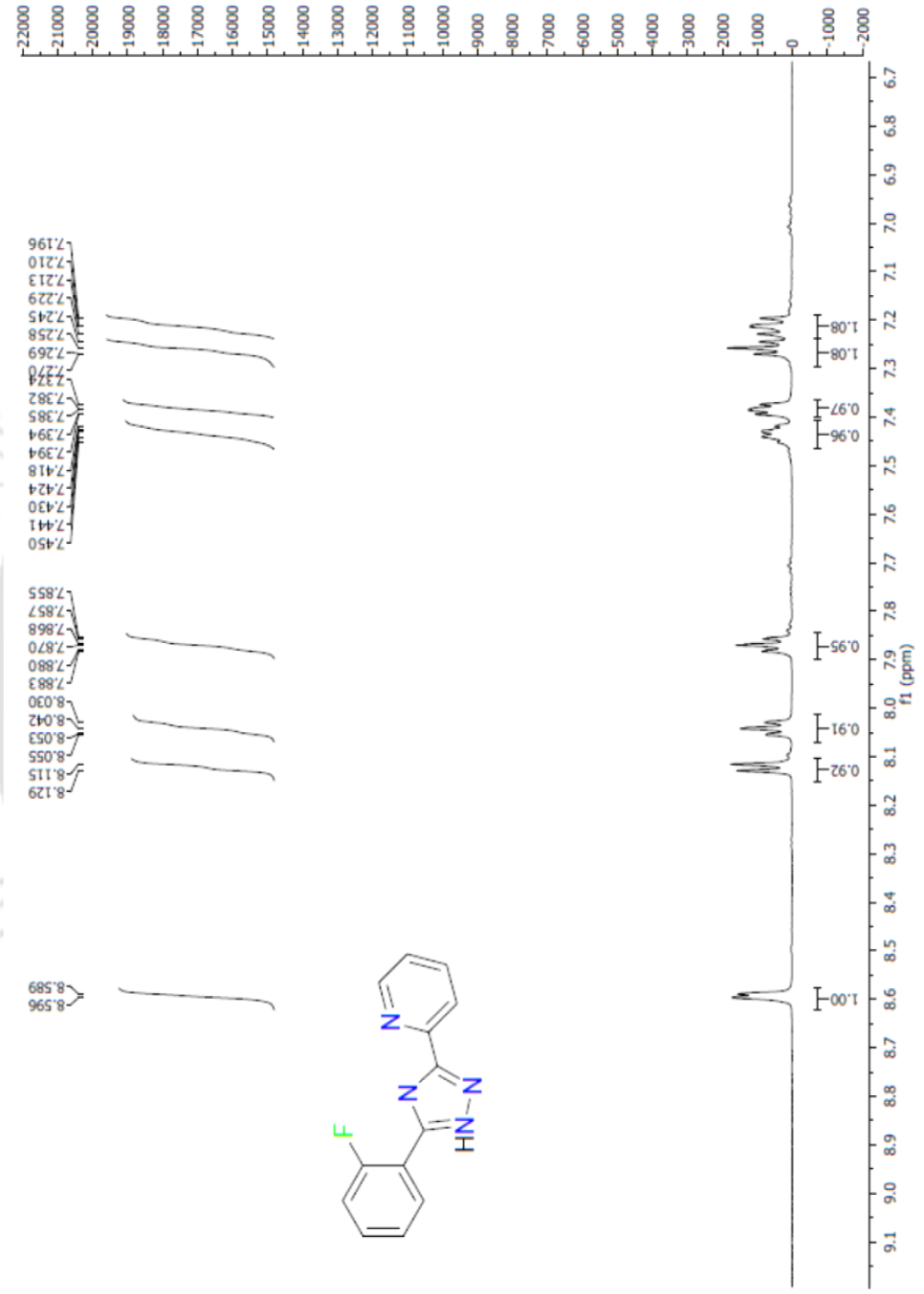

Spectrum 1. ^{1}H NMR spectrum of ligand **trz-F** (600 MHz, DMSO d_6).

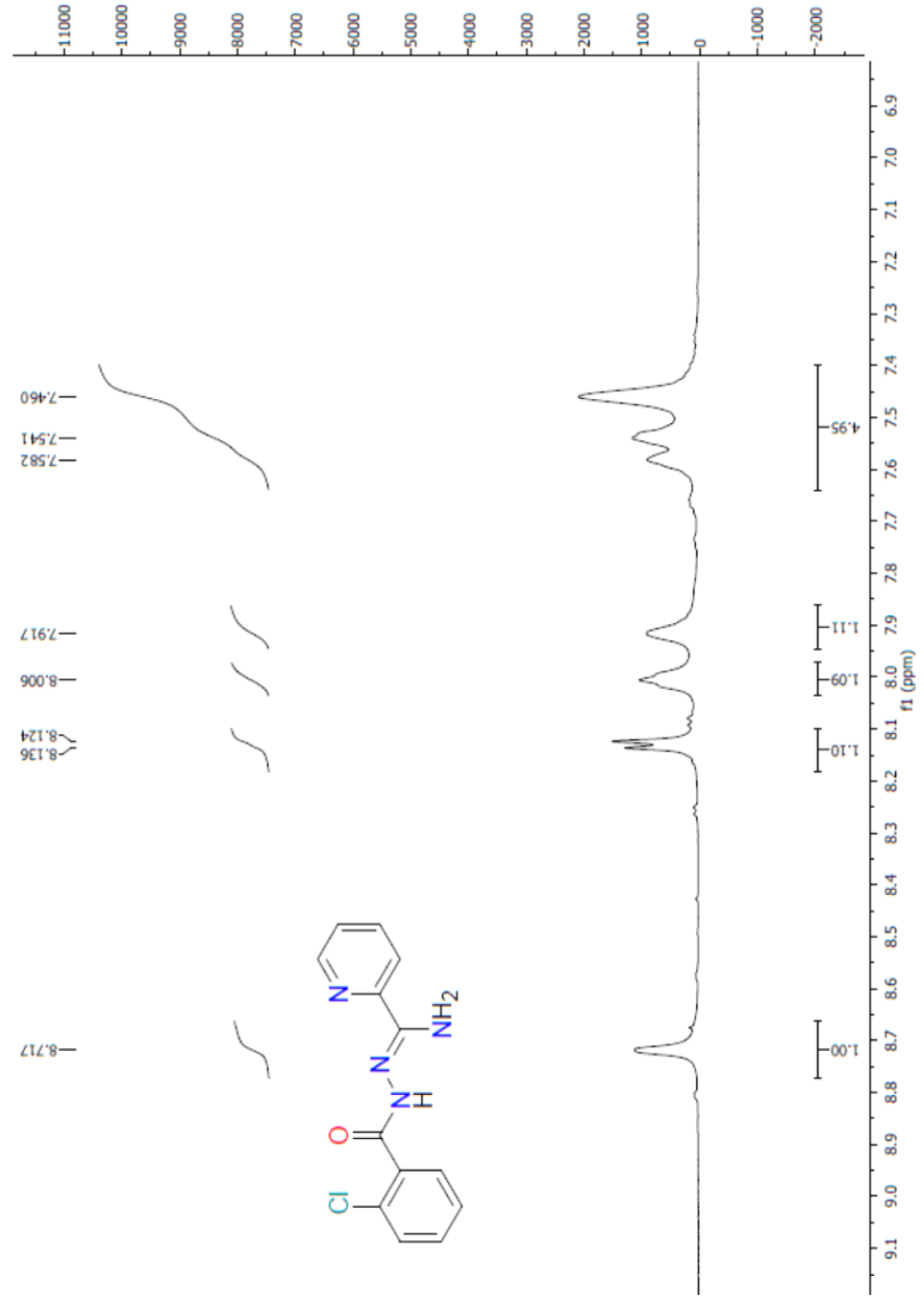

Spectrum 2. ^{1}H NMR spectrum of ligand **hyd-Cl** (600 MHz, DMSO d_6).

Spectrum 3. ESI MS of complex [Zn(**hyd-F**)Cl_2] (**1**).

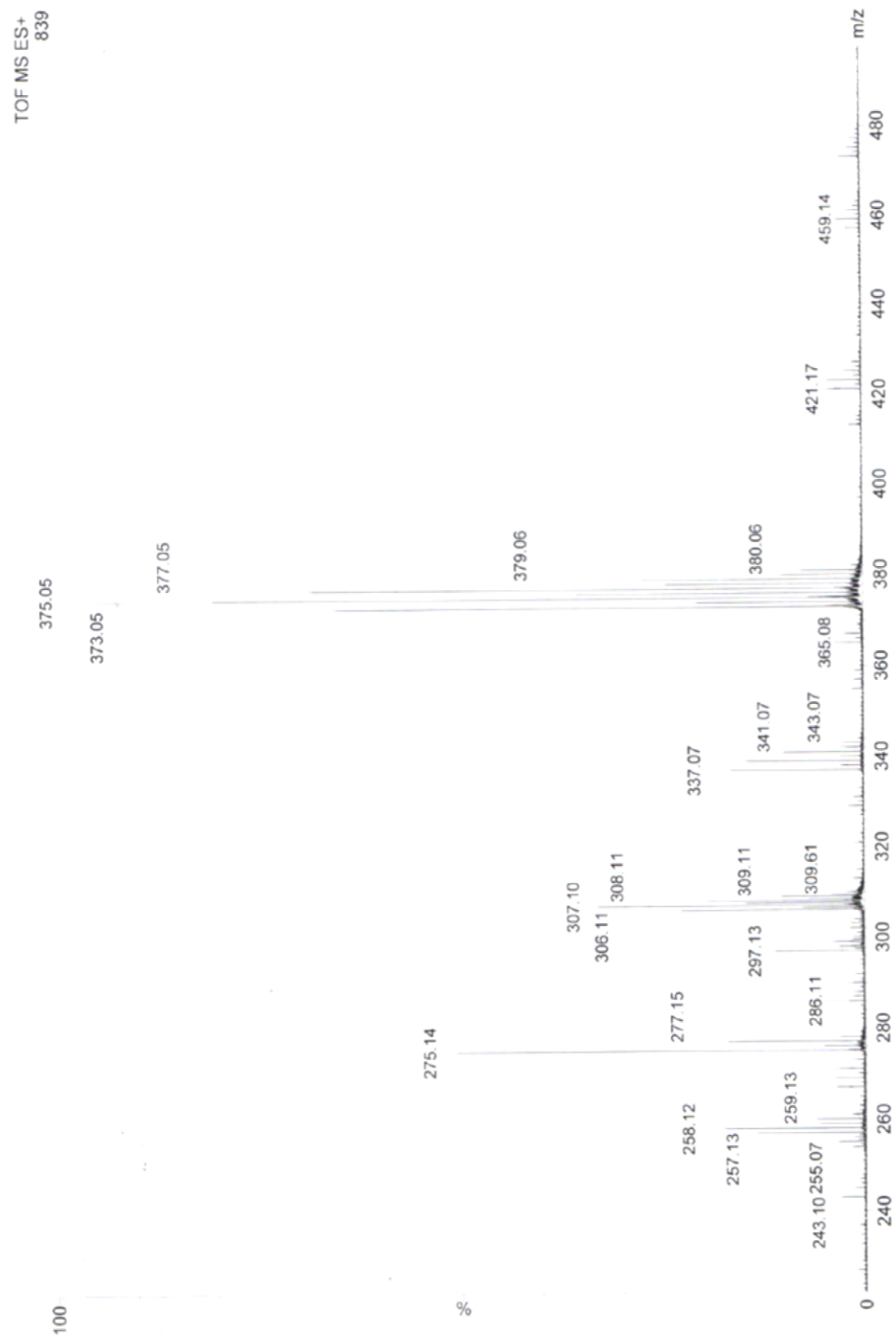

Spectrum 4. ESI MS of complex [Zn(**hyd-Cl**)Cl_2] (**2**).

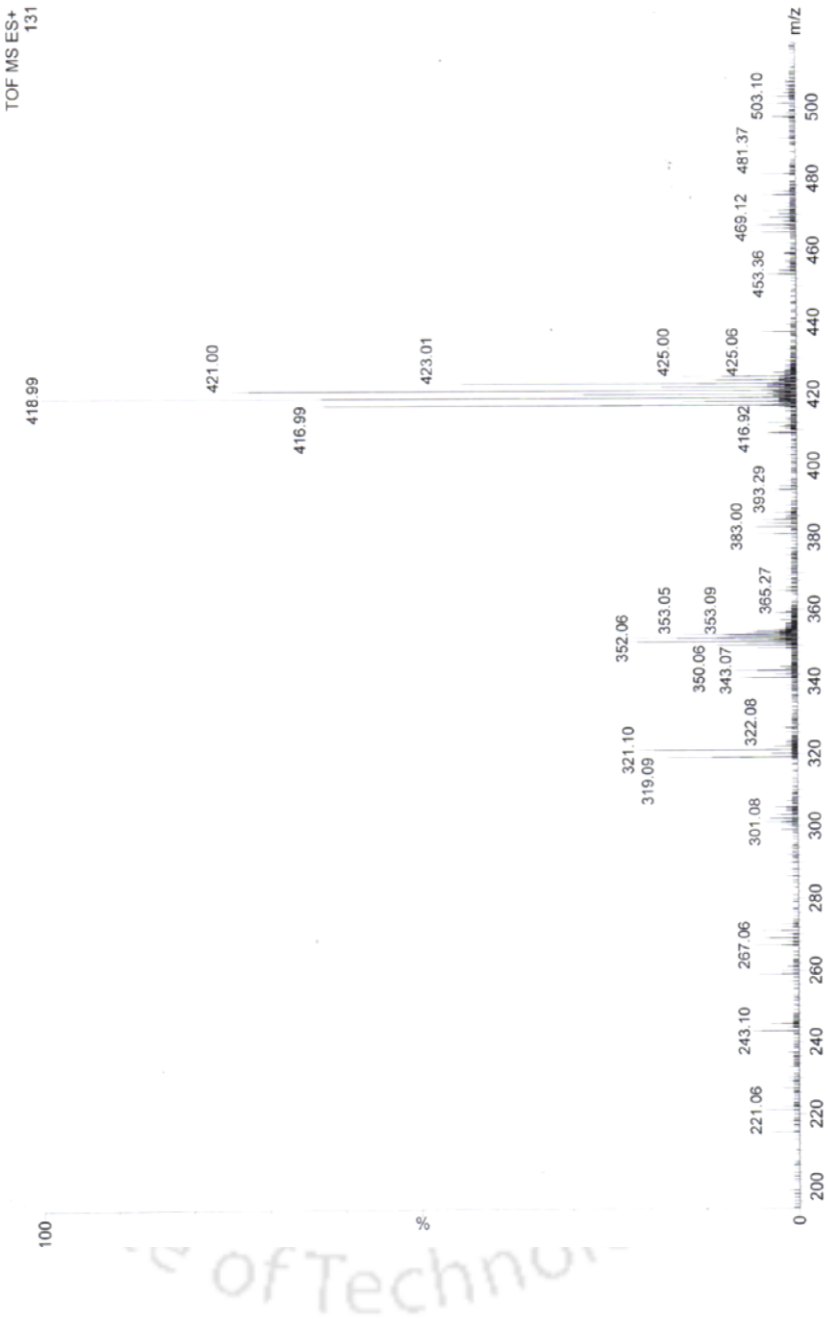

Spectrum 5. ESI MS of complex [Zn(**hyd-Br**)Cl_2] (**3**).

Reference

[1] (a) A. S. Eustaquio, D. O'Hagan, B. S. Moore, *J. Nat. Prod.* **2010**, *73*, 378; (b) D. Seebach, *Angew Chem. Int. Ed. Eng*. **1990**, *29*, 1320.

[2] (a) M. C. Pfrunder, A. S. Micallef, L. Rintoul, D. P. Arnold, J. McMurtrie, *Cryst. Growth Des.* **2016**, *16*, 681; (b) G. M. Espallargas, L. Brammer, P. Sherwood, *Angew. Chem. Int. Ed.* **2006**, *45*, 435; (c) R. Bertani, P. Sgarbossa, A. Venzo, F. Lelj, M. Amati, G. Resnati, T. Pilati, P. Metrangolo, G. Terraneo, *Coord. Chem. Rev*. **2010**, *254*, 677.

[3] (a) A. C. Legon, *Phys. Chem. Chem. Phys.* **2010**, *12*, 7736; (b) S. J. Grabowski, *J. Phys. Chem. A* **2011**, *115*, 12340.

[4] (a) O. Hassel, *Nobel Lectures, Chemistry* 1963; Elsevier: Amsterdam, **1972**; (b) O. Hassel, *Science* **1970**, *170*, 497.

[5] (a) P. Smart, G. M. Espallargas, L. Brammer, *CrystEngComm* **2008**, *10*, 1335; (b) S. Q. Zang, Y. J. Fan, J. B. Li, H. W. Hou, C. W. Mak, T. *Cryst. Growth Des.* **2011**, *11*, 3395.

[6] H. L. Nguyen, P. N. Horton, M. B. Hoursthouse, A. C. Legon, D. C. Bruce, *J. Am. Chem. Soc.* **2004**, *126*, 16.

[7] (a) M. Baldrighi, G. Cavallo, M. R. Chierotti, R. Gobetto, P. Metrangolo, T. Pilati, G. Resnati, G. Terraneo, *Mol. Pharmaceutics* **2013**, *10*, 1760; (b) A. Lemmerer, *CrystEngComm* **2012**, *14*, 2465.

[8] (a) E. Cariati, A. Forni, S. Biella, P. Metragolo, F. Meyer, G. Resnati, S. Righetto, E. Tordin, R. Ugo, *Chem. Commun*. **2007**, 2590; (b) P. Metrangolo, Y. Carcenac, M. Lahtinen, T. Pilati, K. Rissanen, A. Vij, G. Resnati, *Science* **2009**, *323*, 1461.

[9] (a) A. R. Voth, A. F. Hays and P. S. Ho, *J. Nat. Prod.* **2007**, *104*, 6188; (b) S. Sirimulli, J. B. Bailey, R. Vegesma, M. Narayana, *J. Chem. Inf. Model* **2013**, *53*, 2781; (c) K. S. Nayak, K. Reddy, T. N. Guru Row, D. Chopra, *Cryst. Growth Des.* **2011**, *11*, 1578.

[10] (a) D. Chopra, K. Nagarajan, T. N. Guru Row, *Cryst. Growth Des.* **2005**, *5*, 1035; (b) D. Chopra, T. N. Guru Row, *Cryst. Growth Des*. **2005**, *5*, 1679; (c) J. Ridout, M. R. Probert, *Cryst. Growth Des.* **2013**, *13*, 1943.

[11] S. K. Nayak, G. Terraneo, A. Forni, P. Metrangolo, G. Resnati, *CrystEngComm* **2012**, *14*, 4259.

[12] (a) Y. Y. Zhu, H. P. Yi, C. Li, X. K. Jiang, Z. T. Li, *Cryst. Growth Des.* **2008**, *8*, 1294; (b) Y. Y. Zhu, L. Jiang, Z. -T. Li, *CrystEngComm* **2009**, *11*, 235; (b) J. N. Moorthy, R. Natarajan, P. Mal, P. Venugopalan, *J. Am. Chem. Soc.* **2002**, *124*, 6530.

[13] C. Li, S. F. Ren, J. L. Hou, H. P. Yi, S. Z. Zhu, X. K. Jiang, Z. -T. Li, *Angew. Chem. Int. Ed. Eng.* **2005**, *44*, 5725.

[14] D. L. Widner, Q. R. Knauf, M. T. Merucci, T. R. Fritz, J. S. Sauer, E. D. Speetzen, E. Bosch, N. P. Bowling, *J. Org. Chem.* **2014**, *79*, 6269.

[15] (a) M. C. Etter, *Acc. Chem. Res.* **1990**, *23*, 120; (b) M. C. Etter, *J. Phys. Chem. A* **1991**, *95*, 4601.

[16] (a) M. Palusiak, S. J. Grabowski, *Struct. Chem.* **2007**, *18*, 859; (b) M. Jabłoński, *J. Phys. Chem. A* **2012**, *116*, 3753.

[17] M. P. Johansson, M. Swart, *Phys. Chem. Chem. Phys.* **2013**, *15*, 11543.

[18] (a) T. A. O. Fonseca, M. P. Freitas, R. A. Cormanich, T. C. Ramalho, C. F. Tormena, R. Rittner, *Beilstein J. Org. Chem.* **2012**, *8*, 112; (b) D. Dey, S. Bhandary, A. Sirohiwal, V. R. Hathwar, D. Chopra, *Chem. Commun.* **2016**, *52*, 7225; (c) N. Hergué, P. Leriche, P. Blanchard, M. Allain, N. Gallego-Planas, P. Frère, J. Roncali, *New J. Chem.* **2008**, *32*, 932.

[19] (a) V. R. Pedireddi, S. D. Reddy, B. S. Goud, D. C. Craig, A. D. Rae, G. R. Desiraju, *J. Chem. Soc. Perkin Trans. 2*, **1994**, 2353; (b) I. Saraogi, V. G. Vijay, S. Das, K. Sekar and T. N. Guru Row, *Crystallogr. Eng.* **2003**, *6*, 69; (c) B. T. Gowda, B. P. Sowmya, J. Kozísek, M. Tokarcík, H. Fuess, *Acta Crystallogr* **2007**, *E63*, o2906; (d) B. K. Saha, A. Nangia, J. F. Nicoud, *Cryst. Growth Des.* **2006**, *6*, 1278; (e) F. C. Pigge, V. R. Vangala, D. C. Swenson, *Chem. Commun.* **2006**, 2123.

[20] (a) P. Politzer, P. Lane, M. C. Concha, Y. Ma, J. S. Murray, *J. Mol. Model* **2007**, *13*, 305; (b) D. Hauchecorne, B. J. Veken, A. Moiana, W. A. Herrebout, *Chem. Phys.* **2010**, *374*, 30.

[21] L. Brammer, E. A. Bruton, P. Sherwood, *Cryst. Growth Des.* **2001**, *1*, 277; (b) G. Aullón, D. Bellamy, L. Brammer, E. A. Bruto, A. G. Orpen, *Chem. Commun.* **1998**, *6*, 653; (c) H. R. Khavasi, F. Norouzi, A. A. Tehrani, *Cryst. Growth Des.* **2015**, *15*, 2579.

[22] (a) L. Brammer, J. K. Swearingen, E. A. Bruton, P. Sherwood, *Proc. Nat. Acad. Sci., U. S.A.* **2002**, *99*, 4956; (b) J. C. M. Rivas, L. Brammer, *Inorg. Chem.* **1998**, *37*, 4756; (c) G. R. Lewis, A. G. Orpen, *J. Chem. Soc., Chem. Commun.* **1998**, *17*, 1873.

[23] (a) G. M. Espallargas, F. Zordan, L. A. Marín, H. Adams, K. Shankland, J. Streek, L. Brammer, *Chem. Eur. J.* **2009**, *15*, 7554; (b) Y. Wei, B. Xu, C. L. Barnes, Z. Peng, *J. Am. Chem. Soc.* **2001**, *123*, 4083.

[24] B. N. Ghosh, M. Lathinen, E. Kalenius, P. Mal, K. Rissanen, *Cryst. Growth Des.* **2016**, *16*, 2527.

[25] (a) P. Metrangolo, H. Neukirch, T. Pilati, G. Resnati, *Acc. Chem. Res.* **2005**, *38*, 386; (b) A. Mukherjee, S. Tothadi, G. Desiraju, *Acc. Chem. Res.* **2014**, *47*, 2514.

[26] (a) Y. -X. Lu, J. -W. Zou, Y. -H. Wang, Y. -J. Jiang, Q. -S. Yu, *J. Phys. Chem. A* **2007**, *111*, 10781; (b) N. J. M. Amezaga, S. C. Pamies, N. M. Peruchena, G. L. Sosa, *J. Phys. Chem. A* **2010**, *114*, 552; (c) Y. Zeng, X. Zhang, X. Li, L. Meng and S. Zheng, *ChemPhysChem* **2011**, *12*, 1080.

[27] C. F. Matta, N. Castillo, R. J. Boyd, *J. Phys. Chem. A* **2005**, *109*, 3669.

[28] A. Mandal, B. K. Patel, *ChemistrySelect* **2017**, *2*, 494.

[29] S. J. Grabowski, *J. Phys. Chem. A* **2012**, *116*, 1838.

[30] H. A. Bent, *Chem. Rev.* **1961**, *61*, 275.

[31] (a) P. K. Thallupally, A. Nangia, *CrystEngComm* **2001**, *3*, 114; (b) C. B. Aakeröy, T. A. Evans, K. R. Seddon, I. Pálinkó, *New J. Chem.* **1999**, *23*, 145; (c) R. Taylor, *Cryst. Growth Des.* **2016**, *16*, 4165; (d) R. Banerjee, G. R. Desiraju, R. Mondal, J. A. K. Howard, *Chem. Eur. J.* **2004**, *10*, 3373.

[32] (a) M. D. Prasanna, T. N. Guru Row, *Cryst. Eng.* **2000**, *3*, 135; (b) A. N. M. M. Rahman, R. Bishop, D. C. Craig and M. L. Schudder, *CrystEngComm* **2003**, *5*, 422.

[33] (a) D. G. Truhlar and Y. Zhao, *Theor. Chem. Acc.* **2008**, *120*, 215; (b) A. J. Parker, J. Stewart, K. J. Donald, C. A. Parish, *J. Am. Chem. Soc.* **2012**, *134*, 5165; (c) G. Wang, Z. Chen, Z. Xu, J. Wang, Y. Yang, T. Cai, J. Shi,W. Zhu, *J. Phys. Chem. B* **2016**, *120*, 610.

[34] (a) A. D. Becke, *J. Chem. Phys.* **1993**, *98*, 5648; (b) A. D. Becke, *Phys. Rev.* **1988**, *A38*,3098; (c) C. Lee, W. Yang, R. G. Parr, *Phys. Rev.* **1988**, *B37*, 785; (d) B. Civalleri, C. M. Zicovich-Wilson, L. Valenzano, P. Ugliengo, *CrystEngComm* **2008**, *10*, 405.

[35] S. F. Boys, F. L. Bernardi, *Mol. Phys.* **1970**, *19*, 553.

[36] Gaussian 09, M. J. Frisch, G. W. Trucks, J. R. Cheeseman, G. Scalmani, M. Caricato, H. P. Hratchian, X. Li, V. Barone, J. Bloino, G. Zheng, T. Vreven, J. A. Jr. Montgomery, G. A. Petersson, G. E. Scuseria, H. B. Schlegel, H. Nakatsuji, A. F. Izmaylov, R. L. Martin, J. L. Sonnenberg, J. E. Peralta, J. J. Heyd, E. Brothers, F. Ogliaro, M. Bearpark, M. A. Robb, B. Mennucci, K. N. Kudin, V. N. Staroverov, R. Kobayashi, J. Normand, A. Rendell, R. Gomperts, V. G. Zakrzewski, M. Hada, M. Ehara, K. Toyota, R. Fukuda, J. Hasegawa, M. Ishida, T. Nakajima, Y. Honda, O. Kitao, H. Nakai.

[37] T.A. Keith, AIMAll (Version 13.11.04). TK Gristmill Software, Overland Park, KS, USA, 2013.

[38] (a) R. F. W. Bader, *Chem. Rev.* **1991**, *91*, 893; (b) R. F. W. Bader, *Atoms in Molecules: A Quantum Theory*; Oxford University Press: Oxford, U.K., **1990**; (c) C. Matta, R. J. Boyd,

Quantum Theory of Atoms in Molecules: Recent Progress in Theory and Application Eds.; Wiley-VCH: New York, **2007**.

[39] (a) A. L. Spek, *Acta Cryst. D* **2009**, *65*, 148; (b) M. Nardelli, *J. Appl. Cryst.* **1995**, *28*, 659.

[40] (a) A. D. Becke, *J. Chem. Phys.* **1993**, *98*, 5648; (b) C. Lee, W. Yang, R. G. Parr, *Phys. Rev.* B **1988**, *37*, 785.

Chapter 4

Molecular Structures and Fluorescence Property of Zn(II), Cd(II) Complexes of 3-Pyridyl-5-aryl-(1*H*)-1,2,4-triazoles

The reaction of two 3-pyridyl-5-aryl substituted 1,2,4-triazole ligands (**trz-1** and **trz-2**) with $M(NO_3)_2$ and MCl_2 (M = Zn^{II}/Cd^{II}) afforded metal complex [Zn(**trz-1**)Cl_2], [Cd(**trz-1**)$_2(NO_3)_2$] and [Zn^{II}/Cd^{II}(**trz-2**)$_2$]$(NO_3)_2 \cdot H_2O$. Reaction $Cd(NO_3)_2$, **trz-2** and NaNCS in 1:1:1 molar ratio resulted the complex [Cd(**trz-2**)$_2(NCS)_2$]. These complexes have been characterized by spectroscopic analyses and X-ray crystallography. Crystal structures of the complexes show the presence of classical as well as non-classical C−H···O, C−H···F and C−H···S hydrogen bonds along with strong π···π interaction between the triazole moieties. The complexes possess satisfactory photoluminescence property both in solid state and DMSO solution. DFT and TD-DFT studies have been performed to understand emission behavior of the complexes.

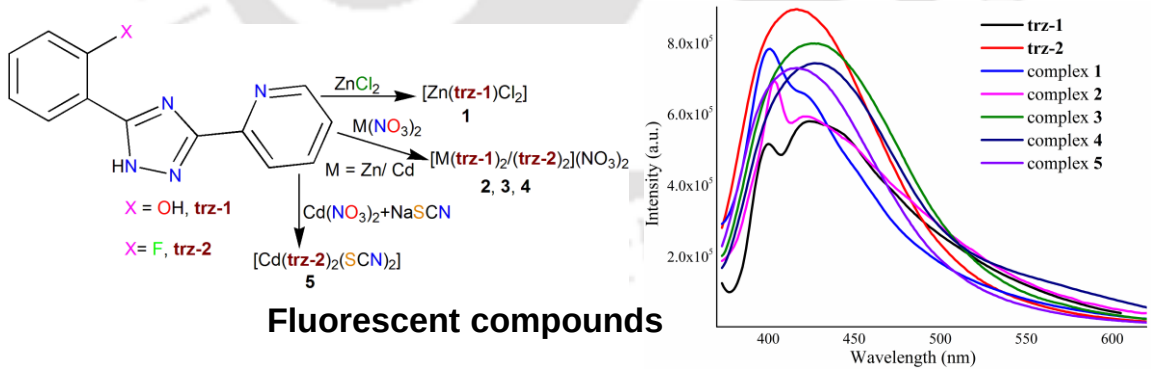

This work has been submitted for publication.

4. 1. Introduction

Triazoles are nitrogen rich heterocycles which can be considered as structural combination of pyrazole and imidazole for the relative disposition for three nitrogen atoms in the heterocyclic backbone.[1] Triazoles are broadly categorised into two classes, namely, 1,2,3-triazole and 1,2,4-triazole.[2] Multidenate 1,2,4-triazole based ligands offer versatile coordination chemistry as tuning of the substituents on triazole ring leads to the formation of various functional materials. Haasnoot[3] and Brooker[4] have reported spin crossover (SCO) property of iron(II) complexes of 4-substitued-1,2,4-triazole ligands. The stabilisation of deprotonated triazolato ring via π-electron delocalisation results in interesting electrochemistry of Ru(II) complexes of 1,2,4-triazole based ligands.[5] Few first row transitional metal complexes of 1,2,4-triazole based ligands demonstrate satisfactory antibacterial, anti-tumor and DNA cleavage property (Figure 1).[6]

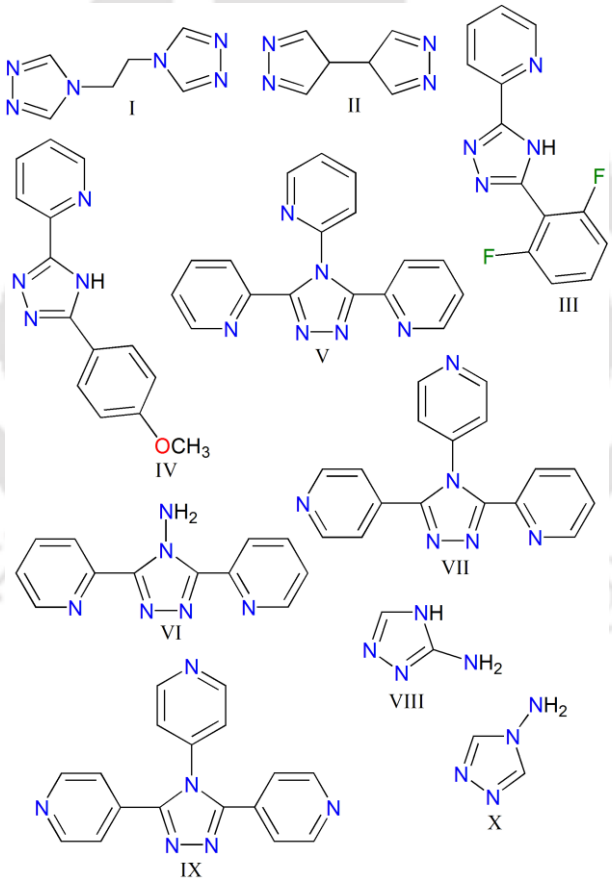

Figure 1. Few 1,2,4-triazole based ligands reported earlier; (I-IV) used to form luminescent Zn(II) and Cd(II) complexes;[12-13] (V-VI) used to form Fe(II) complexes with spin crossover property;[4] (VII-X) used to form metal organic framework (MOF).[8]

1,2,4-triazole based ligands with pyridyl, pyrazinyl substituents are known to form multinuclear metal complexes as well as coordination polymers through bridging nitrogen donor centers.[7-8] Some of the multinuclear complexes of substituted 1,2,4-triazole exhibit antiferromagnetic coupling of metal centers[7] and photoluminescence.[8] In recent years, d^{10} metal complexes heterocyclic ligands have received considerable attention from scientific community for their photoluminescence property and potential use as organic light emitting diode (OLED) materials. Cu(I),[9] Ag(I),[10] Au(I),[11] Zn(II)[12] and Cd(II)[13] should be mentioned in this regard. The d^{10} metal complexes heterocyclic ligands have been proven as judicious choice as luminescent materials as they are not prone to oxidation or reduction at the ligand center.[14] It has been reported earlier that in most of these complexes, d^{10} metal complexes of heterocyclic ligands exhibit intraligand and not ligand to metal charge transfer or metal centered emission.[14]

We have synthesised two fluorescent 1,2,4-triazole ligands *viz.* 3-pyridyl-5-aryl-(1*H*)-1,2,4-triazole ligands, namely, 2-(3-(pyridin-2-yl)-1*H*-1,2,4-triazol-5-yl)phenol (**trz-1**) and 2-[5-(2-fluoro-phenyl)-1*H*-[1,2,4]triazol-3-yl]-pyridine (**trz-2**) (Scheme 1) and their Zn(II), Cd(II) metal complexes. The *ortho* substitution on aryl group of ligand framework has been varied from hydrogen bond donor hydroxy group to non-polarizable organic fluorine (C−F), which exerted remarkable effects in the supramolecular assemblies of the complexes. These ligands as well as their Zn(II) and Cd(II) complexes exhibit fluorescence in both solid state and DMSO solution. Analysing and quantifying non-covalent interactions in the supramolecular assembly of metal complexes is an emerging field of crystal engineering. Recently, the decisive roles of non-classical hydrogen bonds as well as π···π, anion···π and M···π interactions in dictating crystal packing of metal complexes have been reported extensively.[15] Herein, we have investigated the role of non-classical hydrogen bonds and π···π interactions as well as the classical hydrogen bonds in determining the supramolecular assemblies of the metal complexes. In addition, fluorescence property of the metal complexes has been explored with the help of DFT and TD-DFT studies.

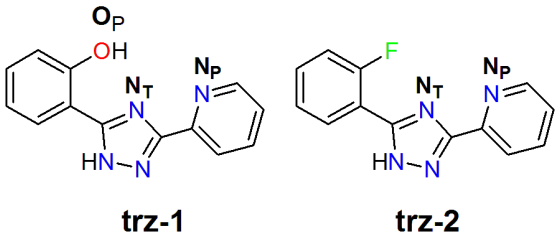

Scheme 1. Ligands used for the study.

4. 2. Results and Discussion

4. 2. 1. IR and UV-Visible spectra

The ligands **trz-1**, **trz-2** and their complexes show characteristic peaks due to C=N and N−N stretching frequencies of the triazole ring respectively in the range 1630-1580 cm^{-1} and 1050-950 cm^{-1}. Pyridine ring C−H bending vibrations are observed in the range of 835-745 cm^{-1} and the peak due to thiocynate stretching appears at 2100 cm^{-1}. Peaks for π→π* and n→π* transitions are observed respectively in the range 236 nm and 288 nm in the UV-visible spectra of ligands **trz-1**, but the π→π* band is considerably red shifted compared to free ligand (261-266 nm) in complexes **1** and **2**. In contrary, the n→π* is red shifted in **1** (320 nm) but not in **2**. The π→π* and n→π* transitions in complexes **3** and **4**, exhibit no practical change from ligand **trz-2**. However, both π→π* and n→π* transitions are significantly blue shifted as compared to free ligand in complex **5** (Figure 2). The intensity of π→π* transitions is many fold higher than n→π* transitions. The metal complexes (**1-5**) exhibit intraligand π→π* and n→π* transitions in their UV-visible spectra. It is pertinent to mention that no ligand to metal charge transfer (LMCT) transition was observed in metal complexes **1-5**. Table 1 contains the characteristic peak values of IR and UV-Visible spectra of complex **1-5** and ligands **trz-1**, **trz-2**. Time dependent DFT (TD-DFT) studies confirm the intraligand nature of transitions observed in metal complexes **1-5**.

Table 1

IR and UV-Visible peak values of **trz-1**, **trz-2** and metal complexes **1-5**

Compound	IR (cm^{-1})	UV-Vis [λ_{max}(nm), ε ($M^{-1}cm^{-1}$)]
trz-1	C=N stretching: 1629, 1593 N−N stretching: 1017, 978 Pyridine ring bending: 834, 800, 749	236 (8870), 288 (4100)
trz-2	C=N stretching: 1620, 1600 N−N stretching: 1033, 1011 Pyridine ring bending: 826, 799, 743	284 (10700), 320 (15390)
Complex **1**	C=N stretching: 1638,1612 N−N stretching: 1015, 991 Pyridine ring bending: 825, 801, 747	272 (5650), 298 (8980), 331 (2170)
Complex **2**	C=N stretching: 1638,1612 N−N stretching: 1040, 986	261 (11175), 292 (14390)

	Pyridine ring bending: 825, 801,747	
Complex **3**	C=N stretching: 1623,1589 N−N stretching: 1036, 1000 Pyridine ring bending: 823, 804, 758	284 (16570), 319 (5800)
Complex **4**	C=N stretching: 1621,1600 N−N stretching: 1018, 984 Pyridine ring bending: 823, 804, 756	276 (15680), 284 (15240), 314 (7990)
Complex **5**	C=N stretching: 1621, 1603 N−N stretching: 1017, 985 Pyridine ring bending: 823, 801, 751 Thiocynate stretching: 2100	248 (16200), 285 (5130)

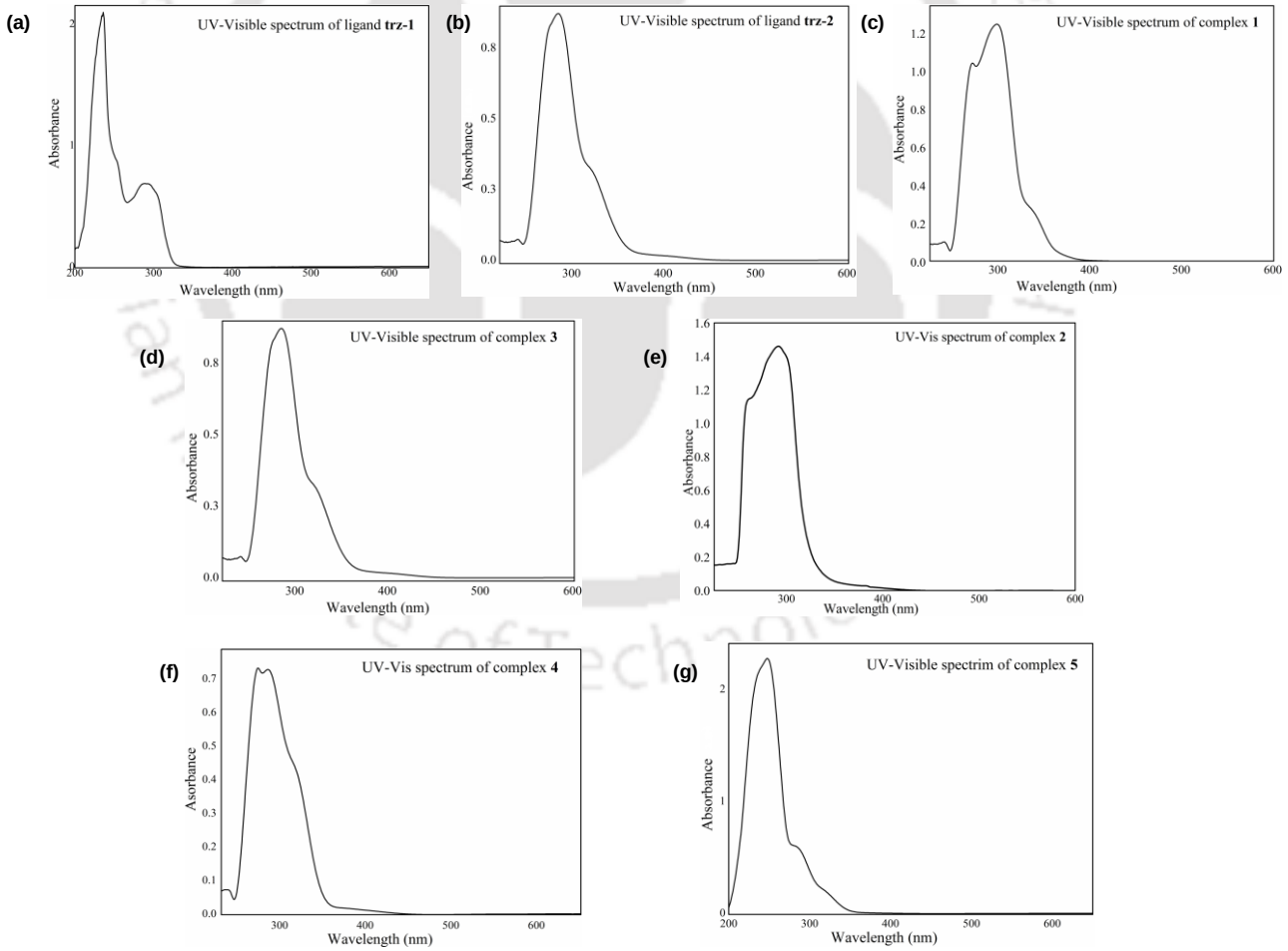

Figure 2. UV-Visible spectra of ligands **trz-1**, **trz-2** and complexes **1-5**.

Table 2

Crystallographic and refinement parameters complexes **1-5**

	1	**2**	**3**
chem formula	$C_{16}H_{17}N_5O_2ZnCl_2$	$C_{26}H_{20}N_{10}O_8Cd$	$C_{26}H_{18}N_{10}O_9F_2Zn$
formula wt	447.64	712.93	719.75
temp (K)	296	296	296
CCDC Number	1451162	1451164	1533713
crystal system	monoclinic	orthorhombic	monoclinic
space group	*C*2/*c*	*Pbcn*	*C*2/*c*
a (Å)	27.1560(2)	17.9094(7)	16.4590(13)
b (Å)	7.5701(6)	10.9211(4)	13.1212(13)
c (Å)	19.4520(2)	14.0541(6)	14.7106(13)
α (°)	90.00	90.00	90.00
β (°)	106.686(7)	90.00	105.787(8)
γ (°)	90.00	90.00	90.00
V (Å^3)	3830.4(6)	2748.86(19)	3057.1(5)
Z	8	4	4
μ (mm^{-1})	1.582	0.865	0.885
ρ_{calcd} (g cm^{-3})	1.553	1.723	1.564
no. of unique rflns	3454	2693	2860
no. of rflns ($I \geq 2\sigma(I)$)	2782	2019	2856
R_1[a], wR_2[b] ($I \geq 2\sigma(I)$)	0.0515, 0.1381	0.0314, 0.0746	0.0457, 0.1212
R_1[a], wR_2[b] (all data)	0.0623, 0.1565	0.0491, 0.0860	0.0457, 0.1212
goodness of fit (F^2)	0.993	1.026	1.000
largest peak/hole (e Å^{-3})	0.970/-0.854	0.427/-0.311	0.418/-0.230

	4	**5**
chem formula	$C_{26}H_{18}N_{10}O_9F_2Cd$	$C_{28}H_{18}N_{10}S_2F_2Cd$
formula wt	764.91	709.06
temp (K)	296	296
CCDC Number	1533714	1533715
crystal system	monoclinic	monoclinic
space group	*C*2/*c*	*C*2/*c*
a (Å)	16.6691(4)	16.3400(9)
b (Å)	13.2767(4)	12.8173(5)
c (Å)	14.7097(5)	14.4706(8)
α (°)	90.00	90.00
β (°)	107.359(2)	102.559(5)
γ (°)	90.00	90.00
V (Å^3)	3107.14(16)	2958.1(2)
Z	4	4
ρ (mm^{-1})	0.783	0.930
μ_{calcd} (g cm^{-3})	1.635	1.592
no. of unique rflns	3812	2757
no. of rflns ($I \geq 2\sigma(I)$)	3088	2242
R_1[a], wR_2[b] ($I \geq 2\sigma(I)$)	0.0379, 0.1122	0.0496, 0.1446
R_1[a], wR_2[b] (all data)	0.0478, 0.1199	0.0615, 0.1630
goodness of fit (F^2)	1.037	1.034
largest peak/hole (e Å^{-3})	0.572/-0.289	0.089/-0.497

Table 3

List of selected bond lengths (Å) and bond angles (°) in **1** and **2**

1		**2**	
Zn1−N1	2.188(3)	Cd1−N1	2.324(3)
Zn1−N2	2.032(3)	Cd1−N2	2.426(2)
Zn1−O1	2.403(3)	Cd1−O2	2.469(3)
Zn1−Cl1	2.225(1)	Cd1−O3	2.762(2)
Zn1−Cl2	2.273(1)	O2−Cd1−O3	47.59(7)
Cl1−Zn1−Cl2	113.61(4)	N1−Cd1−O2	84.74(9)
N1−Zn1−N2	77.8(1)	N1−Cd1−N2	70.93(8)
N2−Zn1−O1	75.0(1)	N1−Cd1−O2′	90.80(9)
N1−Zn1−O1	152.7(1)	N1−Cd1−N1′	153.60(8)
N2−Zn1−Cl1	129.71(8)	N2−Cd1−O2	118.83(8)
N2−Zn1−Cl2	115.84(8)	O2−Cd1−O2′	160.44(7)
N1−Zn1−Cl1	100.31(9)	N1−Cd1−N2′	132.54(8)
O1−Zn1−Cl1	129.71(8)	O2−Cd1−O2′	160.44(7)
N1−Zn1−Cl2	102.36(8)	N2−Cd1−O2′	77.16(8)
		N2−Cd1−N2′	80.15(7)

Table 4

Hydrogen bonding interactions in complex **1** and **2**

Molecule	D–H···A	D···A (Å)	H···A (Å)	∠D–H···A (°)	Symmetry
1	N4−H4A···Cl2	3.207(2)	2.429	150.79	-x,-y,-z+1
	O1−H1P···O2	2.557(2)	1.770	175.74	x,-y+1,z-1/2
	C13−H13···Cl2	3.683(3)	2.838	151.60	-x,-y,-z+1
2	O1−H1A···O3	2.786(4)	1.961	164.71	-x+1,y-1,-z+1/2
	N4−H4A···O1	2.680(4)	2.148	115.38	x,y,z
	N4−H4A···O4	3.513(5)	2.616	158.16	x,-y+1,z+1/2
	Cg···Cg	4.025			-x+1,-y+1,-z+1

Table 5

Selected bond lengths (Å) and angles (°) in complex **3**, **4** and **5**

Zn1−O1	2.108(2)	Cd1−O1	2.290(2)	Cd1−S1	2.631(1)
Zn1−N1	2.148(3)	Cd1−N1	2.350(2)	Cd1−N1	2.355(4)
Zn1−N2	2.217(2)	Cd1−N2	2.369(2)	Cd1−N2	2.446(4)
O1−Zn1−N1	92.21(10)	O1−Cd1−N1	96.61(9)	S1−Cd1−N1	93.22(10)
O1−Zn1−N2	95.66(9)	O1−Cd1−N2	98.86(8)	S1−Cd1−N2	102.57(10)

N1−Zn1−N2	76.96(9)	N1−Cd1−N2	72.39(7)	N1−Cd1−N2	71.48(13)
O1−Zn1−O1′	87.99(13)	O1−Cd1−O1′	86.21(12)	S1−Cd1−S1′	83.05(7)
O1−Zn1−N1	92.79(10)	O1−Cd1−N1′	91.76(9)	S1−Cd1−N1′	102.57(10)
O1−Zn1−N2′	168.70(9)	O1−Cd1−N2′	163.75(9)	S1−Cd1−N2′	172.99(9)
N1−Zn1−N1′	173.05(13)	N1−Cd1−N1′	168.54(11)	N1−Cd1−N1′	158.93(19)
N1−Zn1−N2′	97.74(9)	N1−Cd1−N2′	98.64(7)	N2−Cd1−N2′	76.10(17)
N2−Zn1−N2′	82.80(13)	N2−Cd1−N2′	80.55(10)		

Table 6

Hydrogen bonding interactions in complex **3**, **4** and **5**

Compound	D−H···A	D···A (Å)	H···A (Å)	D−H···A (°)	Symmetry
3	N4−H4···O4	2.770(2)	1.901	162.43	-x+1/2,-y+1/2,-z+1/2
	C12−H12···F1	3.592(3)	2.733	154.03	-x+1/2,-y+1/2, -z+1
	C12−H12···O1	3.684(3)	2.956	136.13	x-1/2, -y+1/2,- z+1
	C2−H2A···N3	3.610(3)	2.696	167.53	-x-1/2,y-1/2,-z+1/2
	O1···O4	2.737(3)			x-1/2, -y+1/2, z+1/2
	O1···O5	2.808(2c)			-x+1/2,y-1/2, -z+1/2
	O2···O2	2.959(6)			-x+1, y,-z+1/2
	O2···O5	2.858(3)			-x+1, y,-z+1/2
	O3···O5	2.995(2)			-x+1, y,-z+1/2
	Cg···Cg	3.674(3)			-x,-y+1,-z+1
4	N4−H4A···O2	2.767(5)	1.932	163.42	-x+1/2,y-1/2, -z+1/2
	C10−H10···F1	3.733(4)	2.859	157.03	-x+1/2,-y+1/2, -z+1
	C10−H10···O1	3.515(3)	2.824	131.99	x-1/2, -y+1/2,- z+1
	C2−H2···N3	3.581(5)	2.682	162.89	-x-1/2,y-1/2,-z+1/2
	O1···O2	2.819(2)			x-1/2,-y+/2, z+1/2
	O1···O5	2.815(5)			x, y, z
	O3···O3	2.980(7)			-x+1, y,-z+1/2
	O3···O5	2.852(6)			-x+1/2,y-1/2,-z+1/2
	O4···O5	3.033(5)			-x+1/2,y+1/2, -z+1/2
	Cg···Cg	3.541(3)			-x,-y+1,-z+1
5	N4−H4A···N5	2.802(8)	1.958	166.68	-x+1, -y+2,- z+1
	C12−H12···F1	3.615(7)	2.720	161.78	-x+3/2,-y+3/2,-z+1
	C11−H11···S1	3.703(5)	3.374	126.35	-x+3/2,-y+3/2,-z+1
	Cg···Cg	3.666(5)			-x+1,-y+2,-z+1

4. 2. 2.Quantitative crystal structure description of complexes 1-5

The crystallographic and refinement parameters of metal complexes [Zn(**trz-1**)Cl_2]·DMF (**1**), [Cd(**trz-1**)$_2$(NO_3)$_2$] (**2**), [Zn(**trz-2**)$_2$(H_2O)$_2$](NO_3)$_2$·H_2O (**3**), [Cd(**trz-2**)$_2$(H_2O)$_2$](NO_3)$_2$·H_2O (**4**) and [Cd(**trz-2**)$_2$(NCS)$_2$] (**5**) are listed in Table 2. In order to maintain uniformity on type of coordination sites and hydrogen donor, acceptor atoms / groups following conventions were utilised throughout the chapter: O_P = phenol-O, O_N = nitrate-O, O_W = water-O, N_T = triazole-N (at 4th position in the ring) and N_P = pyridine-N (Scheme 1).

Crystal structure description of [Zn(trz-1)Cl_2]·DMF (1)

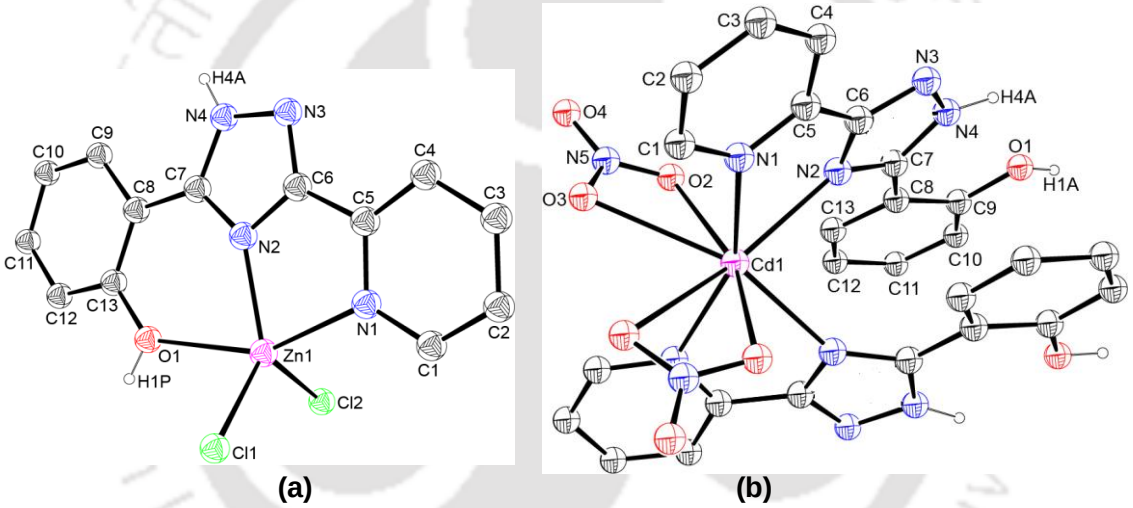

Figure 3. (a) *ORTEP* diagram of complex **1**, displacement ellipsoids are drawn on 30% probability; (b) *ORTEP* diagram of **2**, displacement ellipsoids are drawn on 30% probability level.

Complex **1** crystallizes in *C*2/*c* space group, the asymmetric unit is composed of one molecule of the metal complex and one lattice DMF molecule. In complex **1**, Zn(II) ion is penta-coordinated, ligand **trz-1** chelates the Zn(II) using five and six membered rings (Figure 2a) through O_P, N_P and N_T atoms and two chloride ions occupy remaining coordination sites. The calculated value of τ parameter (0.65) demonstrates that the geometry around the metal ion is a distorted trigonal bipyramidal with N_TCl_2 coordination forming a trigonal plane while O_P and N_P occupying axial sites. Axial O_P–Zn–N_P angle deviate largely from the ideal value by 27.3(1)° due to chelate bite constraints imposed on the ligand framework. The Zn–N_T

bond length is shorter by 0.16(3) Å than Zn−N_P and by 0.37(3) Å than Zn−O_P (Figure 3a). The triazole-NH is involved in intermolecular hydrogen bonding interaction with coordinated chlorine Cl2 of another molecule (N4···Cl2, 3.207(3) Å), thus generating a centrosymmetric dimer (Figure 4). The non-classical C−H···Cl interaction with considerable directionality (C−H···Cl, 151.47°) adds additional stability to this hydrogen bonded dimer. The BSSE corrected interaction energy for this hydrogen bonded dimeric pair is -15.14 kcal/mol. NBO analyses reveal the following values of second order perturbation energy, (lp)Cl→σ*(N−H), 5.33 kcal mol and (lp)Cl→σ*(C−H), 0.90 kcal mol. The centrosymmetric dimer is linked to oxygen atom of lattice DMF molecule through hydrogen bonding involving the phenolic hydrogen (O1···O2, 2.587(3) Å).

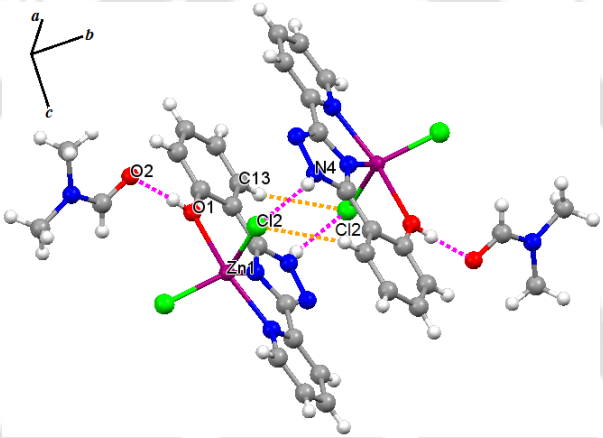

Figure 4. Symmetrical dimeric motif formed by hydrogen bonding in complex **1**.

Crystal structure description of [Cd(trz-1)$_2$(NO$_3$)$_2$] (2)

Bis-chelated cadmium complex **2** crystallized in *Pbcn* space group. The asymmetric unit contains half molecule of **2** with a glide plane passing through the central cadmium atom. Ligand **trz-1** is bound to the bivalent Cd(II) in its neutral form through N_P and N_T sites. The nitrate ion is coordinated as chelating ligand having a chelate bite angle of 47.59(7)° but with one short and another long bond. Ligand **trz-1** show a chelate bite angle of 70.93(8)° in complex **2** which is less than that was observed (77.8(1)°) in complex **1**. The geometry around Cd(II) can be best described as mono-capped pentagonal bipyramidal with four oxygen atoms being part of pentagonal basal plane. Two N_P atoms occupy axial sites and among two N_T atoms, one acts as a capping atom and the other as a part of the basal plane (Figure 2b). Due to capping, N_T atom that is part of basal plane is pushed from the plane as revealed by N_P−Cd−N_P angle 153.60(8)°. The Cd−N_T distance is longer than Cd–N_P distance

by 0.102(2) Å which is opposite to bond length trend found in complex **1**. Among the bound nitrate oxygen distances, Cd−O2 (2.469(3) Å) falls within the range that has been reported for nitrate bound cadmium complexes (Figure 3b).[16] However, Cd−O3 distance (2.762(2) Å) is little longer than that has been found in literature,[16] which certainly puts this bond in the margin between a covalent bond and strong non-bonding dipolar interaction. Selected bond lengths and bond angles for complexes **1** and **2** are given in Table 3.

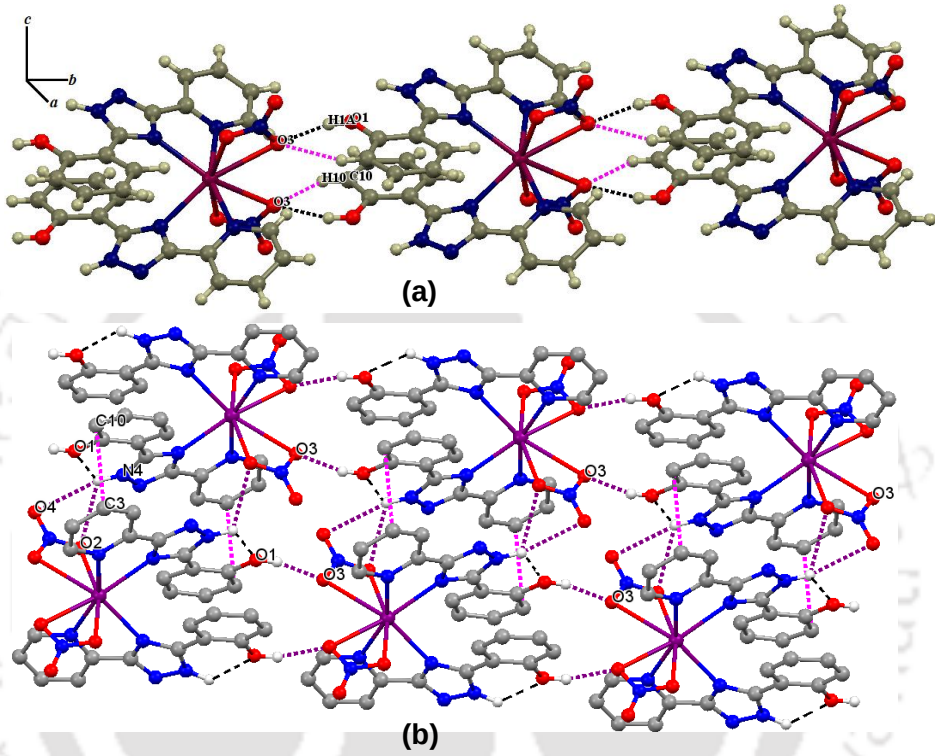

Figure 5. (a) Hydrogen bonded 1D chain in complex **2**; (b) Hydrogen bonding and π···π interaction in complex **2**.

The phenol group is intramolecularly hydrogen bonded with the triazole-NH to form N−H···O hydrogen bond (O1···N4, 2.680(4) Å). This interaction in turn allows the phenolic hydroxyl group to act as intermolecular hydrogen bond donor (O1···O3, 2.787(4) Å) to two nitrate oxygen atoms of neighbouring [Cd(**trz-1**)$_2$(NO$_3$)$_2$] unit. This generates a 1D chain along the crystallographic *b* axis as shown in Figure 5a. The BSSE corrected interaction energy for this hydrogen bonded chain has been calculated by taking two such units in consideration and the energy amounts to -24.29 kcal/mol. NBO analyses show the second order perturbation energy value for intramolecular N−H···O hydrogen bond; (lp)O→σ*(N−H), 2.87 kcal/mol. The values for intermolecular O−H···O hydrogen bonds are the following; (lp)O→σ*(O−H), 5.79 and 3.41 kcal/mol. These one dimensional chains are

joined to each other by hydrogen bonds between triazole-NH and nitrate oxygen (N4···O2, 3.116(4) Å and N4···O4, 3.513(5) Å) and face to face π···π interaction (C3···C10, 3.865(5) Å) to form an infinite two dimensional supramolecular assembly (Figure 5b). Useful donor acceptor distances in complex **1** and **2** are listed in Table 4.

Crystal structure description of $[Zn(trz\text{-}2)_2(H_2O)_2](NO_3)_2{\cdot}H_2O$ (3) and $[Cd(trz\text{-}2)_2(H_2O)_2](NO_3)_2{\cdot}H_2O$ (4)

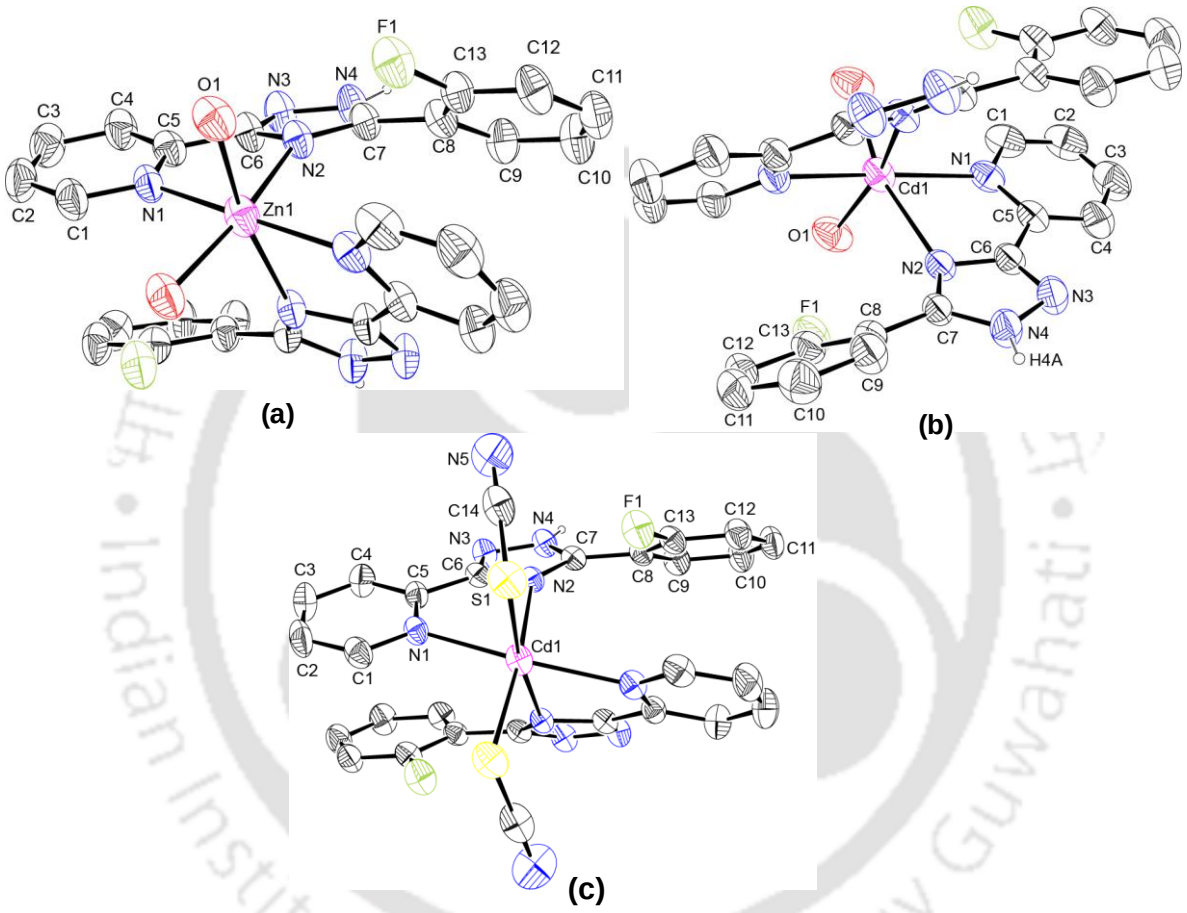

Figure 6. (a) *ORTEP* diagram of **3**, displacement ellipsoids are drawn on 30% probability level; (b) *ORTEP* diagram of **4**, displacement ellipsoids are drawn on 30% probability level; (c) *ORTEP* diagram of **5**, displacement ellipsoids are drawn on 30% probability level.

The *iso*-structural metal complexes **3** and **4** crystallized in *C*2/*c* space group, a glide plane passing through metal centre divides the molecule into two equal halves (Figure 6a and 6b). The asymmetric unit possesses one molecule of complex, one nitrate ion and two half water molecules. The bivalent metal center is bis-chelated by **trz-2** which coordinates through triazole (N_T) and pyridyl (N_P) nitrogen in a bidentate fashion and remaining two co-ordination sites are occupied by water molecules. The coordination environment around the

metal center is $(N_P)_2(N_T)_2(O_w)_2$ having the *trans-cis-cis* stereochemistry respectively (Figure 5a, 5b). The bond lengths in **3** and **4** follow the order $M{-}O_W < M{-}N_P < M{-}N_T$. The chelate bite angle (72.39(7)-76.96(9)°) deviate from ideal value 90°, however, the deviation witnessed is smaller for other *cis* angles with values ranging within 80.55(7)-98.64(7)°. Among the two *trans* angles, $N_T{-}M{-}Ow$ (163.75(9)-168.70(9)°) is less than $N_P{-}M{-}N_P$ (168.54(11)-173.05(13)°). Selected bond parameters found in **3** and **4** are listed in Table 5.

The packing diagrams of complex **3** and **4** (Figure 7) show that the pyrrole type nitrogen N4 on triazole ring acts as a hydrogen bond donor to nitrate oxygen (N4···O4, 2.771(1) Å and N4···O2, 2.767(5) Å). The lattice water molecules donate hydrogen bond to nitrate oxygen; O2···O5, 2.927(4) Å and O3···O5, 2.976(4) Å in **3**, likewise O3···O5, 2.852(6) Å and O4···O5, 3.033(5) Å in **4**. In contrast, it receives hydrogen bond from coordinated water O1 (O1···O5, 2.860(5) Å in **3** and 2.815(5) Å in **4**). The other non-bonded interaction between two nitrate oxygen (O2···O2, 2.922(5) Å in **3**) and (O3···O3, 2.980(7) Å in **4**) helps in forming a two dimensional network in which zigzag chains of complex molecules are separated by nitrate ion-water channel (Figure 7).

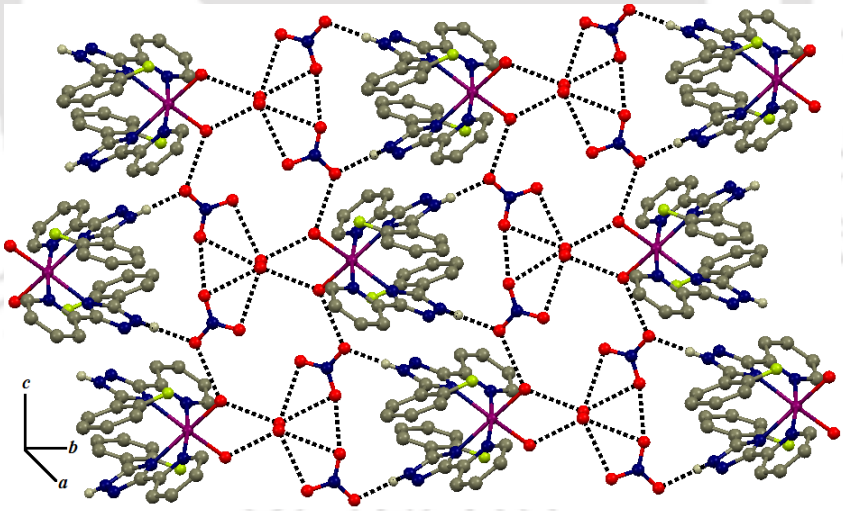

Figure 7. Classical N−H···O and O−H···O hydrogen bonded 3D network observed in the crystal structures of complex **3** and **4**.

Strong π···π interaction (Cg···Cg, 3.541-3.674 Å) between triazole rings form an one dimensional chain along the crystallographic *c* axis (Figure 8a), Cg···Cg distances are in the range reported for π-stacked triazole moities.[17] The BSSE corrected energy for the π···π stacked dimer in complex **4** was calculated to be -8.38 kcal/mol and this indicates a strong interaction. In addition to classical hydrogen bonding interactions, centrosymmetric motifs

formed by weak C−H···F hydrogen bond are observed in complex **3** and **4**. The C−H···F interactions have significant directionality as C−H−F >150° and C···F distances falling in the range 3.592(3)-3.733(3) Å (Figure 8b). Similar parameters were cited earlier for relatively rare C−H···F interactions.[18] Non-classical C−H···O interactions following considerable linearity (C−H−O >150°) are observed in the supramolecular assemblies of complex **3** and **4** with nitrate-O acting as the acceptor and aromatic hydrogen as donor. Useful hydrogen bond donor-acceptor distances in complexes **3** and **4** are listed in Table **6**.

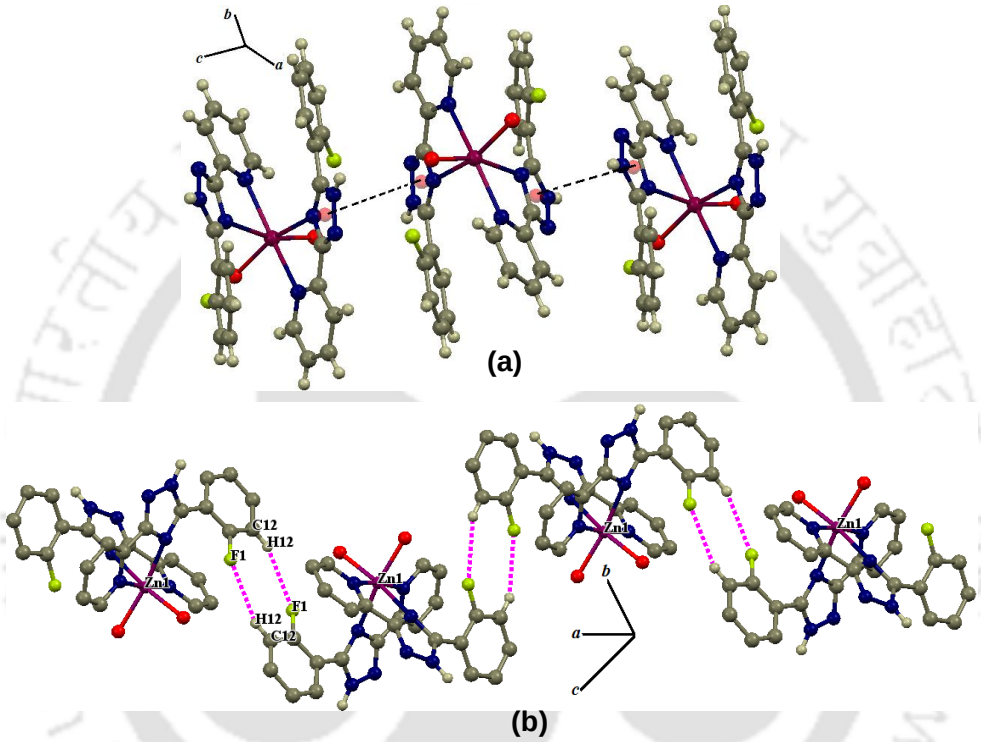

Figure 8. π···π interaction and non-classical C−H···F hydrogen bond observed in crystal structures of complex **3** and **4**.

Crystal structure description of [Cd(trz-2)$_2$(SCN)$_2$] (5)

Complex **5** crystallises in monoclinic *C*2/*c* space group and the asymmetric unit contains one molecule of the complex. The hexa-coordinated Cd(II) centre is bis-chelated by two **trz-2** ligands through its pyridyl (N_P) and triazolyl (N_T) nitrogen and two isothiocyante ligands. Like found in complexes **3** and **4**, a gliding plane passes through the molecule dividing it into two equal halves. The $(N_P)_2(N_T)_2(S_{IT})_2$ coordination geometry is spanned respectively in *trans-cis-cis* fashion with triazolyl-N and isothiocyanate-S being *trans* to each other (Figure 4c). The bond length order in complex **5** is followed as Cd−N_P <Cd−N_T <Cd−S_{IT} (Table **7**). The large deviation of angle N_P−Cd−N_T (71.48(13)°) from ideal 90°

value reflects bite angle constraint on ligand **trz-2**. This is also reflected by trans angle N_P−Cd−N_P value (158.93(19)°) while the value other trans angle N_T−Cd−S_{IT} (172.99(9)°) approaches to ideal 180° (Figure 6c). The packing diagram reveals that an infinite chain of complex **5** propagates along the crystallographic *c* axis through classical N−H···N hydrogen bond between triazole-NH and N-end of isothiocyanate (N···N, 2.802(8) Å). Strong π···π interaction between triazole rings (Cg···Cg, 3.666 Å) imparts extra stabilization to this hydrogen bonded chain (Figure 9a). The interaction energy was calculated by taking a dimeric unit from this polymeric chain in consideration. The BSSE corrected interaction energy for this dimer (-29.38 kcal/mol) is the sum of N−H···N hydrogen bond and π···π interaction energies. NBO analysis shows the following second order perturbation energy value for N−H···N hydrogen bond; (lp)N→σ*(N−H), 10.53 kcal/mol. Polymeric motif formed via non-classical C−H···S (C···S, 3.701(5) Å) and C−H···F (C···F, 3.615(7) Å) interactions is observed in the crystal structure of complex **5** (Figure 9b). Useful hydrogen bonding parameters in complex **5** are included in Table 6.

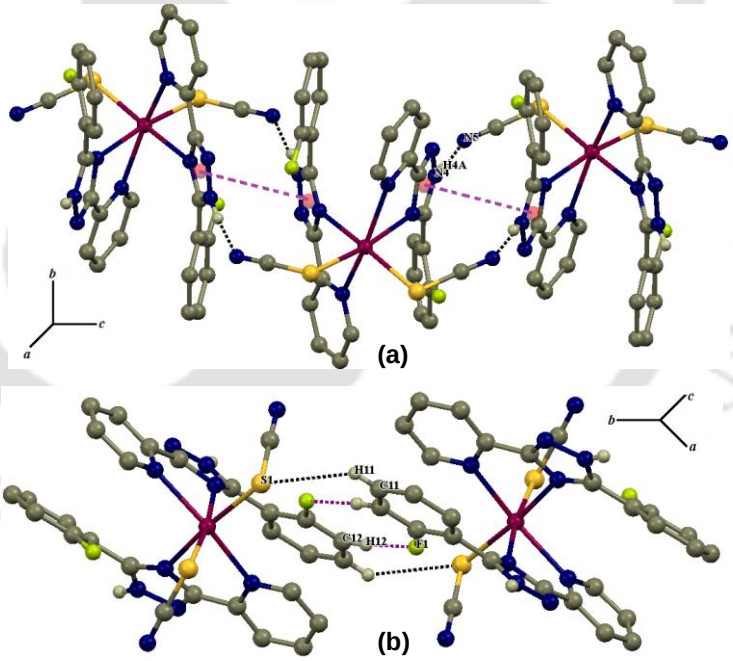

Figure 9. Classical N−H···N, non-classical C−H···S hydrogen bonds and π···π interaction in complex **5**.

4. 4. 3. Fluorescence property of the compounds in solid and DMSO solution

Metal complexes of substituted 1,2,4-triazole based ligands have been tested for high luminescent nature as well as potential use as organic light emitting diodes (OLEDs).[19]

Designing a luminescent material with desired property is considered as a tough goal to achieve and thus syntheses of new fluorescent metal complexes are of practical use. The ligands **trz-1** and **trz-2** are fluorescent at room temperature in solid state and in MeOH/ DMSO solution. The origin of the emission in the complexes are ascribed to intraligand $\pi^* \rightarrow \pi$ transition as evidenced from broad and unstructured fluorescence.[20] The excitation as well as emission wavelengths of the compounds in both solid state and in DMSO solution are included in Table 8.The emission spectra of the complexes **1-5** were recorded in solid state and DMSO solution as they are insoluble in other organic solvents. The ligands as well as the metal complexes in DMSO solution are all blue emitters with their λ_{max} lying in the range 400-440 nm (Figure 10c). Ligand **trz-1** and its metal complexes exhibit two closely spaced emission peaks in DMSO solution, one sharp peak around 400-425 nm and a broad emission around 440 nm. Ligand **trz-1** and its complexes exhibit blue emission in the solid state as their λ_{max} values fall between 449-468 nm. Complex **2** in solid state show two emission peaks (398 and 467 nm) whereas emission spectra of **trz-1** and complex **1** show the presence of only peak corresponding to λ_{max} 449 and 467 nm respectively (Figure 10a).

Table 8

Excitation and emission wavelengths in solid state and DMSO solution

Compound	Solid		DMSO solution	
	Excitation λ_{max} (nm)	Emission λ_{max} (nm)	Excitation λ_{max} (nm)	Emission λ_{max} (nm)
trz-1	255	449	378	395, 419
trz-2	250	394	350	414
Complex **1**	300	468	368	416, 436
Complex **2**	290	398, 467	370	424, 440
Complex **3**	254	396	356	425
Complex **4**	255	395	355	427
Complex **5**	250	393	353	416

The emission maxima in solid state have been blue shifted by 55-70 nm with the change the *ortho* substituent from hydroxy to fluoro. Ligand **trz-2** and its complexes behave as violet emitters in solid state with λ_{max} in the range 394-396 nm (Figure 10b) as well in DMSO solution with λ_{max} 414-425 in the range (Figure 10c). The intensity of fluorescence in

the metal complexes of ligand **trz-1** is higher than the ligand and the reason might be attributed to the decrease in radiation less decay upon chelation.[21] However, the complexes of ligand **trz-2** exhibit more commonly observed trend which is quenching of fluorescence upon coordination.[22] These complexes in addition to the ligands can be used as new luminescent materials for potential use in OLED devices.

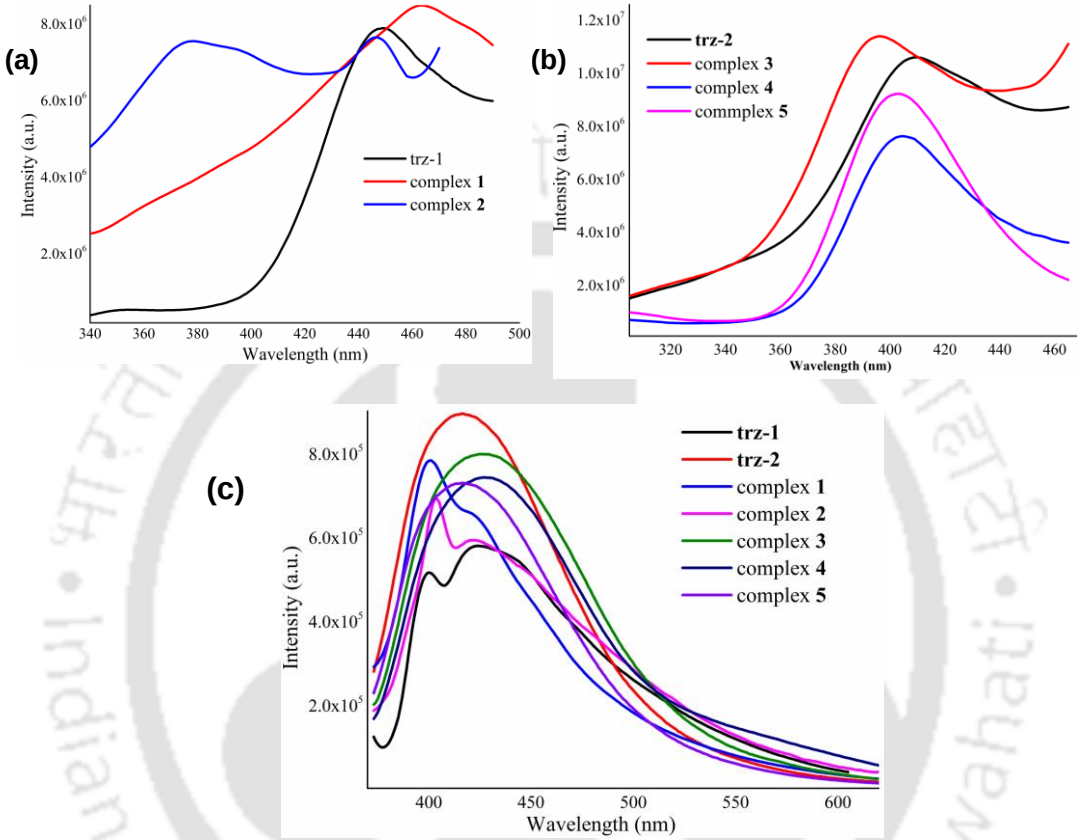

Figure 10. (a) Emission spectra of **trz-1** and complexes **1**, **2** in solid state; (b) Emission complexes **1-5** in DMSO (10^{-5} M) solution.

DFT and TD-DFT studies

Time dependent density functional theory (TD-DFT) has been employed to investigate the origin of absorbance in the metal complexes of **trz-1** and **trz-2**. The bulk solvent effects were corrected with the help of polarization continuum model (PCM) in its integral equation formalism.[23] According to the continuum model, the solution is divided into two parts. The compound lies inside the cavity surrounded by the solvent (DMSO). The absorption corrections in the PCM were computed by 'non-equilibrium' solutions. It has been ascertained from the TD-DFT study that absorbance of the complexes are intraligand charge transfer by origin. The calculated absorbance maxima, oscillator strengths and orbital

contributions to particular electronic transitions for **trz-1**, **trz-2**, complex **1** and **3** calculated by B3LYP/6-31G(d,p) level of theory are listed in Table 9. It has been observed that calculated values of absorbance peaks differ from experimental values by 5-20 nm and are generally blue shifted. The molecular orbital pictures of all orbitals taking part in electronic transitions are given in Figure 11 and 12.

Table 9

Calculated wavelengths, oscillator strengths and orbital contributions in **trz-1**, **trz-2**, complex **1** and **3** using PCM

Compound	Calculated wavelength λ (nm)	Oscillator strength f_1	Orbital contributions
Trz-1	275	0.358	HOMO→LUMO, 0.4789 HOMO→LUMO+1, 0.5032
	230	0.249	HOMO-1→LUMO, 0.1733 HOMO-3→LUMO, 0.2528 HOMO-2→LUMO+1, 0.2515 HOMO-2→LUMO, 0.1740 HOMO-2→LUMO+1, 0.2155 HOMO-1→LUMO+1, 0.1003 HOMO-1→LUMO+2, 0.3686 HOMO→LUMO+3, 0.2684
Trz-2	268	0.597	HOMO→LUMO, 0.2303 HOMO→LUMO+1, 0.6502
Complex **1**	301	0.206	HOMO→LUMO, 0.6606 HOMO→LUMO+1, 0.2365
	288	0.159	HOMO-1→LUMO, 0.1052 HOMO-1→LUMO+1, 0.1703 HOMO→LUMO, 0.2317 HOMO→LUMO+1, 0.6175
	269	0.257	HOMO-1→LUMO+1, 0.6253 HOMO-2→LUMO+2, 0.2809
	306	0.226	HOMO-2→LUMO+1, 0.6686 HOMO→LUMO+5, 0.1542
Complex **2**	296	0.355	HOMO-1→LUMO+2, 0.6632 HOMO-1→LUMO+4, 0.1009 HOMO→LUMO+5, 0.1134

	264	0.164	HOMO-16→LUMO, 0.1293 HOMO-14→LUMO, 0.3464 HOMO-6→LUMO+1, 0.1716 HOMO-4→LUMO+3, 0.3494 HOMO-2→LUMO+3, 0.4081

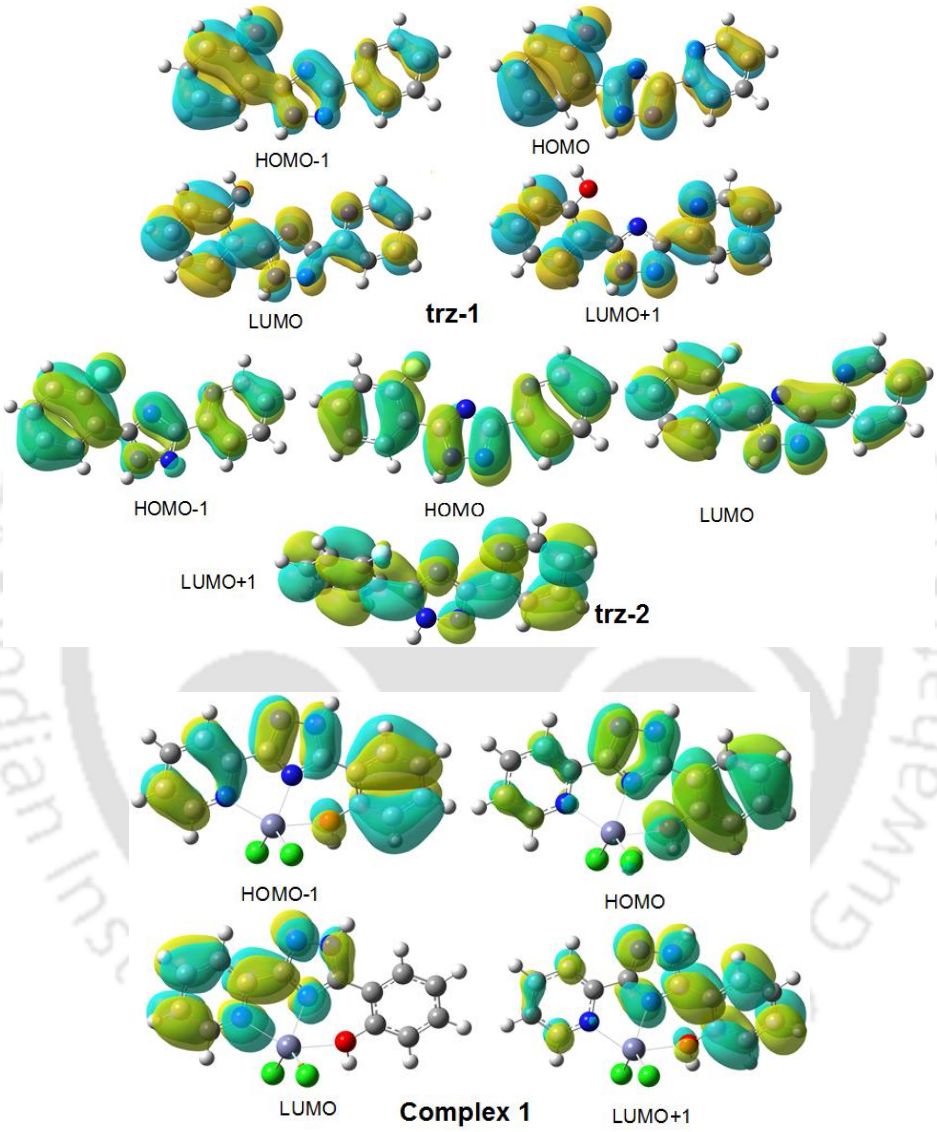

Figure 11. Molecular orbitals of **trz-1**, **trz-2** and complex **1** which take part in electronic transitions.

DFT has been employed to confirm that the HOMO, LUMO and the orbitals possessing energies closer to them are 1,2,4-triazole ligand based rather than M−O/ M−Cl σ* orbitals in complex **1**. These orbitals are spread over 1,2,4-triazole based ligands with most significant contribution from π-conjugated ligand framework. Figure 11 shows the pictures of

HOMO, LUMO and the orbitals having energies close to them in ligands **trz-1**, **trz-2** and complex **1**. However, the HOMO in complex **3** has contributions from the pyridyl ring as well as Zn−O σ* orbitals. In contrast, the HOMO-1, LUMO and LUMO+1 orbitals in complex **3** have major contribution from the π-conjugated ligand framework (Figure 12). Thus it can be assumed that the emission of the complexes have their origin in intraligand π*→π transitions.

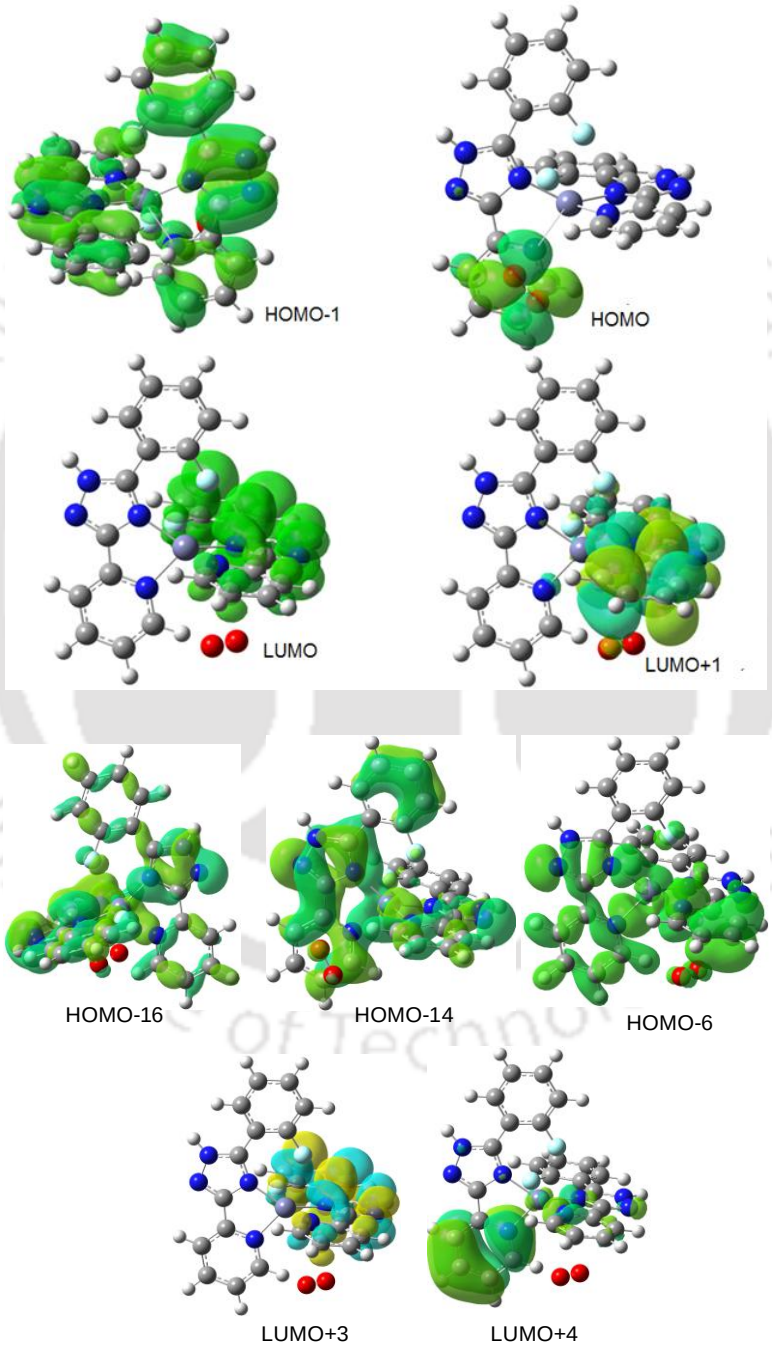

Figure 12. Molecular orbitals which take part in electronic transition in complex **3**.

4. 3. Conclusion

Zn(II) and Cd(II) complexes of two 3-pyridyl-5-aryl-(1*H*)-1,2,4-triazole ligands **trz-1** and **trz-2** have been synthesised and characterised by X-ray crystallography. The crystal structures of these complexes demonstrate weak, non-classical C−H···F, C−H···S and C−H···Cl hydrogen bonds have important roles in determining supramolecular assembly alike the classical hydrogen bonds. The complexes of ligand **trz-2** are characterized with strong π···π interaction which plays a decisive role in the crystal packing. All five complexes as well as the ligands show blue/ blue-violet emission in solid state and DMSO solution. In recent years, the usage of Zn(II)/ Cd(II) complexes of heterocyclic ligands as luminescent and OLED materials has become popular. In this regard, the fluorescent nature of Zn(II) and Cd(II) complexes of these ligands in solid state can be of significant practical application.

4. 4. Experimental section

4. 4. 1. Materials and methods

2-Hydroxybenzhydrazide, 2-fluorobenzhydrazide, 2-cyanopyridine, $Zn(NO_3)_2 \cdot 6H_2O$, anhydrous $ZnCl_2$, $Cd(NO_3)_2 \cdot 4H_2O$, NaSCN and solvents were used as received without further purification. The synthesis procedure of ligand **trz-2** has been described in our previous report[24] and the same procedure was used for the preparation of ligand **trz-1**.

A Perkin Elmer Spectrum FTIR spectrometer (4000-250 cm^{-1}), Perkin Elmer Lambda 25 spectrometer, Perkin Elmer Series II CHNO Analyzer 2400, Bruker 400 MHz and 600 MHz spectrometer. X-ray crystallographic data was collected using a Bruker SMART APEX-CCD diffractometer and Agilent Supernova diffractometer with Mo-Kα radiation (λ= 0.71073 Å). The intensity data were corrected by Lorentz and polarization effects and empirical absorption corrections was applied using SAINT program.[25] All structures were solved by direct methods using SHELX-97. Non hydrogen atoms were refined anisotropically by full matrix least-squares on F^2, using SHEXL-97 and further refined using PLATON.[26] All hydrogen atoms were included in the calculated positions and was refined isotropically using a riding model. Becke's three parameter functional (B3LYP)[27] and 6-31G(d,p) basis set were used for calculation, Stuttgart-Dresden (SDD) pseudo potential for Cd atoms was employed in case of complex **3**, **4** and **5**. TD-DFT calculations were performed using the optimized gas phase geometries. Gaussian09[28] and GaussView05[29] program packages were

used for calculation and visualization purposes. NBO calculations were performed using NBO 3.1[30] implemented in Gaussian09 package.

4. 4. 2. Syntheses and characterisation data

2-(3-(pyridin-2-yl)-1*H*-1,2,4-triazol-5-yl)phenol (trz-1). 2-Hydroxybenzhydrazide (0.913 g, 6 mmol) and 2-cyanopyridine (0.677 g, 6.5 mmol) were taken together in 1.5 mL of PEG 400 and heated for 12 h at 100 °C. To resulting gummy yellow liquid was added to 20 mL water and stirred for 30 minutes to produce pale yellow residue. It was filtered, dried over anhydrous $CaCl_2$ in vaccuo and subjected to basic alumina column chromatography using EtOAc : hexane (1:1) mixture as elutent. Pale yellow solid; yield 1.12 g, 78%. 400 MHz ^{1}H NMR (δ): 4.05 (s, 1H), 7.01 (m, 2H), 7.35 (t, *J* = 10.8 Hz, 1H), 7.56 (s, 1H), 8.03 (d, 2H, *J* = 10.8 Hz), 8.19 (d, *J* = 10.8 Hz, 1H), 8.75 (s, 1H), 11.02 (bs, 1H). ^{13}C NMR 150 MHz, DMSO d_6): δ 114.12, 117.24, 119.86, 112.01, 120.10, 127.38, 131.52, 138.05, 147.85, 150.04, 156.63, 157.21, 158.52. ESI MS *m/z* calcd. $C_{13}H_{11}N_4O^+$ $(M+H)^+$ 239.090 found 239.098.

[Zn(trz-1)Cl$_2$]·DMF (1). To a solution of ligand **trz-1** (50 mg, 0.20 mmol) in methanol, solid anhydrous $ZnCl_2$ (28 mg, 0.25 mmol) was added to result in precipitation of white solid. The precipitate was dissolved in 2 mL DMF and slow evaporation of this solution produced colorless crystals of **1**. Yield: 64 mg (71%). *Anal.* Calcd. for $C_{16}H_{17}N_5O_2Cl_2Zn$: C, 42.93%; H, 3.83%; N, 15.64%. Found: C, 42.80%; H, 3.78%; N, 15.55%. ESI MS: *m/z* found (calcd.): [**trz-1**+H]$^+$ 239.03 (238.09); [^{64}Zn(**trz-1**)$^-$]$^+$ 300.92 (301.00); [^{66}Zn(**trz-1**)$^-$]$^+$ 302.93 (303.00); [^{64}Zn(**trz-1**)(^{35}Cl)]$^+$ 336.92 (336.98); [^{68}Zn(**trz-1**)(^{35}Cl)]$^+$ 340.92 (340.98).

[Cd(trz-1)$_2$(NO$_3$)$_2$] (2). To 120 mg (0.50 mmol) of **trz-1** dissolved in methanol, 91 mg (0.30 mmol) of crystalline $Cd(NO_3)_2·4H_2O$ solid was added and stirred for 1 h. Tiny white crystals were separated after one week from this solution. Yield: 111 mg (62%). *Anal.* Calcd. for $C_{26}H_{20}N_{10}O_8Cd$: C, 43.80%; H, 2.83%; N, 19.64%. Found: C, 43.69%; H, 2.80%; N, 19.51%. ESI-MS: *m/z* found (calcd.): [**trz-1**+H]$^+$ 239.10 (238.09); [^{114}Cd(**trz-1**)(**trz-1**)$^-$]$^+$ 589.07 (589.07).

[Zn(trz-2)$_2$(H$_2$O)$_2$](NO$_3$)$_2$·H$_2$O (3). To 120 mg (0.50 mmol) of **trz-2** dissolved in methanol in 10 mL, 90 mg (0.30 mmol) of solid $Zn(NO_3)_2·6H_2O$ was added and stirred for 1 h. Pale yellow, needle shaped crystals deposited after five days from this solution. Yield: 108

mg (60%). *Anal*. Calcd. for $C_{26}H_{20}N_{10}O_9F_2Zn$: C, 43.38%; H, 2.80%; N, 19.46%. Found: C, 43.31%; H, 2.73%; N, 19.37%. ESI-MS: *m/z* found (calcd.): [**trz-2**+H]$^+$ 241.53 (241.08); [^{64}Zn(**trz-2**)$_2$]$^{2+}$ 272.53 (272.05); [^{64}Zn(**trz-2**)$_2$(NO_3)]$^+$ 366.66 (366.10).

[Cd(trz-2)$_2$(H_2O)$_2$](NO_3)$_2$·H_2O (4). To 120 mg (0.50 mmol) of **trz-2** dissolved in 10 mL methanol, 93 mg (0.30 mmol) of solid Cd(NO_3)$_2$·4H_2O was added and stirred for 1 h. Pale yellow, needle shaped crystals deposited after five days from this solution. Yield: 124 mg (65%). Anal. Calcd. for $C_{26}H_{20}N_{10}O_9F_2Cd$: C, 42.49%; H, 2.74%; N, 19.06%. Found: C, 42.37%; H, 2.82%; N, 19.13%. ESI MS: *m/z* found (calcd.): [**trz-2**+H]$^+$ 241.49 (241.08); [^{114}Cd(**trz-2**)$_2$]$^{2+}$ 297.55 (297.08);

[Cd(trz-2)$_2$(NCS)$_2$] (5). To 120 mg (0.50 mmol) of **trz-2** dissolved in 10 mL methanol, 93 mg (0.30 mmol) of solid Cd(NO_3)$_2$·4H_2O and 25 mg (0.30 mmol) of solid NaSCN were added together. This mixture was stirred for 1 h and left undisturbed. Pale yellow, needle shaped crystals deposited from this mixture after one week. Yield: 121 mg (68%). Anal. Calcd. for $C_{28}H_{18}N_{10}S_2F_2Cd$: C, 47.43%; H, 2.56%; N, 19.75%. Found: C, 47.37%; H, 2.62%; N, 19.73%. ESI MS: *m/z* found (calcd.): [**trz-2**+H]$^+$ 241.11 (241.08); [^{114}Cd(**trz-2**)(SCN)]$^+$ 411.99 (411.96); [^{114}Cd(**trz-2**)$_2$(SCN)]$^+$ 652.10 (652.04).

4. 4. 3. Selected spectra

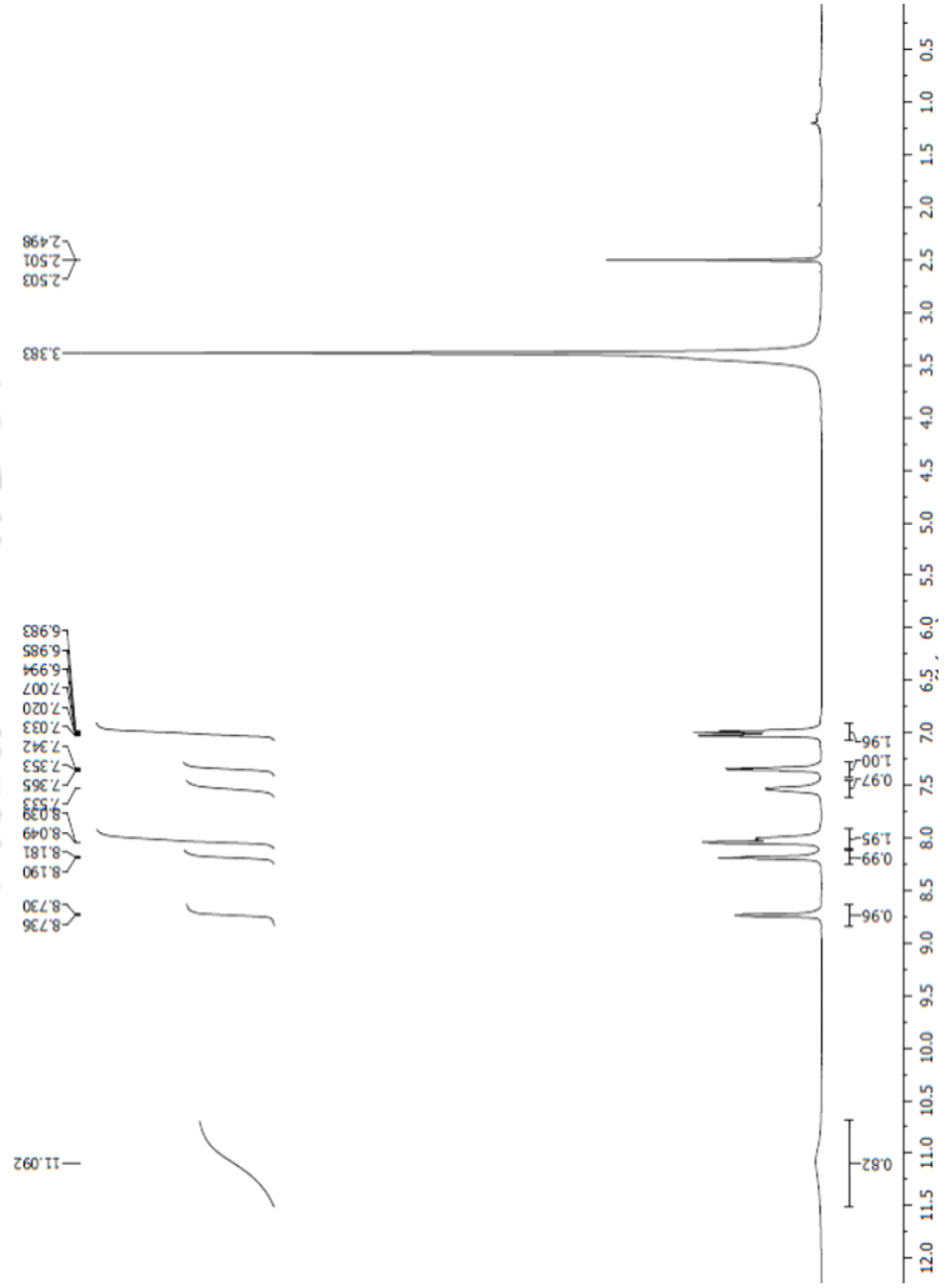

Spectrum 1. ^{1}H NMR (600 MHz, DMSO d_6) of **trz-1**

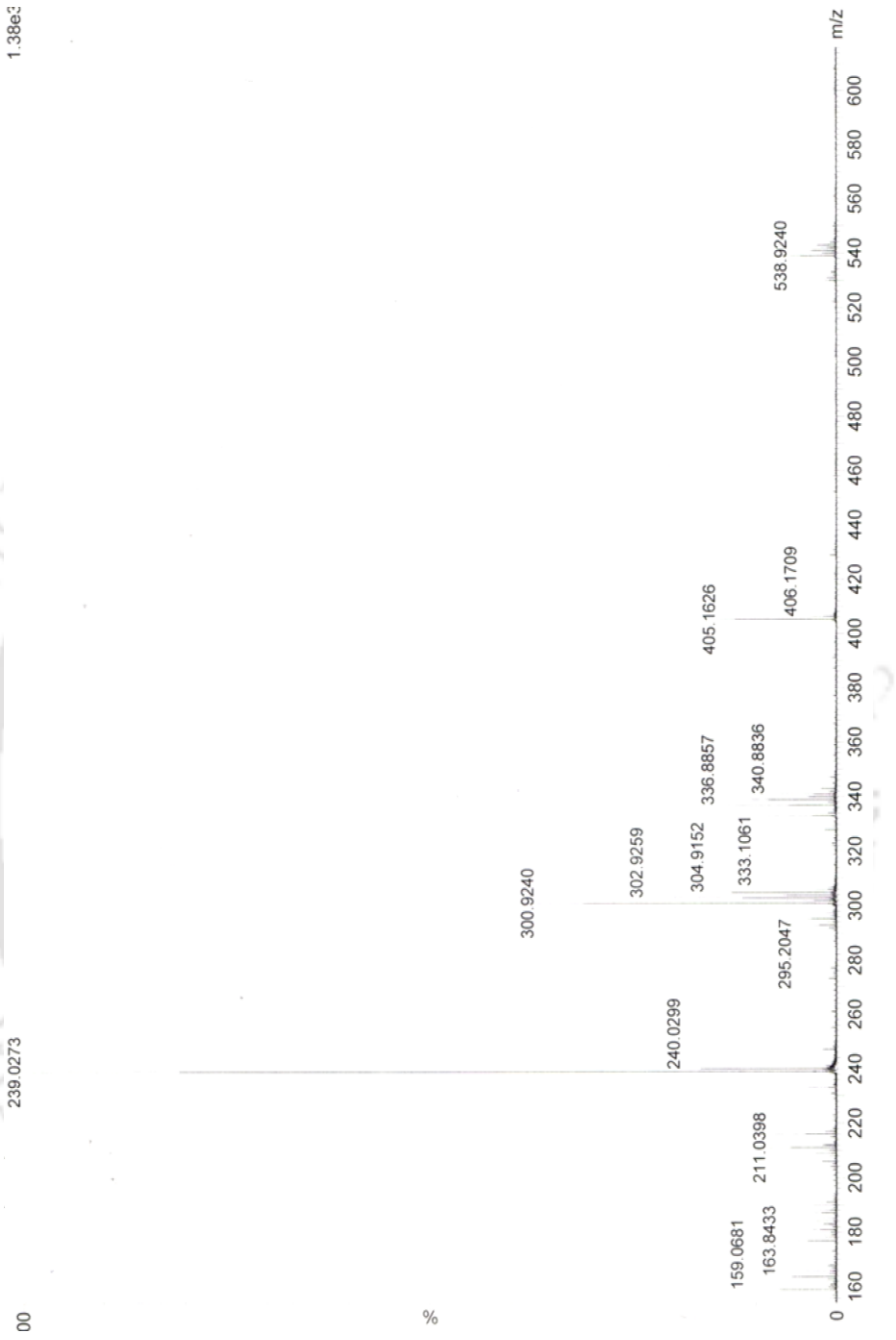

Spectrum 2. ESI-MS of complex [Zn(**trz-1**)Cl_2]·DMF (**1**).

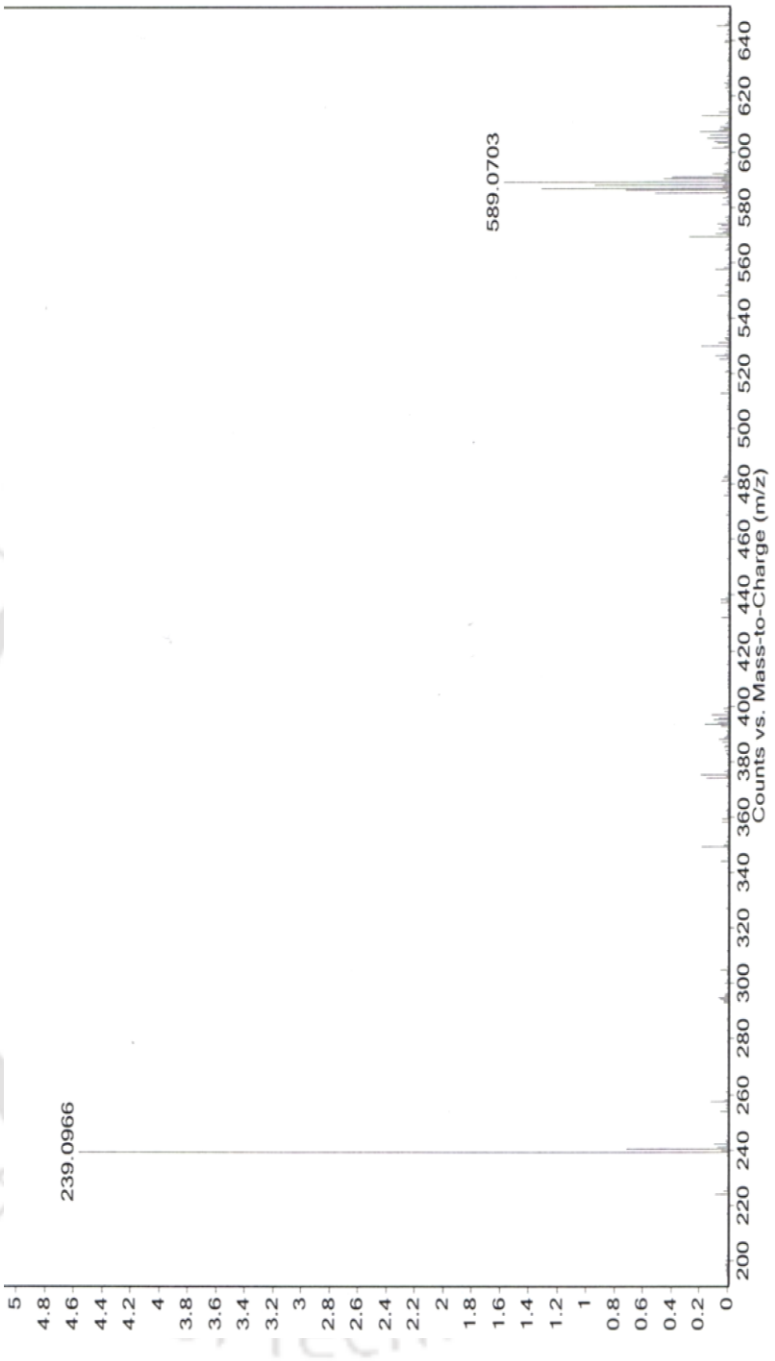

Spectrum 3. ESI-MS of complex [Cd(**trz-1**)$_2$(NO$_3$)$_2$] **(2)**.

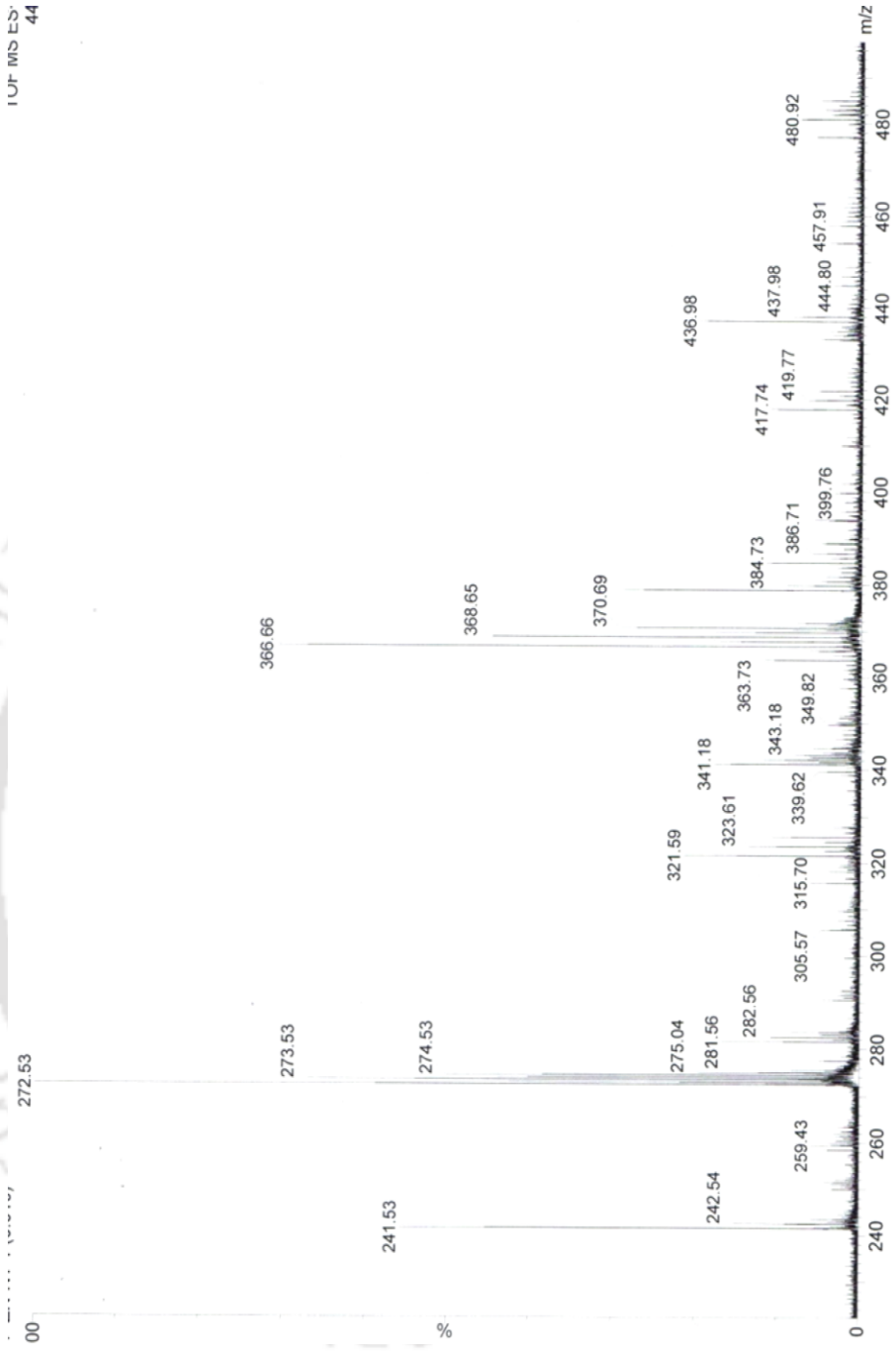

Spectrum 4. ESI-MS of complex [Zn(**trz-2**)$_2$(H_2O)$_2$](NO_3)$_2$·H_2O (**3**).

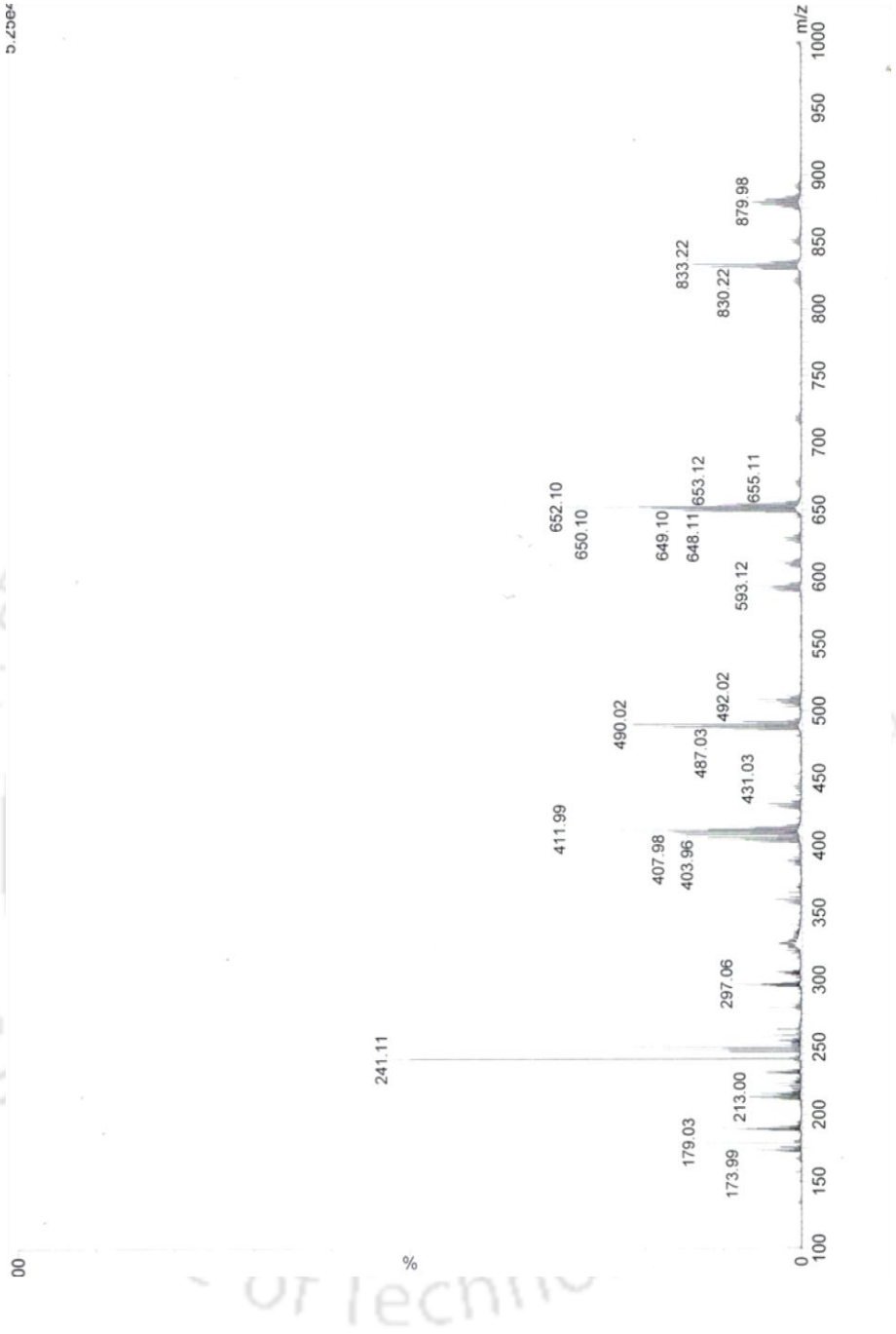

Spectrum 5. ESI-MS of complex [Cd(**trz-2**)$_2$(NCS)$_2$] (**5**).

Reference

[1] A. R. Katritzky, C. A. Ramsden, J. A. Joule, V. V. Zhdankin, *Handbook of Heterocyclic Chemistry*, Elsevier **2010**.

[2] K. T. Potts, *Chem. Rev.* **1961**, *61*, 81.

[3] (a) W. Vreugdenhil, J. H. V. Diemen, R. A. G. D. Graaff, J. G. Haasnoot, J. Reedijk, A. M. V. D. Kraan, O. Kahn, J. Zarembowitch, *Polyhedron* **1990**, *9*, 2971; (b) P. J. Kunkeler, P. J. Koningsbruggen, J. P. Cornelissen, A. N. Horst, A. M. Kraan, A. L. Spek, J. G. Haasnoot, J. Reedijk, *J. Am. Chem. Soc.* **1996**, *118*, 2190; (c) O. Roubeau, M. A. Gomez, E. Balskus, J. J. A. Kolnaar, J. G. Haasnoot, J. Reedijk, *New. J. Chem.* **2001**, *25*, 144.

[4] (a) J. A. Kitchen, S. Brooker, *Coord. Chem. Rev.* **2008**, *252*, 2072; (b) J. A. Kitchen, N. G. White, M. Boyd, B. Moubaraki, K. S. Murray, P. D. W. Boyd, S. Brooker, *Inorg. Chem.* **2009**, *48*, 6670.

[5] (a) R. Hage, A. H. J. Dijkhuis, J. G. Haasnoot, R. Prim, J. Reedijk, B. E. Buchanan, J. G. Vos, *Inorg. Chem.* **1988**, *27*, 2185; (b) O. Roubeau, M. A. Gomez, E. Balskus, J. J. A. Kolnaar, J. J. G. Haasnoot, J. Reedijk, *New. J. Chem.* **2001**, *27*, 2185.

[6] (a) G. B. Bagihalli, P. G. Avaji, S. A. Patil, P. S. Badami, *Eur. J. Med. Chem.* **2008**, *43*, 2639; (b) V. B. Arion, E. Reisner, M. Fremuth, M. A. Jakupec, B. K. Keppler, V. Y. Kukushkin, A. J. L. Pombeiro, *Inorg. Chem.* **2003**, *42*, 6024; (c) S. Ferrer, R. Ballesteros, A. Sambartolom, M. González, G. Alzuet, J. Borrás, M. Liu, *Inorg. Chem.* **2004**, *43*, 7083.

[7] (a) J. C. Liu, D. G. Fu, J. Z. Zhuang, C. Y. Duan, X. Z. You, *J. Chem. Soc., Dalton Trans.* **1999**, 2337; (b) M. H. Klingele, S. Brooker, *Inorg. Chim. Acta* **2004**, 357, 1598.

[8] (a) W. Li, H. -P. Jia, Z. -F. Ju, J. Zhang, *Cryst. Growth Des.* **2006**, *9*, 2136; (b) X. Liu, K. Liu, Y. Yang, B. Li, *Inorg. Chem. Comm.* **2008**, *11*, 1273; (c) R. B. Zhang, Z. -J. Li, J. -K. Cheng, Y. -Y. Qin, J. Zhang, Y. -G. Yao, *Cryst. Growth Des.* **2008**, *8*, 2562.

[9] (a) R. Czerwieniec, K. Kowalski, H. Yersin, *Dalton Trans.* 2013, *42*, 9826; (b) L. Shi, B. Li, S. Yuea, D. Fan, *Sensors Actuat. B* **2009**, *137*, 386; (c) C. Wena, G. Tao, X. Xuc, X. Fengc, R. Luo, *Spectrochim. Acta Part A* **2011**, *79*, 1345.

[10] (a) D. Sun, N. Zhang, R. -B. Huang, L. -S. Zheng, *Cryst. Growth Des.* **2010**, *10*, 3699; (b) D. Marcinkowski, M. W. Chorab, A. Bocian, J. Mikołajczyk, M. Kubicki, Z. Hnatejko, V. Patroniak, *Polyhedron* **2017**, *123*, 243.

[11] (a) M. -L. Zhang, D. -S. Li, J. -J. Wang, F. Fu, M. Du, K. Zoua, X. -M. Gao, *Dalton Trans.* **2009**, 5355; (b) X. -W. Wang, J. -Z. Chen, J. -H. Liu, *Cryst. Growth Des.* **2007**, *7*, 1227; (c) Y. Kang, C. Seward, D. Song, S. Wang, *Inorg. Chem.* 2003, 42, 2789.

[12] (a) Y. Qiu, Y. Li, G. Peng, J. Cai, L. Jin, L. Ma, Deng, H. M. Zeller, S. R. Batten, *Cryst. Growth Des.* **2010**, *10*, 1332; (b) W. Chen, Q. Peng, Y. Li, *Cryst. Growth Des.* **2008**, *8*, 564; (c) J. L. Zhang, Y. L. Gong, J. Wang, J. Wu, J. Feng, C. Zhang, *Polyhedron* **2017**, *123*, 62; (d) S. -M. Yue, H. -B. Xu, J. -F. Ma, Z. -M. Su, Y. -H. Kan, H. -J. Zhang, *Polyhedron* **2006**, *25*, 635.

[13] V. J. Catalano, A. O. Etogo, *Inorg. Chem.* **2007**, *46*, 5608.

[14] (a) Y. -Y. Yang, W. Guo, M. Du, *Inorg. Chem Comm.* **2010**, *13*, 1195; (b) G. Wei, Y. -F. Shen, Y. -R. Li, X. -C. Huang, *Inorg. Chem.* **2010**, *49*, 9191.

[15] (a) P. K. Bhaumik, A. Bauzá, M. G. B. Drew, A. Frontera, S. Chattopadhyay, *CrystEngComm.* **2015**, *17*, 5664; (b) A. Bhattacharyya, A. Bauzá, A. Frontera, S. Chattopadhyay, *Polyhedron* **2016**, *119*, 451; (c) A. Bauzá, T. J. Mooibroek, A. Frontera, *CrystEngComm.* **2016**, *18*, 10; (d) S. Jana, K. Harms, A. Bauzá, A. Frontera, S. Chattopadhyay, *Cryst. Growth Des.* **2015**, *15*, 257.

[16] (a) A. Majumder, G. M. Rosair, A. Mallick, N. Chattopadhyay, S. Mitra, *Polyhedron* **2006**, *25*, 1753; (b) S. Basak, S. Sen, C. Marschner, J. Baumgartner, S. R. Batten, D. R. Turner, S. Mitra, *Polyhedron* **2008**, *27*, 1193; (c) K. Bania, N. Barooah, J. B. Baruah, *Polyhedron* **2007**, *26*, 2612; (d) Y. Dong, M. D. Smith, H. C. Loye, *Inorg. Chem.* **2000**, *39*, 4927.

[17] B. Jing, Y. -C. Du, A. -X. Zhu, *Acta Cryst* **2012**, *E 68*,o1802.

[18] (a) L. Shimoni, J. P. Glusker, *Struct. Chem.* **1994**, 5, 383; (b) P. Murray-Rust, W. C. Stalling, C. T. Monti, R. K. Preston, J. P. Glusker, *J. Am. Chem. Soc.* **1983**,*105*, 3206.

[19] (a) C. -F. Chang, Y. -M. Cheng, Y. Chi, Y. -C. Chiu, C. -C. Lin, G. H. Lee, P. -T. Chou, C. -C. Chen, C. -H. Chang, C. -C. Wu, *Angew. Chem. Int. Ed.* **2008**, *47*, 4542; (b) Y. -Q. Huang, B. Ding, H. -B. Song, B. Zhao, P. Ren, P. Cheng, H. -G. Wang, D. -Z. Liao, S.-P. Yan, *Chem. Commun.* **2006**, 4906.

[20] B. Valeur, *Molecular Fluorescence: Principles and Applications*; Wiley-VCH: Weinheim, **2001**.

[21] M. D. Allendorf, C. A. Bauer, R. K. Bhakta, R. J. T. Houk, *Chem. Soc. Rev.* **2009**, *38*, 1330.

[22] (a) X. Peng, J. Du, J. Fan, J. Wang, Y. Wu, J. Zhao, S. Sun, T. Xu, *J. Am. Chem. Soc.* **2007**, *129*, 1500; (b) K. Rurack, M. Kollamannsberger, U. R. Genger, J. Daub, *J. Am. Chem. Soc.* **2000**,*122*, 968.

[23] J. Tomasi, B. Mennucci, R. Cammi, *Chem. Rev.* **2005**, *105*, 2999.

[24] A. Mandal, B. K. Patel, R. Shukla, D. Chopra, *CrystEngComm.* **2017**, *19*, 1607.

[25] Area-Detector Integration Software. (1995) Siemens Industrial Automation, Inc.: Madison, WI.

[26] A. L. Spek, *Acta Cryst. D* **2009**, *65*, 148.

[27] (a) A. D. Becke, *J. Chem. Phys.* **1993**, *98*, 5648; (b) C. Lee, W. Yang, R. G. Parr, *Phys. Rev. B* **1988**, *37*, 785.

[28] Gaussian 09, M. J. Frisch, G. W. Trucks, J. R. Cheeseman, G. Scalmani, M. Caricato, H. P. Hratchian, X. Li, V. Barone, J. Bloino, G. Zheng, T. Vreven, J. A. Montgomery, G. A. Petersson, G. E. Scuseria, H. B. Schlegel, H. Nakatsuji, A. F. Izmaylov, R. L. Martin, J. L. Sonnenberg, J. E. Peralta, J. J. Heyd, E. Brothers, F. Ogliaro, M. Bearpark, M. A. Robb, B. Mennucci, K. N. Kudin, V. N. Staroverov, R. Kobayashi, J. Normand, A. Rendell, R. Gomperts, V. G. Zakrzewski, M. Hada, M. Ehara, K. Toyota, R. Fukuda, J. Hasegawa, M. Ishida, T. Nakajima, Y. Honda, O. Kitao, H. Nakai.

[29] GaussView, Version 5, R. Dennington, K. Todd, J. Millam, *Semichem Inc.*, Shawnee Mission, KS, 2009.

[30] NBO Version 3.1, E. D. Glendening, A. E. Reed, J. E. Carpenter, F, Weinhold.

Chapter 5

A Three Component Synthesis of 2-Aryl-3-imidamide Substituted 1,2-Dihydroquinazolin-4(1*H*)-ones

An efficient one-pot three component synthesis of 2-aryl-3-imidamide substituted 1,2-dihydroquinazolin-4(*1H*)-ones has been described herein using *o*-aminobenzhydrazide, 2-pyridine/pyrazinecarbonitrile and arylaldehydes as the coupling partners. In the resultant product the 2-position is substituted with various aromatic or heterocyclic groups and substituents at the 3-position are picolinimidamide, 5-phenylpicolinimidamide and pyrazine-2-carboximidamide groups, thus generating an array of compounds. The present synthetic protocol is greener and superior to the existing methods.

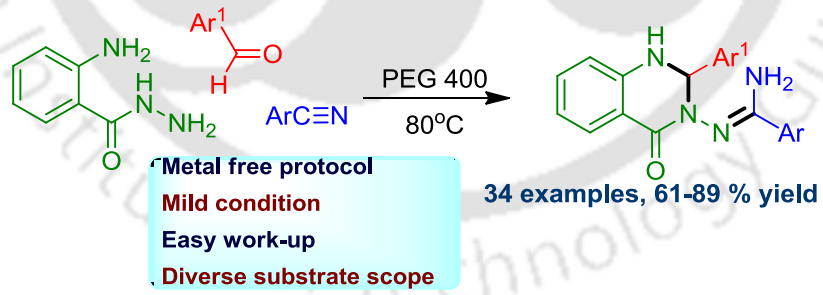

This work has been published in *ChemistrySelect* **2017**, *2*, 1717-1722.

5. 1. Introduction

Quinazolinones are a group of heterocycles having a pyrimidine nucleus fused to a phenyl ring.[1] They are widely studied for their prolific pharmaceutical application, for example some quinazolinone compounds exhibit antifungal and anti-tumor activities (**I-IV** in Figure 1).[2] Few 1,2-dihydroquinazolinones bearing trifluoromethyl group attached to a chiral carbon *viz*. DPC 082, DPC 961 and DPC 963 and other structurally similar compounds are worthy to be mentioned for their use as a non nuclear reverse transcriptase inhibitors (NNRTI) as cure for HIV.[3] Various 1,2-quinazo and dihydroquinazolinones are widely used as anti-tumor,[4] CNS depressant,[5] anti-inflammatory,[6] MAP kinase inhibitor,[7] oxidase inhibitor,[8] anti-hypertensive[9] and diuretic.[10] The enhanced polar surface area of this group of compounds are responsible for their versatile biological activity.[11] 1,2-Quinazo or dihydroquinazolinones bearing N−N linker *i.e.* N3 atom is substituted with an amino or an imino nitrogen are known to exhibit remarkable analgesic (compound **V** in Figure 1),[12-14] and anti-inflammatory (compounds **VI-VII** in Figure 1)[15-18] properties with their activity being comparable to standard anti-inflammatory agent proquazone (compound **IV**). Some C2 aryl substituted 1,2-dihydroquinazolinones inhibit tubulin polymerization and thus act as potential anticancer and antitumor agents (compounds **VIII-IX** in Figure 1).[19-21]

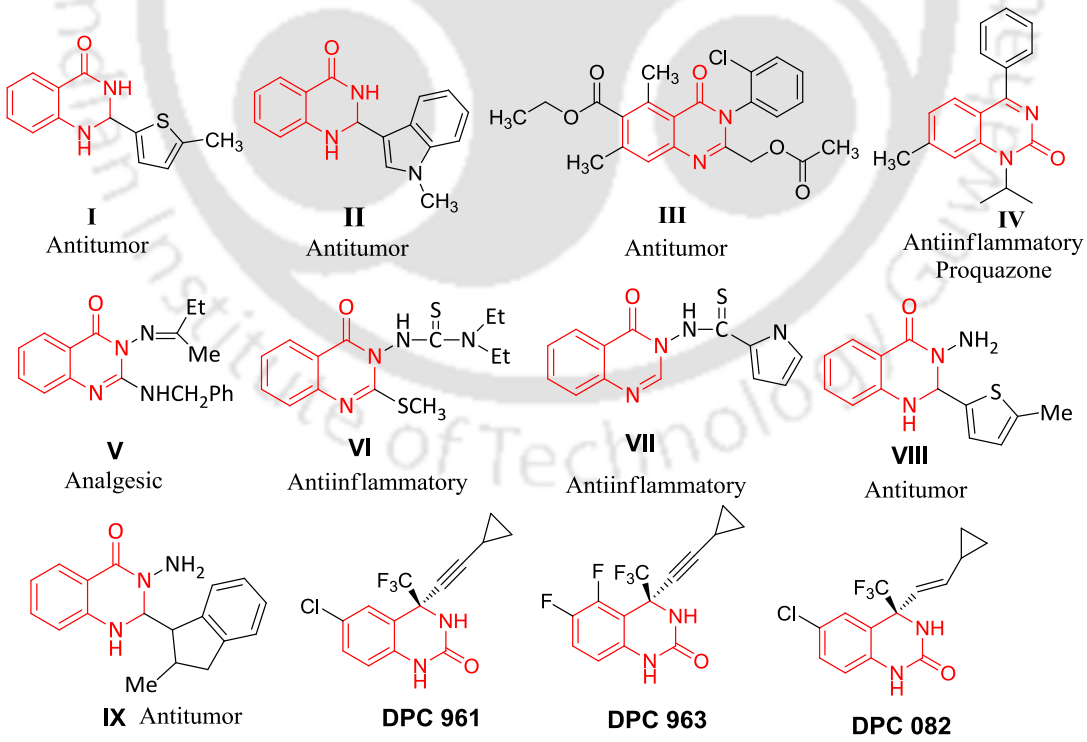

Figure 1. Few biologically active molecules possessing quinazolinone moiety.

Some of the classical methods for the syntheses of 1,2-dihydroquinazolinones involve: (i) reaction of 2-amino-*N*-(aryl)benzamides and phenylisothiocyanate in the presence of hetero polyacids;[22] (ii) reaction of *o*-nitrobenzamide with triethylorthoformate catalysed by $TiCl_4/Zn$;[23] (iii) reaction of anthranilimide with benzil.[24]

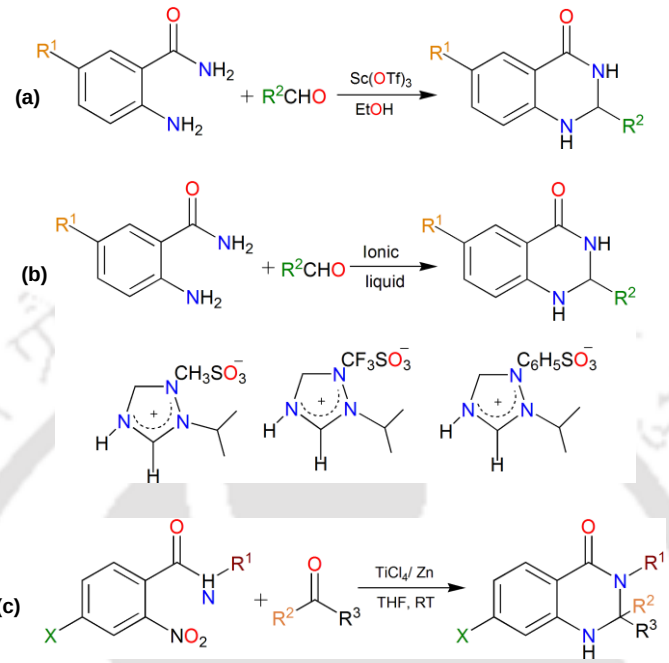

Scheme 1. Reported methods for the synthesis of 1,2-dihydroquinazolinone moiety, (a);[25] (b);[24] (c).[28]

Recently reported synthetic methods describe the condensation of *o*-aminobenzamide or *o*-nitrobenzamide or *o*-azidobenzamide with aldehydes or ketones, in the presence of transition metal triflates,[25] Sm with catalytic amount of iodine,[26] SmI_2,[27] using ionic liquid[28] and hydroxyapatite nanoparticles as heterogeneous catalyst.[29] The use of differently substituted hydrazides in place of amides results in the formation of 1,2-dihydroquinazolin-4(*1H*)-ones bearing a N−N linker. Earlier reported synthetic methods include a $Pd(OAc)_2$/AgOAc catalysed condensation of hydrazides with triethylorthobenzoate[30] and a three component condensation of isatoic anhydride, aldehyde or ketone and aromatic amine in the presence of bentonite as the heterogeneous catalyst under an ultrasonic irradiation.[31] The synthesis of a limited number of biologically active 1,2-dihydroquinazolin-4(1*H*)-one has been achieved by refluxing a mixture of hydrazide and aldehyde/ ketone.[32] However, these methods lack either substituent divergence or require the use of expensive catalysts.

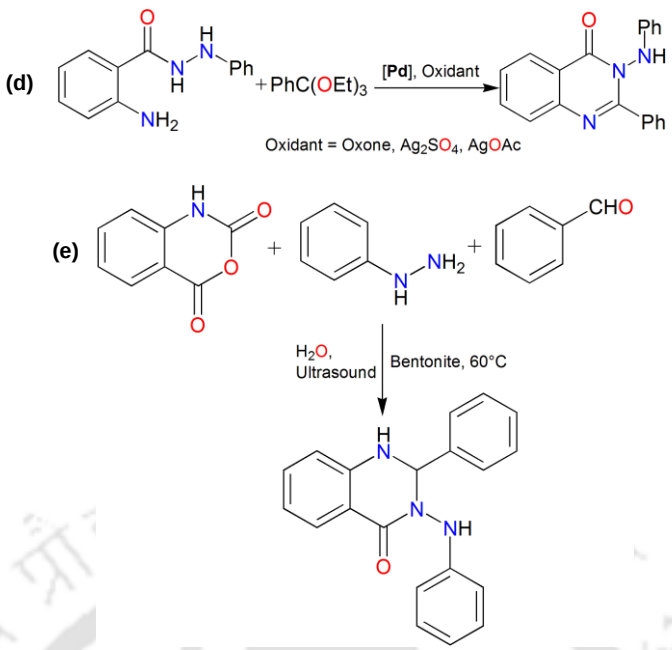

Scheme 2. Synthesis of 1,2-dihydroquinazolinones with N–N linker, (a);[30] (b).[31]

During one of our ongoing projects the condensation of *o*-aminobenzhydrazide (**x**) with 2-picolinonitrile (**1**) in PEG-400 at 80 °C gave *N*′-(2-aminobenzoyl)picolinohydrazonamide (**1x**) (Scheme 3). We envisaged that the condensation of the resultant hydrazonamide (**1x**) with benzaldehyde (**a**) would result in the formation of a Schiff base involving the *o*-amino group of (**1x**). The iminium carbon of the Schiff base may be attacked intramolecularly by the amidic NH group resulting in the formation of 1,2-dihydroquinazolinone (**1ax**) having a N–N linker (Scheme 3). Herein, we describe a successful one pot three component synthesis of 1,2-dihydroquinazolin-4(*1H*)-ones having a N–N linker under a mild condition.

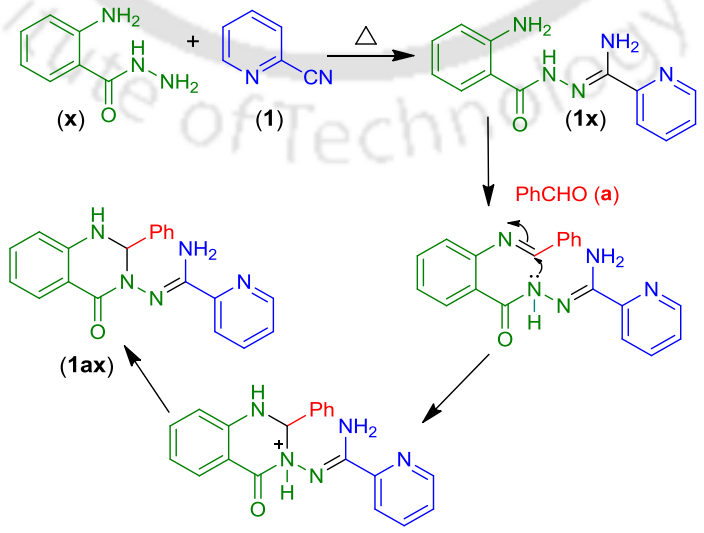

Scheme 3. Our envisaged strategy.

5. 2. Results and Discussion

Initially 2-pyridinecarbonitrile (**1**) (1 equiv) and *o*-aminobenzhydrazide (**x**) (1 equiv) were refluxed in methanol (5 mL) for 6 h. During this time disappearance of both the starting materials and appearance of a new product was observed. The product was analyzed to be a hydrazonamide (**1x**). To this was then added benzaldehyde (**a**) (1 equiv) and the resultant mixture was refluxed for a further period of 4 h. During the course of the reaction a white polycrystalline solid precipitated out (40%) from the reaction medium. Spectroscopic (IR, ^{1}H NMR and ^{13}C NMR), mass analyses and from the crystal structure of one of its derivative the structure of the product was confirmed to be oxo-2-phenyl-1,4-dihydro-2*H*-quinazolin-3-yl)-pyridine-2-carboxamidine *i.e.* 1,2-dihydroquinazolin-4(1*H*)-one (**1ax**). Encouraged by this result some other alcoholic solvents such as EtOH (37%) (entry 2, Table 1) and *i*-PrOH (44%) (entry 3, Table 1) were employed and both gave comparable yields to that using MeOH. When PEG 300 (entry 4, Table 1) was tested as the solvent, a considerable improvement in the yield (63%) of (**1ax**) was found. A further improvement in the yield (81%) was observed using PEG 400 (entry 5, Table 1) as the solvent at 80 °C. During the course of the reaction, the product (**1ax**) started precipitating out from the viscous PEG-400 medium. Further precipitation was achieved by admixing anhydrous EtOH (10 mL) to the reaction medium and the product was separated by simple filtration. Thus there is no requirement of chromatographic purification.

Reaction at temperature lower than 80 °C gave considerably lower yield of the product (entry 6, Table 1). The reaction when carried out at temperature higher than 80 °C (entries 7 and 8, Table 1) leads to the formation of a multitude of products and the yield is also dropped considerably. Table 1 summarises the effects of different solvents and reaction temperature. After screening various reaction conditions, the best optimised condition for this reaction is heating nitrile (**1**) (1 equiv) with *o*-aminobenzhydrazide (**x**) (1 equiv) in PEG 400 for 6 h followed by the addition of aldehyde (1 equiv) and further heating for 4 h. The sequence of the addition is crucial for the success of this reaction, adding all the three reactants together or any other addition sequence leads to the formation undesirable products and by-products.

Table 1. Optimisation of reaction condition for the formation of (**1ax**)

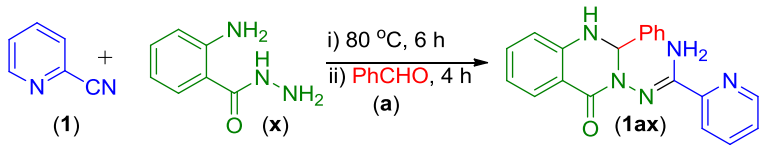

Entry	Solvent	Temperature (°C)	Yield (%)
1	MeOH	80	40
2	EtOH	80	37
3	*i*-PrOH	80	44
4	PEG-300	80	63
5	**PEG-400**	**80**	**81**
6	PEG-400	70	55
7	PEG-400	90	76
8	PEG-400	100	68

The *in situ* generated hydrazonamide (**1x**) obtained by the condensation of *o*-aminobenzhydrazide (**x**) and 2-picolinonitrile (**1**) was then reacted separately with various substituted benzaldehydes possessing electron-donating groups such as *o*-OH (**b**), *p*-OH (**c**), *p*-OMe (**d**) providing their corresponding 1,2-dihydroquinazolin-4(1*H*)-one (**1bx-1dx**) in good yields (Table 2). Similarly, aldehydes possessing electron-withdrawing groups such as *o*-Cl (**e**), *o*-Br (**f**), *m*-F (**g**), *m*-Cl (**h**), *m*-Br (**i**), *p*-F (**j**), *p*-Cl (**k**), *p*-Br (**l**), *p*-NO_2 (**m**) (Table 2) also yielded their corresponding products 1,2-dihydroquinazolin-4(1*H*)-one (**1ex-1mx**) in moderate to good yields when reacted with the *in situ* generated hydrazonamide (**1x**). Heterocyclic aldehydes such as imidazolyl (**n**), pyridyl (**o**) and quinazolinyl (**p**) upon reaction with hydrazonamide (**1x**) gave satisfactory yields of their corresponding 1,2-dihydroquinazolin-4(1*H*)-one (**1nx-1px**) in decent yields (Table 2). From the observations in Table 2 it is evident that no correlation between the yields of the product obtained and the effect of the substituents present in the phenyl ring of the aldehyde could be correlated.

Table 2. Synthesis of various 1,2-dihydroquinazolin-4(1*H*)-one

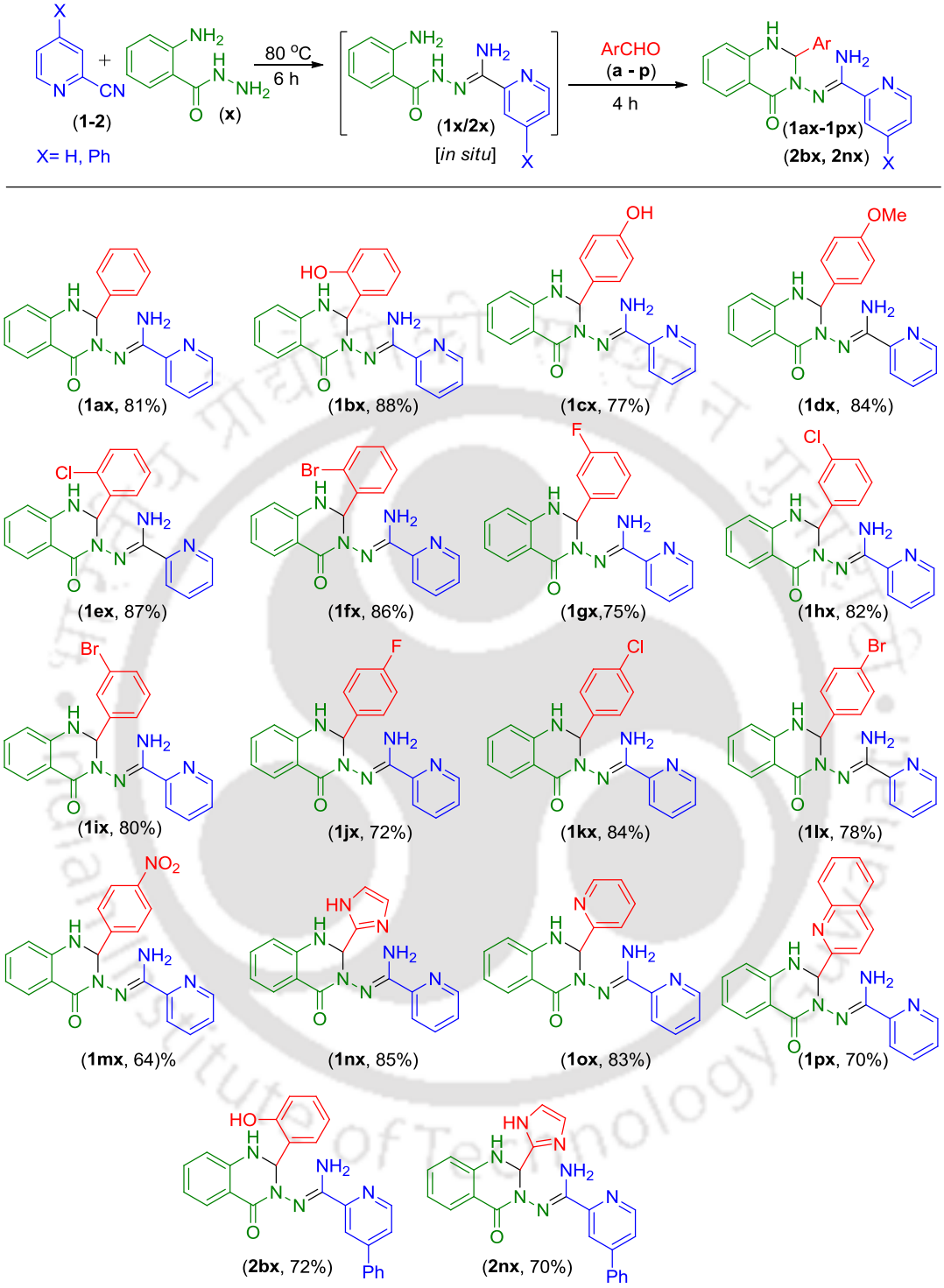

[a]Reaction conditions: 2-aminobenzhydrazide (**x**) (1 mmol), 2-pyridine/4-phenyl-2-pyridinecarbonitrile (**1-2**) (1 mmol), arylaldehydes (**a-p**) (1 mmol) at 80 °C for 6 h in PEG 400.

Further, the *in situ* generated hydrazonamide (**2x**) obtained by the condensation of *o*-aminobenzhydrazide (**x**) and 4-pyridyl-2-picolinonitrile (**2**) when reacted under the present reaction condition with salicylaldehyde (**b**) and 2-imidazolyl aldehyde (**n**) provided their corresponding 1,2-dihydroquinazolin-4(1*H*)-one (**2bx**) and (**2nx**) respectively (Table 2). It should be mentioned here that aliphatic nitriles such as acrylonitrile and allyl nitrile and aromatic nitriles such as benzonitrile, *p*-bromobenzonitrile and *p*-nitrobenzonitrile all failed to give their intermediate hydrazonamide and eventually the final product 1,2-dihydroquinazolin-4(1*H*)-one. Surprisingly, both 3-pyridyl and 4-pyridyl nitriles also failed to condense with *o*-aminobenzhydrazide to give any trace of the 1,2-dihydroquinazolin-4(1*H*)-one. The latter two heterocyclic nitriles did not produce their intermediate hydrazonamides even at higher temperature (up to 100 °C) and longer reaction time (24 h).

The successful condensation 2-picolinonitrile (**1**) with *o*-aminobenzhydrazide (**x**) giving intermediate hydrazonamide (**1x**) prompted us to test whether similar condensation with pyrazine-2-carbonitrile (**3**) and *o*-aminobenzhydrazide (**x**) is possible or not? When pyrazine-2-carbonitrile (**3**) and *o*-aminobenzhydrazide (**x**) were reacted under the present experimental condition, it provided the corresponding hydrazonamide (**3x**) (Table 3). This *in situ* hydrazonamide (**3x**) was then reacted separately with various aromatic aldehydes possessing electron-neutral (**a**), electron-donating groups such as *o*-OH (**b**), *p*-OH (**c**), *p*-OMe (**d**) all of which provided their corresponding 1,2-dihydroquinazolin-4(1*H*)-one (**3ax-3dx**) in good yields (Table 3). Here again, aromatic aldehydes possessing electron-withdrawing groups such as *o*-Cl (**e**), *o*-Br (**f**), *m*-F (**g**), *m*-Cl (**h**), *m*-Br (**i**), *p*-F (**j**), *p*-Cl (**k**), *p*-Br (**l**), *p*-NO_2 (**m**) groups (Table 3) resulted their corresponding products 1,2-dihydroquinazolin-4(1*H*)-one (**3ex-3mx**) in decent yields when reacted with the *in situ* generated hydrazonamide (**3x**). The structure of the product **3kx** has been confirmed by X-ray crystallography as shown in Figure 2. Further, heterocyclic aldehydes such as imidazolyl (**n**), pyridyl (**o**) and quinazolinyl (**p**) all reacted with the *in situ* generated hydrazonamide (**3x**) giving good yields of their corresponding 1,2-dihydroquinazolin-4(1*H*)-one (**3nx-3px**). As observed in Table 2, here as well neither the steric nor the electronic effect of substituents on the aryl ring of the aromatic aldehyde could be ascertained.

Table 3. Synthesis of various 1,2-dihydroquinazolin-4(1*H*)-one

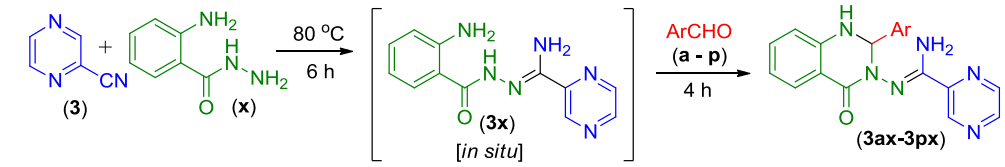

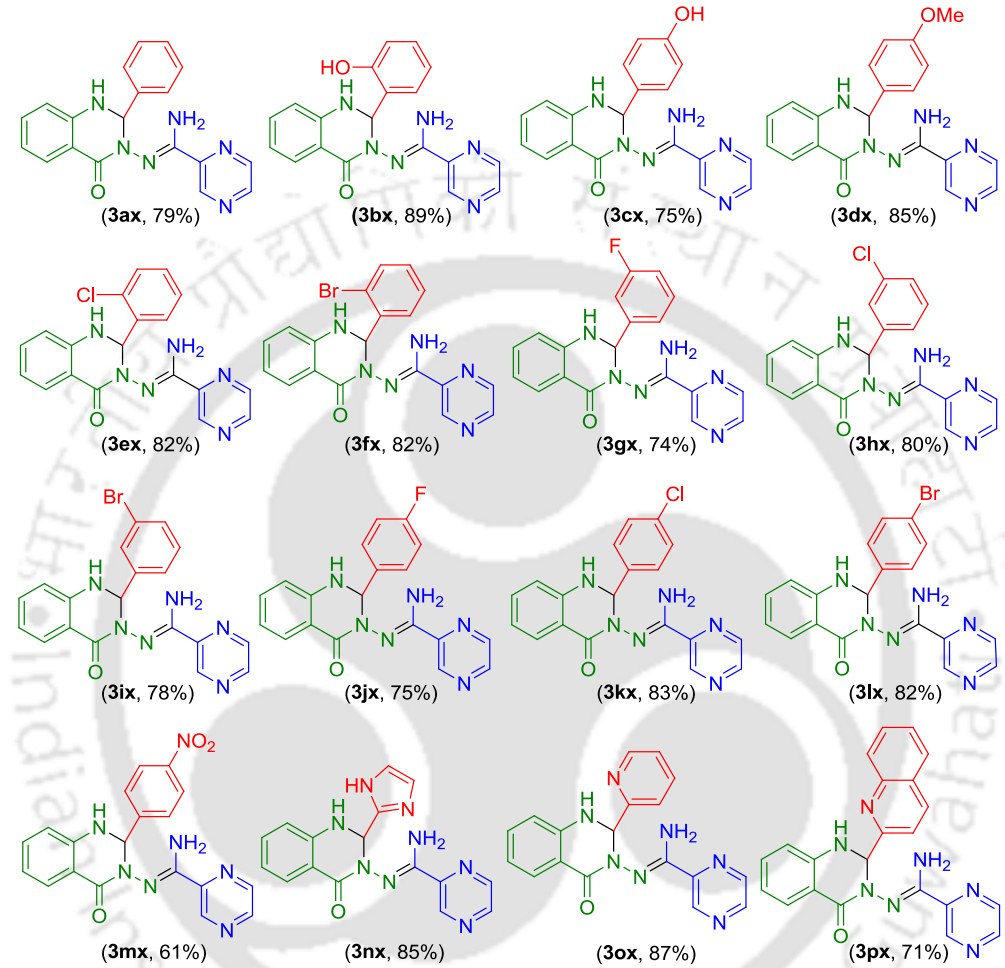

[a]Reaction conditions: 2-aminobenzhydrazide (**x**) (1 mmol), 2-pyrazine-carbonitrile (**3**) (1 mmol), arylaldehydes (**a**-**p**) (1 mmol) at 80 °C for 6 h in PEG 400.

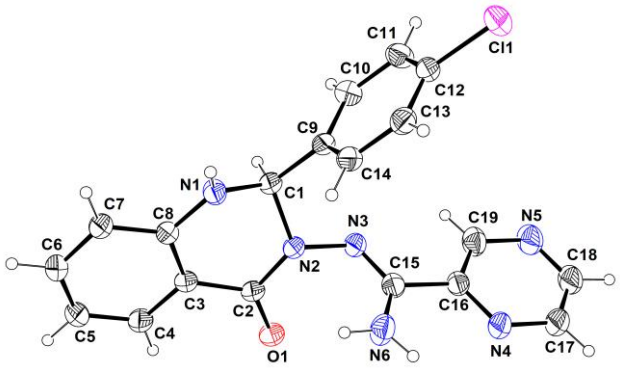

Figure 2. *ORTEP* diagram of compound **3kx.**

Aliphatic aldehydes such as heptaldehyde and cyclohexaldehyde failed to react under the present reaction condition to give their desired products. However, both the reactions gave dihydro-5*H*-1,3-4-benzotrizepin-5-one (**4a**) as the only isolable product (Figure 3).[33] The formation of **4a** might be due to the slow production of intermediate Schiff base which undergoes intramolecular cyclisation. Mechanism for the formation of product (**4a**) is shown in Scheme 4.

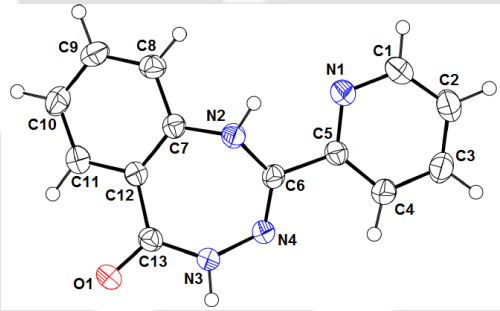

Figure 3. *ORTEP* diagram of compound **4a**.[33]

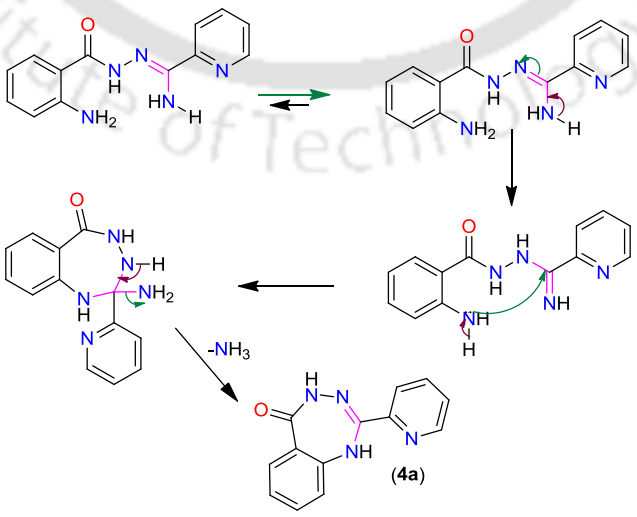

Scheme 4. Mechanism for the formation of product (**4a**).

This first step of the reaction is the condensation between *o*-aminobenzhydrazide (**x**) with picolinonitrile (**1**) to yield aroylhydrazonamide (**1x**). The *o*-amino group of **1x** reacts with an aldehyde to generate a Schiff base intermediate (**1ax′**). Subsequent intramolecular attack of the amidic NH at the imine carbon results in the formation of a fused heterocyclic intermediate (**1ax′′**). The loss of a proton from the intermediate results in the formation of racemic product **1ax** (Scheme 5). The formation of intermediate **1a** has been confirmed by isolation and characterization.

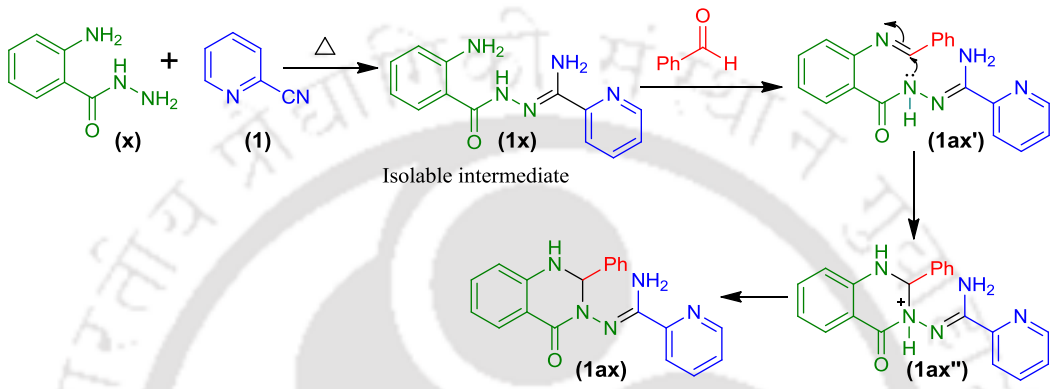

Scheme 5. Plausible mechanism for formation of 1,2-dihydroquinazolin-4(1*H*)-one.

5. 3. Conclusions

A series of 3-aryl-2-substituted-1,2-dihydroquinazolin-4(1*H*)-one were synthesized *via* an one pot three-component method using *o*-aminobenzhydrazide, *N*-heterocyclic nitriles and various aromatic/ heterocyclic aldehydes. The advantages of this method are one pot synthesis, metal free protocol, easy work-up and isolation procedure with wide substituent divergence.

5. 4. Experimental Section

The synthesis procedure and characterisation data for **2-amino-benzoic acid (amino-pyridin-2-yl-methylene)-hydrazide** (**1x**) has been earlier described in chapter 2. The same synthesis procedure was followed for the synthesis of **2-amino-benzoic acid [amino-(4-phenyl-pyridin-2-yl)-methylene]-hydrazide** (**2x**) and **2-amino-benzoic acid (amino-pyrazin-2-yl-methylene)-hydrazide** (**3x**), by using respectively 4-phenyl-2-carbonitrile and 2-pyrazinyl-carbonitrile.

5. 4. 1. General procedure for the synthesis of 2-aryl-3-imidamide substituted 1,2-dihydroquinazolin-4(1*H*)-ones

The specific procedure for *N*-(4-oxo-2-phenyl-1,4-dihydro-2*H*-quinazolin-3-yl)-pyridine-2-carboxamidine (**1ax**) is detailed below. 2-Aminocarbhydrazide (236 mg, 1.50 mmol), 2-cyanopyridine (161 mg, 1.55 mmol) were suspended in PEG 400 (3 mL) and heated at 80 °C for 6 h. The reaction mixture was cooled to room temperature, to this was added benzaldehyde (165 mg, 1.55 mmol) and heated at 80 °C for another 2 h. The resultant white precipitate was filtered, washed with methanol (2 x 5 mL) dried in vacuum desiccators over anhydrous $CaCl_2$ to give product (**1ax)**. White solid; yield 416 mg, 81%. Mp 224−226 °C. ^{1}H NMR (DMSO-d_6, 600 MHz) δ 5.94 (s, 1H), 6.31–7.00 (m, 4H), 7.24 (t, *J* = 7.3 Hz, 2H), 7.29 (t, *J* = 7.4 Hz, 2H), 7.33 (s, 1H), 7.42–7.48 (m, 1H), 7.56 (d, *J* = 7.4 Hz, 2H), 7.67 (d, *J* = 7.6 Hz, 1H), 7.79 (t, *J* = 7.5 Hz, 1H), 7.84 (d, *J* = 7.8 Hz, 1H), 8.55 (d, *J* = 4.3 Hz, 1H). ESI MS calcd. for $C_{20}H_{18}N_5O$ ($M+H^+$) 344.1506, found: 344.1503. The same procedure was followed for the synthesis of **1bx-3px** using respective aldehydes and *N*-heterocyclic nitriles in the same molar quantities.

5. 4. 2. Characterisation data of compounds 2x-3x and 1bx-3px

2-Amino-benzoic acid [amino-(4-phenyl-pyridin-2-yl)-methylene]-hydrazide (2x)

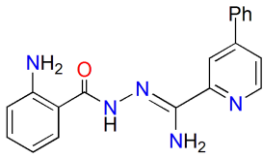

Yellow solid; yield 354 mg, 71%. Mp 148−150 °C. IR (KBr, cm^{-1}) 3495, 3403, 1807, 1658, 1427, 1366, 1257, 1161. ^{1}H NMR (DMSO-d_6, 600 MHz) δ 6.19 (s, 2H), 6.57 (t, *J* = 7.2 Hz, 1H), 6.73 (d, *J* = 7.8 Hz, 1H), 6.99 (s, 2H), 7.17 (t, *J* = 6.6 Hz, 1H), 7.52–7.54 (m, 1H), 7.58 (t, *J* = 6.9 Hz, 3H), 7.82 (s, 3H), 8.43 (s, 1H), 8.67 (s, 1H), 10.14 (s, 1H). ^{13}C NMR (DMSO-d_6, 150 MHz) δ 175.10, 149.96, 149.50, 148.48, 147.49, 137.72, 132.11, 130.13, 129.99, 29.36, 127.54, 122.77, 118.43, 116.59, 115.27. HR-MS (ESI) calcd. for $C_{19}H_{18}N_5O$ ($M+H^+$) 332.1513, found 332.1503.

2-Amino-benzoic acid (amino-pyrazin-2-yl-methylene)-hydrazide (3x)

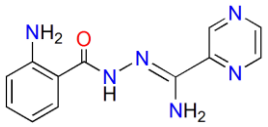

Yellow solid; yield 335 mg, 87%. Mp 253−255 °C. IR (KBr, cm^{-1}) 3489, 3454, 3358, 3214, 3032, 1665, 1625, 1582, 1547, 1521, 1474, 1449, 1431, 1375, 1313, 1261, 1178, 1063, 1017, 908, 758. ^{1}H NMR (DMSO-d_6, 400 MHz) δ 6.19 (s, 2H), 6.56 (t, J = 7.0 Hz, 3H), 6.73 (d, J = 7.9 Hz, 1H), 6.97 (s, 2H), 7.17 (t, J = 7.0 Hz, 1H), 7.55 (d, J = 7.2 Hz, 1H), 8.67 (d, J = 17.7 Hz, 2H), 9.32 (s, 1H), 10.14 (s, 1H). ^{13}C NMR (DMSO-d_6, 150 MHz) δ 165.38, 149.40, 146.36, 145.33, 144.86, 142.85, 142.80, 131.73, 128.67, 116.07, 115.17, 114.69. HR-MS (ESI) calcd. for $C_{12}H_{13}N_6O$ ($M+H^+$) 257.1145, found 257.1144.

N-[2-(4-Oxo-2-phenyl-1,4-dihydro-2*H*-quinazolin-3-yl]-pyridine-2-carboximidine (1ax)

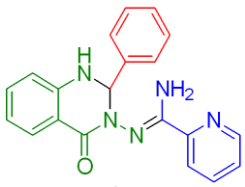

White solid; yield 416 mg, 81%. Mp 224−225 °C. IR (KBr, cm^{-1}) 3490, 1652, 1546, 1510, 1483, 1397, 1364, 1292, 1153, 998, 952, 798, 748. ^{1}H NMR (DMSO-d_6, 600 MHz) δ 5.94 (s, 1H), 6.31–7.00 (m, 4H), 7.24 (t, J = 7.3 Hz, 2H), 7.29 (t, J = 7.4 Hz, 2H), 7.33 (s, 1H), 7.42–7.48 (m, 1H), 7.56 (d, J = 7.4 Hz, 2H), 7.67 (d, J = 7.6 Hz, 1H), 7.79 (t, J = 7.5 Hz, 1H), 7.84 (d, J = 7.8 Hz, 1H), 8.55 (d, J = 4.3 Hz, 1H). ^{13}C NMR (DMSO-d_6, 150 MHz) δ 161.09, 156.03, 150.62, 148.85, 147.34, 141.52, 137.61, 133.59, 128.82, 128.50, 128.06, 127.96, 126.02, 121.87, 117.76, 115.66, 114.80, 75.06. HR-MS (ESI) calcd. for $C_{20}H_{18}N_5O$ ($M+H^+$) 344.1506, found 344.1503.

N-[2-(2-Hydroxy-phenyl)-4-oxo-1,4-dihydro-2*H*-quinazolin-3-yl]-pyridine-2-carboximidine (1bx)

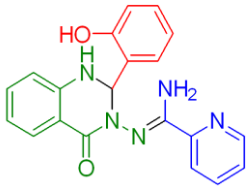

White solid; yield: 474 mg, 88%. Mp 231−233 °C. IR (KBr, cm^{-1}) 3487, 3350, 2730, 2601, 1951, 1915, 1799, 1747, 1650, 1555, 1495, 1459, 1432, 1390, 1320, 1283, 1266, 1240, 1199, 1154, 1099, 1043, 996, 958, 896, 866, 799, 760. ^{1}H NMR (DMSO-d_6, 600 MHz) δ 6.19 (s, 1H), [6.70 (q, J = 7.7 Hz, 2H), 6.81 (dd, J_1 = 17.0 Hz and J_2 = 8.1 Hz, 2H), 6.25–6.90 (b, 2H for NH_2 merged along with these two aromatic protons)], 7.04 (dd, J_1 = 15.6 Hz, J_2 = 8.2 Hz, 2H), 7.04–7.08 (m, 2H), 7.23 (d, 7.2, 1H), 7.36 (d, J = 7.8 Hz, 1H), 7.48 (t, J = 6.6 Hz, 1H), 7.67−7.82 (m, 3H), 8.59 (d, J = 4.8 Hz, 1H), 9.98 (s, 1H). ^{13}C NMR (DMSO-d_6,100 MHz): δ 161.15, 156.01, 155.44, 150.29, 148.71, 147.17, 137.45, 133.31, 129.42, 127.93, 127.80, 126.94, 125.89, 121.76, 118.92, 117.44, 116.04, 115.45, 114.81, 69.48. HR-MS (ESI) calcd. for $C_{20}H_{18}N_5O_2$ ($M+H^+$) 360.1455, found 360.1457.

N-[2-(4-Hydroxy-phenyl)-4-oxo-1,4-dihydro-2*H*-quinazolin-3-yl]-pyridine-2-carboximidine (1cx)

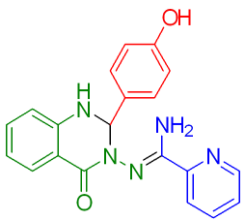

White solid; yield 415 mg, 77 %. Mp 223−225 °C. IR (KBr, cm^{-1}) 3300, 1620, 1485, 1511, 1399, 1330, 1190, 1261, 1190, 1168, 1156, 1110, 1102, 1076, 1030, 985, 951, 852, 820, 792, 782, 782, 761. ^{1}H NMR (DMSO-d_6, 400 MHz) δ 4.76 (s, 2H), 5.68 (s, 1H), 6.52–6.80 (m, 4H), 7.14 (dd, J_1 = 15.5 Hz and J_2 = 9.5 Hz, 4H), 7.58 (d, J = 7.6 Hz, 1H), 9.43 (s, 1H). ^{13}C NMR (DMSO-d_6, 100 MHz) δ 162.81, 157.99, 146.97, 133.61, 131.73, 128.29, 127.62, 117.41, 115.45, 114.50, 114.17, 74.38. HR-MS (ESI) calcd. for $C_{20}H_{18}N_5O_2$ ($M+H^+$) 360.1455, found 360.1462.

N-[2-(4-Methoxy-phenyl)-4-oxo-1,4-dihydro-2*H*-quinazolin-3-yl]-pyridine-2-carboximidine (1dx)

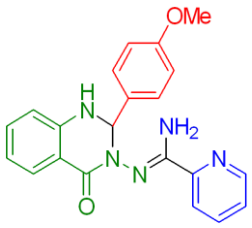

White solid; yield 476 mg, 85%. Mp 242−243 °C. IR (KBr, cm^{-1}) 3494, 3294, 1630, 1563, 1511, 1485, 1394, 1371, 1294, 1252, 1175, 1030, 952, 837, 799, 752. ^{1}H NMR (DMSO-d_6, 400 MHz) δ 5.92 (s, 1H), 6.20–6.79 (m, 3H), 6.85 (d, J = 8.6 Hz, 2H), 7.16–7.34 (m, 2H), 7.48 (dd, J_1 = 12.0 and J_2 = 8.0 Hz, 3H), 7.68 (d, J = 7.7 Hz, 1H), 7.84 (m, 2H), 8.57 (d, J = 4.5 Hz, 1H). ^{13}C NMR (DMSO-d_6, 100 MHz) δ 160.43, 159.06, 155.30, 149.96, 148.15, 146.72, 136.93, 132.88, 128.52, 127.37, 125.33, 121.19, 116.99, 114.94, 114.09, 113.12, 73.99, 54.98. HR-MS (ESI) calcd. for $C_{21}H_{20}N_5O_2$ ($M+H^+$) 374.1612, found 374.1625.

N-[2-(2-Chloro-phenyl)-4-oxo-1,4-dihydro-2*H*-quinazolin-3-yl]-pyridine-2-carboximidine (1ex)

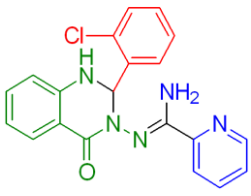

White solid; yield 492 mg, 87%. Mp 228−230 °C. IR (KBr, cm^{-1}) 3394, 3311, 1804, 1670, 1564, 1526, 1502, 1466, 1444, 1386, 1342, 1321, 1258, 1241, 1208, 1151, 1112, 1087, 1065, 999, 894, 862, 832, 756. ^{1}H NMR (DMSO-d_6, 400 MHz) δ 6.42 (s, 1H), [6.72–6.77 (m, 2H), 6.50–7.00 (b, 2H for NH_2 merged along with these two aromatic protons)], 7.27−7.29 (m, 4H), 7.39–7.42 (m, 1H), 7.46 (dd, J_1 = 8.7 Hz and J_2 = 4.7 Hz, 1H), 7.72 (d, J = 7.6 Hz, 1H), 7.77–7.81 (m, 3H), 8.55 (d, J = 4.8 Hz, 1H). ^{13}C NMR (DMSO-d_6, 100 MHz) δ 160.80, 155.96, 149.82, 148.22, 146.45, 137.60, 137.02, 133.13, 132.43, 129.92, 129.11, 128.93, 127.46, 127.05, 125.45, 121.17, 117.33, 114.56, 114.19, 70.86; HR-MS (ESI) calcd. for $C_{20}H_{17}N_5O^{35}Cl$ ($M+H^+$) 378.1116, found 378.1122.

N-[2-(2-Bromo-phenyl)-4-oxo-1,4-dihydro-2*H*-quinazolin-3-yl]-pyridine-2-carboximidine (1fx)

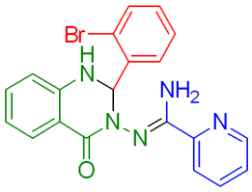

White solid; yield 542 mg, 86%. Mp 229−231 °C. IR (KBr, cm^{-1}) 3381, 3311, 3182, 1658, 1630, 1564, 1485, 1386, 1321, 1208, 1151, 1028, 859, 829, 797, 756. ^{1}H NMR (DMSO-d_6, 600 MHz) δ 6.40 (s, 1H), [6.73 (m, 2H), 6.50–7.10 (b, 2H for NH_2 merged along with these two aromatic protons)], 7.19 (t, 6.9, 1H), 7.25–7.28 (m, 2H), 7.32 (t, *J* = 7.5 Hz, 1H), 7.43–7.50 (bs, 1H), 7.55 (d, *J* = 7.8 Hz, 1H), 7.70 (d, *J* = 7.8 Hz, 1H), 7.80 (d, *J* = 7.2 Hz, 3H), 8.54 (d, *J* = 4.2 Hz, 1H). ^{13}C NMR (DMSO-d_6, 150 MHz) δ 160.71, 155.92, 149.85, 148.18, 146.46, 139.11, 136.97, 133.12, 132.26, 130.25, 129.20, 127.61, 127.45, 125.39, 122.91, 121.16, 117.33, 114.50, 114.16, 73.55; HR-MS (ESI) calcd. for $C_{20}H_{17}N_5O^{79}Br$ ($M+H^+$) 422.0611, found 422.0619.

N-[2-(3-Fluoro-phenyl)-4-oxo-1,4-dihydro-2*H*-quinazolin-3-yl]-pyridine-2-carboximidine (1gx)

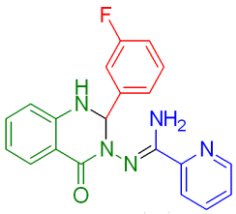

White solid; yield: 388 mg, 75%. Mp 244−245 °C. IR (KBr, cm^{-1}) 3380, 3247, 2935, 1652, 1588, 1505, 1560, 1485, 1454, 1435, 1400, 1368, 1317, 1290, 1267, 1239, 1140, 997, 967, 870, 805, 756. ^{1}H NMR (DMSO-d_6, 600 MHz) δ 6.26 (s, 1H), [6.70–6.74 (m, 2H), 6.50–6.90 (b, 2H for NH_2 merged along with these two aromatic protons)], 7.11–7.17 (m, 2H), 7.25 (t, *J* = 7.5 Hz, 1H), 7.29 (s, 2H), 7.45 (bs, 1H), 7.65 (t, *J* = 7.5 Hz, 1H), 7.70 (d, *J* = 7.8 Hz, 1H), 7.80 (s, 2H), 8.55 (d, *J* = 4.2 Hz, 1H). ^{13}C NMR (DMSO-d_6, 150 MHz) δ 160.40, 155.68, 149.85, 148.25, 146.40, 143.46, 137.01, 133.05, 132.57, 129.76, 128.11, 127.43, 127.24, 126.03, 125.44, 121.20, 117.33, 114.99, 114.22, 73.61. HR-MS (ESI) calcd. for $C_{20}H_{17}N_5OF$ ($M+H^+$) 362.1418, found: 362.1424.

N-[2-(3-Chloro-phenyl)-4-oxo-1,4-dihydro-2*H*-quinazolin-3-yl]-pyridine-2-carboximidine (1hx)

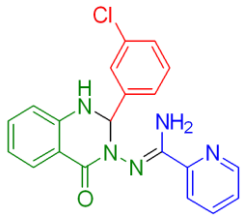

White solid; yield 464 mg, 82%. Mp 205−207 °C. IR (KBr, cm^{-1}) 3484, 3359, 3319, 1672, 1650, 1564, 1538, 1502, 1483, 1451, 1414, 1396, 1368, 1324, 1292, 1254, 1202, 1182, 1153, 996, 953, 880, 848, 753. ^{1}H NMR (DMSO-d_6, 400 MHz) δ 5.98 (s, 1H), [6.70–6.76 (m, 2H) 6.30–7.10 (b, 2H for NH_2 merged along with these two aromatic protons)], 7.27 (t, J = 7.4 Hz, 1H), 7.32−7.34 (m, 2H), 7.40 (s, 1H), 7.49–7.54 (m, 2H), 7.65 (s, 1H), 7.67 (d, J = 7.6 Hz, 1H), 7.82–7.89 (m, 2H), 8.57 (d, J = 3.6 Hz, 1H). ^{13}C NMR (DMSO-d_6,100 MHz) δ 160.87, 156.14, 150.25, 148.69, 146.83, 144.09, 137.46, 133.50, 131.45, 130.59, 130.51, 127.88, 126.83, 125.90, 121.64, 117.76, 115.38, 114.65, 74.00. HR-MS (ESI) calcd. for $C_{20}H_{17}N_5O^{35}Cl$ ($M+H^+$) 378.1116, found 378.1127.

N-[2-(3-Bromo-phenyl)-4-oxo-1,4-dihydro-2*H*-quinazolin-3-yl]-pyridine-2-carboximidine (1ix)

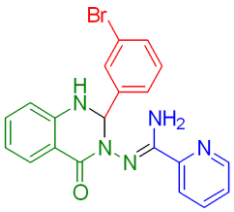

White solid; yield 505 mg, 80%. Mp 221−223 °C. IR (KBr, cm^{-1}) 3477, 3375, 1951, 1926, 1812, 1666, 1564, 1507, 1485, 1448, 1427, 1395, 1322, 1290, 1255, 1213, 1176, 1151, 1119, 1063, 1017, 997, 962, 884, 866, 854, 800, 784. ^{1}H NMR (DMSO-d_6, 400 MHz): δ 5.96 (s, 1H), [6.69 (t, J = 7.4 Hz, 1H), 6.74 (d, J = 8.4 Hz, 1H), 6.45–6.95 (b, 2H) for NH_2 merged along with these two aromatic protons)], 7.25–7.28 (m, 2H), 7.40 (s, 1H), 7.44 (d, J = 7.8 Hz, 1H), 7.47 (t, J = 6.9 Hz, 1H), 7.55 (d, J = 7.8 Hz, 1H), 7.67 (d, J = 7.2 Hz, 1H), 7.78 (s, 1H), 7.82 (t, J = 7.5 Hz, 1H), 7.87 (d, J = 7.8 Hz, 1H), 8.57 (d, J = 4.8 Hz, 1H). ^{13}C NMR (DMSO-d_6, 150 MHz) δ 161.07, 156.35, 150.48, 148.91, 147.05, 144.31, 137.67, 133.72, 131.66, 130.80, 130.73, 128.10, 127.05, 126.12, 121.86, 117.99, 115.61, 114.87, 74.22. HR-MS (ESI) calcd. for $C_{20}H_{17}N_5O^{79}Br$ ($M+H^+$) 422.0611, found: 422.0592.

N-[2-(4-Fluoro-phenyl)-4-oxo-1,4-dihydro-2*H*-quinazolin-3-yl]-pyridine-2-carboximidine (1jx)

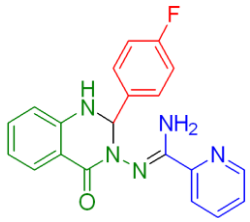

White solid; yield 390 mg, 72%. Mp 245−247 °C. IR (KBr, cm^{-1}) 3489, 3379, 3339, 3270, 3060, 1654, 1565, 1547, 1509, 1480, 1441, 1421, 1392, 1366, 1331, 1291, 1253, 1221, 1154, 997, 949, 906, 863, 840, 796, 748. ^{1}H NMR (DMSO-d_6, 600 MHz) δ 5.98 (s, 1H), [6.69−6.76 (m, 2H), 6.40–7.10 (b, 2H for NH_2 merged along with these two aromatic protons)], 7.14 (t, 8.7, 2H), 7.26 (t, *J* = 7.5 Hz, 1H), 7.32 (s, 1H), 7.48 (t, *J* = 6.0 Hz, 1H), 7.60−7.69 (m, 3H), 7.80−7.84 (m, 2H), 78.56 (d, *J* = 4.2, 1H). ^{13}C NMR (DMSO-$d_6$150 MHz): δ 161.09, 160.44, 155.53, 149.89, 148.20, 146.61, 137.11, 136.96, 132.97, 129.46, 129.46, 127.41, 125.38, 121.16, 117.20, 114.94, 114.66, 114.52, 114.15, 73.74. HR-MS (ESI) calcd. for $C_{20}H_{17}N_5OF$ ($M+H^+$) 362.1418, found 362.1410.

N-[2-(4-Chloro-phenyl)-4-oxo-1,4-dihydro-2*H*-quinazolin-3-yl]-pyridine-2-carboximidine (1kx)

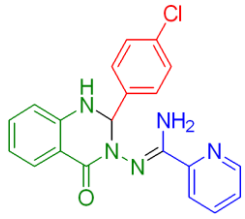

White solid; yield 475 mg, 84%. Mp 232−233 °C. IR (KBr, cm^{-1}) 3486, 3376, 3340, 3276, 1920, 1805, 1753, 1664, 1546, 1507, 1484, 1440, 1414, 1389, 1370, 1331, 1292, 1254, 1226, 1201, 1154, 1087, 1012, 999, 948, 905, 831, 796, 745. ^{1}H NMR (DMSO-d_6, 600 MHz) δ 5.99 (s, 1H), [6.70−6.75 (m, 2H), 6.40–7.10 (b, 2H for NH_2 merged along with these two aromatic protons)], 7.25(t, *J* = 7.5, 1H), 7.34–7.38 (m, 3H), 7.50 (t, *J* = 6.0, 1H), 7.54 (d, *J* = 7.8, 2H), 7.67 (d, *J* = 7.8, 1H), 8.64 (s, 1H), 8.71 (s, 1H), 8.96 (s, 1H). ^{13}C NMR (DMSO-d_6, 150 MHz) δ 160.40, 155.57, 149.82, 148.21, 146.47, 139.91, 136.99, 133.00, 132.66, 129.21, 127.84, 127.41, 125.42, 121.19, 117.24, 114.93, 114.17, 73.63. HR-MS (ESI) calcd. for $C_{20}H_{17}N_5O^{35}Cl$ ($M+H^+$) 378.1116, found 378.1114.

N-[2-(4-Bromo-phenyl)-4-oxo-1,4-dihydro-2*H*-quinazolin-3-yl]-pyridine-2-carboximidine (1lx)

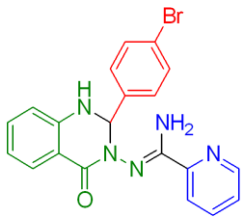

White solid; yield 493 mg, 78%. Mp 242−244 °C. IR (KBr, cm^{-1}): 3383, 3374, 3339, 3282, 1654, 1630, 1565, 1548, 1508, 1482, 1439, 1367, 1331, 1291, 1155, 1070, 1010, 949, 905, 829, 796, 748. 400 MHz ^{1}H NMR (DMSO-d_6, 400 MHz) δ 5.97 (s, 1H), [6.70–6.76 (m, 2H), 6.45–7.05 (b, 2H for NH_2 merged along with these two aromatic protons)], 7.26 (t, *J* = 7.6 Hz, 1H), 7.38 (d, *J* = 7.2 Hz, 3H), 7.48 (t, *J* = 6.0 Hz, 1H), 7.60 (d, *J* = 7.6 Hz, 2H), 7.69 (d, *J* = 8.0 Hz, 1H), 7.84 (t, *J* = 7.6 Hz, 1H), 7.88 (d, *J* = 8.0 Hz, 1H), 8.58 (d, *J* = 4.0 Hz, 1H). ^{13}C NMR (DMSO-d_6, 150 MHz) δ 161.15, 156.38, 150.39, 148.92, 147.08, 140.91, 137.70, 133.75, 131.45, 130.19, 128.08, 126.16, 121.99, 121.89, 118.02, 115.54, 114.86, 73.34. HR-MS (ESI) calcd. for $C_{20}H_{17}N_5O^{79}Br$ ($M+H^+$) 422.0611, found 422.0630.

N-[2-(4-Nitro-phenyl)-4-oxo-1,4-dihydro-2*H*-quinazolin-3-yl]-pyridine-2-carboximidine (1mx)

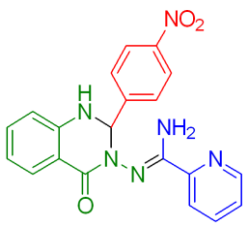

White solid; yield 374 mg, 64 %. Mp 264−266 °C; IR (KBr, cm^{-1}): 3502, 3463, 3384, 32060, 2829, 1926, 1811, 1662, 1586, 1564, 1526, 1480, 1440, 1391, 1368, 1345, 1288, 1256, 1231, 1170, 1152, 1104, 949, 910, 867, 856, 831, 800, 753. ^{1}H NMR (DMSO-d_6, 600 MHz) δ 6.12 (s, 1H), [6.72−6.78 (m, 2H), 6.55–7.10 (b, 2H for NH_2 merged along with these two aromatic protons)], 7.27 (t, *J* = 7.6 Hz, 1H), 7.46–7.55 (m, 2H), 7.71 (d, *J* = 7.2 Hz, 1H), 7.82 (t, *J* = 7.2 Hz, 1H), 7.86 (d, *J* = 8.4 Hz, 2H), 7.90 (d, *J* = 7.8 Hz, 1H), 8.20 (d, *J* = 7.8 Hz, 2H), 8.57 (d, *J* = 3.6 Hz, 1H). ^{13}C NMR (DMSO-d_6, 150 MHz) δ 160.37, 155.86, 149.73, 148.47, 148.30, 147.36, 146.24, 137.09, 133.19, 128.67, 127.51, 125.55, 123.18, 121.30, 117.55, 115.00, 114.33, 73.33. HR-MS (ESI) calcd. for $C_{20}H_{17}N_6O_3$ ($M+H^+$) 389.1357, found 389.1358.

N-[2-(1H-Imidazolyl-2-yl)-4-oxo-1,4-dihydro-2*H*-quinazolin-3-yl]-pyridine-2-carboximidine (1nx)

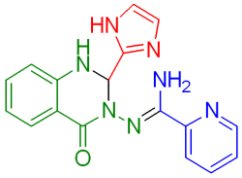

White solid; yield 424 mg; 85%. Mp 256−258 °C. IR (KBr, cm^{-1}) 3457, 1806, 1707, 1657, 1519, 1485, 1440, 1394, 1349, 1320, 1289, 1267, 1233, 1195, 1149, 1115, 1078, 894, 854, 821, 799, 766. ^{1}H NMR (DMSO-d_6, 600 MHz) δ 5.94 (s, 1H), [6.70 (t, J = 7.5 Hz, 1H), 6.73– 6.75 (m, 2H), 6.35– 6.90 (b, 2H for NH_2 merged along with these two aromatic protons)], 7.03 (s, 1H), 7.24 (t, J = 7.5 Hz, 1H), 7.34 (s, 1H), 7.50 (t, J = 6 Hz, 1H), 7.65 (d, J = 7.2 Hz, 2H), 7.86 (t, J = 7.8 Hz, 1H), 8.01 (d, J = 7.8 Hz, 1H), 8.58 (d, J = 4.2 Hz, 1H), 11.96 (s, 1H). ^{13}C NMR (100 MHz, DMSO-d_6) δ 159.55, 156.60, 149.81, 148.19, 146.72, 146.35, 136.96, 132.83, 127.34, 125.52, 121.57, 117.27, 115.07, 114.27, 68.99. HR-MS (ESI) calcd. for $C_{17}H_{16}N_7O$ ($M+H^+$) 334.1411, found 334.1418.

N-[2-(4-oxo-2-pyridin-2-yl-1,4-dihydro-2*H*-quinazolin-3-yl)-pyridine-2-carboximidine (1ox)

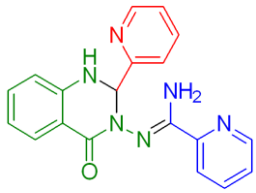

White solid; yield 428 mg, 83%. Mp 237−239 °C. IR (KBr, cm^{-1}) 3432, 3321, 3248, 1650, 1570, 1508, 1587, 1508, 1482, 1442, 1396, 1297, 1271, 1247, 1213, 1153, 954, 858, 805, 753. ^{1}H NMR (DMSO-d_6, 600 MHz) δ 5.85 (s, 1H), [6.67−6.72 (m, 2H), 6.50–7.10(b, 2H for NH_2 merged along with these two aromatic protons)], 7.22 (t, J = 8.1 Hz, 1H), 7.29 (d, J = 5.4 Hz, 1H), 7.46–7.49 (m, 2H), 7.57 (d, J = 7.8 Hz, 1H), 7.69 (d, J = 6.6 Hz, 1H), 7.77−7.81 (m, 2H), 7.85 (d, J = 7.8 Hz, 1H), 8.50 (d, J = 4.8 Hz, 1H), 8.59 (d, J = 4.4 Hz, 1H). ^{13}C NMR (DMSO-d_6, 150 MHz) δ 160.08, 159.49, 155.71, 149.81, 148.66, 148.22, 146.16, 136.99, 136.57, 132.84, 127.23, 125.44, 123.36, 121.26, 121.13, 117.01, 115.05, 114.10, 75.17. HR-MS (ESI) calcd. for $C_{19}H_{17}N_6O$ ($M+H^+$) 345.1458, found 345.1457.

N-[2-(4-Oxo-2-quinolin-2-yl-1,4-dihydro-2*H*-quinazolin-3-yl)-pyridine-2-carboximidine (1px)

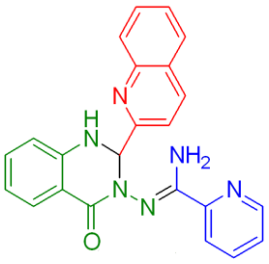

White solid; yield 414 mg, 65%. Mp 222−223 °C. IR (KBr, cm^{-1}) 3419, 3345, 3208, 1669, 1631, 1581, 1550, 1518, 1474, 1452, 1431, 1375, 1320, 1303, 1260, 1176, 1114, 1061, 1017, 911, 854, 753. ^{1}H NMR (DMSO-d_6, 600 MHz) δ 6.13 (d, J = 1.2 Hz, 1H), 6.71−6.74 (m, 2H), 6.75–7.10 (bs, 2H for NH_2), 7.24 (t, J = 8.4 Hz, 1H), 7.41 (t, J = 6.0 Hz, 1H), 7.51 (s, 1H),7.58 (t, J = 7.2 Hz, 1H), 7.73−7.75 (m, 4H), 7.83 (d, J = 8.4 Hz, 1H), 7.92 (d, J = 8.4 Hz, 1H), 8.01 (d, J = 8.4 Hz, 1H), 8.34 (d, J = 8.4 Hz, 1H), 8.54 (d, J = 4.8 Hz, 1H). ^{13}C NMR (DMSO-d_6, 150 MHz) δ 160.35, 160.02, 156.20, 149.79, 148.31, 146.48, 146.36, 137.06, 136.78, 133.16, 129.83, 128.79, 127.92, 127.66, 127.49, 126.84, 125.54, 121.30, 119.22, 117.39, 114.91, 114.21, 76.40. HR-MS (ESI) calcd. for $C_{23}H_{19}N_6O$ ($M+H^+$) 395.1615, found 395.1614.

N-[2-(2-Hydroxy-phenyl)-4-oxo-1,4-dihydro-2*H*-quinazolin-3-yl]-4-phenyl-pyridine-2-carboximidine (2bx)

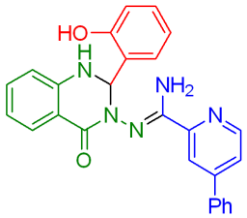

White solid; yield 479 mg, 72%. Mp 240−242 ° C. IR (KBr, cm^{-1}) 3436, 3339, 3302, 3302, 1643, 1621, 1581, 1563, 1543, 1499, 1485, 1460, 1435, 1410, 1373, 1357, 1333, 1311, 1284, 1244, 1158, 1102, 1067. ^{1}H NMR (DMSO-d_6, 600 MHz) δ 6.27 (s, 1H), [6.71 (q, J = 6.8 Hz, 2H), 6.81 (t, J = 9.6 Hz, 2H), 6.40–7.00 (bs, 2H for NH_2 merged along with these two aromatic protons)], 7.05– 7.09 (m, 2H), 7.25 (t, J = 7.5, 1H), 7.42 (d, J = 7.2 Hz, 1H), 7.50 (t, J = 7.2 Hz, 1H), 7.55 (t, J = 7.5 Hz, 2H), 7.70 (t, J = 7.8 Hz, 3H), 7.81(d, J = 5.4 Hz, 1H), 8.06 (s, 1H), 8.64 (d, J = 4.8 Hz, 1H), 9.96 (s, 1H). ^{13}C NMR (DMSO-d_6, 150 MHz) δ 160.83, 155.58, 155.20, 150.93, 149.07, 147.90, 147.07, 136.85, 132.93, 129.56, 129.40, 129.09, 127.77, 127.44, 126.94, 126.81, 126.42, 122.87, 118.56, 117.06, 115.56, 115.00, 114.30, 68.96. HR-MS (ESI) calcd. for $C_{26}H_{22}N_5O_2$ ($M+H^+$) 436.1768, found 436.1774.

N-[2-(1*H*-Imidazolyl-2-yl)-4-oxo-1,4-dihydro-2*H*-quinazolin-3-yl]-4-phenyl-pyridine-2-carboximidine (2nx)

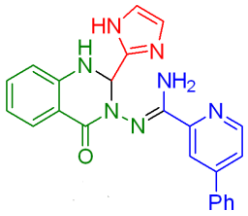

White solid; yield 430 mg, 70%. Mp 260−262 °C. IR (KBr, cm^{-1}): 3455, 3338, 3196, 1668, 1622, 1590, 1551, 1521, 1482, 1450, 1376, 1351, 1298, 1154, 1091. ^{1}H NMR (DMSO-d_6, 600 MHz) δ 6.01 (s, 1H), [6.71 (t, J = 7.5 Hz, 1H), 6.75 (d, J = 6.6 Hz, 1H), 6.50–6.80 (b, 2H for NH_2 merged along with these two aromatic protons)], 7.05 (s, 1H), 7.25 (t, J = 7.5 Hz, 1H), 7.37(s, 1H), 7.50(t, J = 7.5 Hz, 1H), 7.55 (t, J = 7.5 Hz, 2H), 7.62 (d, J = 7.2 Hz, 1H), 7.77 (d, J = 7.2 Hz, 2H), 7.82 (d, J = 4.8 Hz, 1H), 8.23 (s, 1H), 8.64 (d, J = 4.8 Hz, 1H), 12.06 (s, 1H). ^{13}C NMR (DMSO-d_6, 150 MHz) δ 159.72, 156.59, 150.76, 149.00, 147.89, 146.63, 146.50, 136.84, 132.93, 129.57, 129.37, 127.40, 126.97, 126.88, 122.93, 118.77, 117.38, 117.02, 115.06, 114.34, 69.13. HR-MS (ESI) calcd. for $C_{23}H_{20}N_7O$ ($M+H^+$) 410.1724, found 410.1723.

N-[2-(4-Oxo-2-phenyl-1,4-dihydro-2*H*-quinazolin-3-yl]-pyrazdine-2-carboximidine (3ax)

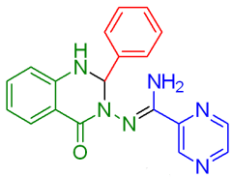

White solid; yield 481 mg, 79%. Mp 216−218 °C. IR (KBr, cm^{-1}) 3428, 3374, 1652, 1603, 1565, 1490, 1449, 1399, 1325, 1288, 1253, 1195, 1150, 1073, 1018, 958, 834, 792, 749. ^{1}H NMR (DMSO-d_6, 400 MHz) δ 6.20 (s, 1H), 6.75 (dd, J = 13.0, 7.6 Hz, 2H), 7.06 (s, 2H), 7.27 (t, J = 7.5 Hz, 1H), 7.58 (dd, J = 15.1, 7.4 Hz, 2H), 7.76 (t, J = 7.7 Hz, 2H), 7.90 (dd, J_1 = 22.2 Hz and J_2 = 8.2 Hz, 2H), 8.03 (d, J = 8.3 Hz, 1H), 8.63 (d, J = 14.8 Hz, 2H), 8.88 (s, 1H). ^{13}C NMR (DMSO-d_6, 100 MHz) δ 160.16, 159.81, 146.40, 146.33, 145.90, 145.48, 143.09, 142.85, 136.66, 133.08, 128.69, 127.80, 127.53, 127.42, 126.72, 117.23, 114.66, 114.08, 76.49. HR-MS (ESI) calcd. for $C_{19}H_{17}N_6O$ ($M+H^+$) 345.1458, found 345.1466.

N-[2-(2-Hydroxy-phenyl)-4-oxo-1,4-dihydro-2*H*-quinazolin-3-yl]-pyrazdine-2-carboximidine (3bx)

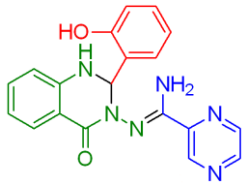

White solid; yield 481 mg, 89%. Mp 257−259 °C. IR (KBr, cm^{-1}) 3428, 3355, 1660, 1494, 1411, 1322, 1285, 1267, 1240, 1203, 1160, 1110. ^{1}H NMR (DMSO-d_6, 600 MHz) δ 6.30 (s, 1H), 6.72 (q, *J* = 7.1 Hz, 2H), [6.82 (d, *J* = 7.8 Hz, 1H), 6.85 (d, *J* = 7.8 Hz, 1H), 6.80–7.00 (b, 2H for NH_2 merged along with these two aromatic protons)], 7.09 (m, 2H), 7.24 (t, *J* = 7.5 Hz, 1H), 7.44 (d, *J* = 7.2 Hz, 1H), 7.73 (d, *J* = 7.2 Hz, 1H), 8.64 (s, 1H), 8.70 (s, 1H), 8.98 (s, 1H), 9.84 (s, 1H); ^{13}C NMR (DMSO-d_6, 150 MHz) δ 161.51, 155.71, 154.94, 147.65, 146.54, 146.41, 143.80, 143.73, 133.59, 129.71, 128.33, 128.08, 126.90, 119.18, 117.65, 116.07, 115.45, 114.95, 69.53. HR-MS (ESI) calcd. for $C_{19}H_{17}N_6O_2$ ($M+H^+$) 361.1408, found 361.1424.

N-[2-(4-Hydroxy-phenyl)-4-oxo-1,4-dihydro-2*H*-quinazolin-3-yl]-pyrazdine-2-carboximidine (3cx)

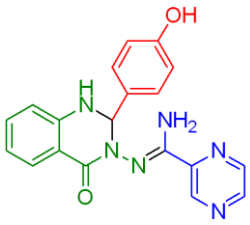

White solid; yield 465 mg, 86%. Mp 262−263 °C. IR (KBr, cm^{-1}) 3400, 1655, 1624, 1510, 1458, 1377, 1355, 1291, 1258, 1174, 1051, 1018, 959, 854, 783, 753. ^{1}H NMR (DMSO-d_6, 600 MHz) δ 5.91 (s, 1H), 6.50–6.88 (m, 6H), 7.21 (s, 1H), 7.25 (t, *J* = 7.5 Hz, 1H), 7.39 (d, *J* = 8.4 Hz, 2H), 7.67 (d, *J* = 7.6 Hz, 1H), 8.62 (s, 1H), 8.69 (d, *J* = 2.3 Hz, 1H), 8.93 (s, 1H), 9.37 (s, 1H). ^{13}C NMR (DMSO-d_6, 150 MHz) δ 161.24, 158.03, 154.79, 147.73, 146.48, 146.45, 143.76, 143.67, 133.61, 131.58, 129.45, 128.13, 117.65, 115.39, 115.14, 114.75, 75.24. HR-MS (ESI) calcd. for $C_{19}H_{17}N_6O_2$ ($M+H^+$) 361.1408, found 361.1404.

N-[2-(4-Methoxy-phenyl)-4-oxo-1,4-dihydro-2*H*-quinazolin-3-yl]-pyrazdine-2-carboximidine (3dx)

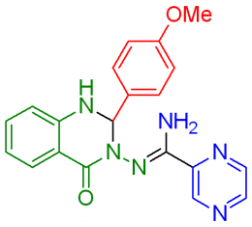

White solid; yield 482 mg, 85%. Mp 232−234 °C. IR (KBr, cm^{-1}) 3452, 3317, 3278, 1659, 1610, 1581, 1508, 1483, 1365, 1293, 1246, 1171, 1029, 955, 909, 856, 836, 797, 756. ^{1}H NMR (DMSO-d_6, 400 MHz) δ 3.69 (s, 3H), 5.98 (s, 1H), 6.45–7.09 (m, 6H), 7.14–7.41 (m, 2H), 7.53 (d, *J* = 7.9 Hz, 2H), 7.69 (d, *J* = 7.7 Hz, 1H), 8.68 (d, *J* = 26.2 Hz, 2H), 8.98 (s, 1H). ^{13}C NMR (DMSO-d_6,100 MHz) δ 160.51, 159.15, 154.11, 146.91, 145.82, 145.70, 143.08, 142.97, 132.96, 132.69, 128.70, 127.45, 117.03, 114.76, 114.10, 113.14, 74.27, 55.00. HR-MS (ESI) calcd. for $C_{20}H_{19}N_6O_2$ ($M+H^+$) 375.1464, found 375.1566.

N-[2-(2-Chloro-phenyl)-4-oxo-1,4-dihydro-2H-quinazolin-3-yl]-pyrazine-2-carboximidine (3ex)

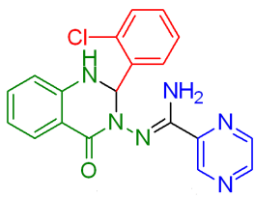

White solid; yield 465 mg, 82%. Mp 231−233 °C. IR (KBr, cm^{-1}) 3457, 3432, 3373, 1662, 1524, 1503, 1468, 1446, 1409, 1370, 1325, 1292, 1256, 1206, 1154, 1042, 1018, 959, 859, 828, 797, 761. ^{1}H NMR (600 MHz, DMSO-d_6): δ 6.47 (s, 1H), 6.74 (q, *J* = 5.2 Hz, 2H), 6.88 (bs, 2H for NH_2), 7.27–7.29 (m, 4H), 7.41–7.42 (m, 1H), 7.72 (d, *J* = 5.2 Hz, 1H), 7.81–7.82 (m, 1H), 8.62 (s, 1H), 8.68 (d, *J* = 2.5 Hz, 1H), 8.88 (s, 1H). ^{13}C NMR (100 MHz, DMSO-d_6) δ 160.90, 154.98, 146.96, 146.35, 145.96, 143.64, 143.56, 143.36, 133.59, 133.02, 130.19, 128.65, 127.92, 127.77, 126.60, 117.81, 115.19, 114.65, 74.28. HR-MS (ESI) calcd. for $C_{19}H_{16}N_6O^{35}Cl$ ($M+H^+$) 379.1069, found 379.1077.

N-[2-(2-Bromo-phenyl)-4-oxo-1,4-dihydro-2H-quinazolin-3-yl]-pyrazine-2-carboximidine (3fx)

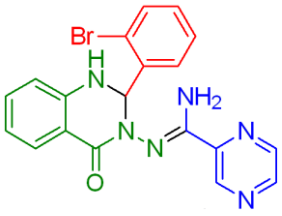

White solid; yield 519 mg, 82%. Mp 258−260 °C. IR (KBr, cm^{-1}) 3366, 3299, 3204, 1662, 1638, 1613, 1525, 1486, 1463, 1442, 1429, 1387, 1341, 1322, 1284, 1258, 1241, 1213, 1153, 1115, 1021, 961, 851, 839, 757. ^{1}H NMR (DMSO-d_6, 600 MHz) δ 6.48 (s, 1H), 6.77 (q, J = 8.0 Hz, 2H), 6.87 (bs, 2H for NH_2), 7.21 (t, J = 7.5 Hz, 1H), 7.30−7.34 (m, 3H), 7.59 (d, J = 8.4 Hz, 1H), 7.73 (d, J = 7.2 Hz, 1H), 7.86 (d, J = 8.4 Hz, 1H), 8.61 (s, 1H), 8.69 (d, 2.4, 1H), 8.92 (s, 1H). ^{13}C NMR (DMSO-d_6, 150 MHz) δ 160.80, 154.82, 146.71, 145.93, 145.60, 143.16, 142.99, 138.99, 133.29, 132.27, 130.39, 129.43, 127.70, 127.57, 123.15, 117.46, 114.39, 114.22, 73.76. HR-MS (ESI) calcd. for $C_{19}H_{16}N_6O^{79}Br$ ($M+H^+$) 423.0563, found 423.0565.

N-[2-(3-Fluoro-phenyl)-4-oxo-1,4-dihydro-2*H*-quinazolin-3-yl]-pyrazine-2-carboximidine (3gx)

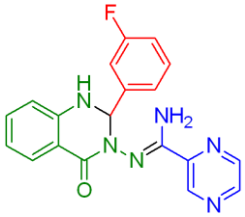

White solid; yield 402 mg, 74%. Mp 270−272 °C. IR (KBr, cm^{-1}) 3430, 3385, 1651, 1608, 1571, 1525, 1494, 1445, 1398, 1371, 1330, 1291, 1263, 1242, 1229, 1173, 1153, 1019, 959, 862, 776. ^{1}H NMR (DMSO-d_6, 600 MHz) δ 6.03 (s, 1H), [6.73−6.78 (m, 2H), 6.85 (bs, 2H for NH_2 merged along with these two aromatic protons)], 7.11 (s, 1H), 7.28−7.44 (m, 4H), 7.55 (s, 1H) 7.68 (d, J = 7.6 Hz, 1H), 8.65 (s, 1H), 8.72 (d, J = 2.5 Hz, 1H), 8.98 (s, 1H). ^{13}C NMR (DMSO-d_6, 150 MHz) δ 160.43, 154.52, 146.59, 145.94, 145.60, 143.64, 143.16, 142.92, 133.14, 129.83, 127.47, 123.62, 117.35, 115.18, 115.04, 114.78, 114.20, 114.04, 73.88. HR-MS (ESI) calcd. for $C_{19}H_{16}N_6OF$ ($M+H^+$) 363.1364, found 363.1360.

N-[2-(3-Chloro-phenyl)-4-oxo-1,4-dihydro-2*H*-quinazolin-3-yl]-pyrazine-2-carboximidine (3hx)

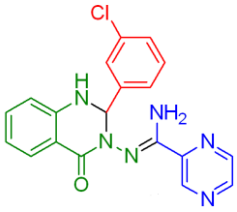

White solid; yield 454 mg, 80%. Mp 220−222 °C. IR (KBr, cm^{-1}) 3422, 3396, 1653, 1610, 1524, 1489, 1428, 1393, 1326, 1290, 1254, 1195, 1171, 1154, 1071, 1154, 1017, 956, 857, 804. ^{1}H NMR (DMSO-d_6, 600 MHz) δ 6.03 (s, 1H), 6.72−6.77 (m, 2H), 6.87 (bs, 2H for NH_2), 7.27–7.41 (m, 4H), 7.55 (d, J = 6.6 Hz, 1H), 7.68 (d, J = 11.4 Hz, 2H), 8.65 (s, 1H), 8.72 (s, 1H), 8.98 (s, 1H). ^{13}C NMR (DMSO-d_6, 150 MHz) δ 160.47, 154.57, 146.59, 146.00, 145.63, 143.26, 143.22, 142.97, 133.21, 132.60, 129.81, 128.26, 127.53, 127.38, 126.22, 117.42, 114.81, 114.26, 73.88. HR-MS (ESI) calcd. for $C_{19}H_{16}N_6O^{35}Cl$ ($M+H^+$) 379.1069, found 379.1072.

N-[2-(3-Bromo-phenyl)-4-oxo-1,4-dihydro-2*H*-quinazolin-3-yl]-pyrazine-2-carboximidine (3ix)

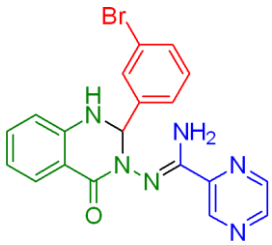

White solid; yield 494 mg, 78%. Mp 235−237 °C. IR (KBr, cm^{-1}) 3477, 3314, 1650, 1626, 1557, 1506, 1480, 1432, 1364, 1294, 1276, 1227, 1199, 1165, 1017, 955, 855, 783, 753. ^{1}H NMR (DMSO-d_6, 600 MHz) δ 6.08 (s,1H), 6.74 (t, J = 7.3 Hz, 1H), 6.82 (d, J = 7.5 Hz, 1H), 6.94 (bs, 2H for NH_2), 7.28 (t, J = 7.5 Hz, 2H), 7.45 (s, 2H), 7.64 (d, J = 6.8 Hz, 1H), 7.73 (d, J = 7.2 Hz, 1H), 7.87 (s, 1H), 8.61 (s, 1H), 8.69 (s, 1H), 9.06 (s, 1H). ^{13}C NMR (DMSO-d_6, 150 MHz) δ 160.35, 154.45, 146.52, 145.93, 145.60, 143.15, 142.91, 133.11, 131.06, 130.25, 130.05, 127.46, 126.50, 121.11, 117.31, 114.76, 114.17, 73.77. HR-MS (ESI) calcd. for $C_{19}H_{16}N_6O^{79}Br$ ($M+H^+$) 423.0563, found 423.0552.

N-[2-(4-Fluoro-phenyl)-4-oxo-1,4-dihydro-2*H*-quinazolin-3-yl]-pyrazine-2-carboximidine (3jx)

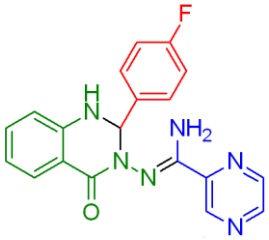

White solid; yield 402 mg, 74%. Mp 227−229 °C. IR (KBr, cm^{-1}) 3476, 3341, 3310, 3064, 1665, 1642, 1558, 1506, 1482, 1436, 1372, 1351, 1290, 1261, 1221, 1159, 1097, 950, 862, 841, 790, 755. ^{1}H NMR (DMSO-d_6, 600 MHz) δ 6.03 (s, 1H), 6.70−6.75 (m, 2H), 6.77 (bs, 2H for NH_2 merged with aromatic protons), 6.80 (s, 1H), 7.14 (t, J = 8.8 Hz, 2H), 7.23 – 7.28 (m, 1H), 7.33 (s, 1H), 7.64 (dd, J_1 = 8.5 Hz and J_2 = 5.7 Hz, 2H), 7.67 (d, J = 7.5Hz, 1H), 8.63 (dd, J_1 = 2.3 Hz and J_2 = 1.6 Hz, 1H), 8.70 (d, J = 2.5 Hz, 1H), 8.94 (s, 1H). ^{13}C NMR (DMSO-d_6, 100 MHz) δ 163.17, 160.74, 160.50, 154.39, 146.78, 145.90, 145.62, 143.12, 142.93, 136.95, 136.92, 133.08, 129.65, 129.57, 127.49, 117.24, 114.76, 114.73, 114.52, 114.15, 74.00. HR-MS (ESI) calcd. for $C_{19}H_{16}N_6OF$ ($M+H^+$) 363.1364,

N-[2-(4-Chloro-phenyl)-4-oxo-1,4-dihydro-2*H*-quinazolin-3-yl]-pyrazine-2-carboximidine (3kx)

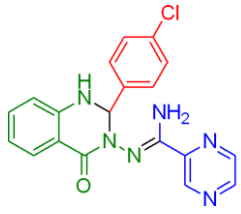

White solid; yield 471 mg, 83%. Mp 240−242 ° C. IR (KBr, cm^{-1}) 3466, 3289, 1661, 1571, 1511, 1483, 1438, 1412, 1375, 1328, 1293, 1259, 1227, 1157, 1087. ^{1}H NMR (DMSO-d_6, 600 MHz) δ 6.02 (s, 1H), 6.70−6.75 (m, 2H), 6.84 (bs, 2H for NH_2), 7.25–7.29 (m, 1H), 7.37 (m, 3H), 7.61−7.68 (m, 3H), 7.68 (d, J = 7.7 Hz, 1H), 8.64−8.70 (m, 2H), 8.96 (s, 1H). ^{13}C NMR (150 MHz, DMSO-d_6) δ 161.11, 155.09, 147.33, 146.61, 146.26, 143.83, 143.61, 140.43, 133.77, 133.44, 130.04, 128.55, 128.15, 117.95, 115.44, 114.84, 74.53. HR-MS (ESI) calcd. for $C_{19}H_{16}N_6O^{35}Cl$ ($M+H^+$) 379.1069, found 379.1075.

N-[2-(4-Bromo-phenyl)-4-oxo-1,4-dihydro-2*H*-quinazolin-3-yl]-pyrazine-2-carboximidine (3lx)

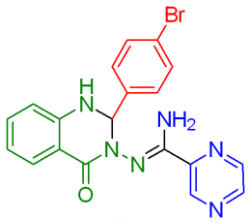

White solid; yield 519 mg, 82%. Mp 270−272 °C. IR (KBr, cm^{-1}) 3462, 3294, 1649, 1626, 1568, 1508, 1483, 1435, 1409, 1367, 1328, 1292, 1225, 1156. ^{1}H NMR (600 M MHz, DMSO-d_6) δ 5.96 (s, 1H), [6.74−6.79 (m, 2H), 6.45–6.95 (b, 2H for NH_2 merged along with these two aromatic protons)], 7.24 (d, *J* = 7.6 Hz, 1H), 7.34–7.37 (m, 3H), 7.47 (d, *J* = 6.0 Hz, 1H), 7.58 (d, *J* = 7.8 Hz, 2H), 7.67 (d, *J* = 7.8 Hz, 1H), 7.82 (t, *J* = 7.2 Hz, 1H), 7.86 (d, *J* = 7.8 Hz, 1H), 8.56 (d, *J* = 4.8 Hz, 1H). ^{13}C NMR (DMSO-d_6, 100 MHz) δ 161.07, 155.02, 147.03, 146.29, 145.87, 143.48, 143.37, 140.42, 133.59, 131.21, 130.06, 127.92, 121.92, 117.83, 115.17, 114.62, 74.47. HR-MS (ESI) calcd. for $C_{19}H_{16}N_6O^{79}Br$ ($M+H^+$) 423.0563, found 423.0571.

N-[2-(4-Nitro-phenyl)-4-oxo-1,4-dihydro-2*H*-quinazolin-3-yl]-pyrazine-2-carboximidine (3mx)

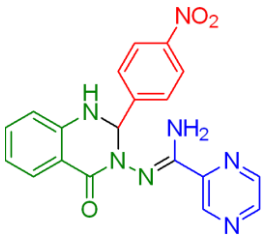

White solid; yield 356 mg, 61%. Mp 271−273 °C. IR (KBr, cm^{-1}) 3502, 3391, 3334, 3259, 1665, 1565, 1524, 1484, 1442, 1423, 1371, 1286, 1259, 1229, 1156, 1102, 1070. ^{1}H NMR (DMSO-d_6, 600 MHz) δ 6.10 (s, 1H), 6.50–7.05 (m, 4H), 7.23–7.30 (m, 1H), 7.44–7.55 (m, 2H), 7.69 (d, *J* = 7.7 Hz, 1H), 7.78–7.92 (m, 4H), 8.18 (d, *J* = 8.7 Hz, 2H), 8.56 (d, *J* = 4.3 Hz, 1H). ^{13}C NMR (DMSO-d_6, 100 MHz) δ 160.35, 154.45, 146.52, 145.93, 143.44, 143.15, 142.91, 133.11, 131.06, 130.25, 130.05, 127.46, 126.50, 121.11, 117.31, 114.76, 114.17, 73.77. HR-MS (ESI) calcd. for $C_{19}H_{16}N_7O_3$ ($M+H^+$) 390.1309, found 390.1299.

N-[2-(1*H*-Imidazolyl-2-yl)-4-oxo-1,4-dihydro-2*H*-quinazolin-3-yl]-pyrazine-2-carboximidine (3nx)

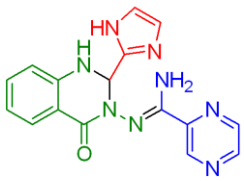

White solid; yield 426 mg, 85%. Mp 267−269 °C. IR (KBr, cm^{-1}) 3435, 3354, 1657, 1561, 1509, 1472, 1432, 1397, 1350, 1324, 1287, 1267, 1249, 1227, 1196, 1173, 1110, 1074, 1016, 959, 904, 857, 779, 759. ^{1}H NMR (DMSO-d_6, 600 MHz) δ 5.97 (s, 1H), 6.71 (t, *J* = 7.5 Hz, 1H), 6.75–6.76 (m, 2H), 7.05 (s, 1H), 7.25 (t, *J* = 7.8 Hz, 1H), 7.39 (s, 1H), 7.65 (d, *J* = 7.7 Hz, 1H), 8.67 (s, 1H), 8.74 (d, 2.4, 1H), 9.16 (s, 1H), 12.00 (s, 1H). ^{13}C NMR (DMSO-d_6, 150 MHz) δ 159.69, 156.74, 149.84, 148.28, 146.75, 146.40, 143.20, 137.05, 132.97, 127.42, 125.62, 125.38, 121.65, 117.42, 115.13, 114.37, 69.03. HR-MS (ESI) calcd. for $C_{16}H_{15}N_8O$ ($M+H^+$) 335.1363, found 335.1372.

N-[2-(4-Oxo-2-pyridin-2-yl-1,4-dihydro-2*H*-quinazolin-3-yl)-pyrazine-2-carboximidine (3ox)

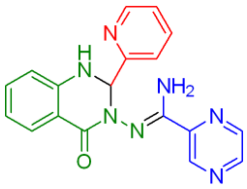

White solid; yield 450 mg, 87%. Mp 267−269 °C. IR (KBr, cm^{-1}) 3445, 3326, 3256, 1655, 1572, 1506, 1470, 1442, 1398, 1374, 1339, 1321, 1297, 1271, 1243, 1215, 1201, 1157, 1098. ^{1}H NMR (DMSO-d_6, 600 MHz) δ 5.89 (s, 1H), 6.66−6.71 (m, 2H), 6.90 (bs, 2H for NH_2), 7.21 (t, *J* =7.8 Hz, 1H), 7.29 (t, *J* = 6.3 Hz, 1H), 7.48 (s, 1H), 7.60 (d, *J* = 7.8 Hz, 1H), 7.67 (d, *J* = 6.6 Hz, 1H), 7.77 (t, *J* = 7.8 Hz, 1H), 8.49 (d, *J* = 4.8 Hz, 1H), 8.65 (s, 1H), 8.71 (d, *J* = 3.0 Hz, 1H), 8.94 (s, 1H). ^{13}C NMR (DMSO-d_6, 100 MHz) δ 160.20, 159.38, 154.57, 148.67, 146.30, 145.96, 145.54, 143.13, 143.04, 136.64, 133.00, 127.36, 123.45, 121.30, 117.13, 114.96, 114.19, 75.37. HR-MS (ESI) calcd. for $C_{18}H_{16}N_7O$ ($M+H^+$) 346.1411, found 346.1421.

N-[2-(4-Oxo-2-quinolin-2-yl-1,4-dihydro-2*H*-quinazolin-3-yl)-pyrazine-2-carboximidine (3px)

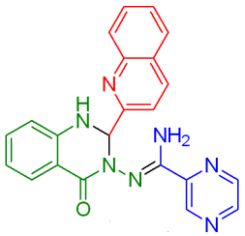

White solid; yield 421 mg, 71%. Mp 244−246 °C. IR (KBr, cm^{-1}) 3423, 3316, 3229, 3006, 2942, 1655, 1633, 1606, 1564, 1511, 1483, 1442, 1397, 1377, 1329, 1311, 1282, 1258, 1204, 1175, 1147, 1119, 1071. ^{1}H NMR (DMSO-d_6, 600 MHz) δ 6.12 (s, 1H), 6.68 (m, 2H), 7.02 (bs, 2H for NH_2), 7.21 (t, J = 7.5 Hz, 1H), 7.49 (s, 1H), 7.54 (t, J = 7.5 Hz, 1H), 7.69 (q, J = 7.4 Hz, 2H), 7.80 (d, J = 8.4 Hz, 1H), 7.87 (d, J = 8.4 Hz, 1H), 7.96 (d, J = 8.4 Hz, 1H), 8.30 (d, J = 8.4 Hz, 1H), 8.57 (s, 1H), 8.60 (s, 1H), 8.79 (s, 1H). ^{13}C NMR (DMSO-d_6, 100 MHz) δ 160.41, 159.87, 155.11, 146.52, 146.47, 145.59, 143.32, 143.00, 136.91, 129.95, 128.82, 127.99, 127.70, 127.60, 126.97, 119.33, 117.52, 114.82, 114.30, 76.58. HR-MS (ESI) calcd. for $C_{22}H_{18}N_7O$ ($M+H^+$) 396.1567, found 396.1581.

Table 4. Crystallographic and refinement parameters of compound **3kx** and **4a**.

	3kx	**4a**
chem formula	$C_{19}H_{15}N_6OCl$	$C_{13}H_{10}N_4O$
formula wt	378.81	238.25
temp (K)	296	296
crystal system	monoclinic	monoclinic
space group	$P2_1/n$	$P2_1/n$
a (Å)	8.0529(4)	12.0686(10)
b (Å)	13.5876(7)	5.4446(5)
c (Å)	16.3708(9)	16.8697(17)
α (°)	90.00	90.00
β(°)	97.133(3)	96.673(8)
γ(°)	90.00	90.00
V ($Å^3$)	1777.42(16)	1100.98(17)
Z	4	4
R_1^a, wR_2^b ($I \geq 2\sigma(I)$)	0.0506, 0.1244	0.0454, 0.0632
R_1^a, wR_2^b (all data)	0.0965, 0.1438	0.1362, 0.1508
goodness of fit (F^2)	1.023	1.010

5. 4. 3. Selected spectra

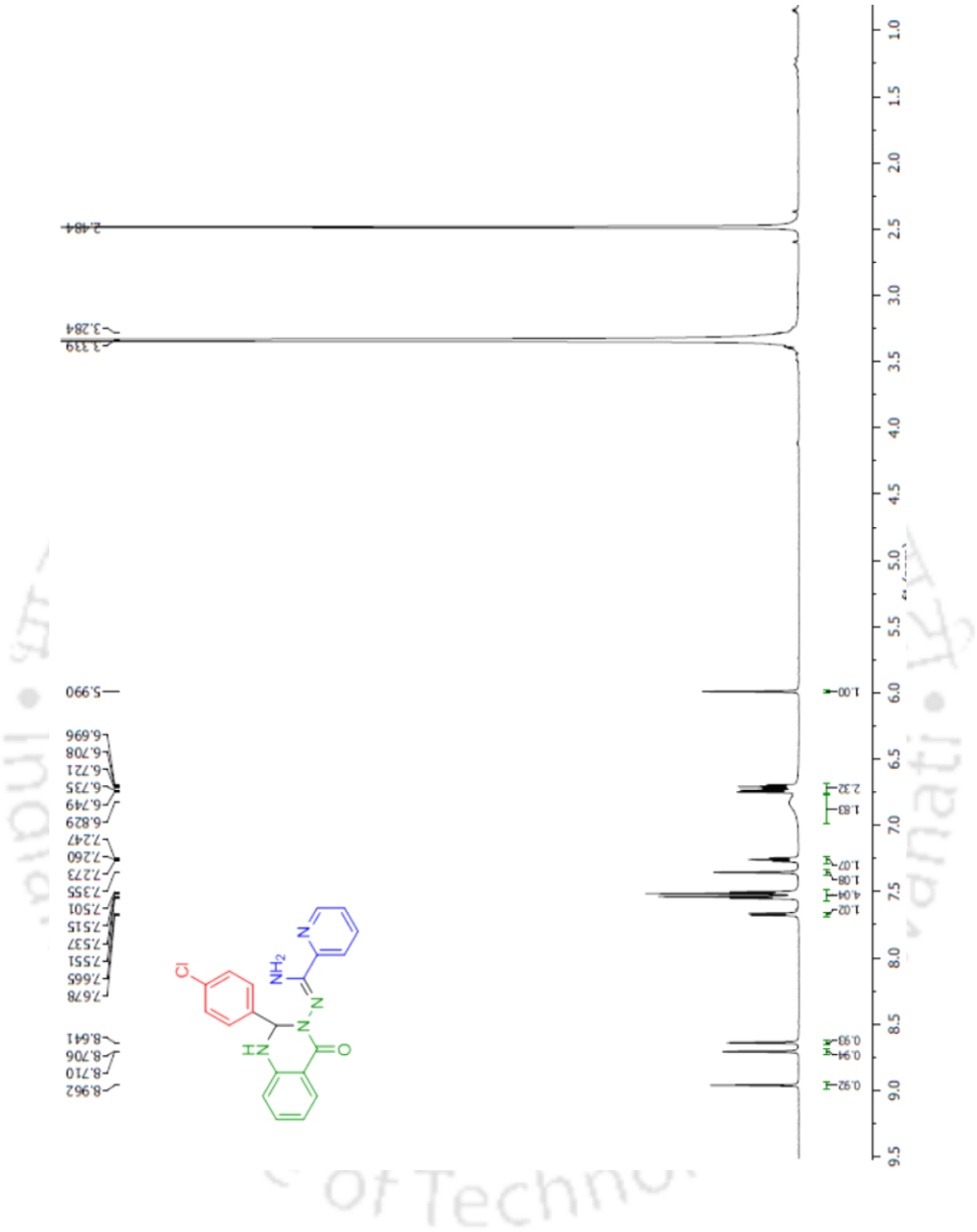

Spectrum 1. ^{1}H (600 MHz, DMSO d_6) NMR of **1kx**.

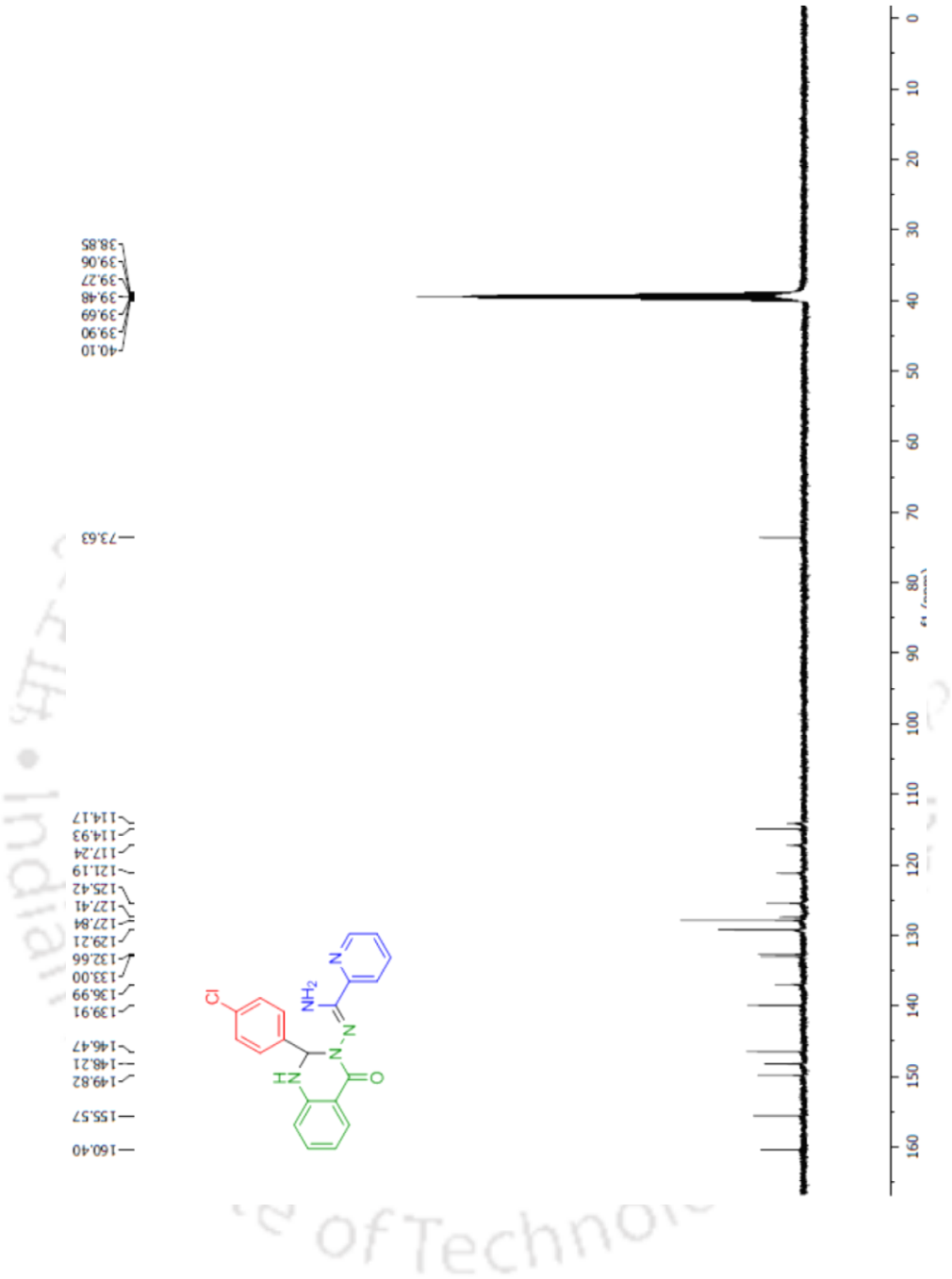

Spectrum 2. ^{13}C (100 MHz, DMSO d_6) NMR of **1kx**.

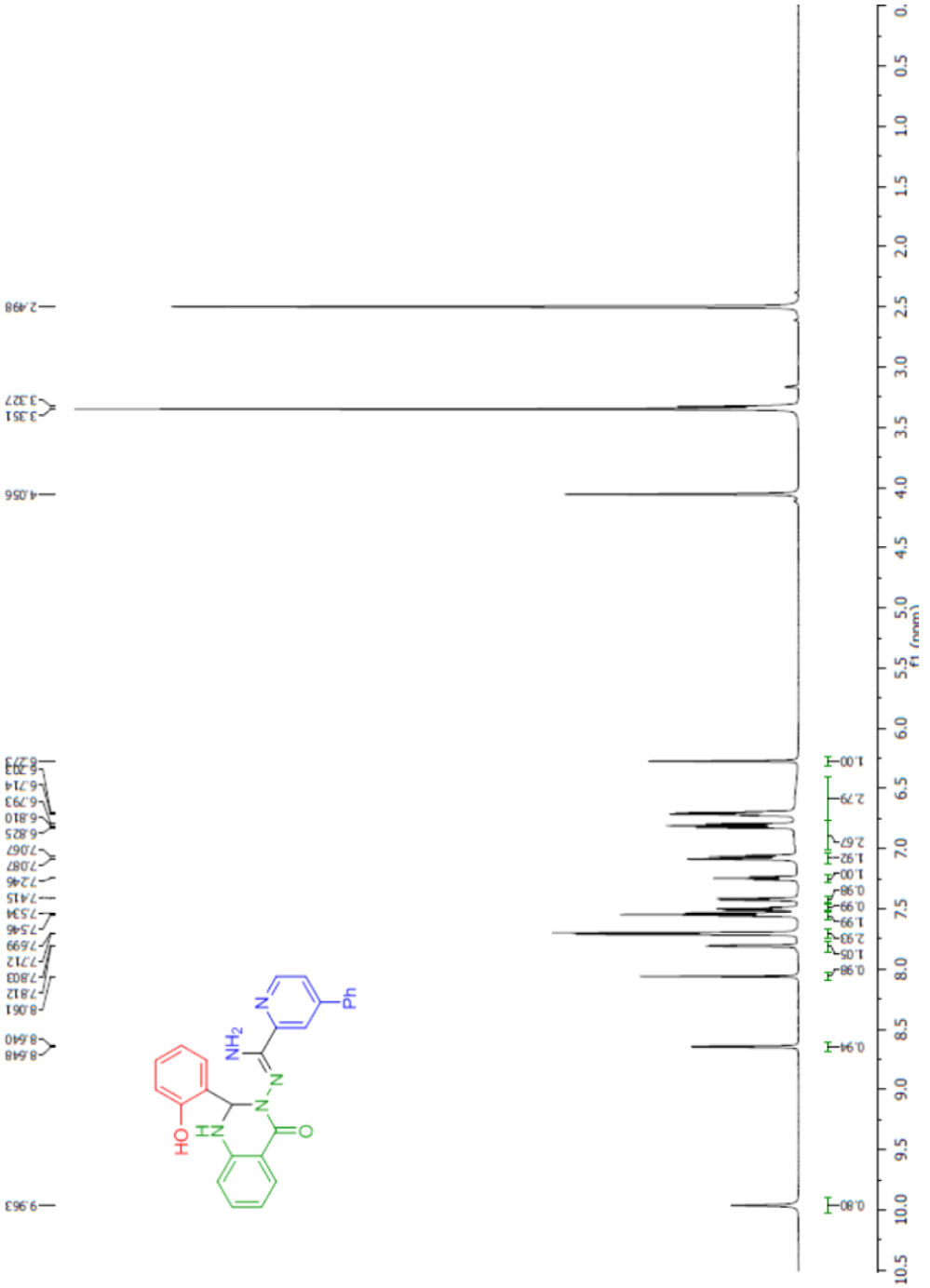

Spectrum 3. ^{1}H NMR (600 MHz, DMSO d_6) of **2bx**.

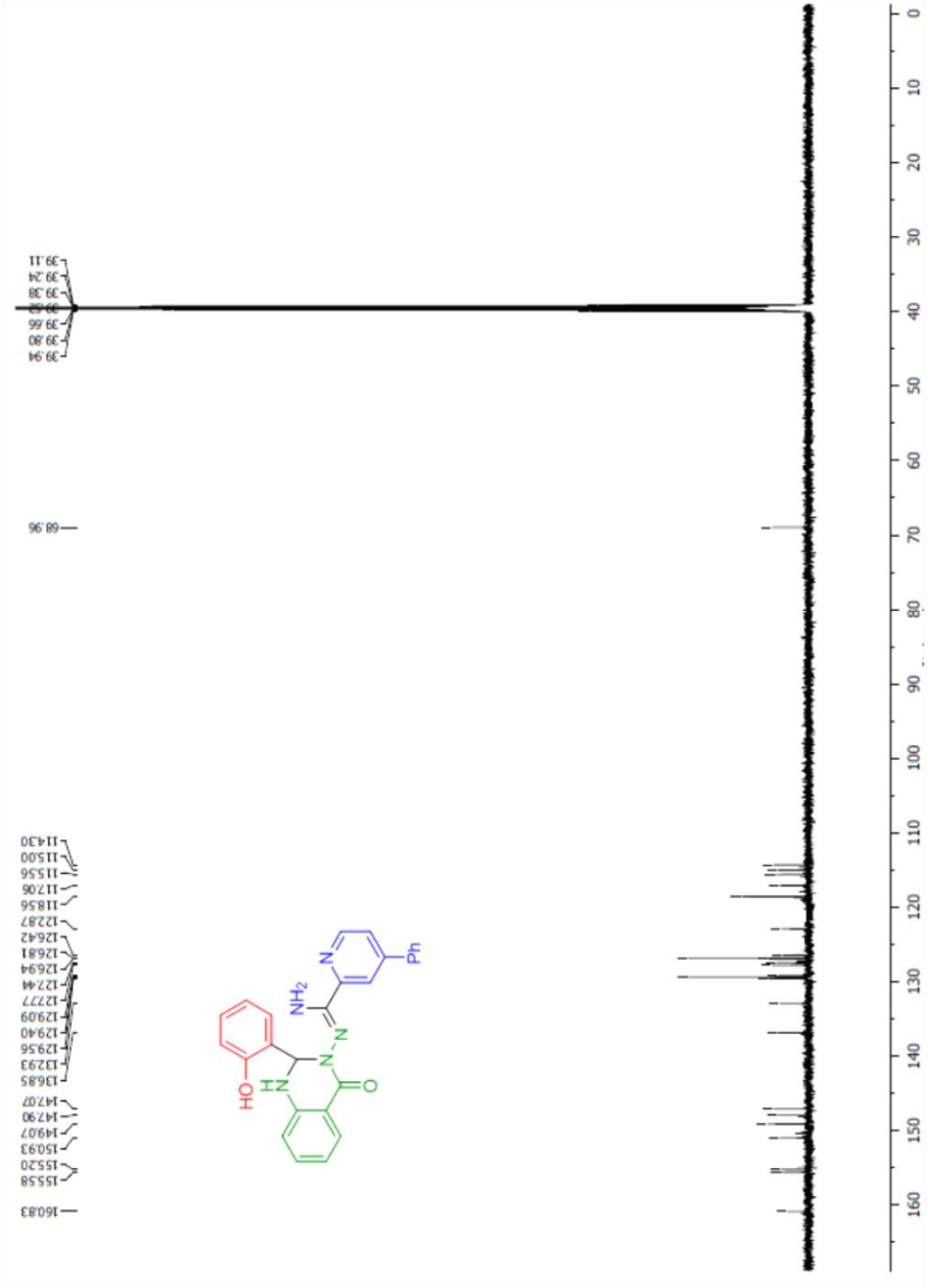

Spectrum 4. ^{13}C NMR (150 MHz, DMSO d_6) of **2bx**.

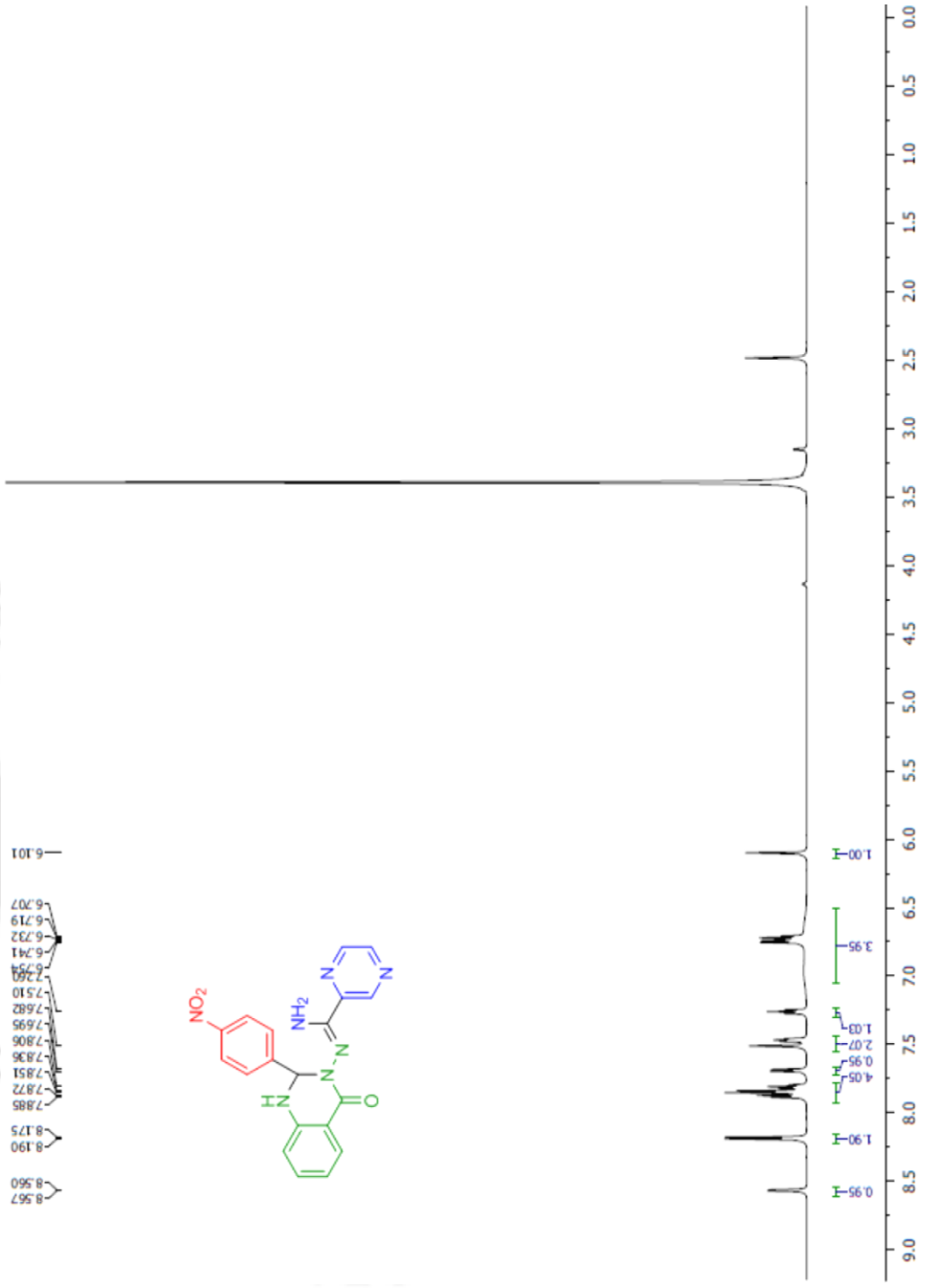

Spectrum 5. ^{1}H NMR (600 MHz, DMSO d_6) of **3mx**.

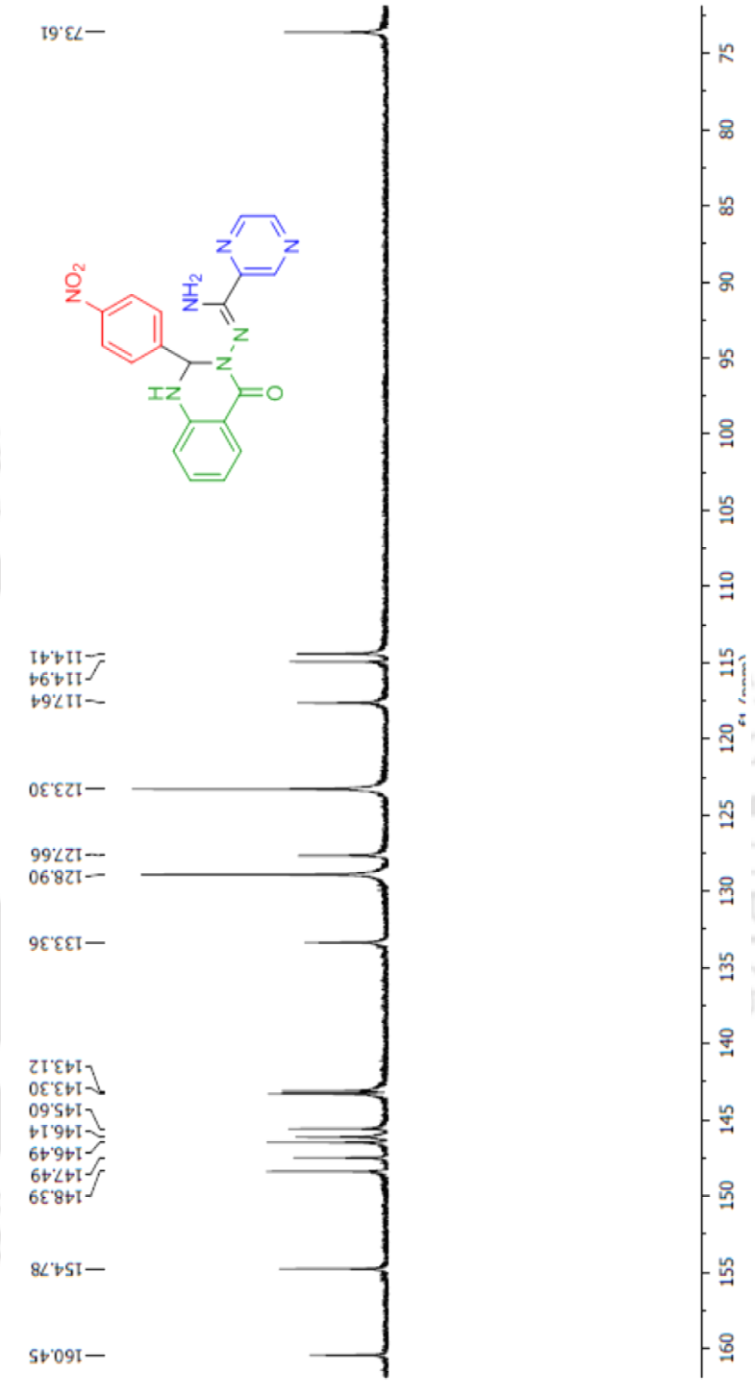

Spectrum 6. ^{13}C NMR (100 MHz, DMSO d_6) of **3mx**.

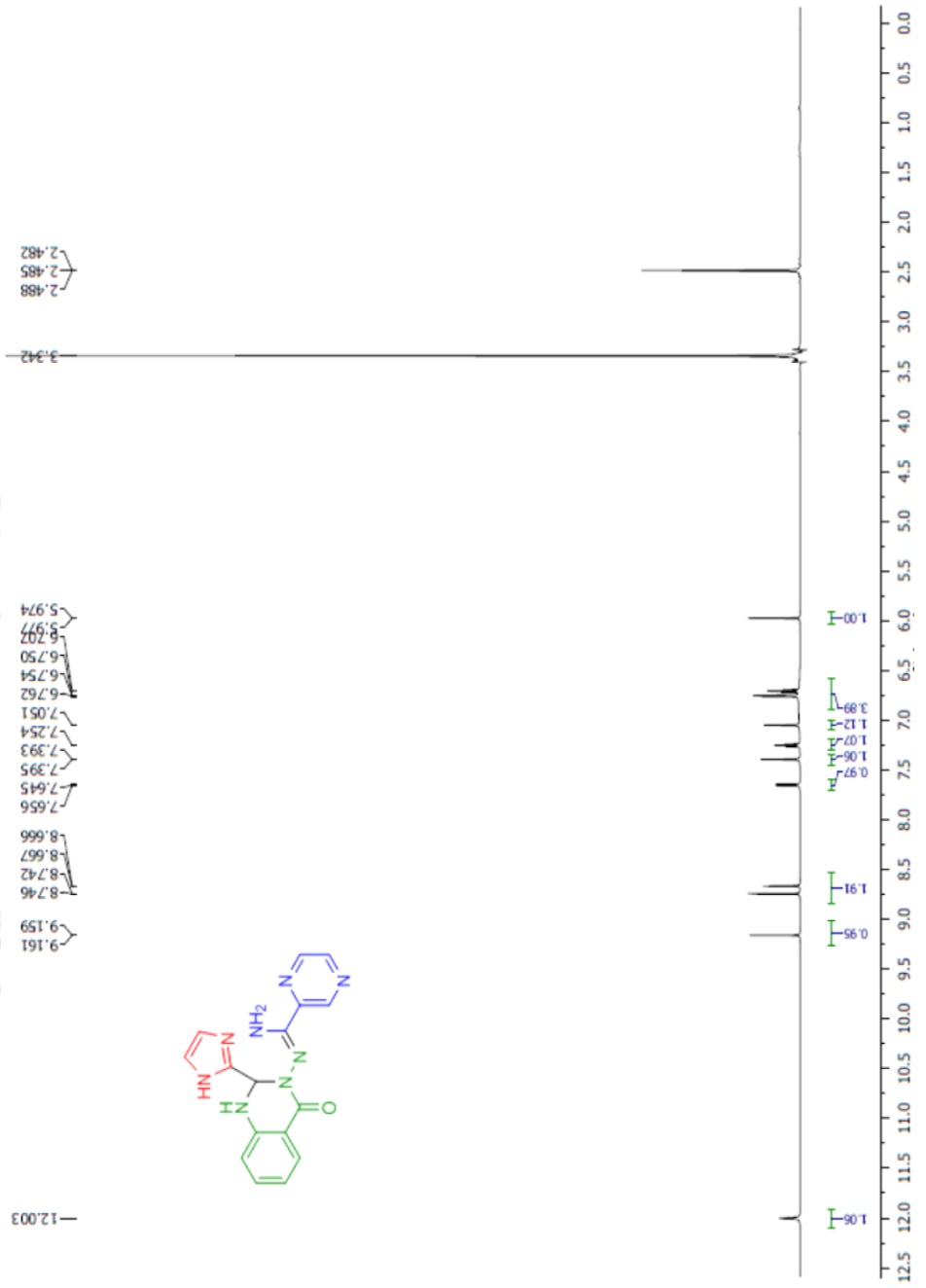

Spectrum 7. ^{1}H NMR (600 MHz, DMSO d_6) of **3nx**.

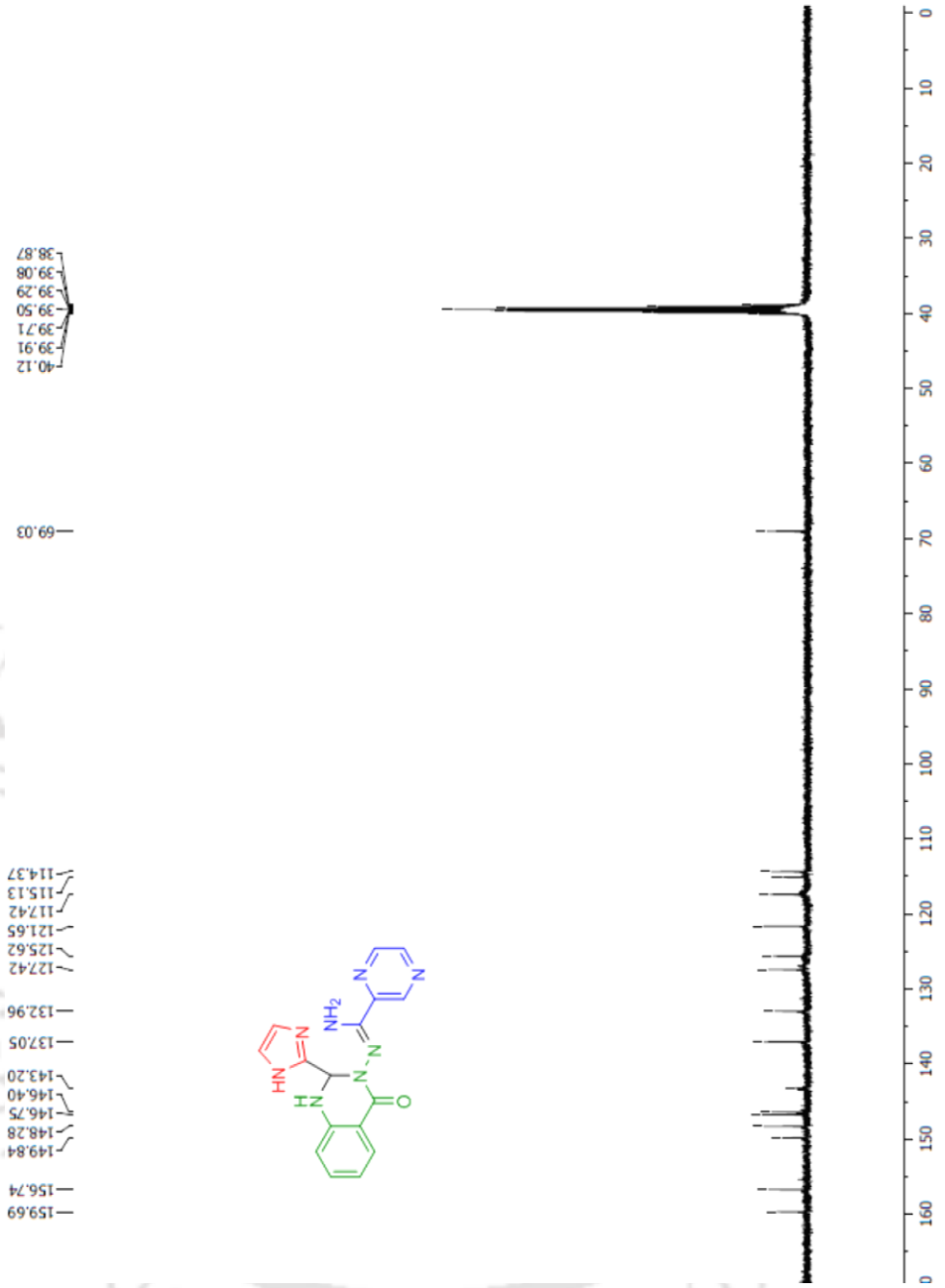

Spectrum 8. ^{13}C NMR (100 MHz, DMSO d_6) of **3nx**.

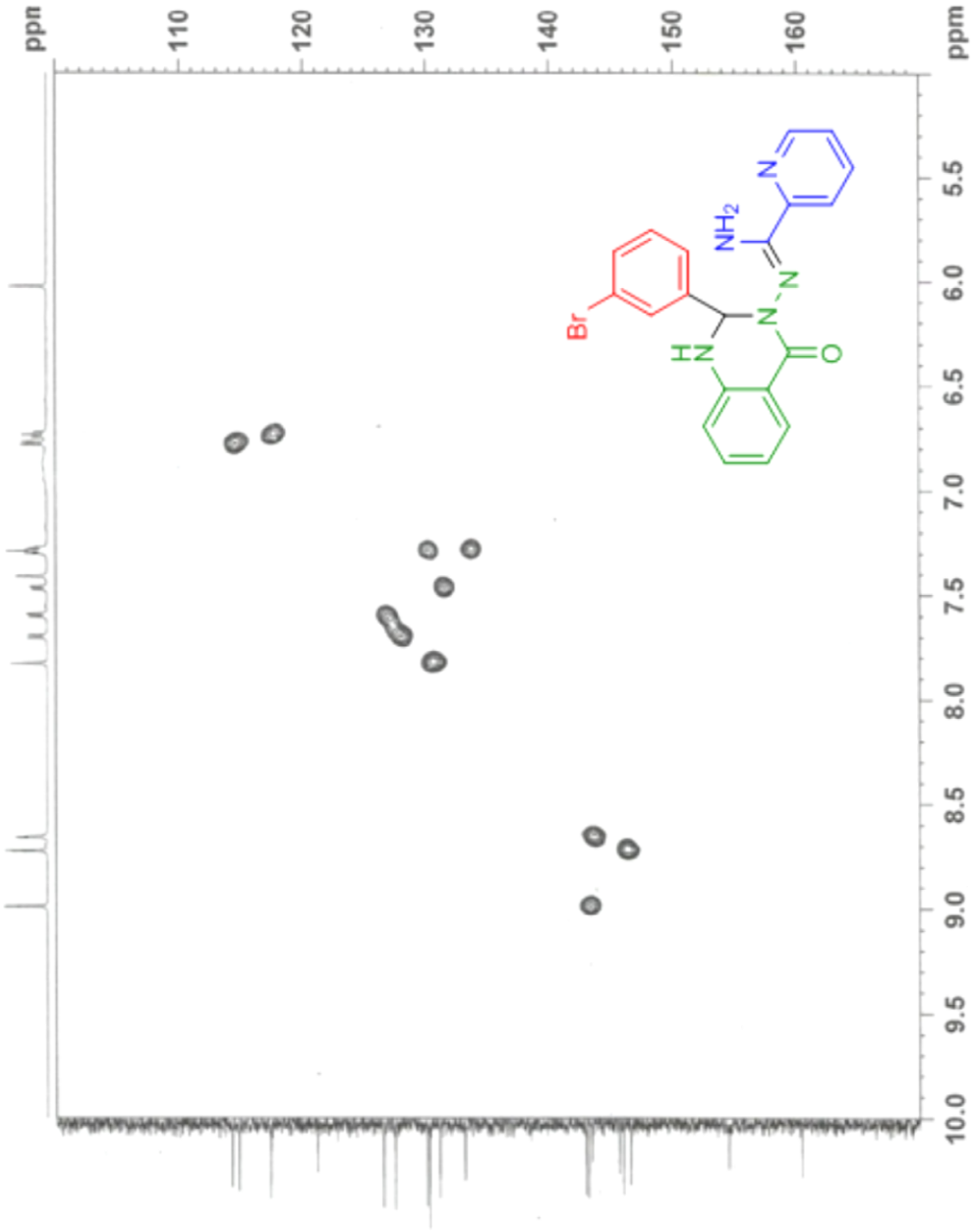

Spectrum 9. Two dimensional HMQC NMR spectrum of **3ix**.

References

[1] G. W. Rewcastle, A. R. Katritzky, C. W. Rees, E. F. V. Scriven, '*Comprehensive Heterocyclic Chemistry II*', Eds. Pergamon, Oxford, **1996**, vol. *8*, pp 120−272.

[2] (a) J. Bartroli, E. Turmo, M. Algueró, E. Boncompte, M. L. Vericat, L. Conte, J. Ramis, M. Merlos, J. G. Rafanell, J. Forn, *J. Med. Chem.* **1998**, *41*, 1869; (b) V. Bavetsias, J. H. Marriott, C. Melin, R. Kimbell, Z. S. Matusiak, F. T. Boyle, A. L. Jackman, *J. Med. Chem.* **2000**, *43*, 1910.

[3] (a) J. W. Corbett, S. S. Ko, J. D. Rodgers, L. A. Gearhart, N. A. Magnus, L. T. Bacheler, S. Diamond, S. Jeffrey, R. M. Klabe, B. C. Cordova, S. Garber, K. Logue, G. L. Trainor, P. S. Anderson, S. K. Erickson-Viitanen, *J. Med. Chem.*, **2000**, *43*, 2019; (b) B. Jiang, J. J. Dong, Y. G. Si, X. L. Zhao, Z. G. Huang, M. Xua, *Adv. Synth. Catal.* **2008**, *350*, 1360; c) N. A. Magnus, P. N. Confalone, L. Storace, *Tetrahedron Lett*. **2000**, *41*, 3015; (d) R. Ragno, A. Mai, G. Sbardella, M. Artico, S. Massa, C. Musiu, M. Mura, F. Marturana, A. Cadeddu, P. L. Colla, *J. Med. Chem.* **2004**, *47*, 928.

[4] (a) S. L. Cao, Y. P. Feng, Y. Y. Jiang, S. Y. Liu, G. Y. Ding, R. T. Li, *Bioorg. Med. Chem. Lett.* **2000**, *15*, 1915; (b) D. J. Baek, Y. K. Park, H. I. Heo, M. Lee, Z. Yang, M. Choi, *Bioorg. Med. Chem. Lett.* **1998**, *8*, 3287; (c) S. Xue, J. McKenna, W. C. Shieh, O. Repic, *J. Org. Chem.* **2004**, *69*, 6474.

[5] (a) V. Jatav, P. Mishra, S. Kashaw, J. P. Stables, *Eur. J. Med. Chem.* **2008**, *43*, 135; (b) V. Jatav, P. Mishra, S. Kashaw, J. P. Stables, *Eur. J. Med. Chem.* **2008**, *43*, 1945.

[6] (a) K. Ozaki, Y. Yamada, T. Oine, T. Ishizuka, Y. Iwasawa, *J. Med. Chem.* **1985**, *26*, 568; (b) Q. Chao, L. Deng, H. Shih, L. M. Leoni, D. Genini, D. A. Carson, H. B. Cottam, *J. Med. Chem.* **1999**, *42*, 3860; (c) R. S. Giri, H. M. Thaker, T. Giordano, J. Williams, D. Rogers, V. Sudersanam, K. K. Vasu, *Eur. J. Med. Chem.* **2009**, *44*, 2184.

[7] J. E. Stelmach, L. Liu, S. B. Patel, J. V. Pivnichny, G. Scapin, S. Singh, C. E. C. A. Hop, Z. Wang, J. R. Strauss, P. M. Cameron, E. A. Nichols, S. J. O'Keefe, E. A. O'Neill, D. M. Schmatz, C. D. Schwartz, C. M. Thompson, D. M. Zallerd, J. B. Doherty, *Bioorg. Med. Chem. Lett.* **2003**, *13*, 277.

[8] D. Dorsch, W. W. K. R. Medederski, M. Osswall, R. M. Devant, C. J. Schmitges, *Bioorg. Med. Chem. Lett.* **2009**, *17*, 275.

[9] H. J. Hess, T. H. Cronin, A. Scriabine, *J. Med. Chem.* **1969**, *42*, 130.

[10] T. R. Kleyman, J. E. Cragoe, *J. Membr. Biol.* **1988**, *105*, 1.

[11] P. Ertl, B. Rohde, P. Selzer, *J. Med. Chem.* **2000**, *43*, 3714.

[12] E. Hamel, C. M. Lin, J. Plowman, H. K. Wang, K. H. Lee, K. D. Paull, *Biol. Pharmacol*, **1996**, *51*, 53.

[13] J. B. Jiang, D. P. Hesson, B. A. Dusak, D. L. Dexter, G. I. Kang, E. Hamel, *J. Med. Chem.* **1990**, *33*, 1721.

[14] C. M. Lin, G. J. Kang, M. C. Roach, J. B. Jiang, D. P. Hesson, R. F. Ludeuena, E. Hamel, *Mol. Pharmacol.* **1991**, *40*, 827.

[15] R. Nigam, S. Swarup, V. K. Saxena, *Indian Drugs* **1990**, *27*, 238.

[16] V. Alagarsamy, V. Muthukumar, N. Pavalarani, R. Revathi, *Biol. Pharm. Bull.* **2003**, *26*, 557.

[17] V. Alagarsamy, V. R. Solomon, M. Murugan, K. Dhanabal, P. Parthiban, G. V. Anjana, *J. Enzyme. Inhib. Med. Chem.* **2008**, *23*, 839.

[18] V. Alagarsamy, K. Dhanabal, P. Parthiban, G. Anjana, G. Deepa, B. Murugesan, S. Rajkur, A. J. Beevi, *J Chem. Biol. Drug. Des.* **2007**, *70*, 254.

[19] (a) V. Alagarsamy, V. R. Solomon, M. Murugan, R. Sankaranarayanan, P. Periyasamy, R. Deepa, T. D. Anandkumar, *J. Pharm. Pharmacol.* **2007**, *59*, 669.

[20] V. Alagarsamy, S. Meena, K. V. Ramaseshu, V. R. Solomon, T. D. Kumar, K. Thirumurugan, *Biomed. Pharmacoether* **2008**, *62*, 454.

[21] A. A. Bekhit, M. A. Khalil, *Pharmazie* **1998**, *53*, 539.

[22] (a) S. D. Sharma, V. Kaur, *Synthesis* **1989**, 677; (b) S. Allameh, M. M. Heravi, M. M. Hashemi, F. F. Bamoharram, *Chinese Chem. Lett.* **2011**, *22*, 131.

[23] D. Shi, L. Rong, J. Wang, Q. Zhuang, X. Wang, H. Hu, *Tetrahedron Lett.* **2003**, *44*, 3199.

[24] J. A. Mooreg, G. J. Sutherland, G. J. Sowerby, E. G. Kelly, S. Palermo, W. Webster, *J. Org. Chem.* **1969**, *4*, 887.

[25] J. X. Chen, H. Y. Wu, W. K. Su, *Chinese Chem. Lett.* **2007**, *18*, 536.

[26] W. K. Su, B. B. Yang, *Aust. J. Chem.* **2002**, *55*, 695.

[27] W. K. Su, B. B. Yang, *J. Chem. Res. Synop.* **2002**, 604.

[28] J. Chen, W. Su, H. Wu, M. Liu, C. Jin, *Green Chem.* **2007**, 972.

[29] N. Razavi, B. Akhlaghinia, *New J. Chem*. **2016**, *40*, 447.

[30] W. Yang, R. Qiao, J. Chen, X. Huang, M. Liu, W. Gao, J. Ding, H. Wu, *J. Org. Chem.* **2015**, *80*, 482.

[31] Y. Ma, D. Ren, J. Zhang, J. Liu, J. Zhao, L. Wang, F. Zhang, *Tetrahedron Lett.* **2015**, *56*, 4076.

[32] (a) K. B. Gudasi, R. S. Vadavi, R. V. Shenoy, S. A. Patil, *Trans. Met. Chem.* **2006**, *31*, 374; (b) R. S. Hoonur, B. R. Patil, D. S. Badiger, R. S. Vadavi, K. B. Gudasi, P. R. Dandawate, M. M. Ghaisas, S. B. Padhye, M. Nethaji, *Eur. J. Med. Chem.* **2010**, *45*, 2277; (c) K. B. Gudasi, R. V. Shenoy, R. S. Vadavi, M. S. Patil, S. Patil, *Indian J. Chem. Sec. A* **2005**, *44*, 2247.

[33] A. N. Gusev, V. F. Shul'gin, M. A. Kiskin, I. L. Eremenko, *Russ. J. Coord. Chem.* **2011**, *37*, 589.

Publications and Presentations

List of publications

[1] 'Metal Ion Directed Tautomeric Polymorphism in a Hydrazonamide/ Hydrozonate System'

Arkalekha Mandal, Bhisma K. Patel*, *ChemistrySelect* **2017**, *2*, 494–503.

[2] 'A Three Component Synthesis of 2-Aryl-3-imidamide Substituted 1,2-Dihydroquinazolin-4(1*H*)-ones'

Arkalekha Mandal, Bhisma K. Patel*, *ChemistrySelect* **2017**, *2*, 1717–1722.

[3] 'Impact of the Complementary Electronic Nature of C–X and M–X Halogens and Intramolecular X···O Interaction on Supramolecular Assemblies of Zn(II) Complexes of *O*-halophenyl Substituted Hydrazides'

Arkalekha Mandal, Bhisma K. Patel,* Rahul Shukla, Deepak Chopra*, *CrystEngComm.* **2017**, *CrystEngComm.* **2017**, *19*, 1607−1619.

[4] 'Molecular Structures and Fluorescence Property of Zn(II), Cd(II) Complexes of 3-Pyridyl-5-aryl-(1*H*)-1,2,4-triazoles'

Arkalekha Mandal, Bhisma K. Patel*, communicated.

List of Presensntations

[1] 'Coordination Chemistry with Ligands Derived from 2-Cyanopyridine and Substituted Hydrazide'

Frontiers in Chemical Science (FICS), December 2014; held in IIT Guwahati, Guwahati, India.

[2] 'Role of Intramolecular Hydrogen and Halogen Bonding in Determining Molecular Conformation of Ligands in Their Transition Metal Complexes'

Modern Trends in Inorganic Chemistry (MTIC), December 2015; held in Jadavpur University, Kolkata, India.

[3] 'Metal Ion Directed Tautomeric Polymorphism in a Hydrazonamide/ Hydrozonate System'

CRSI Symposium, February 2017; held in Gauhati University, Guwahati, India.